

Review

# Recent Progress with Pincer Transition Metal Catalysts for Sustainability

Luca Piccirilli , Danielle Lobo Justo Pinheiro  and Martin Nielsen \* 

Department of Chemistry, Technical University of Denmark, DK-2800 Kgs. Lyngby, Denmark;  
lucpic@kemi.dtu.dk (L.P.); dane@kemi.dtu.dk (D.L.J.P.)

\* Correspondence: marnie@kemi.dtu.dk; Tel.: +45-24651045

Received: 11 June 2020; Accepted: 6 July 2020; Published: 11 July 2020



**Abstract:** Our planet urgently needs sustainable solutions to alleviate the anthropogenic global warming and climate change. Homogeneous catalysis has the potential to play a fundamental role in this process, providing novel, efficient, and at the same time eco-friendly routes for both chemicals and energy production. In particular, pincer-type ligation shows promising properties in terms of long-term stability and selectivity, as well as allowing for mild reaction conditions and low catalyst loading. Indeed, pincer complexes have been applied to a plethora of sustainable chemical processes, such as hydrogen release, CO<sub>2</sub> capture and conversion, N<sub>2</sub> fixation, and biomass valorization for the synthesis of high-value chemicals and fuels. In this work, we show the main advances of the last five years in the use of pincer transition metal complexes in key catalytic processes aiming for a more sustainable chemical and energy production.

**Keywords:** pincer complexes; sustainability; biomass valorization; hydrogen; carbon dioxide valorization; nitrogen fixation

## 1. Introduction

During the last 15 years, organometallic pincer-type complexes have emerged as a highly promising group of catalysts for numerous processes within sustainable chemistry. They have been applied in energy production through hydrogen generation, dehydrogenative synthesis of high-value chemicals, as well as CO<sub>2</sub> and N<sub>2</sub> hydrogenations for carbon dioxide capture and recycling and a more sustainable ammonia production, respectively. As such, the use of this family of homogeneous catalysts enhances the sustainability of an incredible number of chemical processes. High catalytic activity at mild reaction conditions, low catalyst loading, combined with high selectivity and excellent atom efficiency are the general main advantages. Notably, all these aspects are crucial when considering the sustainability of chemical processes, as dictated by the green chemistry guidelines [1]. Unfortunately, catalyst deactivation and/or degradation are usually the main drawbacks of homogeneous catalysis, otherwise excellent systems in terms of activity, selectivity, and reaction conditions. The currently employed heterogeneous alternatives are more robust and with an established know-how on the processes, but they usually require high temperatures and hence are high-energy demanding. Pincer-type ligations provides increased robustness because of the stabilization of the tridentate coordination, resulting in homogeneous catalytic systems with increased chemical and thermal stability [2–4].

The ligand design of pincer complexes offers numerous possibilities as well as potential catalytic applications [5,6]. For example, the pincer arm can bear an array of different heteroatoms and functionalities. In addition to affording chemical stability, the pincer ligand can take active part of the catalytic cycle by providing a suitable coordination site for the substrate, weakening selected bonds (H-X bonds), or accepting/donating electrons and protons. Moreover, the cooperation between the

central metal atom and the ligand is tunable based on the desired steric/electronic environment and catalytic application.

After the first family of PCP complexes was synthesized by Shaw in 1976 [7], numerous research groups have applied this concept for almost all types of homogeneously catalyzed chemical reactions. A myriad of novel complexes with different pincer arms have been synthesized and characterized, including a vast family of carbene pincers [8–23], PNP [24–29], PNN [30,31], POP [32], PCP [33–38], SNS [39,40], NCN [41], NSiN [42], CNC [43], CNN [44], NNN [45], as well as sulfur- [46–48], silicon- [49,50], selenium- [51,52], and boron-functionalized [53,54] pincer ligands. Indeed, this topic represents one of the most attractive areas in homogeneous catalysis [55–63]. Many of the most promising results in sustainable transformations have been achieved with second and third-row transition metals, such as Ru [40,64–72], Os [73–76], Ir [77–81], Rh [82,83], and Pd [84–89]. Nevertheless, the current trend in the scientific community is to identify cheaper alternatives based on earth-abundant metals such as Fe [90–96], Mn [97–100], Ni [101–105], V [106–108], and Co [109–114]. In particular, iron and manganese PNP pincer complexes show optimal performance in many relevant sustainable transformations in the optic of the hydrogen economy. Several excellent reviews cover this relevant transition toward first-row metals for a more sustainable chemical production [115–124].

More recently, the incorporation of pincer complexes into porous materials acting as supports has been investigated using the supported (ionic) liquid phase catalysis (SILP or SLP) [125,126]. The idea is to combine the excellent activity of homogeneous systems with the robustness given by the heterogeneous nature of the support. Important examples using pincer-type homogeneous catalysts can be found in aldehyde hydrogenation using Fe(II)-PNP complexes [127,128], and continuous-flow alkane dehydrogenation [129].

Furthermore, several groups have been exploring the use of pincer complexes for a wide series chemical transformations, further expanding the applicability of this family of catalysts. Representative examples include olefination [130–132], hydroamination [133–135], hydrocarboxylation [136], hydrovinylation [137], aminomethylation [138], dehydrogenation of alkanes [139–144], alkane metathesis [145], N-formylation of amines [146,147], C-alkylation of secondary alcohols [148,149],  $\alpha$ -alkylation of ketones [150,151], and alkylation of amines [152–156] and anilines [157].

The deoxydehydrogenation (DODH) of biomass-derived vicinal diols and polyols has also been explored by employing metal pincer complexes. The reaction proceeds in the presence of a sacrificial reducing agent and results in the formation of alkenes, relevant building blocks for the polymer industry. Some examples using pincer ligation are reported with vanadium [106,107], rhenium [158], as well as molybdenum pincer catalysts [159]. The field is relatively immature and further optimization is necessary. A comprehensive overview of the best catalytic systems for DODH reactions, including the aforementioned pincer complexes, is provided in the detailed reviews of Fristrup [160] and Monbaliu [161].

Remarkably, there are several reports in literature using pincer-type metal complexes as suitable catalysts for water splitting reactions. The process is key for the development of the hydrogen economy that requires green and sustainable hydrogen produced via solar or wind energy. Many groups explored various combinations of metals and pincer ligation [14,162,163]; in particular, several works report the use of Milstein Ru-PNP catalyst **3** for this transformation [164–169].

The purpose of this review is to show the very recent advances in pincer-type catalysis for sustainable chemistry. Research in this area centers on achieving zero-CO<sub>2</sub> emissions and sustainable, eco-friendly chemistry and energy production. Literature is already rich with numerous excellent works reviewing pincer complex chemistry as well as its applications in homogeneous catalysis for sustainable reactions [170–175]. As such, in this review we will confine ourselves to discuss the recent progress in the use of pincer complexes as catalysts for sustainable chemistry. Moreover, we will mainly cover work from the second half of the previous decade, i.e., 2015–2020. Dehydrogenation of bio-resourced substrates, hydrogenation of CO<sub>2</sub> and N<sub>2</sub>, processes for the synthesis of high-value

chemicals with lowered waste and enhanced atom efficiency, as well as hydrogen storage systems, are the main areas of interest of this review.

## 2. Dehydrogenation Reactions

Acceptorless alcohol dehydrogenation (AAD) by homogeneous catalysis represents a powerful and sustainable route for synthetic purposes as well as for energy production/storage [176,177]. Mild reaction conditions, high selectivity, and excellent atom efficiency are the main advantages of the process. The sustainability of homogeneous catalytic AAD relies on the absence of any Meerwein-Ponndorf-Verley type sacrificial reagents, which traditionally promote the Oppenauer oxidation of the alcoholic moiety in transfer hydrogenation reactions. In addition, even when molecules that are more complex are formed, valuable hydrogen is often the only byproduct, which can be directly used in-house to provide energy to the process, perfectly in line with the idea of new integrated bio-refineries. These facets render AAD dramatically more atom- and energy efficient, respectively, compared to conventional synthetic procedures.

In the optics of abandoning fossil feedstock, the dehydrogenation of biomass-derived molecules is one of the explored alternatives. Formic acid, ethanol, glycerol, and carbohydrates already represent an accessible, sustainable source for the production of chemicals and fuels by acceptorless dehydrogenation. Importantly, they are abundant and easily obtainable from biomasses. Hence, this field holds great potential, and the transformation of these substrates into high-value chemicals or direct hydrogen release by homogeneous pincer catalysis is promising.

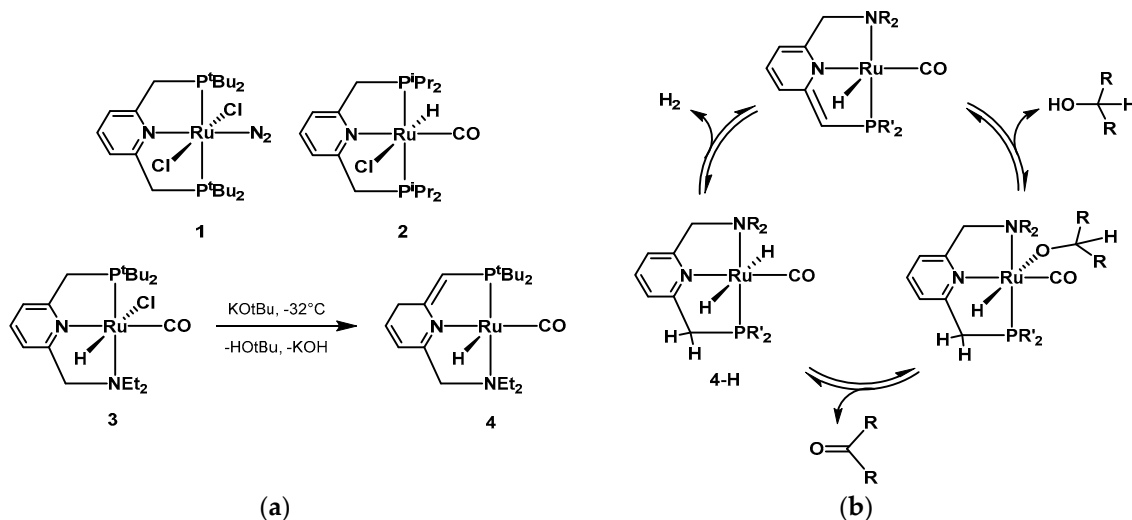
Pincer-type complexes have been extensively applied for AAD reactions with a plethora of bio-substrates, ranging from ethanol [178–181] to lignocellulose [182], as described in Section 2.1. The applied transition metal complexes generally show good performance in terms of stability and activity, with the advantage of carrying out selective reactions at mild conditions and low catalyst loading. Often, the pincer ligand plays an active part of the catalytic cycle (metal–ligand cooperativity), which seemingly is determinant for the catalyst's stability as well as reactivity. The mechanistic details of AAD are beyond the scope of this review and can be found elsewhere [183–195]. The topic is of great importance and a deeper understanding of the reaction mechanisms is still necessary [196,197]. Nevertheless, some representative examples of catalytic cycles involving pincer ligand participation are provided throughout the review.

### 2.1. Early Works

The first example of AAD by homogeneous catalysis dates back to 1960s with the work by Charman, using rhodium chloride as catalyst [198]. In the mid-1970s, Robinson described the ruthenium complex  $[\text{Ru}(\text{OCOCF}_3)_2(\text{CO})(\text{PPh}_3)_2]$  in combination with trifluoroacetic acid for the dehydrogenation of isopropanol, 1-butanol, ethanol, methanol, and glycerol [199–202]. Several improvements were achieved in the subsequent 20 years, using various type of homogeneous systems in combinations with a range of additives, including light irradiation.

In 2004, Milstein presented the first example of metal–ligand cooperating pincer ligands in AAD for synthetic purposes [203,204]. In a series of ruthenium(II)-based complexes, the PNP pincer bearing a pyridine moiety and various phosphine substituted side arms was found to be very active for the dehydrogenation of simple secondary alcohols. Some examples of the first generations of Milstein's catalysts can be found in Scheme 1a. In most cases, there is a direct participation of the pincer ligands in the catalytic cycle. The pyridine moiety rearranges by aromatization-dearomatization [64,177,205–209], facilitating the coordination of the alcoholic substrate and the subsequent hydrogen release from the dihydride species, as depicted in the catalytic cycle in Scheme 1b. The involvement of the pincer moiety in the catalytic cycle has been investigated by many groups [210–215]. In 2015, Li reported computational mechanistic studies on several reactions using the Milstein PNP and PNN catalysts [216]. The authors recalculated rate-determining steps and investigated the aromatization-dearomatization equilibria. It was found that aromatic PNP and PNN ligands often provide the lowest activation energy

for some steps, whereas for other steps, the aromatization–dearomatization process was not involved in the lowest energy pathway. Very recently, Gusev investigated the mechanism of AAD of alcohols, as well as ester hydrogenation, using catalyst **4**, and identified the dihydrido complex **4-H** (Scheme 1b) as the active species for both dehydrogenation and hydrogenation reactions [217].



**Scheme 1.** (a) Examples of Milstein's first generation pincer catalysts [204]; (b) example of acceptorless alcohol dehydrogenation (AAD) reaction mechanism using Milstein's type PNN pincer complexes based on aromatization/dearomatization of the pyridine moiety.

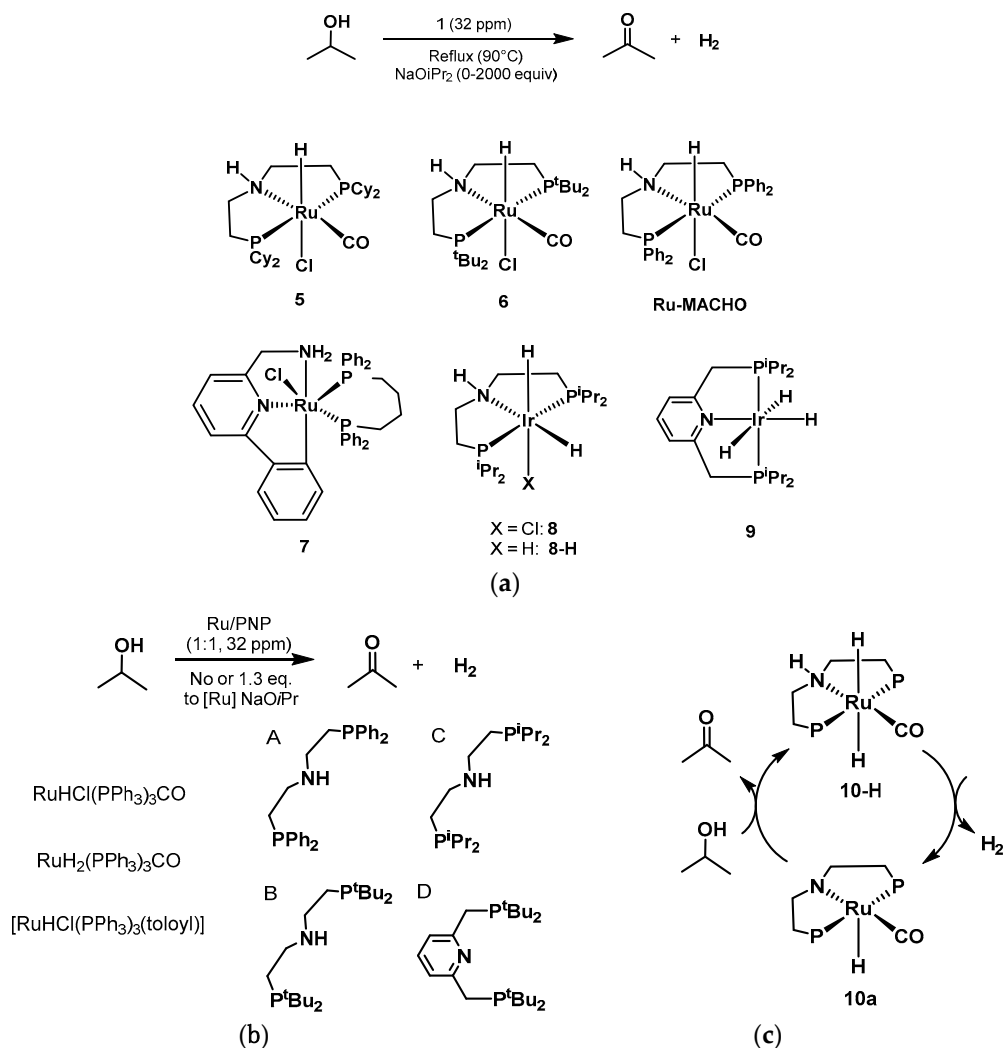
Simultaneously, the Beller group started exploring the in situ influence of various phosphines and nitrogen containing ligands mixed with ruthenium catalyst precursors for the dehydrogenation of isopropanol [218]. For the first time, they demonstrated the possibility to generate hydrogen from this substrate at temperatures below  $100^\circ\text{C}$ . A dramatic increase in activity was observed with addition of multidentate *N*-ligands, with particularly TMEDA being the most prominent promoter for catalytic activity. Remarkably, the catalyst was active over a period of up to 11 days. The authors applied the same system for ethanol dehydrogenation but no significant  $\text{H}_2$  formation was detected.

In a following work from 2011, Beller tested both known catalyst as well as the in situ formation of active species using combinations of Ru-precursors and *N*-containing pincer ligands. They showed that the ruthenium complex  $[\text{RuH}_2(\text{CO})(\text{PPh}_3)_3]$ , in the presence of the  $i\text{PrPNP}$  ligand **C** shown in Scheme 2, was able to efficiently dehydrogenate isopropanol without the need of any additive [219].

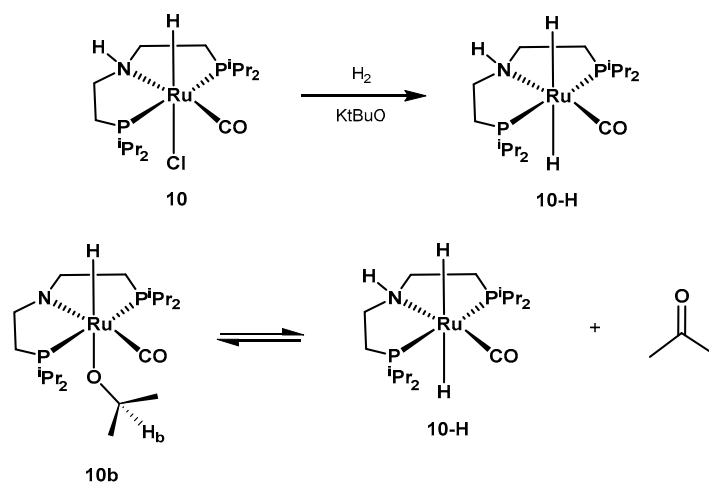
The system showed in Scheme 2 represents the current state-of-the-art of homogeneous isopropanol acceptorless dehydrogenation. The reaction was performed for the first time at mild conditions ( $90^\circ\text{C}$ , refluxing isopropanol) and importantly, without additives. The in situ formed active catalyst **10-H** (Scheme 3) resulted in a turnover frequency higher than  $8000\text{ h}^{-1}$  using 4 ppm of catalyst.

Almost simultaneously, Gusev presented a range of ruthenium and osmium PNP and POP pincer catalysts for the transformation of alcohols into ketones, widening the applicability of metals to osmium for this type of transformation [73]. The  $i\text{PrPNP}$ -Ru- $\text{H}_2$  active dihydrido catalyst **10-H** formed in situ in the work of Beller, was synthesized and characterized starting from the chlorido precursor **10** (Scheme 3). NMR analysis revealed the equilibrium between the dihydrido species and the model substrate isopropanol, and isopropoxo complex **10b** was isolated. Importantly, while the Os-POP catalysts **11** and **11-H** (Figure 1) did not show significant catalytic activity, the Os-PNP complexes **12** and **12-H** demonstrated good air, moisture, and thermal stability, together with outstanding versatility for dehydrogenation of primary alcohols for reactions of transfer hydrogenation, dehydrogenative coupling, and amine alkylation.





**Scheme 2.** (a) Pincer complexes screened by Beller in 2011; (b) low temperature isopropanol dehydrogenation; (c) proposed outer-sphere mechanism [219].



**Scheme 3.** Ru-<sup>i</sup>PrPNP catalysts synthesized and characterized by Gusev and equilibrium between 10-H and 10 [73].

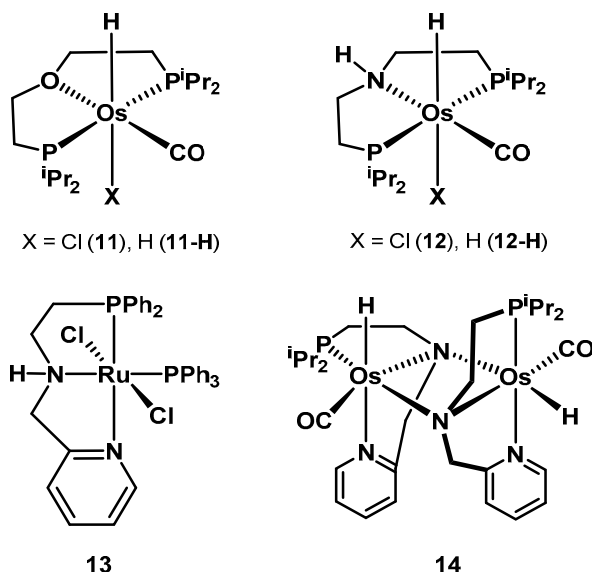
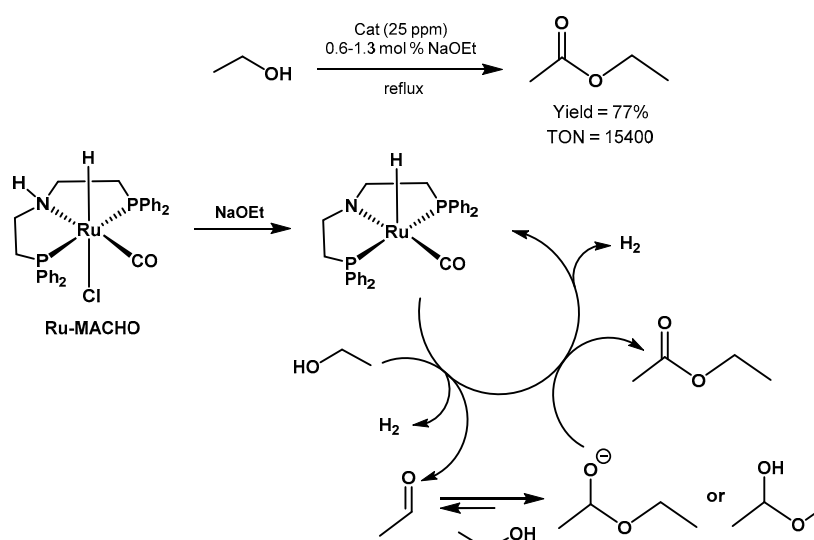


**Figure 1.** Representative examples of ruthenium and osmium pincer catalysts reported by Gusev [73,178,179].

In 2013, Beller showed the efficient conversion of ethanol into ethyl acetate using **Ru-MACHO**, reported in 2012 to efficiently catalyze ester hydrogenation [220]. The reactions were performed at refluxing conditions and in the presence of NaOEt, necessary for the catalyst activation through Cl<sup>−</sup> elimination (Scheme 4) [180]. Furthermore, it was speculated whether the ethoxide plays an active role in driving the reaction further from the acetaldehyde intermediate to the ethyl acetate product. Under optimized conditions, the reaction afforded 77% yield in ethyl acetate (TON = 15,400) using 50 ppm of **Ru-MACHO**, 0.6% mol of NaOEt, at 90 °C, after 46 h. Curiously, in the screening of catalysts, the Ir-PNP catalyst (**8** in Scheme 2) synthesized by Abdur-Rashid [79], as well as the Milstein PNP catalyst **4** [204], were found to be practically inactive for this transformation under the given reaction conditions.



**Scheme 4.** Ethanol transformation to ethyl acetate using **Ru-MACHO** and proposed reaction mechanism by Beller [180].

The same year, Gusev reported the same transformation catalyzed by the Ru-PNN complex **13** in Figure 1. By applying 50 ppm of **13** in a refluxing solution of EtOH/NaOEt (1 mol%), it was possible to achieve 85% conversion after 40 h [179]. Also the same year, Gusev presented the osmium dimer **14** (Figure 1) as well [178]. This PNN osmium congener to the ruthenium complex **13** is particularly

active in ethanol dehydrogenation into ethyl acetate. As such, the system affords 96% conversion of neat ethanol into ethyl acetate and 2 equivalents of hydrogen after 8 h at 78 °C, with toluene as solvent, 0.5 mol% of KtBuO, and a molar ratio of substrate to metal equal to 1000.

In 2014, Beller showed that it is feasible to generate hydrogen from ethanol/water mixtures as well as from industrial bio-ethanol obtained from fermentation processes, without prior removal of the water content (5%) [181]. Catalyst **10** was active using various water contents (EtOH/H<sub>2</sub>O [*v/v*] 9:1, 7.5:2.5, 5:5), producing only trace amounts of CO<sub>2</sub> and CO (<10 ppm), of key importance for the direct use of hydrogen in fuel cells. Under optimized conditions, using 25 ppm of catalyst **10** (Scheme 3) and 8 M NaOH, the reaction resulted in TOF of 1707 h<sup>−1</sup> and 1613 h<sup>−1</sup> after 1 and 3 h, respectively. A long-term experiment was also carried out, affording 70% yield after 98 h at 88 °C, resulting in a TON as high as 80,000 and 7.8 L of hydrogen gas produced. Remarkably, the system showed comparable activity to the aqueous ethanol solution also when applying real fermented bio-ethanol (TOF = 1770 h<sup>−1</sup> and 1686 h<sup>−1</sup> after 1 and 3 h, respectively).

Since their seminal work, the Milstein group has continued exploring novel pincer complexes leading to a series of novel synthetic applications using the AAD methodology [205]. As previously mentioned, the sustainability effect of carrying out dehydrogenation reactions by AAD relies not only on the concomitant production of H<sub>2</sub>, but also on the absence of waste, and hence an excellent atom efficiency. The field is extensively growing, and pincer complexes are contributing to the main advances. Several groups have explored new routes for the syntheses of numerous new product types by means of AAD reactions. For example, starting from alcohols and amines, it is now possible to selectively obtain amides [221–225], imines [226–228], imides [229], polyamides [230], pyrroles [231–235], pyridines [236], pyrazines [237–239], pyrimidines [240], hydrazones [241], quinolines [242], or aldimines [243,244]. AAD of alcohols also provide access to clean, efficient routes to carboxylic acids [245–248], ketones or aldehydes [249–251], esters [252–256], acetals [257], alkenes [258], as well as lactones [259–261].

In most of the cited works, homogeneous pincer-type catalysis often provides milder reaction conditions, as well as enhanced atom efficiency compared to the classical synthetic routes. In addition, several of the cited works employ first-row metal complexes, further increasing the sustainability of the processes. The electronic configuration of the metal center, the design of the pincer ligand, together with specific reaction conditions favors the desired reaction mechanism leading to certain products. These possibilities demonstrate the synthetic versatility of AAD and the very high flexibility, selectivity, and activity of pincer catalysts. These complexes might even be considered a privileged family of catalysts [262–266].

## 2.2. Dehydrogenation Reactions for a Hydrogen Economy

There are many alternatives for continuous hydrogen release from liquid organic hydrogen carriers (LOHCs), such as methanol, formic acid, up to bigger aromatic molecules, and carbohydrates. The topic has been widely reviewed, offering comparison with established energy systems, applicability, and potential impact of LOHCs for the future of energy [267–288]. The H<sub>2</sub> content stored in each of these molecules varies (Table 1), as well as the catalytic pathway involved in their dehydrogenation. In most cases, several reaction mechanisms are competing, each of them releasing different equivalents of hydrogen gas. Together with CO<sub>2</sub> hydrogenation, this topic currently represents one of the more intense research areas within sustainable catalysis.

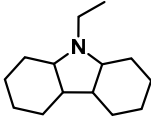
The dehydrogenation of alcohols in a hydrogen economy perspective has been well-reviewed in the last 10 years by many authors, providing a comprehensive overview of the many possibilities offered by homogeneous catalysis, including pincer-type catalysis [289–293]. The release of hydrogen from LOHCs has been proposed and achieved using different approaches, with either methanol, formic acid, or formaldehyde/water as hydrogen storage systems [294–298]. Methanol and formic acid represent nowadays the most studied technologies for efficient hydrogen release at low temperatures (*vide infra*), hence being promising candidates for acting as LOHCs in the transportation sector, where lower temperatures are required [299–305]. Hydrogen release from methanol, as well as from formic

acid, should be envisioned as part of a wider concept including CO<sub>2</sub> capture and recycling [306,307]. Green hydrogen produced via water electrolysis using e.g., wind- or solar energy can sustain the inverse process of CO<sub>2</sub> hydrogenation to methanol, formic acid, or any favorable LOHC, closing an ideal CO<sub>2</sub>-free energy production cycle [308–314].

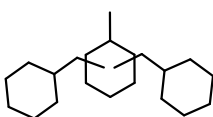
**Table 1.** Hydrogen weight percentage stored in some representative liquid organic hydrogen carriers (LOHCs).

LOHC	H <sub>2</sub> wt%
Methanol	12.6
Formic Acid	4.4
Ethanol	12
Formaldehyde	6.6
Glycerol	9.6
Sugar Alcohols	8.9–9.3
N-ethylcarbazole (NEC)	5.8
Dibenzyltoluene (DBT)	6.2
1,2-BN-cyclohexane	7.1
BuPy	3.14
MePHI	5.76

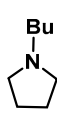
  



NEC

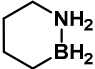


DBT

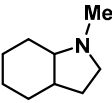


BuPy

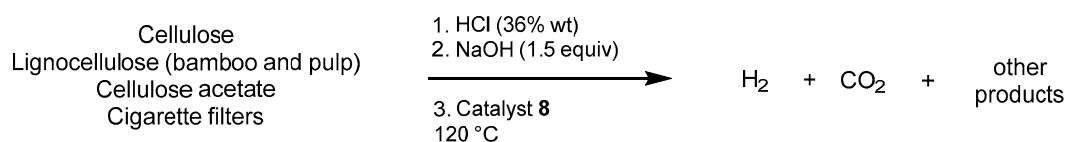


1,2-BN-cyclohexane



MePHI

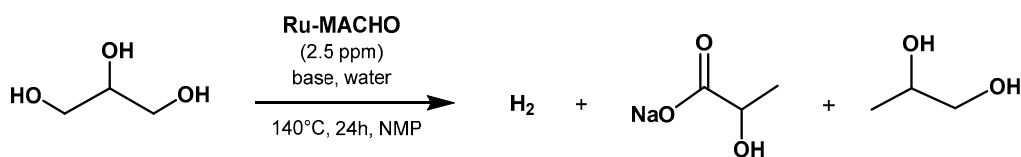
Polyols such as glycerol or carbohydrates might be considered as direct biomass-to-hydrogen suppliers, but their more complicated dehydrogenation pathways as well as lower hydrogen content currently render them unfavorable as hydrogen sources. In this light, Beller screened in 2015 a series of PN<sup>H</sup>P-Ru and -Ir complexes (**Ru-MACHO**, **Ru-MACHO-BH**, **5**, **8**, **10**) for hydrogen production from several bio-substrates obtained from biomass [182]. Hydrogen evolution was observed from cellulose, fructose, glucose, lignocellulose, as well as from (used) cigarette filters (cellulose acetate). After optimization, it was possible to release hydrogen at temperatures at 120 °C using ppm amounts of catalyst **8** and stoichiometric amounts of NaOH in a one-pot protocol (Scheme 5). A remarkable TON of about 6000 after 3 h was obtained using 20 ppm of complex **8** in the conversion of cellulose resulting in a 1.00:1.09 mixture of H<sub>2</sub>/CO<sub>2</sub>.



**Scheme 5.** Conversion of cellulose and other biomass-derived substrates using catalyst **8** in a one-pot protocol proposed by Beller [182].

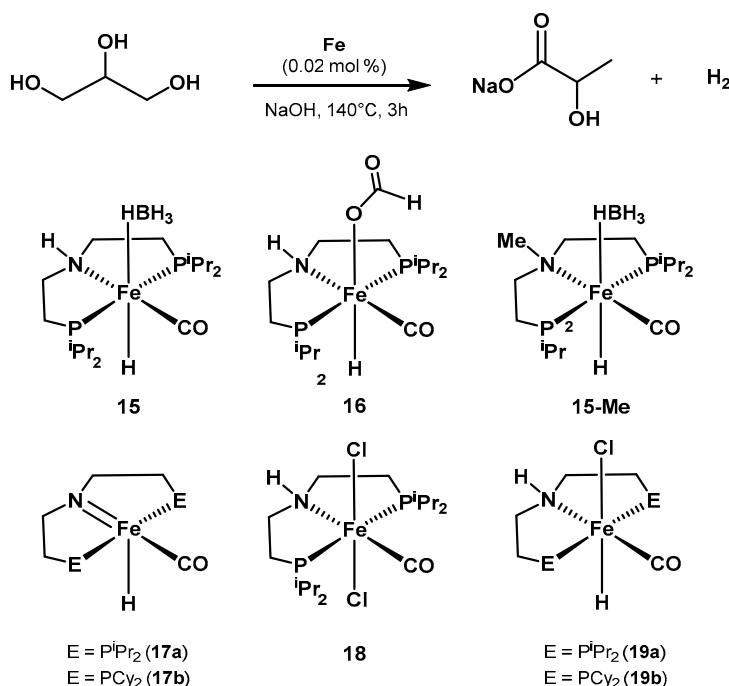
The same group also proposed a Ru-catalyzed hydrogen production from glycerol accompanied by the selective synthesis of sodium lactate, the monomer for the synthesis of polylactic acid (Scheme 6) [315]. The screening involved the same family of catalysts used in the above-mentioned

work. Using only 2.5 ppm of **Ru-MACHO** and 1.08 eq. of KOH (7.3 M), it was possible to obtain full conversion and 67% yield of sodium lactate.



**Scheme 6.** Beller's glycerol dehydrogenation to lactic acid [315].

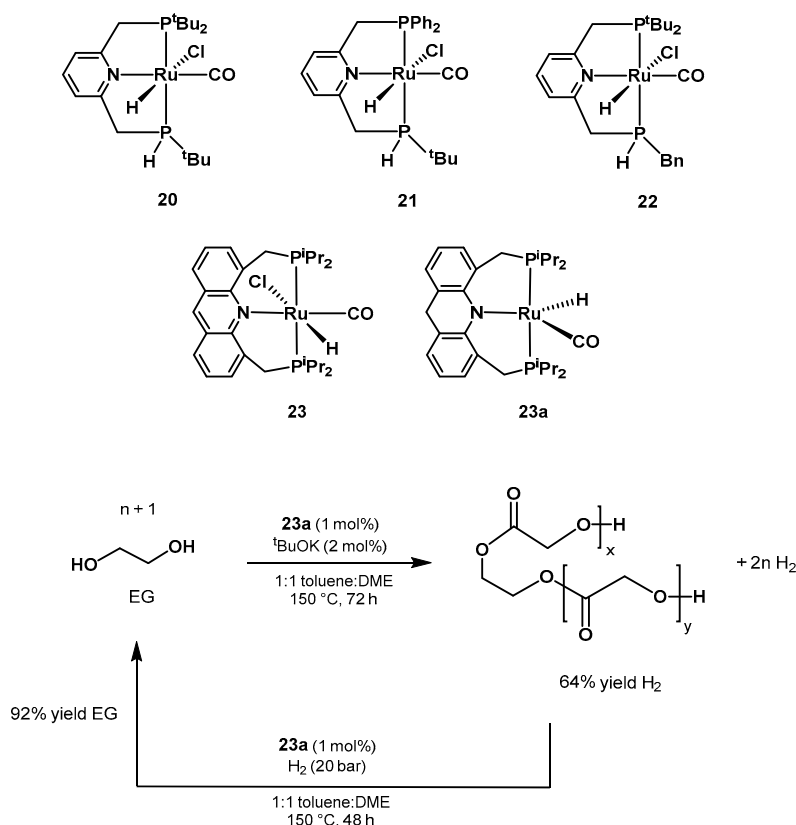
Contemporarily, Hazari and Crabtree showed the same transformation applying the family of iron-PNP complexes showed in Scheme 7 [316]. The formate complex **16** showed the highest activity with 24% conversion and 81% selectivity toward sodium lactate. In addition, the authors proposed a transfer hydrogenation of acetophenone to 1-phenylethanol using complex **15**. The yield increase with the amount of KOH vs. substrate, with a maximum of 90% yield after 20 h using 2.5 mol% of **15** and 10 eq. KOH/substrate in *N*-methyl-2-pyrrolidinone. As described later, both complexes **15** and **16** are efficient catalysts for methanol and formic acid dehydrogenations as well. Catalyst **17a**, which is obtained after basic treatment of **15**, was shown to be active in the dehydrogenation of primary alcohols such as 1-butanol to the corresponding esters [317], as well as highly selective urea synthesis by dehydrogenative coupling of methanol and amines, as reported by Hazari and Bernskoetter in 2018 [318].



**Scheme 7.** Screening of iron pincer complexes performed by Hazari and Crabtree for glycerol conversion to lactic acid [316].

Recently, Milstein proposed a reversible and efficient liquid-organic hydrogen carrier using ethylene glycol (EG) [319]. The authors screened various Ru-PNP catalysts bearing different substituents in the *N* and *P* arms (Scheme 8). After optimization, catalyst **23a** reached 97% conversion and 64% yield of H<sub>2</sub>. In addition, it was possible to hydrogenate the reaction mixture using the same catalyst and same reaction conditions, resulting in full conversion to ethylene glycol.

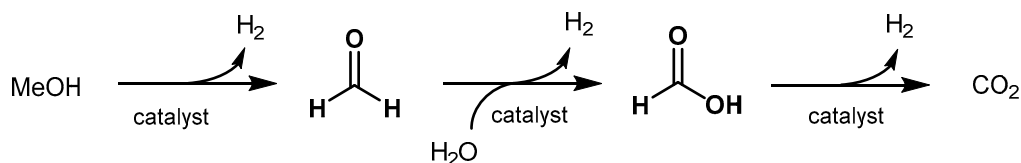




**Scheme 8.** Hydrogen storage system based on ethylene glycol proposed by Milstein [319].

### 2.2.1. Methanol Dehydrogenation

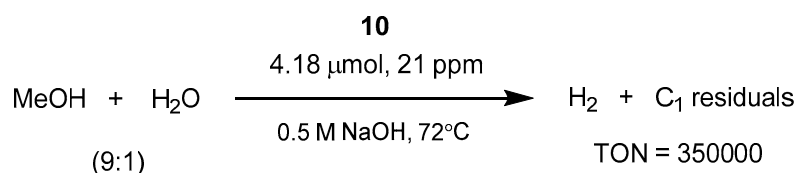
The homogeneous dehydrogenation of methanol to  $\text{H}_2$  and  $\text{CO}_2$  in the optic of a methanol-based economy has been intensively studied over the past decade. The topic has been reviewed by Alberico and Nielsen in 2015 [320], by Prakash in 2018 [321], and very recently by Araya, Liso, Cui, and Knudsen Kær [322]. Importantly, methanol is currently produced from fossil fuels through syngas, hence a sustainable production from biomass or/and atmospheric  $\text{CO}_2$  is highly desirable (see Section 3.1.2). The aqueous reforming of methanol involves three consecutive steps yielding three molecule of hydrogen for each molecule of methanol (Scheme 9). The first step is the dehydrogenation of methanol to afford formaldehyde and the first equivalent of hydrogen. Then, formaldehyde reacts with water to form methanediol that can undergo a second dehydrogenation resulting in formic acid. The latter is further dehydrogenated to finally produce  $\text{CO}_2$  and the third molecule of hydrogen.



**Scheme 9.** Reaction pathway of aqueous methanol reforming.

The reforming of methanol to produce hydrogen is currently carried out at elevated temperatures ( $>200\text{ }^\circ\text{C}$ ) and pressures ( $>25\text{ bar}$ ) by means of heterogeneous catalysts such as  $\text{Pt}/\text{Al}_2\text{O}_3$ , as well as the less expensive  $\text{Cu}/\text{ZnO}/\text{Al}_2\text{O}_3$  [323–328]. As discussed below, pincer complexes allow the direct release of hydrogen gas from aqueous methanol at temperatures below  $100\text{ }^\circ\text{C}$ , with low catalyst loadings as well as promising stability properties.

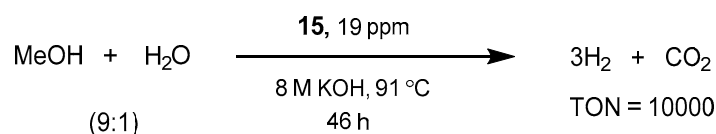
In 2013, Beller showed that the two catalysts **10** and **Ru-MACHO** are able to efficiently dehydrogenate methanol in a one-pot synthesis toward CO<sub>2</sub> (Scheme 10) [329]. The authors investigated the performance of the known Ru-PNP systems under different natures of the base, its concentration, the water content, and the reaction temperature. After optimization of the amount of base (8.0 M KOH), catalyst **10** showed the best performance affording a TOF = 2,668 h<sup>-1</sup> in a 9:1 MeOH:H<sub>2</sub>O mixture, and a TOF of 4719 h<sup>-1</sup> in neat CH<sub>3</sub>OH, at 91 °C and with 1.6 ppm catalyst loading. The system showed a turnover number of 350,000 after 23 days of continuous reaction. Merely <10 ppm of CO and CH<sub>4</sub> were detected. Because of the highly alkaline nature of the reaction mixture, most of the CO<sub>2</sub> initially produced is trapped as carbonate; hence, the authors performed an experiment with low base loading (0.1 M of NaOH in a 4:1 MeOH/H<sub>2</sub>O). Indeed, CO<sub>2</sub> was eventually released instead of being trapped, and the expected 3:1 H<sub>2</sub>/CO<sub>2</sub> gas composition was observed, indicating a direct correlation between solution pH and the observed gas composition. The authors also proposed a catalytic cycle based on the observed species using in situ NMR experiments; all the catalytic steps were believed to follow a conventional outer-sphere mechanism.



**Scheme 10.** Ru-PNP catalyzed methanol dehydrogenation showed by Beller [329].

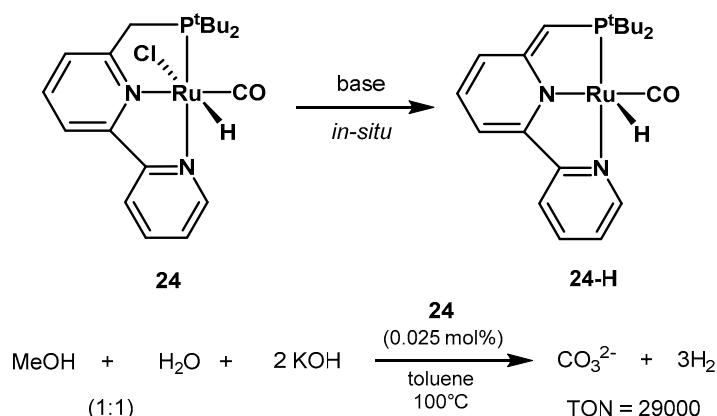
Later, Grützmacher and Trincado reported the homogeneous transition metal complex [K(dme)<sub>2</sub>][Ru(H)(trop<sub>2</sub>dad)] for clean hydrogen release from methanol–water mixtures. Total of 0.5 mol% of the ruthenium catalyst at 90 °C achieved up to 80% methanol conversion [330]. In 2015, Yamaguchi demonstrated the low temperature (<100 °C) hydrogen release from methanol–water using an anionic iridium complex bearing a functional bipyridonate ligand [331].

Beller showed that also the iron-<sup>iPr</sup>PNP complex **15** is able to perform the same transformation in the presence of base [332]. Catalyst **15** dehydrogenated aqueous methanol (9:1 CH<sub>3</sub>OH/H<sub>2</sub>O) at 91 °C with turnover frequencies of 702 h<sup>-1</sup> after 1 h (Scheme 11). CO levels < 10 ppm were detected. Lowering the catalyst loading from 4.2 μmol to 1 μmol resulted in a TOF = 617 h<sup>-1</sup> and TON = 10,000 after 46 h. Remarkably, the system was active in neat methanol, as well as without addition of base, although the best performance was obtained in the presence of 8M KOH.



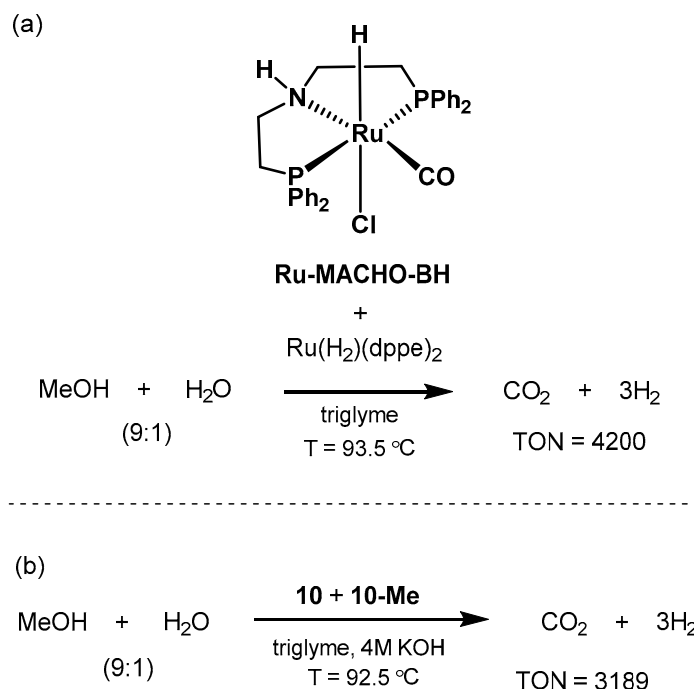
**Scheme 11.** Fe-PNP catalyzed methanol dehydrogenation showed by Beller [332].

A year later, Milstein applied the Ru-PNN complex **24**, known to be active in the AAD of alcohols to carboxylic acid salts and H<sub>2</sub>, for aqueous methanol dehydrogenation as well [333]. Catalyst **24** (Scheme 12) showed promising activity and could be effectively recycled, remaining stable for 1 month and reaching TON values of 29,000. 0.025 mol% of **24** produced an overall H<sub>2</sub> yield of 80% starting from a 1:1 CH<sub>3</sub>OH/H<sub>2</sub>O mixture, in the presence of 2 equivalents KOH at 100 °C in toluene. Higher water loadings were detrimental for catalytic activity since the formation of a hydroxo complex inhibits the coordination of formic acid in the last reaction step. In order to gain insights on the reaction mechanism, the authors also performed experiments on formic acid dehydrogenation, accompanied by the isolation and characterization of the formic acid adduct by NMR and X-ray crystallography. When ~2 equivalents of NEt<sub>3</sub> were used in the absence of water, 0.09 mol% of catalyst **24** dehydrogenated formic acid with 98% yield of hydrogen at room temperature after 24 h.



**Scheme 12.** Ru-PNP catalyzed methanol dehydrogenation showed by Milstein [333].

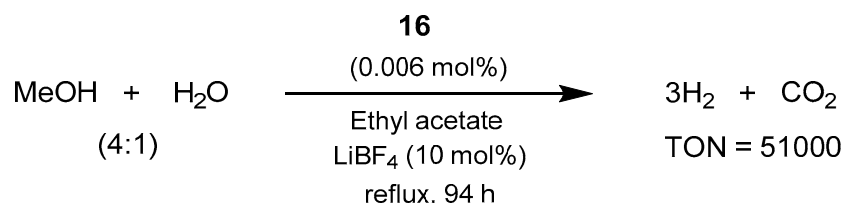
In 2014, Beller proposed a base-free, bi-catalytic system formed by **Ru-MACHO-BH** and  $\text{Ru}(\text{H}_2)(\text{dppe})_2$  ( $\text{dppe}$  = 1,2-bis(diphenylphosphino)ethane) as shown in Scheme 13a [334]. The former catalyst is similar to **Ru-MACHO** but, importantly, can be activated by heat instead of by base within the reaction temperature window employed here. The authors screened several co-catalysts in order to improve the step of formic acid dehydrogenation. After optimization,  $\text{Ru}(\text{H}_2)(\text{dppe})_2$  was found to be the optimal option. The authors proposed a synergetic interaction between the two catalysts; indeed, the volume of gas produced by the bi-catalytic system was much bigger than the gas evolution observed with the single catalysts separately, which showed very little gas evolution. The optimized system gave a turnover number >4200 with very low catalyst loading (5  $\mu\text{mol}$  of each catalyst) and only traces of CO impurity (<8 ppm), yielding 26% of hydrogen (based on water).



**Scheme 13.** Beller's bi-catalytic systems for methanol dehydrogenation catalyzed by Ru-PNP complexes [334,335]. (a) **Ru-MACHO-BH** +  $\text{Ru}(\text{H}_2)(\text{dppe})_2$  (2014) and (b) **10** + **10-Me** (2019).

In 2015, Bernskoetter, Hazari, and Holthausen showed that not only strong basic conditions, but also Lewis acid additives enhance the performance of PNP-based complexes [336]. In this work, the authors screened the same family of catalysts showed in Scheme 7. Using 0.006 mol%, or 60 ppm,

of the iron complex **16** in the presence of 10 mol% LiBF<sub>4</sub> in refluxing ethyl acetate, it was possible to convert a 4:1 methanol/water mixture to 3:1 H<sub>2</sub> and CO<sub>2</sub> in 50% yield after 94 h. Increasing the catalyst loading to 0.01 mol% led to full conversion in 52 h. The system produced a turnover number of 51,000, the highest reported for earth-abundant metals (Scheme 14). The work also provides DFT calculations to explain the role of the Lewis acid additive, suggesting that the competitive lithium coordination promotes the rate of formate abstraction, thus resulting in a higher proportion of the catalytically active amido complex.



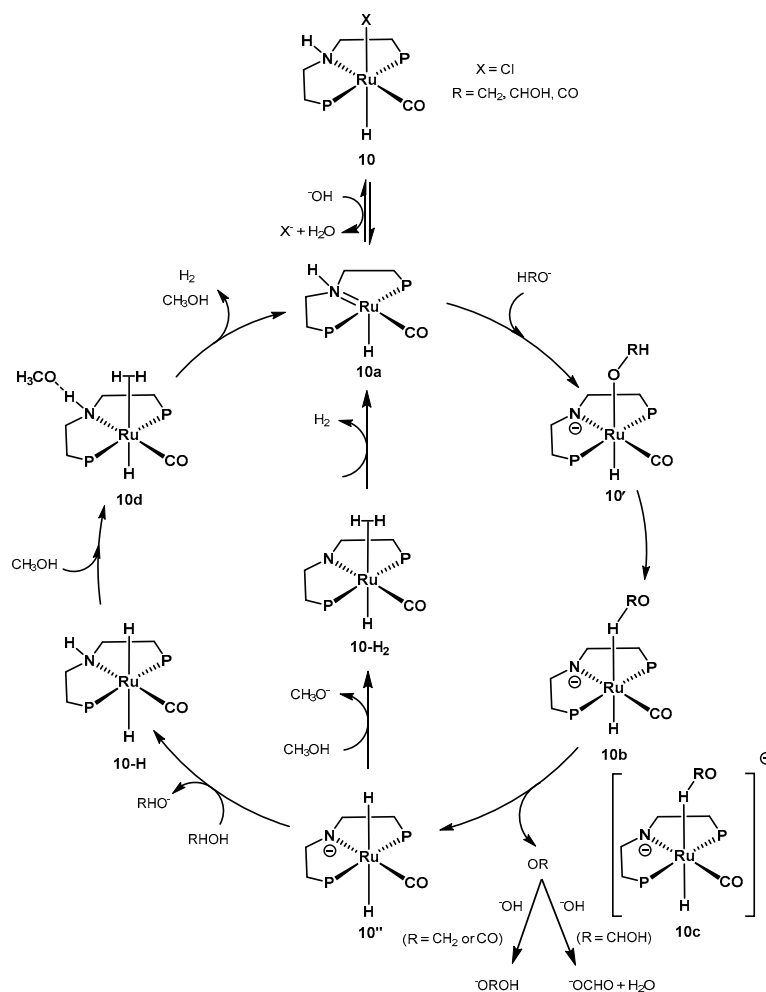
**Scheme 14.** Iron-catalyzed methanol reforming in the presence of Lewis acids proposed by Bernskoetter, Hazari, and Holthausen [336].

In 2016, Beller investigated the mechanism of aqueous methanol dehydrogenation using the state-of-the-art catalyst under highly alkaline conditions, complex **10**, and compared with its N-Me congener **10-Me**. The proposed catalytic cycle depicted in Scheme 15 was obtained combining experiments, isolation of key intermediates, NMR characterization, single crystal X-ray crystallography, and DFT calculations [337]. Contrarily to the previously invoked outer sphere mechanisms, the authors proposed an inner sphere pathway for the C-H cleavage step, promoted by base. The required amount of base is essential to increase the reaction rate; the authors noted an increase in the ratio of **10''/10'**, indicating the “inner-sphere” C-H cleavage, via C-H coordination of the methoxide to the ruthenium center. The lower, but comparable, catalytic activity of **10-Me** with its PNH<sub>2</sub>P counterpart provides further experimental evidence to the role of the N-H moiety in PNP-catalyzed dehydrogenation reactions [193,338–340].

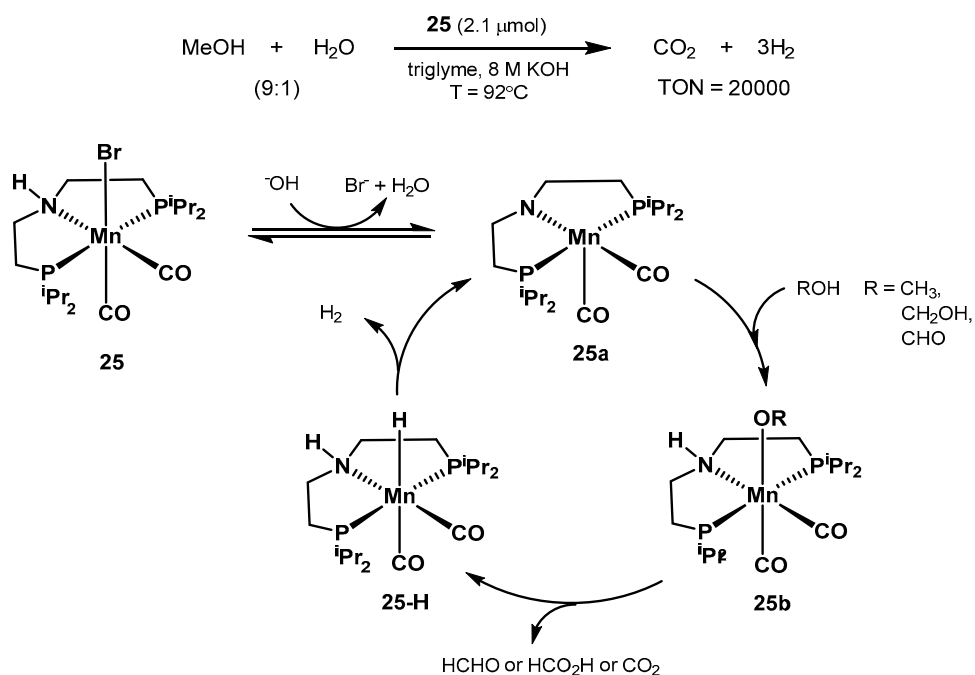
The same group carried out mechanistic studies on aqueous methanol dehydrogenation using well-defined manganese and rhenium catalysts, under both base-free as well as strongly basic conditions [341]. Fu used DFT calculations to propose a self-catalytic role of methanol in ruthenium PNP-catalyzed dehydrogenation [342]. Several authors have studied the process in depth, using inter alia, DFT calculations, NMR spectroscopy, or Raman-GC techniques [343–345].

In 2017, Beller proposed the structurally defined manganese complex **25** as an active catalyst for aqueous methanol dehydrogenation (Scheme 16) [346]. The optimized conditions resulted in 20,000 turnovers after 900 h at 92 °C, starting from a 9:1 CH<sub>3</sub>OH/H<sub>2</sub>O mixture in triglyme, with 8M KOH, and in the presence of 10 equivalents of the PNP ligand to the catalyst (2.1 μmol). Moreover, other organic carriers such as ethanol, paraformaldehyde, and formic acid were successfully dehydrogenated as well. Unlike the previous work by Bernskoetter, Hazari, and Holthausen [336], the presence of Lewis acid additives resulted in no observable improved catalytic activity.

The same group showed that, similar to the PNP complexes of ruthenium, iron, and manganese, also the iridium-PNP catalyst **8** is able to promote methanol dehydrogenation under mild conditions albeit with lower catalytic activity [347]. Complex **8** afforded a TON of 1900 after 60 h at 92 °C, showing promising stability over time. In this case too, highly basic conditions were required (8M KOH) for consistent catalytic activity starting from a 9:1 mixture of CH<sub>3</sub>OH/H<sub>2</sub>O.



**Scheme 15.** Proposed inner-sphere catalytic cycle for aqueous methanol dehydrogenation by Beller [337].



**Scheme 16.** Manganese-catalyzed methanol reforming and proposed catalytic cycle proposed by the group of Beller [346].



In 2019, Beller improved the performance of Ru-PNP catalysts for methanol dehydrogenation using another bi-catalytic system formed by the catalysts **10/10-Me** (Scheme 13b) [335]. Based on observations on the formic acid dehydrogenation step [348], the addition of catalyst **10-Me** promotes the rate of hydrogen release from formic acid in the last step. The combination of the two catalysts together was 1.5 times more active than individually. Employing 8.56–9.62  $\mu\text{mol}$  of **10** + **10-Me** in a 9:1 MeOH:H<sub>2</sub>O mixture in triglyme, with 40 mmol KOH at 92.5 °C, afforded a clean 3:1 H<sub>2</sub>/CO<sub>2</sub> mixture with TOF = 1063 h<sup>−1</sup> and a TON = 3189 (calculated based on total amount of catalysts present) after 3 h. This work further shows that applying bi-catalytic systems in cascade reactions is a promising solution to improve the catalytic performance, taking advantage of synergetic effects between two active catalytic species.

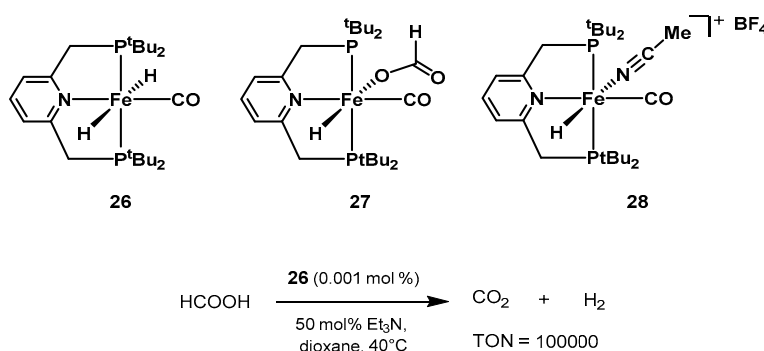
The same year, Haumann explored the immobilization of the known ruthenium <sup>i</sup>PrPNP catalyst **10** for the continuous gas-phase steam reforming of methanol [349]. Using the supported liquid phase (SLP) technology, the authors investigated the activities of the prepared catalysts using an array of support materials. The best result in terms of activity and stability was achieved using pure KOH deposited onto alumina support. The system was stable for 70 h on stream and only trace amounts of CO were observed.

## 2.2.2. Formic Acid Dehydrogenation

The use of formic acid as hydrogen carrier and storage system has been widely investigated and reviewed in various works [299,300,350–359]. A variety of both heterogeneous and homogeneous catalytic systems have been applied for its decomposition, including the use of light irradiation [360–381].

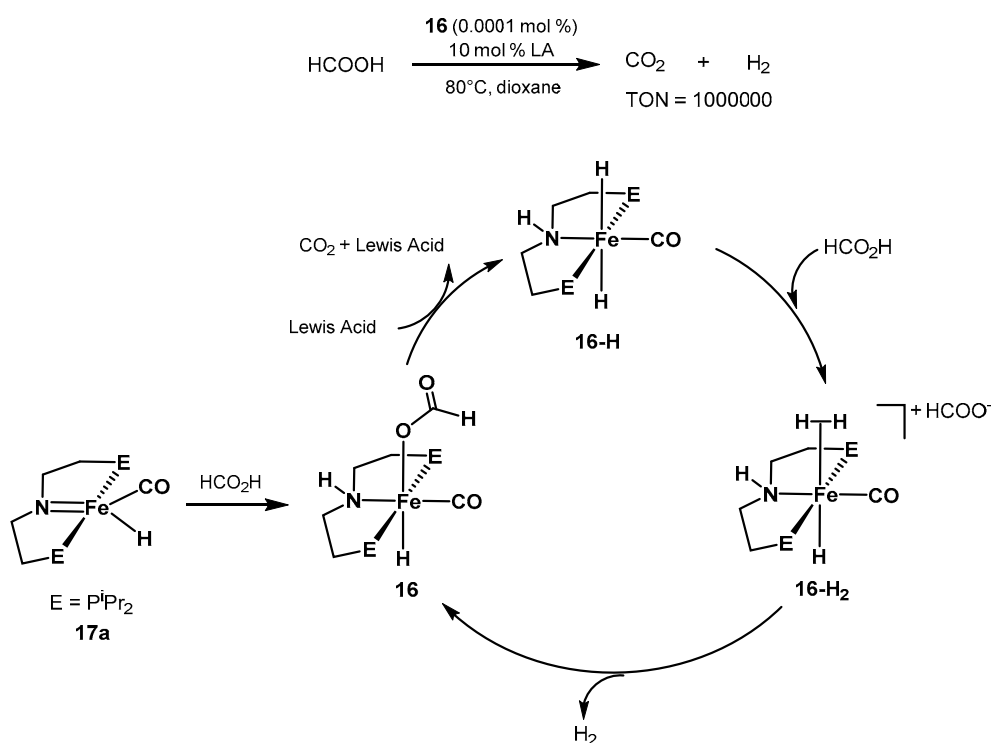
In 2011, following previously reported works on iron-catalyzed formic acid dehydrogenation [382,383], Beller reported the remarkable activity of an iron complex bearing the tetradentate tripodal ligand tris[(2-diphenylphosphino)ethyl]phosphine [P(CH<sub>2</sub>CH<sub>2</sub>PPh<sub>2</sub>)<sub>3</sub> (PP<sub>3</sub>) [384]. The authors tested both the in situ formation of the active species, as well as various synthesized iron hydride complexes bearing the same PP<sub>3</sub> ligand. The activity of the synthesized catalysts was found to be comparable with that of the in situ formed systems in the presence of 2 equivalents of PP<sub>3</sub> ligand. After optimization, simply applying 5 mmol of Fe(BF<sub>4</sub>)<sub>2</sub>·6H<sub>2</sub>O and 2 equivalents of PP<sub>3</sub> to a solution of formic acid in propylene carbonate, afforded a TOF of 9425 h<sup>−1</sup> and a surprising TON of 92,000 at 80 °C.

Contemporarily, Milstein was also investigating the performance of iron pincer complexes based on the lutidine moiety, reporting suitable catalysts for the hydrogenation of ketones [385,386], as well as CO<sub>2</sub> hydrogenation to formate [387]. In 2013, the group showed a series of iron pincer complexes as active catalysts for formic acid dehydrogenation (Scheme 17) [388]. The dihydrido complex *trans*-[Fe-(<sup>t</sup>BuPNP)(H)<sub>2</sub>(CO)] **26** showed the best performance, reaching TON values up to 100,000 at 40 °C in the presence of trialkylamines. 0.001 mol% of **26** in 1,4-dioxane, in the presence of 50 mol% NEt<sub>3</sub>, resulted in full conversion of formic acid after 10 days.



**Scheme 17.** PNP pincer catalysts screened by Milstein for low-temperature formic acid dehydrogenation [388].

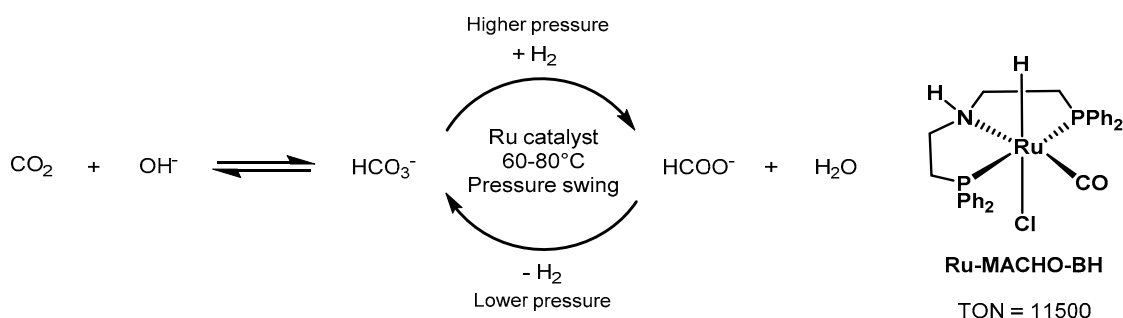
Inspired by the afore-mentioned works carried out by Beller and Milstein using first row transition metals, Schneider and Hazari showed in 2014 that the formate iron-PNP complex **16**, combined with a suitable Lewis acid co-catalyst, is particularly active for formic acid dehydrogenation [389]. As such, employing 0.0001 mol%, or merely 1 ppm, of **16** in the presence of 10 mol% of LiBF<sub>4</sub>, a TOF of 196,728 h<sup>−1</sup> was obtained after one hour and a remarkable TON of 983,642 after 9.5 h. As mentioned earlier, the role of the LA is supposed to facilitate the release of formate from the iron formate intermediate, a task usually carried out by basic additives. The reactions were performed at 80 °C in dioxane (Scheme 18). The gaseous products consisted in a 1:1 mixture of H<sub>2</sub> and CO<sub>2</sub> with CO concentration less than 0.5%. The activity of the system showed in this work (TON = 1,000,000) is the highest reported for non-precious transition metals.



**Scheme 18.** Schneider and Hazari's Lewis acid assisted formic acid dehydrogenation with the Fe-PNP catalyst **16** [389].

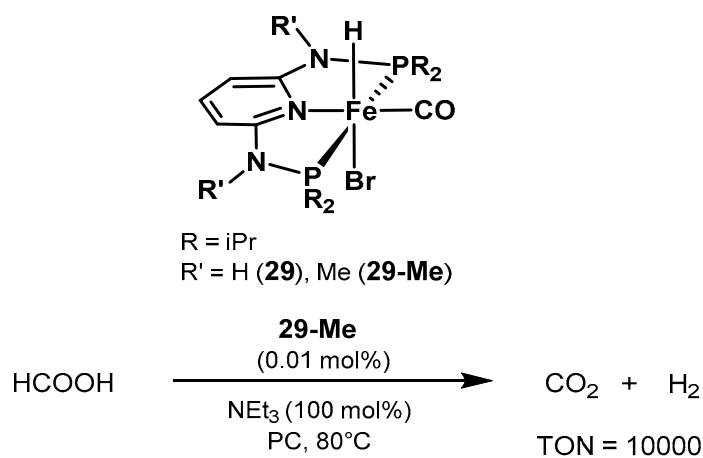
In 2015, Prakash and Olah proposed a remarkable example of CO<sub>2</sub>-free energy storage and release based on the formate/bicarbonate couple, which act as both hydrogen carrier and CO<sub>2</sub> storage system [390]. The authors showed a continuous cyclic system of either CO<sub>2</sub> or bicarbonate hydrogenation to formate and subsequent hydrogen release from formate (Scheme 19). The catalyst screening involved the well-known and robust **Ru-MACHO**, **Ru-MACHO-BH**, and the *N*-methylated MePNP congener of **Ru-MACHO**. The system is amine-additive free and requires neither pH control nor change of solvent between the cycles; the same catalyst performs in both the hydrogenation and dehydrogenation steps. In a combined experiment, and by simply changing the reaction pressure, it was possible to obtain 90% conversion in both directions with a combined turnover number of 11,500 obtained after six full cycles of hydrogenation/dehydrogenation with **Ru-MACHO-BH**. The possibility of performing both transformation by only changing one parameter, such as pressure, is highly favorable for hydrogen-storage batteries. Importantly, the two *N*-H and *N*-Me PNP catalysts showed similar catalytic activities under the same reaction conditions and for both directions, with the *N*-Me PNP complex being the most active in the dehydrogenation of sodium formate, resulting in a TON of 1000 (TOF = 430 h<sup>−1</sup> after 2 h) with 0.1 mol% catalyst loading in a 2:1 mixture H<sub>2</sub>O:1,4-dioxane as

solvent. A TON of 5000 was achieved lowering the catalyst loading down to 0.01 mol%, albeit with only 50% yield in H<sub>2</sub>.



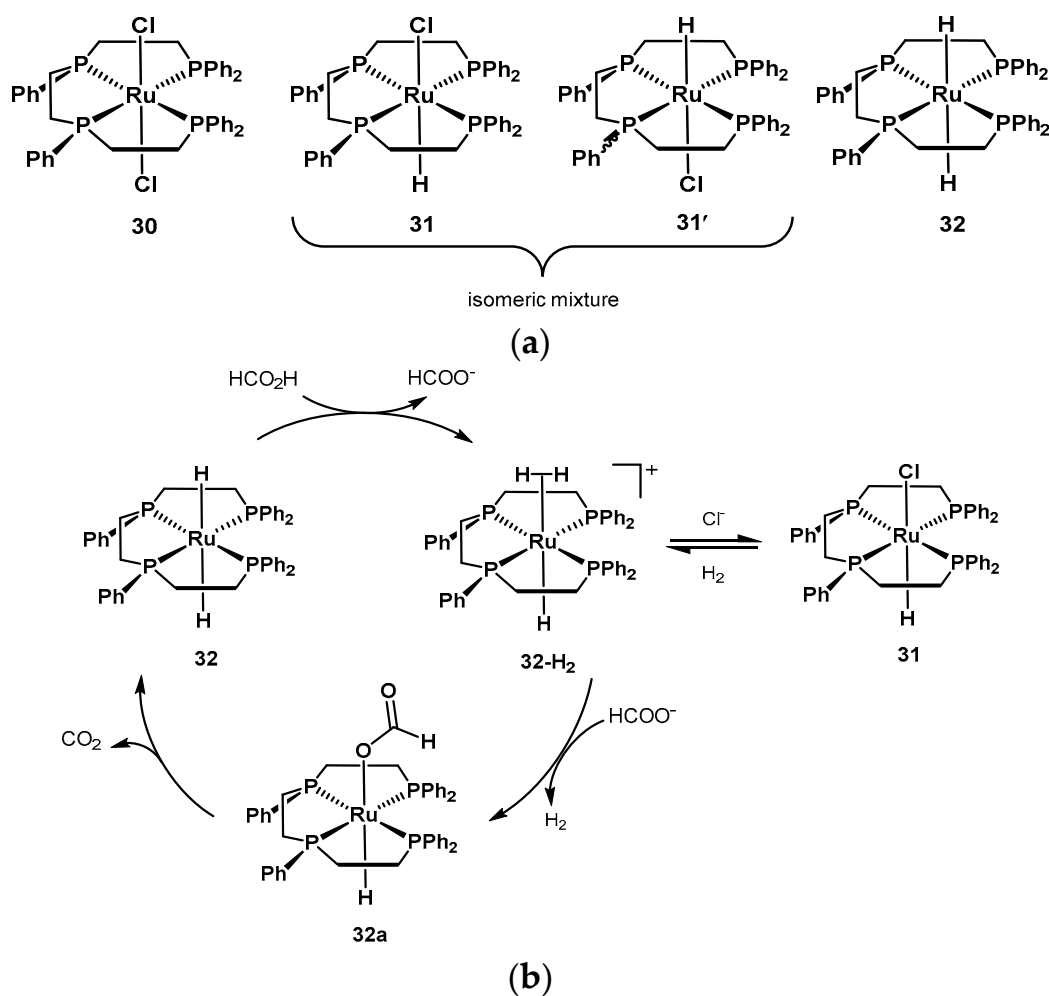
**Scheme 19.** Reversible formic acid hydrogen release and capture performed by Prakash and Olah using Ru-PNP catalysts [390].

Continuing the exploration of iron pincer complexes, Gonsalvi and Kirchner proposed in 2016 a series of Fe-PNP complexes bearing the 2,6-diaminopyridine scaffold (Scheme 20) [391]. Using propylene carbonate (PC) as solvent and 100 mol% of NEt<sub>3</sub> as base additive, led to full conversion of formic acid into H<sub>2</sub> and CO<sub>2</sub> at 80 °C. A TOF = 2635 h<sup>−1</sup> after one hour and a turnover number of 10,000 after six hours were achieved using 0.01 mol% of catalyst **29-Me**. Curiously, the authors explored the effect of Lewis acid additives as well. Contrarily to the results reported by Schneider and Hazari using Fe-PNP catalysts [389], this work showed that replacing the base with 10 mol% of LiBF<sub>4</sub> resulted in no conversion of formic acid.



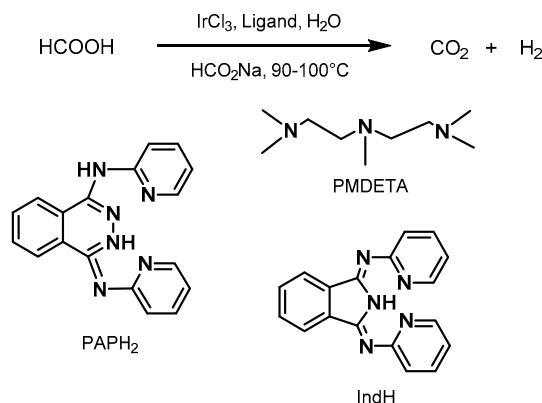
**Scheme 20.** Iron-PNP catalysts for low-temperature hydrogen release from formic acid reported by Gonsalvi and Kirchner [391].

Also in 2016, Gonsalvi proposed a series of well-defined, in situ formed Ru(II) complexes of the linear tetraphosphine ligand meso-1,1,4,7,10,10-hexaphenyl-1,4,7,10-tetraphosphadecane (tetraphos-1, P4), as shown in Scheme 21a [392]. The system was active for formic acid dehydrogenation in both batch and continuous feed conditions, in the presence of an amine additive. The authors investigated the reaction mechanism using NMR experiments and DFT calculations. The *trans*-[Ru(H)<sub>2</sub>(meso-P4)] **32** was found to be the key intermediate in the proposed catalytic cycle, suggesting that formic acid activation occurs on only one of the hydrides of the octahedral specie (Scheme 21b).



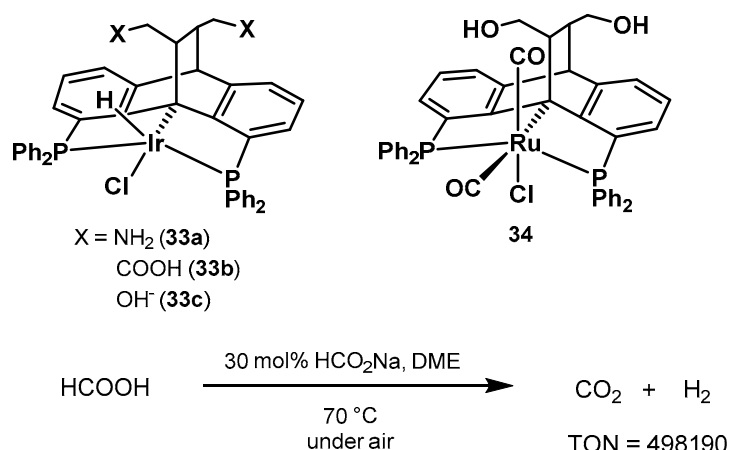
**Scheme 21.** (a) Gonsalvi's ruthenium complexes  $\text{trans-[RuCl}_2(\text{meso-P4})]$  (**30**),  $\text{trans-[Ru(H)Cl(meso-P4)]}$  (**31** and **31'**) and  $\text{trans-[Ru(H)}_2\text{(meso-P4)]}$  (**32**) studied by Gonsalvi; (b) proposed reaction mechanism [392].

The same year, Czaun, Olah, and Prakash investigated the in situ formation of active catalytic systems from mixtures of  $\text{IrCl}_3 \cdot x\text{H}_2\text{O}$  and *N*-donor ligands in aqueous solution of formate at temperatures between 90 and 100 °C (Scheme 22) [393]. Among other tested mono- and bidentate ligands, there were the tridentate  $\text{N,N,N',N',N''}$ -pentamethyldiethylenetriamine (PMDETA), and the multidentate 1,3-bis(2'-pyridyl-imino)-isoindoline (IndH) and 1,4-di(2'-pyridyl)aminophthalazine (PAPH<sub>2</sub>). The catalytic system derived from  $\text{IrCl}_3$  and IndH in aqueous sodium formate showed the best results in terms of high selectivity and robustness for hydrogen generation. Furthermore, the system remained active under both high and moderate pressure conditions (3–50 bar), used to suppress the formation of CO impurity. Importantly from a practical perspective, neither the precursors (including  $\text{IrCl}_3 \cdot \text{H}_2\text{O}$  and IndH) nor the in situ formed species are air sensitive. The catalyst remains active for up to 20 days, and retains a similar activity even after one year when kept under  $\text{H}_2/\text{CO}_2$  pressure. The authors also proposed a prototype of an integrated formic acid decomposition and hydrogen–air PEM fuel cell, demonstrating the feasibility of this approach for a continuous hydrogen production and its conversion into clean energy.



**Scheme 22.** Screening of ligands and in situ formation of iridium pincer ligands by Prakash [393].

In 2017, Gelman explored a series of new bi-functional iridium-PC(sp<sup>3</sup>)P complexes for the dehydrogenation of formic acid at low temperature (Scheme 23) [394]. Catalyst **33a** (cat/FA = 1:2000) reached a turnover number up to  $5 \times 10^5$  and a TOF of  $2 \times 10^4 \text{ h}^{-1}$  ( $3.8 \times 10^5$  and  $1.2 \times 10^4 \text{ h}^{-1}$  with no additives) in 30 mol% sodium formate in DME and, importantly, under air. Three different pincer ligands with pendant groups of varying basicity were investigated: neutral –OH, basic –NH<sub>2</sub> and acidic –COOH. While the complexes containing –OH and –COOH decomposed through liberation of H<sub>2</sub> at  $\text{rt} < T < 60^\circ\text{C}$ , the complex bearing the NH<sub>2</sub> group was found to be the most stable and active catalyst showing selective formic acid decomposition to hydrogen and carbon dioxide with no presence of carbon monoxide (by GC-TCD). Supported by experimental studies and quantum chemical calculations, hydrogen is released by protonolysis of the Ir–H bond and formation of a cationic species stabilized by the amine chelation from the amino group in the backbone. Regeneration of the active hydride catalyst is performed via an outer-sphere intramolecular  $\beta$ -H elimination of formic acid while concomitantly forming CO<sub>2</sub>.



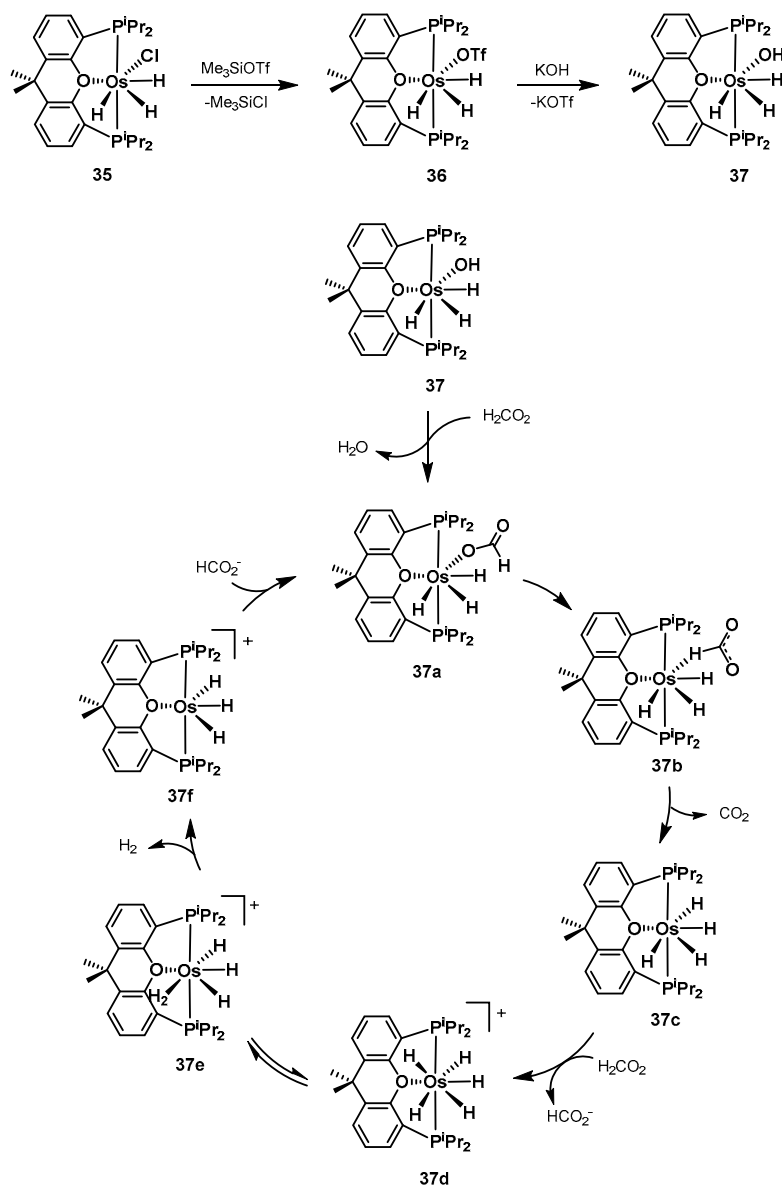
**Scheme 23.** Iridium-PCP complexes explored by Gelman bearing different outer-sphere pendant ligands [394].

Of the same family of bi-functional PCP complexes, Gelman demonstrated that the ruthenium catalyst **34** is active for the acceptorless dehydrogenative coupling of alcohols and amines [395], as well as the *E*-selective semihydrogenation of alkynes with formic acid [396].

In 2018, Esteruelas demonstrated hydrogen production from formic acid using a trihydridohydroxoosmium(IV)-POP catalyst [397]. The reactions were performed at temperatures between 25–45 °C, yielding turnover number values between 17 and 87 (calculated at 20% conversion). Catalyst **37** is obtained starting from the corresponding chloride complex following the route in Scheme 24. The authors also proposed the catalytic cycle shown in Scheme 24 based on kinetic



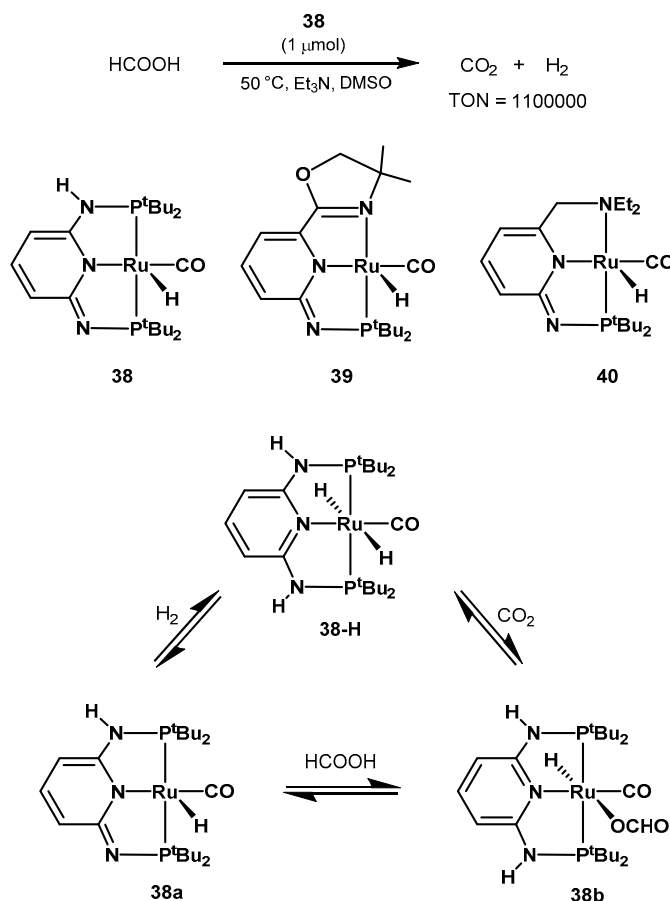
analysis of the catalysis, isolation of the intermediates and kinetic analysis of their decomposition pathways, as well as DFT calculations on the rate-determining step. Complex **37a** was fully isolated and characterized. The release of CO<sub>2</sub> was found to occur through complex **37b**, resulting in the formation of **37c** which is protonated by formic acid to give the pentahydrido complex **37d** in equilibrium with **37e**. The liberation of H<sub>2</sub> affords the unsaturated cationic complex **37f**, which can coordinate a new formate anion.



**Scheme 24.** Synthesis of trihydrido osmium-POP catalysts prepared by Esteruelas as well as their proposed catalytic cycle for formic acid decomposition to H<sub>2</sub> and CO<sub>2</sub> [397].

Zheng and Huang reported a series of new PNP and PNN ruthenium complexes (Scheme 25) as suitable catalysts for formic acid dehydrogenation [398]. The pyridine moiety is dearomatized by deprotonation of one of the arms, leading to an imine functionality, responsible for the catalyst activation/formic acid deprotonation step. Interestingly, the prepared catalysts are both air and water stable. No CO gas is produced together with the CO<sub>2</sub> and H<sub>2</sub>. As expected, the performance of the catalyst dramatically increases in the presence of a base such as  $\text{NEt}_3$ . The system was shown to be active already at 50 °C, but the highest TON of 1,100,000 was obtained at 90 °C, using catalyst **38** in the

presence of triethylenediamine as additive and DMSO as solvent. The same family of catalysts was reported to be active in several promising transformations, i.e., selective dehydrogenation (oxidation) of benzylamines into imines [399], hydrogenation of esters in the presence of water [400], as well as the electrocatalytic reduction of CO<sub>2</sub> to CO and formic acid in aqueous solution with negligible formation of H<sub>2</sub> [401]. In addition, a hydride nickel(I) counterpart of **38** was showed to be active for the cycloaddition of CO<sub>2</sub> and epoxide affording carbonates [402].

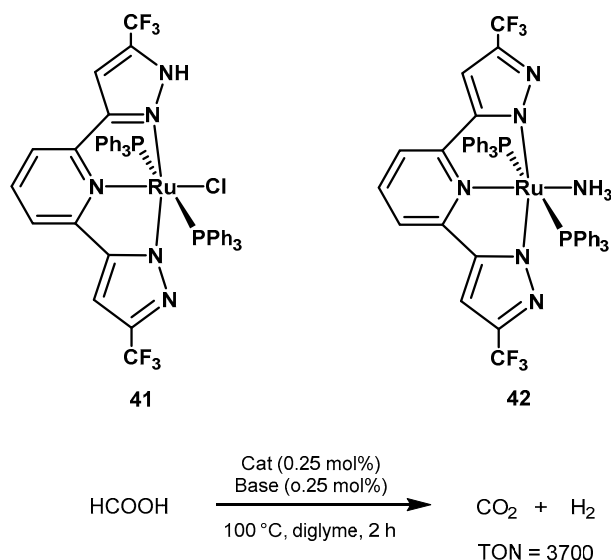


**Scheme 25.** New PNP complexes studied by Huang and proposed plausible mechanism for hydrogen release from formic acid [398].

With the purpose of increasing the long-term stability of homogeneous catalysis, Lai and Huang recently investigated the immobilization of catalyst **38** knitted into porous organic polymers [403]. The supported catalyst was found to be active for dehydrogenation of formic acid in both organic and aqueous media. The system showed excellent stability affording a turnover number of 145,300 after 50 cycles over a period of three months, using a 1:2500 ratio catalyst to formic acid (calculated by measuring the ruthenium content by ICP). A considerably lower TON (5600) was obtained using the homogeneous analog under the same reaction conditions, because of deactivation of the catalyst.

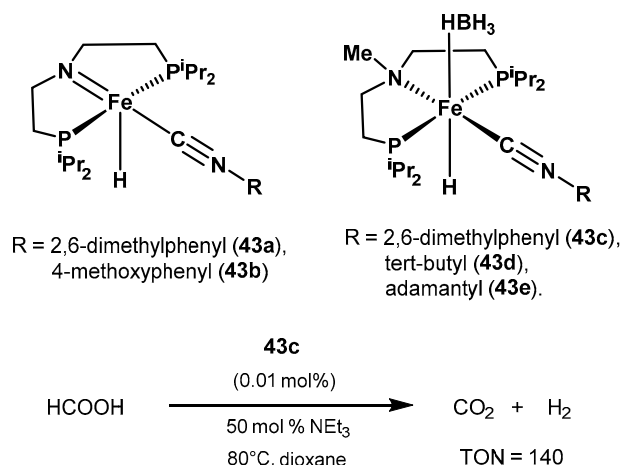
Kuwata showed a series of ruthenium-NNN pincer complexes bearing protic (trifluoromethyl)pyrazole arms for formic acid dehydrogenation [404]. The complexes were synthesized and characterized, and the impact of the perturbations on the catalytic properties was examined. The authors demonstrated the increased Brønsted acidity given by the N-H groups by protonation–deprotonation experiments, whereas the high electron-withdrawing properties of the CF<sub>3</sub> pendants was found to not affect the electron density around the metal center. The NNN pincer complexes **41** and **42** exhibited high catalytic activity; the reaction in the presence of KN(SiMe<sub>3</sub>)<sub>2</sub> as

additive afforded TONs of 3000 and 3700, respectively (Scheme 26). Importantly, using catalyst **42** the reaction proceeds even without the addition of base additives, resulting in the highest TON of 3700.



**Scheme 26.** Novel Ru-NNN catalysts reported by Kuwata for formic acid dehydrogenation [404].

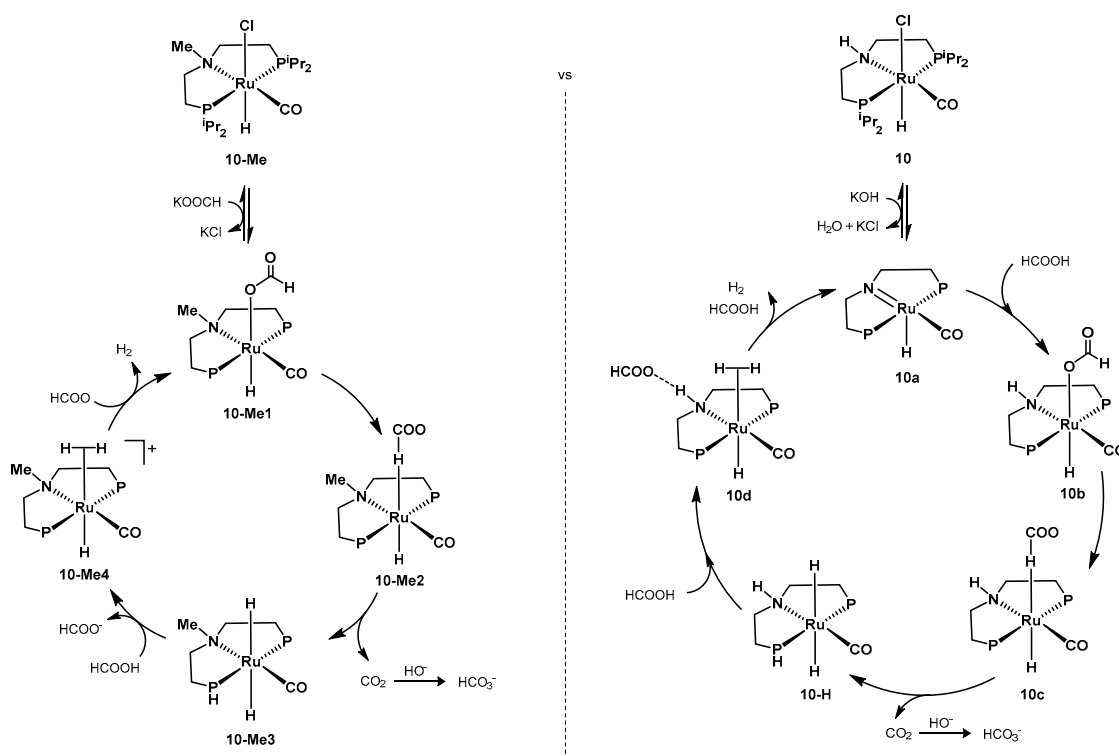
In 2018, Bernskoetter and Hazari proposed three well-defined, single crystal X-ray crystallographically characterized,  $\text{PN}^{\text{Me}}\text{P}$  iron pre-catalysts containing isonitrile ligands, in the form of  $(i\text{PrPN}^{\text{Me}}\text{P})\text{Fe}(\text{H})(\text{HBH}_3)(\text{C}\equiv\text{NR})$ , as shown in Scheme 27 [405]. The catalysts are analogs of the previously showed PNP iron carbonyl complexes, already studied extensively in the literature. A first generation of isonitrile  $\text{Fe-PN}^{\text{H}}\text{P}$  catalysts was reported a year before for the hydrogenation of  $\text{CO}_2$  to formate [406], albeit showing lower activity compared to the first generation iron carbonyl complexes. In this work, a second-generation  $\text{PN}^{\text{Me}}\text{P}$  complexes has been investigated. The new isonitrile catalysts showed to be active in both  $\text{CO}_2$  hydrogenation and formate dehydrogenation, although with one-order magnitude inferior activity compared to the corresponding carbonyl complexes. The reaction using 0.1 mol% of **43c**, 50 mol%  $\text{NEt}_3$  in 5 mL of dioxane at  $80^\circ\text{C}$  resulted in a TON of merely 140 after 4 h.



**Scheme 27.** Isonitrile  $\text{Fe-PN}^{\text{R}}\text{P}$  complexes synthesized by Bernskoetter and Hazari [405].

Very recently, the group of Beller studied the effect of the methylation of the nitrogen atom of the PNP pincer, comparing the activities of the active complexes **10** and **10-Me** for the dehydrogenation of formic acid [348]. This work follows a previously reported article by the same group, where the authors unraveled the mechanism of aqueous methanol dehydrogenation (see Section 2.2.1) [337].

The authors screened the two catalysts at various pH values; under all the tested conditions, complex **10-Me** showed superior activity to **10**. In a first screening in basic conditions (pH = 13), catalyst **10-Me** was found to be approximately twice as active as its  $\text{PN}^{\text{HP}}$  congener, with  $\text{TOF}(\text{N}^{\text{Me}}) = 4251 \text{ h}^{-1}$  and  $\text{TOF}(\text{N}^{\text{H}}) = 2099 \text{ h}^{-1}$  after 1 h. The complexes showed similar activity at neutral pH, while the best activity for both systems was obtained in acidic conditions (pH = 4.5). Catalyst **10-Me** resulted in TOF of  $8981 \text{ h}^{-1}$  superior to **10** ( $5263 \text{ h}^{-1}$ ). In line with the increase in TOF values, the conversion after 3 h also increased: for catalyst **10**, 69% at pH 13 vs 85% at pH 4.5, while catalyst **10-Me** resulted in 82% at pH 13, and in almost full conversion under acidic conditions. After optimization, applying 0.01 mol% of **10-Me** provided a TOF of  $6492 \text{ h}^{-1}$  after 1 h at  $92^\circ\text{C}$ , with 20 mmol of KOH in a aqueous formic acid solution in triglyme. Extending the reaction time to 6 h resulted in full conversion and a TON = 26,388 after four consecutive additions of formic acid. The authors proposed two different catalytic cycles for the two catalysts (Scheme 28), concluding that in both cases the protonation of the complex resulting in the dihydrogen specie is the key step in formic acid dehydrogenation [337]. Curiously, the effect was different with the Mn-PNP **25**, which showed decreased activity in the presence of the N-Me moiety, but still with increased activity in acidic conditions rather than basic ones.

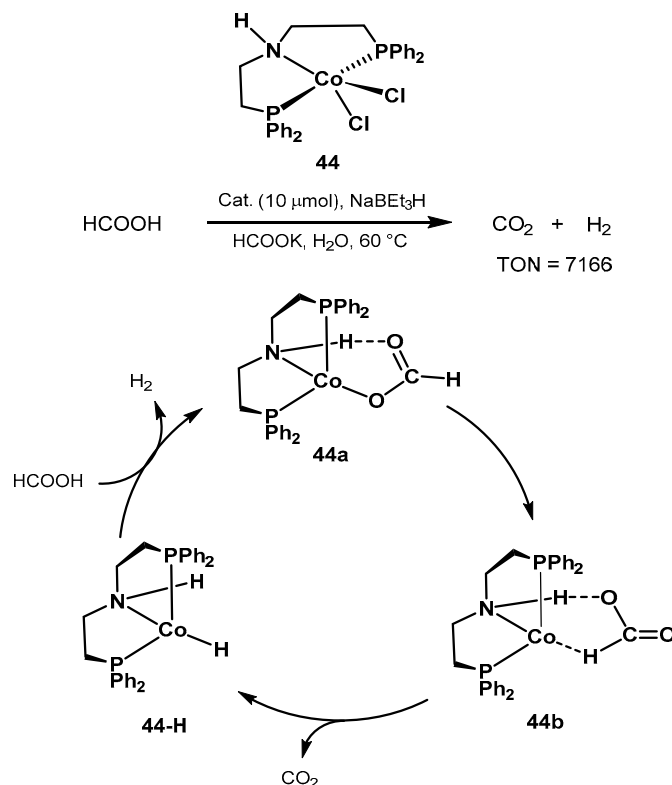


**Scheme 28.**  $\text{PN}^{\text{MeP}}$  vs.  $\text{PN}^{\text{HP}}$  pincer complexes and proposed catalytic cycle for formic acid dehydrogenation proposed by Beller [348].

In 2018, Beller reported that also the known ruthenium dihydride  $[\text{RuH}_2(\text{PPh}_3)_4]$  is a suitable catalyst for the dehydrogenation of aqueous formic acid at low temperature (TOF up to  $36,000 \text{ h}^{-1}$  at  $60^\circ\text{C}$  in THF) [407]. The catalyst was active for 120 days and it does not require basic additives.

The same group also proposed the cobalt catalyst precursor **44** shown in Scheme 29 for formic acid dehydrogenation in aqueous media and at mild conditions [408]. Reactions were performed at  $60\text{--}80^\circ\text{C}$  in the presence of HCOOK. Since the catalytically active species are air-sensitive, the authors investigated the in situ activation of the pre-catalyst **44** in the presence of  $\text{NaBEt}_3$ , resulting in the active hydrido complex **44-H** (Scheme 29). Importantly, under optimized conditions, the benchmark **Ru-MACHO** resulted in scarce H<sub>2</sub> evolution, whereas the manganese catalyst **25** showed no activity in aqueous conditions. The authors proposed an outer-sphere mechanistic cycle similar to the classic

Ru-PNP catalyst, with the amine proton taking active part in the catalytic cycle. The authors concluded that the rate-determining step is the C-H activation resulting in CO<sub>2</sub> release and formation of the amine complex. The work provides useful information for the development of non-noble metal catalysts for formic acid dehydrogenation.



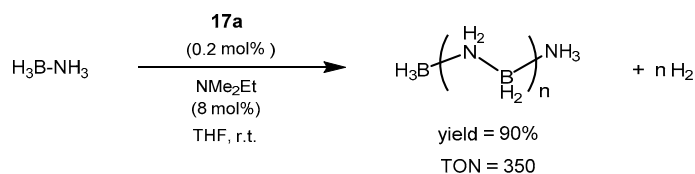
**Scheme 29.** Novel cobalt-PNP pincer complex for low-temperature formic acid dehydrogenation proposed by Beller [408].

### 2.2.3. Other Hydrogen Storage Systems

There are other potential solutions for hydrogen storage based on the LOHC technology, where pincer complexes have been applied as well. Some of these include ammonia-borane, amine-borane, hydrazine-borane, as well as pyrrolidine-based liquid organic hydrogen carriers [409–418]. The inverse hydrogenation process of the obtained products has also been explored [419–423]. Several metal catalysts have been investigated for the dehydrocoupling of these hydrogen reservoirs [424–431]; among these, pincer complexes have showed promising features and remarkable activity [432–440]. A comprehensive review on the main progresses in this field can be found in the work of Rossin and Peruzzini [441], whereas Schneider investigated the ruthenium-catalyzed amino-borane dehydrocoupling in 2013 [442]. Herein, we show representative examples of the more recent works from 2015 up to date involving the use of pincer-type catalysts.

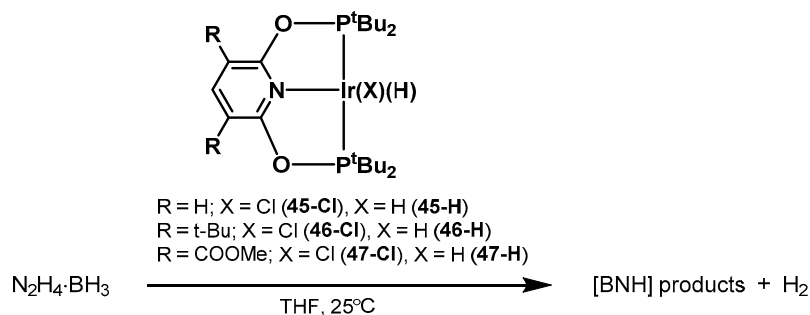
In 2015, Schneider proposed the iron-PNP complex **17a** for ammonia-borane dehydrocoupling at room temperature [443]. Ammonia-borane represents a promising hydrogen storage system, storing up to 19.5 wt% of H<sub>2</sub> at ambient conditions [444]. The dehydrogenation proceeds via an aminoborane complex and results in 90% conversion to the linear polyaminoborane polymer (Scheme 30). Catalyst deactivation due to the presence of free BH<sub>3</sub> can be prevented by addition of a simple amine, resulting in high TON up to 350 using 0.2 mol% of **17a** and 0.8 mol% of NMe<sub>2</sub>Et. In 2009, the same author showed Ru-PNP catalysts similar to **17a**, but where the CO ligand is exchanged with PMe<sub>3</sub> groups, as active catalyst for the same transformation [445,446].





**Scheme 30.** Iron-catalyzed dehydrogenation of ammonia borane performed by Schneider [443,445].

In 2016, Beweries compared new 3,5-disubstituted cyclometalated iridium(III)-hydrido complexes with the non-substituted counterparts in the dehydrogenation of hydrazine borane (Scheme 31) [447]. All catalysts were active, but when  $\text{R} = \text{COOMe}$ , the derived active species outperformed the other catalysts significantly, resulting in full conversion after 28 s (**47-Cl**) and 18 s (**47-H**) using 2 mol% catalyst loading. In addition, both catalysts **47-H** and **47-Cl** showed promising recyclability properties. The dehydrogenation products were characterized by solid state NMR and FT-IR spectroscopy, while DFT studies were performed using catalyst **45-H** to rationalize the mechanism of hydrazine borane dehydrogenation. The reaction proceeds through coordination of hydrazine borane by either  $\text{NH}_2$  or  $\text{H-BH}_2$ , coexisting in equilibrium; later, the dehydrogenation occurs resulting in a dihydrogen complex and liberation of  $\text{H}_2\text{B=NHNH}_2$ . Finally, the active specie **45-H** is regenerated after  $\text{H}_2$  dissociation.



**Scheme 31.** Dehydrogenation of hydrazine-borane hydrogen storage system by Ir-PNP pincer complexes reported by Beweries [447].

In 2015, Jensen performed kinetic studies on the iridium  $^t\text{BuPCP}$  complex **48** for the dehydrogenation of several pyrrolidine based LOHCs, such as butyl pyrrolidine (BuPy), *N*-ethylcarbazole (NEC) and methyl perhydroindole (MePHI) (see Table 1) [448]. The authors investigated reaction kinetics in terms of dehydrogenation onset temperatures, activation energies, and frequency factor when catalyst **48** was used in the presence of  $\text{NaOtBu}$  as additive. The authors concluded that the steric constraints of these LOHCs, rather than the C-H activation at the metal center, represent the main issue preventing higher rates of reaction.

Continuing the exploration of iridium-based pincer complexes, Belkova investigated the mechanism of dimethylamine-borane (DMAB) dehydrogenation using the iridium(III)-PCP complex **49** in Figure 2 [449]. It is possible to use the hydridochlorido complex precursor as precatalyst, which is activated in situ resulting in the active specie **49-H**, as was found for ammonia-borane dehydrogenation by Heinekey and Goldberg in 2006 [450].

In 2016, Esteruelas investigated the monohydride rhodium  $\{\text{xant}(\text{P}^i\text{Pr}_2)_2\}$  complex **50** for the dehydrocoupling of ammonia-borane, dimethylamine-borane, and a combined system with ammonia-borane dehydrogenation and cyclohexane hydrogenation, as shown in Scheme 32 [451]. Using 1 mol% of catalyst **50** in THF at  $31^\circ\text{C}$  resulted in a TOF of  $3150 \text{ h}^{-1}$  (calculated at 50% conversion) using  $\text{BH}_3\text{NH}_3$  and  $1725 \text{ h}^{-1}$  when employing  $\text{BH}_3\text{NHMe}_2$ . The system releases 1 equivalent of hydrogen via stepwise hydrogen transfer from the substrate to the catalyst, involving the formation of a five-coordinate dihydridorhodium(III) intermediate. Based on DFT calculations, the authors proposed a non-classical dihydrido route for the dehydrogenation step.

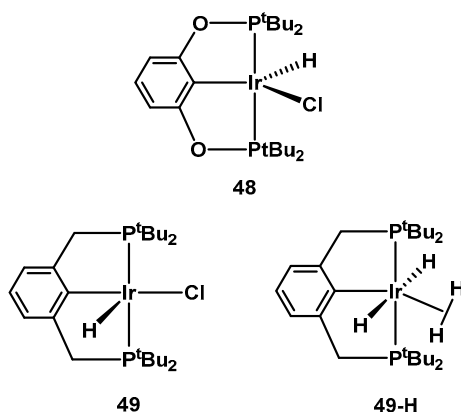
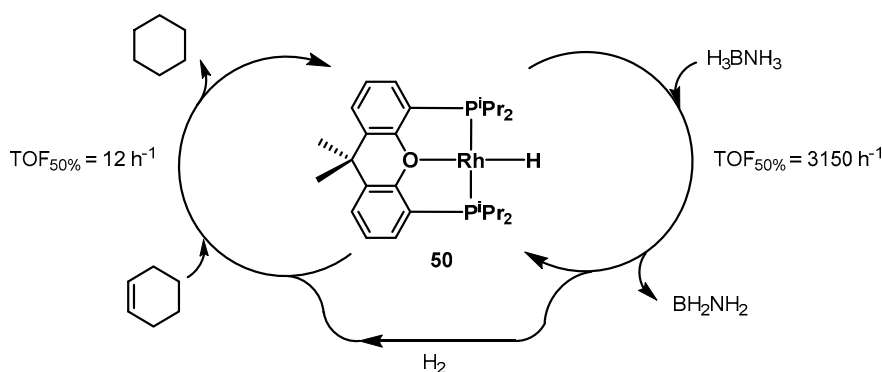


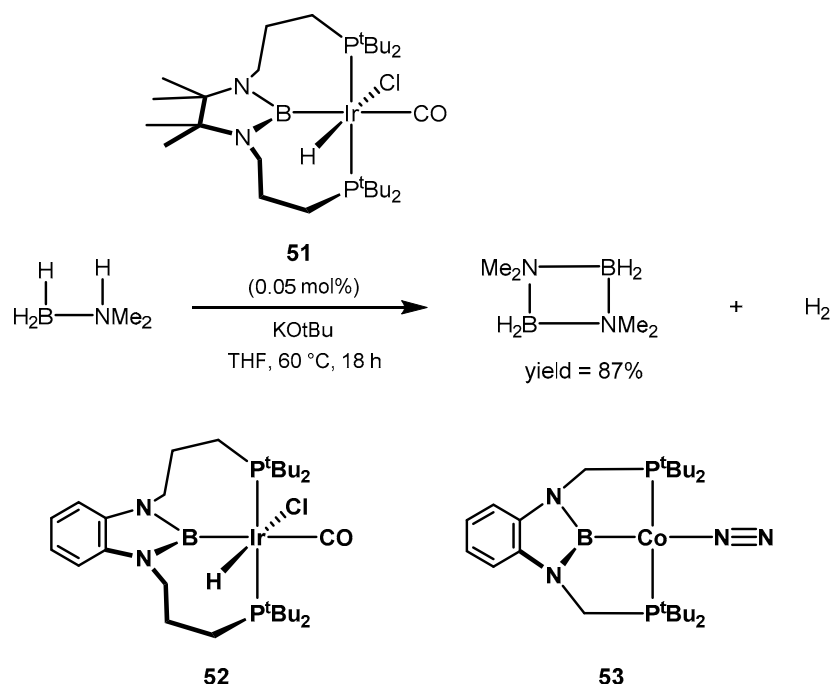
**Figure 2.** Iridium pincer catalysts investigated by Jensen for hydrogen release from pyrrolidine-based LOHCs [448], as well as dimethylamine–borane dehydrogenation by Belkova [449].



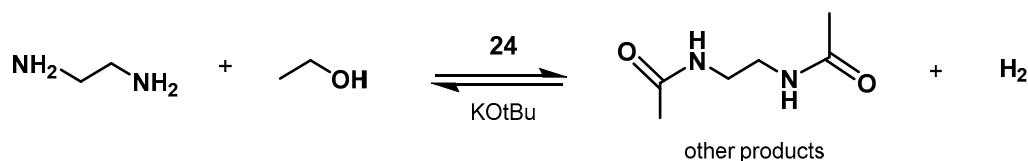
**Scheme 32.** Rhodium-POP catalyst for the dehydrogenation of ammonia-borane and dimethylamine-borane by Esteruelas [451].

In 2017, Yamashita showed the novel iridium PBP pincer complex **51** in Scheme 33 for the dehydrogenation of dimethylamine–borane (DMAB) [452]. The catalyst is a modification of a previously reported Ir-PBP complex (**52**), active for transfer dehydrogenation of alkanes [453]. In this work, the PBP ligand is modified by changing the benzene ring of the benzodiazaborole with the aliphatic tetramethylethylene functionality, hence decreasing the Lewis acidity on the boron center. The active dihydrido species can be obtained from the chloride precursor after treatment with  $n\text{BuLi}$  at room temperature. The complexes were also characterized by NMR spectroscopy, high-resolution mass spectrometry (HRMS), as well as single-crystal X-ray diffraction analysis. Catalyst **51** catalyzes the dehydrogenation of  $\text{Me}_2\text{NH}\cdot\text{BH}_3$  to form the cyclic dimer and releasing 1 equivalent of hydrogen. A turnover frequency of  $3400 \text{ h}^{-1}$  was obtained, with 0.05 mol% of **51** in THF at  $60^\circ\text{C}$ , with a final yield of 87% after 18 h (Scheme 33). Of the same family of PBP catalyst, Peters showed in 2013 that 2 mol% of the cobalt(I)- $\text{N}_2$  complex **53** catalyzes the release of hydrogen from DMAB in 6 h and at room temperature, resulting in full conversion to the cyclic  $(\text{Me}_2\text{N}-\text{BH}_2)_2$  [437].

Using a different approach, Milstein proposed in 2016 a new hydrogen storage system based on the dehydrogenative coupling of ethylenediamine with ethanol, as depicted in Scheme 34 [454]. Complex **24** was able to perform the dehydrogenation step with a 0.1 mol% catalyst loading, 1.2 equivalents of  $\text{KO}^t\text{Bu}$  at  $105^\circ\text{C}$  for 24 h resulting in full conversion. Remarkably, the same catalyst was applied for both hydrogenation and dehydrogenation steps; thus, employing 0.2 mol% of **24**, 2.4 equivalents of  $\text{KO}^t\text{Bu}$ , 50 bar of  $\text{H}_2$  in dioxane at  $115^\circ\text{C}$ , it was possible to fully hydrogenate  $N,N'$ -diacetylenediamine with 100% yield of ethylenediamine. This result expanded the concept of LOHC systems, paving the way for further optimization as well as applying combinations of amine-alcohol with even higher hydrogen capacity, such as ethylenediamine and methanol.



**Scheme 33.** Yamashita's PBP-Ir and Co-catalysts for hydrogen release from dimethylamine–borane (DMAB) hydrogen storage system [452].

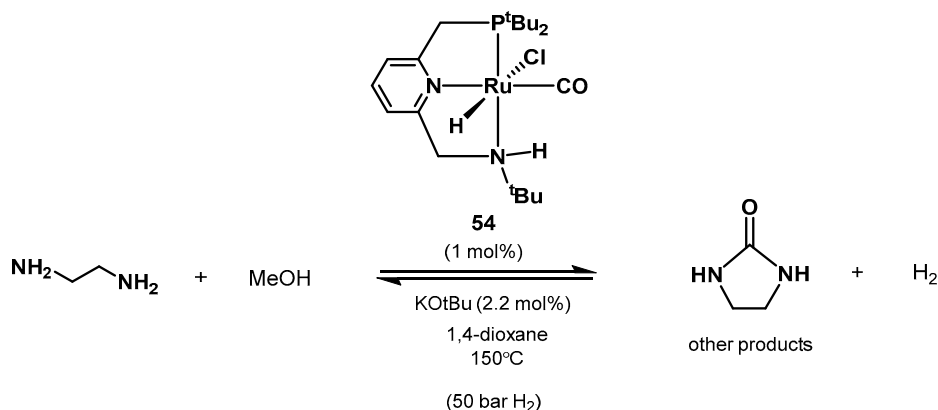


**Scheme 34.** Hydrogen storage system based on ethylenediamine with alcohol proposed by Milstein, and its reversible (de)hydrogenation catalyzed by complex **24** [454].

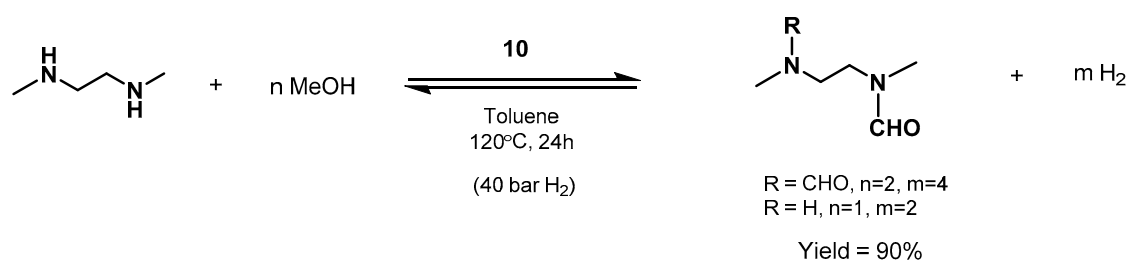
Indeed, very recently Milstein demonstrated the hydrogenation of ethylene urea to ethylenediamine and methanol and the reverse dehydrogenative coupling (Scheme 35) resulting in a mixture of ethylene urea, *N*-(2-aminoethyl)formamide and *N,N'*-(ethane-1,2-diyl)diformamide [319]. The system is rechargeable and has a high theoretic hydrogen capacity (6.52 wt%). Applying 1 mol% of the Ru-PNN catalyst **54**, 2.2 mol% KOtBu in 1,4-dioxane at 150 °C for 24 h, it was possible to obtain high yields of dehydrogenated products and hydrogen released (>90%). The system was also able to perform the hydrogenation step under the same conditions; by simply applying 50 bar of hydrogen gas, the reaction afforded full conversion to a mixture of ethylenediamine and methanol.

After screening a range of amines, Prakash and Olah demonstrated the same concept using **Ru-MACHO-BH** and dimethylethylenediamine (5.3 wt% H<sub>2</sub>) which was successfully dehydrogenated in the presence of methanol resulting in a mixture of formamides [455]. The authors proposed a reversible hydrogen storage system in which both H<sub>2</sub> “loading” and “unloading” can be performed by the same ruthenium pincer catalyst by a simple H<sub>2</sub> pressure swing (Scheme 36). The explorative dehydrogenative reaction using benzylamine in the presence of 1 mol% of **Ru-MACHO-BH** in toluene resulted in 88% yield in *N,N'*-dibenzylurea after 24 h at 140 °C, whereas 99% yield was afforded in the inverse hydrogenation of *N,N'*-dibenzylurea under 60 bar of hydrogen. The authors then screened other Ru- and Fe-PNP catalysts. Complex **10** combined with dimethylethylenediamine (1:4 molar ratio with respect to MeOH) as substrate and 5 mol% K<sub>3</sub>PO<sub>4</sub> as a basic additive afforded 90% yield hydrogen at 120 °C in toluene after 24 h. Importantly, the catalyst retained more than 80% of its catalytic activity after three cycles of reactions. The reverse hydrogenation was carried out using catalyst **10** under 40 or

60 bar of hydrogen resulting in 92% and 95% yield of amine, respectively. Curiously, the *N*-methylated congener of **Ru-MACHO** showed low activity, indicating the presence of an *N*-H assisted outer sphere mechanism. **Ru-MACHO-BH** was also reported by Hong to perform a ruthenium-catalyzed urea synthesis using methanol as the C1 source, with no additive, such as a base, oxidant, or hydrogen acceptor [456].



**Scheme 35.** Reversible hydrogen storage system formed by the couple ethylenediamine and methanol catalyzed by the Ru-PNN complex **53**, as showed by Milstein [319].



**Scheme 36.** Dehydrogenation of dimethylethylenediamine hydrogen storage system by **Ru-MACHO-BH** reported by Prakash and Olah [455].

### 3. Hydrogenation Reactions

For case of brevity, the focus will be on processes involving carbon dioxide and dinitrogen as the main substrates of interests, as well as chemical transformations promoting the valorization of biomass-derived molecules. Nevertheless, pincer complexes have achieved remarkable results in the (transfer) hydrogenation of a wide series of substrates such as ketones [385,457–462], esters [40,179,220,386,400,463–477], aldehydes [478–480], amides [67,481–485], and imines [486,487].

Carbon dioxide is sadly known to be the main responsible for the anthropogenic climate change and global warming [488–491]. At the same time, CO<sub>2</sub> represents an easily accessible C1 building block with the potential to replace the commonly used petrochemical carbon sources in a plethora of useful chemical transformations, dramatically increasing their intrinsic sustainability [492–494]. Several approaches have been investigated for its capture from the atmosphere, as well as from localized emission sources [495–504]. The desorbed CO<sub>2</sub> is subsequently compressed and stored in underground rock formations or utilized in the direct synthesis of value-added products [505–510]. Indeed, the industry already uses several million tons of CO<sub>2</sub> for the production of e.g., urea, salicylic acid, cyclic carbonates, and polypropylenecarbonate [511–513].

In the past decades, the catalytic hydrogenation of CO<sub>2</sub> has gained attention as a powerful tool to store green hydrogen, thereby electrical energy, as introduced by the seminal works by Asinger [514], Leitner [515,516], Noyori [517], as well as Olah [301,518–520]. The process, combined with the aforementioned methanol/formic acid dehydrogenation reactions, has the potential to close

the ideal cycle of CO<sub>2</sub>-free energy release and storage. Currently, both methanol and formic acid are industrially produced using fossil feedstock via carbon monoxide, which has lower kinetic and thermodynamic stability compared to CO<sub>2</sub>. The direct synthesis from CO<sub>2</sub> is traditionally carried out at high temperatures and pressures with heterogeneous metal catalysts such as Cu/ZnO/Al<sub>2</sub>O<sub>3</sub> [521–524]. Thus, the sustainability of the direct CO<sub>2</sub>-route is strictly dependent on the use of green hydrogen produced without contemporary CO<sub>2</sub> release in the atmosphere, as well as catalytic systems operating efficiently under milder reaction conditions. A variety of homogeneous catalytic systems has been employed for the direct hydrogenation of CO<sub>2</sub> into green fuels [213,214,517,525–535], including first-row metal complexes [536–544]. Pincer-type ligation shows again very encouraging features in terms of stability and mild reaction conditions, with promising possibility of further optimization. In addition, often the same catalyst is active in both directions of hydrogenation and dehydrogenation, expanding the applicability and robustness of this family of catalysts.

One of the most relevant and energy consuming industrial transformations is the conversion of N<sub>2</sub> for the production of ammonia through the Haber-Bosch process, a synthesis that requires harsh conditions and, hence, high operative costs [545–548]. Ammonia is widely used in the global economy as a fertilizer feedstock, industrial and household chemical, as well as chemical precursor in many chemical transformations [549–553]. In addition, it has been considered a future fuel alternative as a hydrogen storage molecule [554–556]. The possibility to perform nitrogen fixation at mild reaction conditions and less energetic costs by means of homogeneous catalysis is of key importance for the future sustainable chemical production, and as discussed in Section 3.2, pincer complexes are protagonists in the development of the best performing homogeneous systems developed to date.

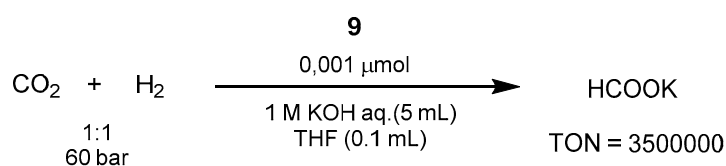
Finally, in Sections 3.3 and 3.4, discuss the main advances in relevant sustainable transformations involving the use of bio-substrates which are already easily accessible from biomasses, representing useful building blocks for the bulk chemical production. In addition, pincer complexes achieved remarkable results also in transfer hydrogenation reactions involving the use of ethanol as the hydrogen source, as well as the upgrading of ethanol to butanol and other C<sub>4</sub> molecules to be used as bio-fuel and fuel additives.

### 3.1. CO<sub>2</sub> Hydrogenation

#### 3.1.1. Early Works

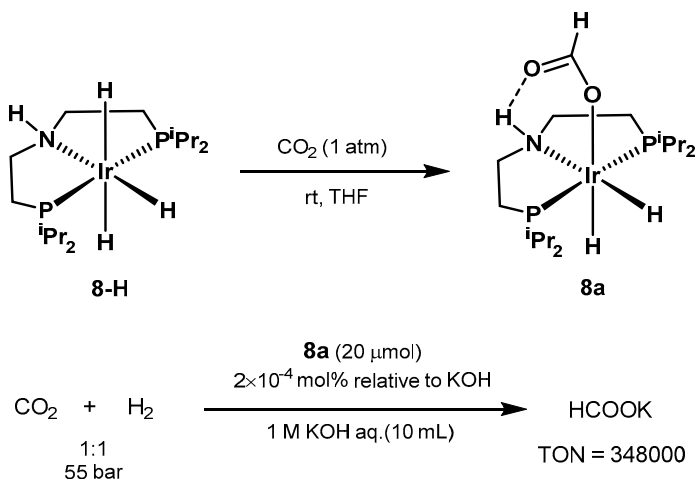
The hydrogenation of carbon dioxide by means of homogeneous catalysis has grown extensively in the last decade. An overview of the best performing systems for CO<sub>2</sub> hydrogenation up to 2010 can be found in the work of Beller [557], while in 2018 and 2019 Prakash reviewed the topic in depth including the use of pincer type complexes [558,559]. In this review, we will focus mostly in CO<sub>2</sub> conversion to formic acid (and/or formate salts) as well as to methanol, both of them representing accessible green fuel and hydrogen carriers.

Up to 2010, the best performing catalytic system was represented by the iridium-PNP catalyst **9** (shown in Scheme 2), reported by Nozaki in 2009, which overcame previously reported Ru [560–563], Rh [564–566], and Ir [567] homogeneous systems. In the work by Nozaki, the reactions were carried out in aqueous KOH, resulting in potassium formate (HCOOK) as the product [568]. Thus, using the trihydrido-iridium(III)-PNP complex **6** at 120 °C and 60 bar of 1:1 CO<sub>2</sub>/H<sub>2</sub> in 1.0 M aqueous KOH it was possible to achieve excellent TON and TOF values of 3,500,000 and 150,000 h<sup>−1</sup>, respectively (Scheme 37).



**Scheme 37.** CO<sub>2</sub> hydrogenation with Ir-PNP catalyst reported by Nozaki in 2009 [568].

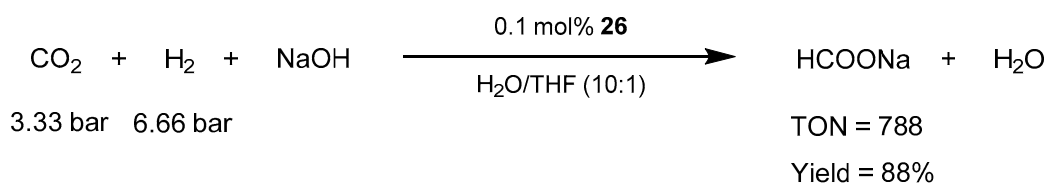
The use of iridium pincer complexes was further explored by Hazari in 2011 [569]. The authors were able to isolate the air and moisture stable catalyst **8a**, obtained from **8-H** in the presence of CO<sub>2</sub>. Under optimized conditions, the system resulted in yields up to 70% in formate, with TON of 348,000 and TOF of 14,500 h<sup>-1</sup> (Scheme 38).



**Scheme 38.** CO<sub>2</sub> hydrogenation with Ir-PNP catalyst proposed by Hazari [569].

In 2010, Beller and Laurenczy showed the hydrogenation of bicarbonates and carbon dioxide to formates, alkyl formates, and formamides catalyzed by the in situ formed system Fe(BF<sub>4</sub>)<sub>2</sub>·6H<sub>2</sub>O and the tetraphos ligand P(CH<sub>2</sub>CH<sub>2</sub>PPh<sub>2</sub>)<sub>3</sub> (PP<sub>3</sub>) [570]. In the presence of 0.14 mol% of this catalyst at 80 °C with 60 bar of hydrogen, sodium formate was obtained in an excellent yield of 88% with TON of 630 after 20 h.

Encouraged by these findings on iron complexes, Milstein proposed the dihydrido Fe-PNP complex **26** for the low-pressure hydrogenation of carbon dioxide [387]. 0.1 mol% of catalyst **26** (catalyst **27** is formed during the reaction in the presence of CO<sub>2</sub>) in a 10:1 mixture H<sub>2</sub>O/THF, with 2M NaOH at room temperature, converted CO<sub>2</sub> and H<sub>2</sub> into sodium formate with a TON of 788, TOF of 156 h<sup>-1</sup>, and 39.4% yield (Scheme 39).

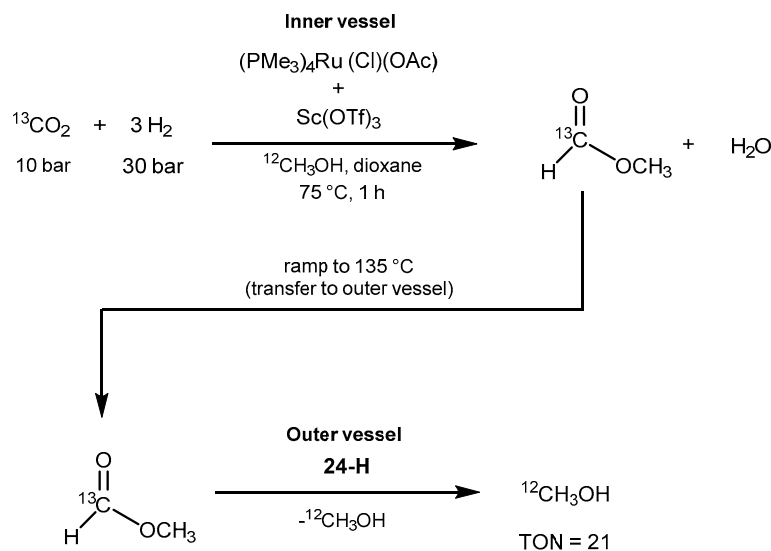


**Scheme 39.** CO<sub>2</sub> hydrogenation with catalyst **26** proposed by Milstein in 2011 [387].

In 2011, Milstein and co-workers published the first example of hydrogenation of carbonates into alcohols and carbamates into alcohol and amines as an indirect route for the synthesis of methanol from CO<sub>2</sub> [571]. 0.02 mol% of catalyst **24-H** in THF, in the presence of 50 bar of H<sub>2</sub>, catalyzed the conversion of dimethyl carbonate into methanol with a TON of 4400, 89% conversion and 88% yield, at 110 °C and after 14 h. With 1 mol% of catalyst **24-H**, in THF and with 10 bar of hydrogen, it was possible to convert *N*-benzyl carbamate into methanol and the corresponding amine with 97% yield, at 110 °C, after 48 h. Finally, the authors tested the hydrogenation of alkyl formates to methanol and the corresponding alcohol. A TON of 4700 and a yield of 94% was achieved applying 0.02 mol% of catalyst **24-H** in THF, 50 bar of H<sub>2</sub>, at 110 °C, and after 14 h.

The same year, Sanford proposed a cascade reaction mechanism for CO<sub>2</sub> hydrogenation using the Milstein catalyst **24-H** in combination with other two homogeneous catalysts, i.e., (PMe<sub>3</sub>)<sub>4</sub>Ru-(Cl)(OAc) and Sc(OTf)<sub>3</sub> (Scheme 40) [572]. The first two steps consist in the hydrogenation of CO<sub>2</sub> to formic acid,

followed by esterification to generate a formate ester. Later, complex **24-H** catalyzes the hydrogenation of the ester to release methanol. In order to prevent the deactivation of catalyst **24-H** by  $\text{Sc}(\text{OTf})_3$ , the former was placed in the outer vessel of the Parr reactor where it promotes methyl formate hydrogenation to methanol. The protocol was successfully demonstrated resulting in an overall TON of 21 under optimized conditions.



**Scheme 40.** Cascade reactions promoting  $\text{CO}_2$  hydrogenation to methanol using catalyst **24-H** in combination with  $(\text{PMe}_3)_4\text{Ru}(\text{Cl})(\text{OAc})$  and  $\text{Sc}(\text{OTf})_3$  as showed by Sanford [572].

Catalyst **24-H** was also employed by Milstein to demonstrate the hydrogenation of urea derivatives (easily obtained from  $\text{CO}_2$  and amines) to amines and methanol [573]. Catalyst **24-H** promotes the double cleavage of the robust C-N bonds under mild, neutral conditions. 1,3-dimethylurea was used as benchmark substrate to identify the optimized reaction conditions. 2 mol% of catalyst **24-H** in THF, heated at 110 °C and in the presence of 13.8 bar of hydrogen, afforded 96% conversion and 93% yield in methanol after 72 h. With the optimized conditions, the authors screened a wide range of urea derivatives that were converted in good to excellent yields.

In 2011, Leitner performed computational studies on 38 different rhodium pincer alkyl complexes with varied steric and electronic environment for the  $\text{CO}_2$  association and insertion into the metal–carbon bond, resulting in the corresponding carboxylate species [574]. Several of the tested catalysts showed insertion barriers with energies that encourage their use within an effective catalytic cycle. The authors pointed out three main features that facilitate  $\text{CO}_2$  insertion: (a) the anionic complexes were more reactive than neutral congeners. (b) The activity decreased based on the central donor atom of the pincer arm in the order of  $\text{C}^- \approx \text{B}^- > \text{Si}^- > \text{N} > \text{carbene} > \text{O}$ . (c) Higher basicity is typically associated with higher reactivity, with the side arm of the pincer that can further tune the electronics around the metal center.

The same author proposed a novel protocol for the direct synthesis of free carboxylic acids via hydrocarboxylation using  $\text{CO}_2$  as a C1 building block and simple non-activated olefins [575]. The reactions were carried out in acetic acid using 1:10  $[\{\text{RhCl}(\text{CO})_2\}_2]$  and  $\text{PPh}_3$  in the presence of 60 bar of  $\text{CO}_2$ , 10 bar of  $\text{H}_2$ ,  $\text{CH}_3\text{I}$  as a promotor, and  $p\text{-TsOH}\cdot\text{H}_2\text{O}$  as acid additive. With cyclohexene as a substrate, the reaction afforded full conversion and 92% yield in the carboxylic acid, with only 5% of cyclohexane as the co-product, after 16 h at 180 °C. With optimized conditions, the authors scoped various substrates and it was possible to obtain the corresponding carboxylic acids in good to excellent yields, with only minor amounts of the hydrogenated olefin. After evaporation of the solvent, the authors isolated and characterized the complex  $[\text{CH}_3\text{PPh}_3][\text{RhI}_4(\text{CO})(\text{PPh}_3)]$  using X-ray crystallographic analysis.



In 2012, Klankermayer and Leitner demonstrated the homogeneous hydrogenation of carbon dioxide to methanol using a catalytic system based on the tripodal PPP Triphos ligand showed in Figure 3 [576]. Both the combination of the precursor  $\text{Ru}(\text{acac})_3$  and the Triphos ligand, as well as catalyst **55** were active in the hydrogenation of both  $\text{CO}_2$  and formate esters. In particular, 25  $\mu\text{mol}$  of catalyst **55**, with 1 equivalent of  $\text{HNTf}_2$ , at 60:20 bar of  $\text{CO}_2:\text{H}_2$  in THF/EtOH, afforded a TON of 221 after 24 h. Mechanistic studies indicate the active species **57** and **58** as key intermediate in this transformation, with enhanced activity in the presence of weakly coordinating anions [577].

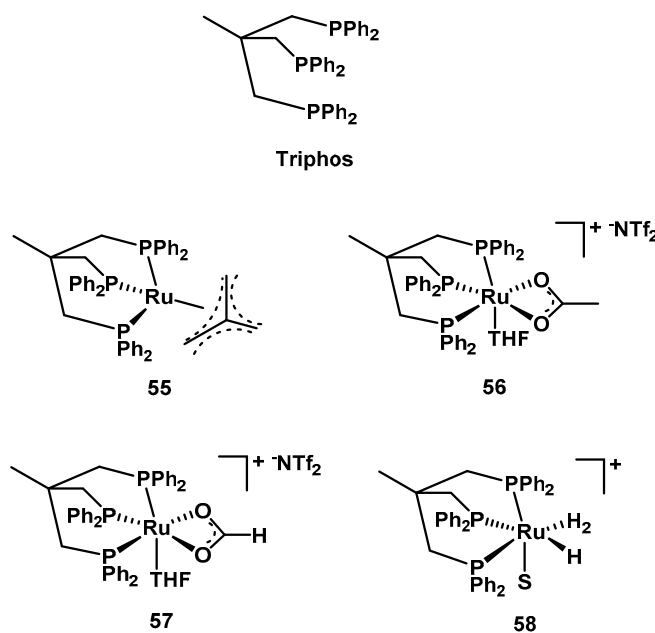
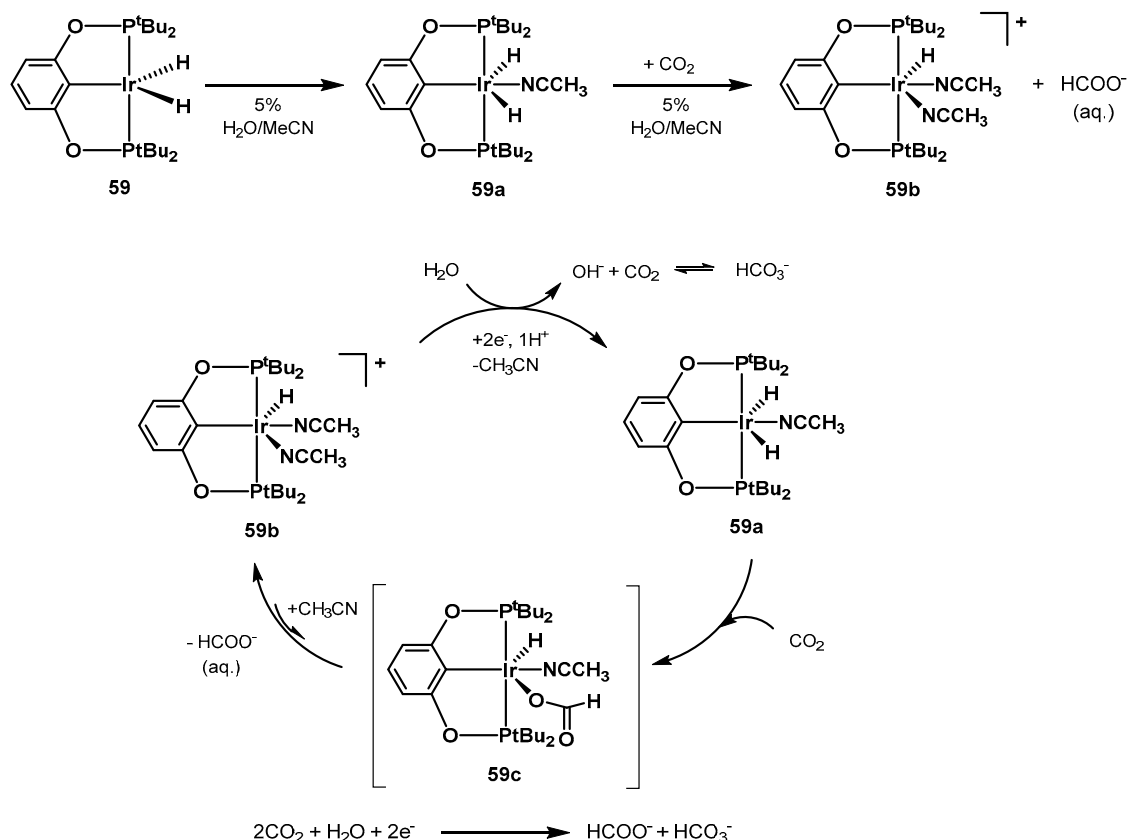


**Figure 3.** Ruthenium catalysts **55** and **56** based on the triphos ligand, and active formate species **57** and **58** (S = solvent or substrate) [576–579].

In 2015, Leitner employed catalyst **55** for the hydrogenation of  $\text{CO}_2$  into methanol without the need of an alcohol additive [578]. Catalysts **55** and **56** were used as pre-catalysts leading to the formation of the active species **57** under the reaction conditions. Applying only 6.3  $\mu\text{mol}$  of **55**, 1 equivalents of  $\text{HNTf}_2$ , 20:60 bar of  $\text{CO}_2:\text{H}_2$  in THF, afforded the best TON of 442 at 140 °C after 24 h.

The same group also showed the direct methylation of primary and secondary amines catalyzed by the PPP complex  $[\text{Ru}(\text{Triphos})(\text{tmm})]$  **55** without the use of reducing agents [579]. The authors found the optimized conditions for the methylation of *N*-methyl aniline, and extended the scope to a wide range of substituted aromatic amines as well as primary anilines. Quantitative yields were obtained for the conversion of *N*-methyl aniline into dimethylaniline by applying 2.5 mol% of  $[\text{Ru}(\text{triphos})(\text{tmm})]$ , 5 mol% of  $\text{HNTf}_2$ , 20:60 bar of  $\text{CO}_2:\text{H}_2$  in THF at 150 °C.

Meyer and Brookhart proposed the iridium PCP pincer catalyst for the electrocatalytic conversion of  $\text{CO}_2$  to formate [580]. The reactions were carried out in acetonitrile with 5% of water. Water promotes the reaction with  $\text{CO}_2$  with consequent formation of the cationic specie **59b** coordinated with a formate anion. The electrochemical observations suggest that the catalyst resides largely as **59a** in the electrocatalytic steady state, whereas **59** is the reactive specie (Scheme 41). In 2016, Ahlquist performed computational studies on the electrochemical  $\text{CO}_2$  hydrogenation catalyzed by the iridium complex **59**, identifying the in situ reduced cationic iridium(I)-H complex as the active specie for the transformation [581].



**Scheme 41.** CO<sub>2</sub> insertion to the Ir-PCP catalyst **59** showed by Meyer and Brookhart [580].

Müller investigated the insertion of CO<sub>2</sub> into metal–phenoxide bonds using homogeneous cobalt and zinc catalysts typically used in the copolymerization of epoxides and CO<sub>2</sub> and shown in Figure 4 [582]. The authors followed the mechanism of insertion resulting in the carbonate species by means of in situ ATR-IR spectroscopy. It was noted that, despite the differences in the two species, the neighboring donor groups of the pincer arm (NO<sub>2</sub> in the case of **60**, amides in the case of **61**) allow the carbonates to remain attached to the ligand sphere, enhancing the nucleophilicity of CO<sub>2</sub>, hence favoring the easy transfer to other organic substrates, such as epoxides.

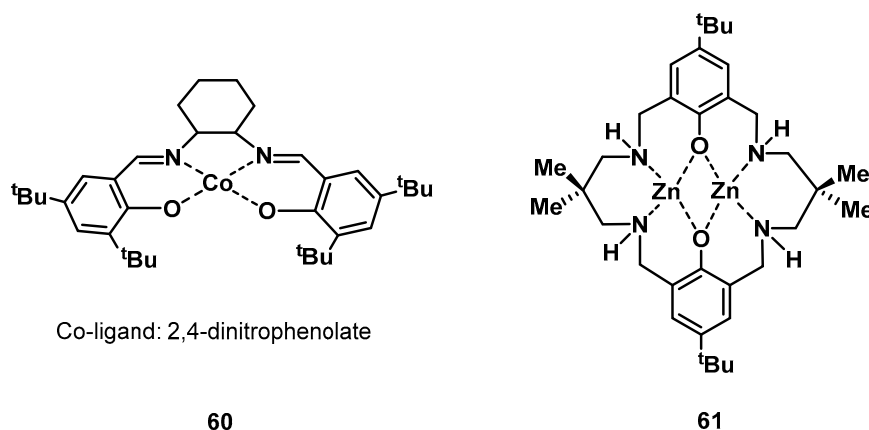
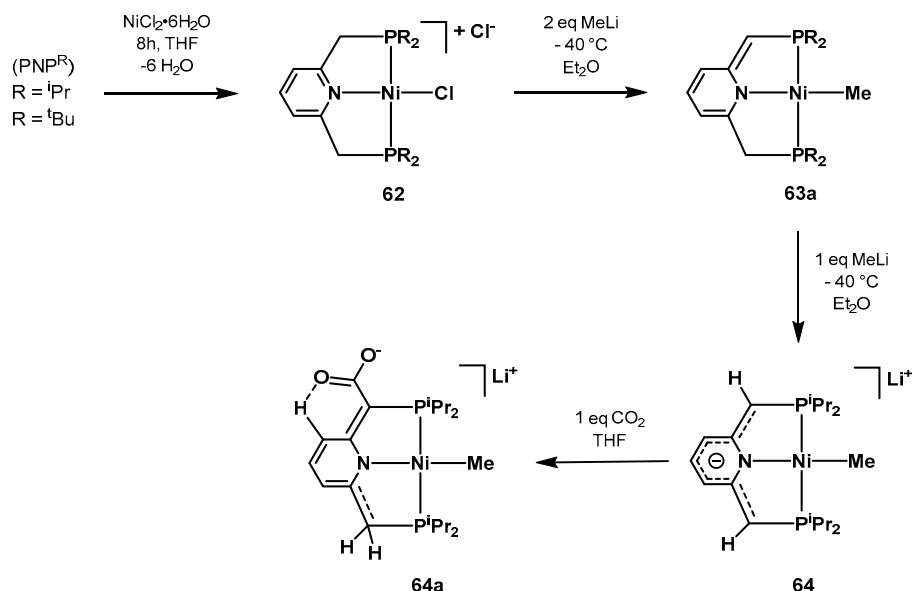


**Figure 4.** Cobalt and zinc pincer complexes reported to activate carbon dioxide by Müller [582].

In 2013, Milstein synthesized and characterized a series of novel pyridine-based Ni-PNP complexes with the aim of investigating the aromatization/dearomatization equilibria prompted by double protonation-deprotonation of the pincer arm [583]. Complex **64** can be readily prepared starting from

$\text{NiCl}_2 \cdot 6\text{H}_2\text{O}$  and the  $\text{PNP}^{\text{R}}$  ligand in a cascade reaction as depicted in Scheme 42. Complex **64**, where the negative charge is delocalized in the pincer moiety, was characterized by single-crystal X-ray diffraction studies. In the presence of  $\text{CO}_2$ , it undergoes electrophilic attack resulting in the anionic specie **64a**, observed by NMR spectroscopy.



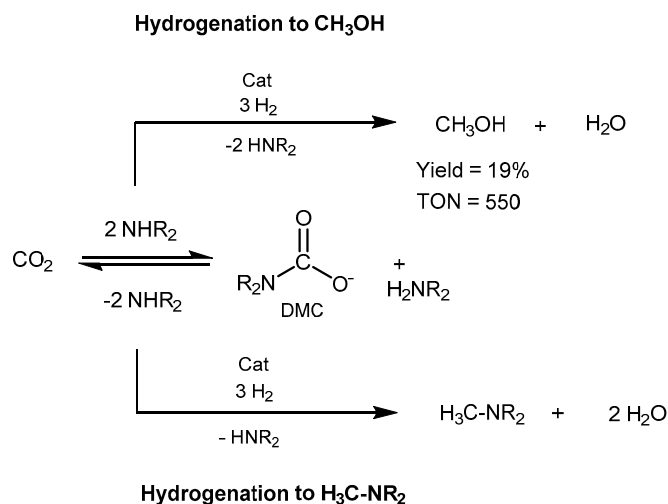
**Scheme 42.** Synthesis and  $\text{CO}_2$  coordination of the Ni-PNP catalyst **64** proposed by Milstein [583].

Goldman performed DFT studies on the hydrogenation of dimethyl carbonate to methanol using the Milstein-type PNN catalyst **4** [215]. The work provided new insights on the mechanism for the C-OMe bond cleavage. The authors proposed an ion-pair-mediated metathesis pathway in which the formed alkoxide C–H bond binds to the ruthenium atom. By simple reorientation of the dimethoxymethanoxide anion formed upon transfer of a hydride to dimethyl carbonate, the methoxy group of the  $[\text{OCH}(\text{OMe})_2]^-$  anion is in a close proximity to the metal, allowing the C–OMe bond cleavage.

### 3.1.2. $\text{CO}_2$ Hydrogenation to Methanol

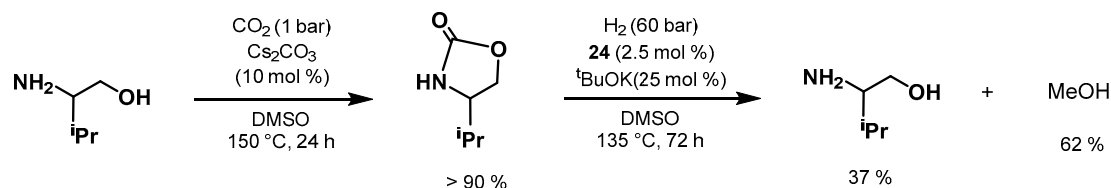
Himeda and Laurency reported in 2016 the iridium complex  $[(\text{Cp}^*)\text{Ir}(\text{dhbp})(\text{OH}_2)][\text{SO}_4]$  (dhbp = 4,4'-dihydroxy-2,2'-bipyridine), already showed for bicarbonate hydrogenation to formate and formic acid dehydrogenation [584], for the production of methanol from  $\text{CO}_2$  at room temperature as well [585]. The catalyst was active for both  $\text{CO}_2$  hydrogenation to formic acid in acidic media, without additives, as well as formic acid disproportionation into methanol, achieving 98% conversion and 96% selectivity after 72 h. Formic acid was obtained by pressurization of a solution of the catalyst with 20 bar  $\text{CO}_2$  and 50 bar  $\text{H}_2$  at ambient temperature. Methanol was observed by only increasing the temperature, whereas the addition of an optimized sulfuric acid concentration resulted in the enhanced activity of the system. No carbon monoxide was observed, indicating that decarbonylation of formic acid did not occur.

In 2015, Sanford proposed a ruthenium-catalyzed hydrogenation of  $\text{CO}_2$  to methanol with dimethylamine as capturing agent [586]. The reduction proceeds in basic conditions through the in situ formation of dimethylammonium dimethylcarbamate (DMC) as a key intermediate (Scheme 43). **Ru-MACHO-BH** (0.03 mol%) was used as catalyst, in the presence of 2.5:50 bar of  $\text{CO}_2/\text{H}_2$ , and 0.25 mmol of  $\text{K}_3\text{PO}_4$ . The reaction afforded a TON of 550 in methanol and an overall 82% conversion of  $\text{CO}_2$  to methanol and a mixture of dimethylformamide and dimethylammonium formate, which raises to 96% total conversion when applying 0.1 mol% of catalyst loading. The work represented a step forward toward the integrated  $\text{CO}_2$  capture and direct conversion to methanol.



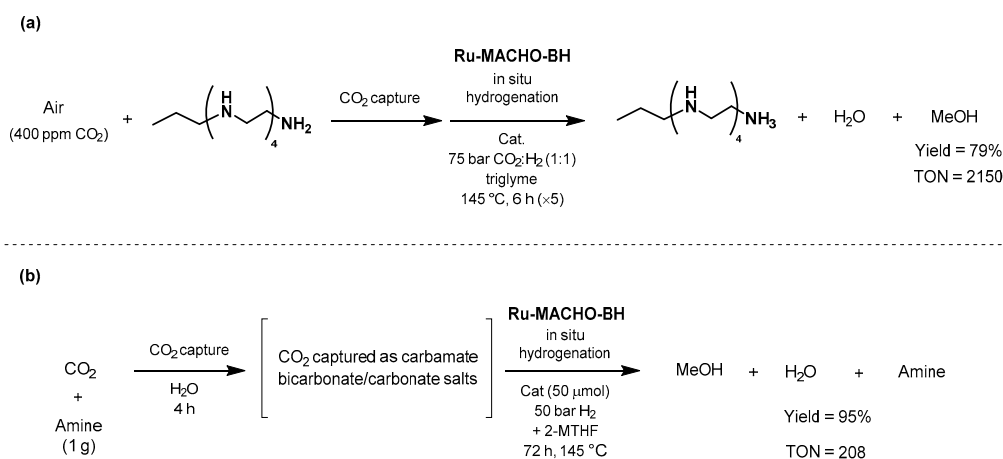
**Scheme 43.** CO<sub>2</sub> capture and conversion to MeOH proposed by Sanford [586].

The same year, Milstein developed an innovative methodology for indirect CO<sub>2</sub> hydrogenation by means of prior capture by amino alcohols at low pressure followed by the hydrogenation of the generated oxazolidinone to form MeOH (Scheme 44) [587]. Moreover, this approach is inspired by the CO<sub>2</sub> capture industry that uses amino alcohols to capture CO<sub>2</sub> from waste streams [588]. The work provides new possibilities for the use of oxazolidinone, which can be useful for the production of a liquid fuel such as MeOH. Three Ru-NNP complexes (**3**, **24**, and **54**) were tested for this transformation, with complex **24** being the most active catalyst. The authors screened both 2-(methylamino)ethanol and valinol for the first step of CO<sub>2</sub> capture; valinol was chosen considering its ability to capture CO<sub>2</sub> more selectively under only 1 bar of CO<sub>2</sub>. Employing Cs<sub>2</sub>CO<sub>3</sub> (10 mol%), DMSO as solvent, and at 150 °C under 1 bar of CO<sub>2</sub>, for 24 h afforded the oxazolidinone in >90% yield. The product is not purified or isolated and the leftover CO<sub>2</sub> is simply removed under vacuum. Then, the subsequent hydrogenation of the formed oxazolidinone was performed with **24** (2.5 mol%) and KOtBu (25 mol%) under 60 bar of H<sub>2</sub>, at 135 °C, for 72 h, producing MeOH and the amino alcohol precursor in 37% and 62% yields, respectively. Remarkably, the process allows direct CO<sub>2</sub> capture with consequent MeOH formation, avoiding the energy-demanding steps of CO<sub>2</sub> regeneration from capture products and subsequent pressurization.



**Scheme 44.** Milstein's CO<sub>2</sub> capture/hydrogenation to MeOH using amino alcohol [587].

The year after, Olah and Prakash reported an efficient catalytic system for the one-pot CO<sub>2</sub> capture and conversion to methanol, using polyamine and **Ru-MACHO-BH** (Scheme 45a) [589]. The first step of CO<sub>2</sub> capture was achieved by bubbling synthetic air (400 ppm of CO<sub>2</sub> in N<sub>2</sub>/O<sub>2</sub> 80/20) in an aqueous solution of pentaethylenhexamine (PEHA) for 64 h. **Ru-MACHO-BH** (20 μmol) was applied in the presence of 50 bar of H<sub>2</sub> in triglyme, and 6% of the captured CO<sub>2</sub> (5.4 mmol) was converted into methanol after 55 h in 79% yield (determined by NMR). The authors confirmed the robustness of the method by recycling the catalyst over five consecutive runs of 5 h without significant loss of activity; only 20 μmol of catalyst afforded an overall TON of 2150 at 145 °C under 75 bar pressure of a 1:9 mixture of CO<sub>2</sub>:H<sub>2</sub>.

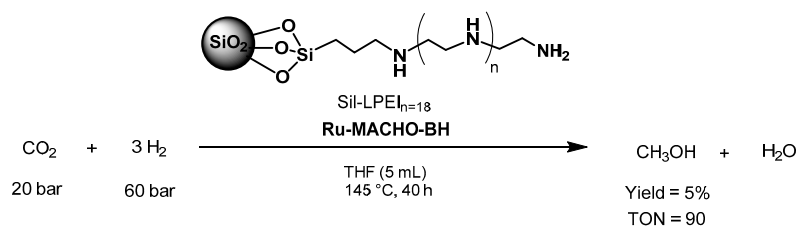


**Scheme 45.** CO<sub>2</sub>-capture and direct conversion to methanol using **Ru-MACHO-BH** as showed by Olah (a) and Prakash (b) [589,590]

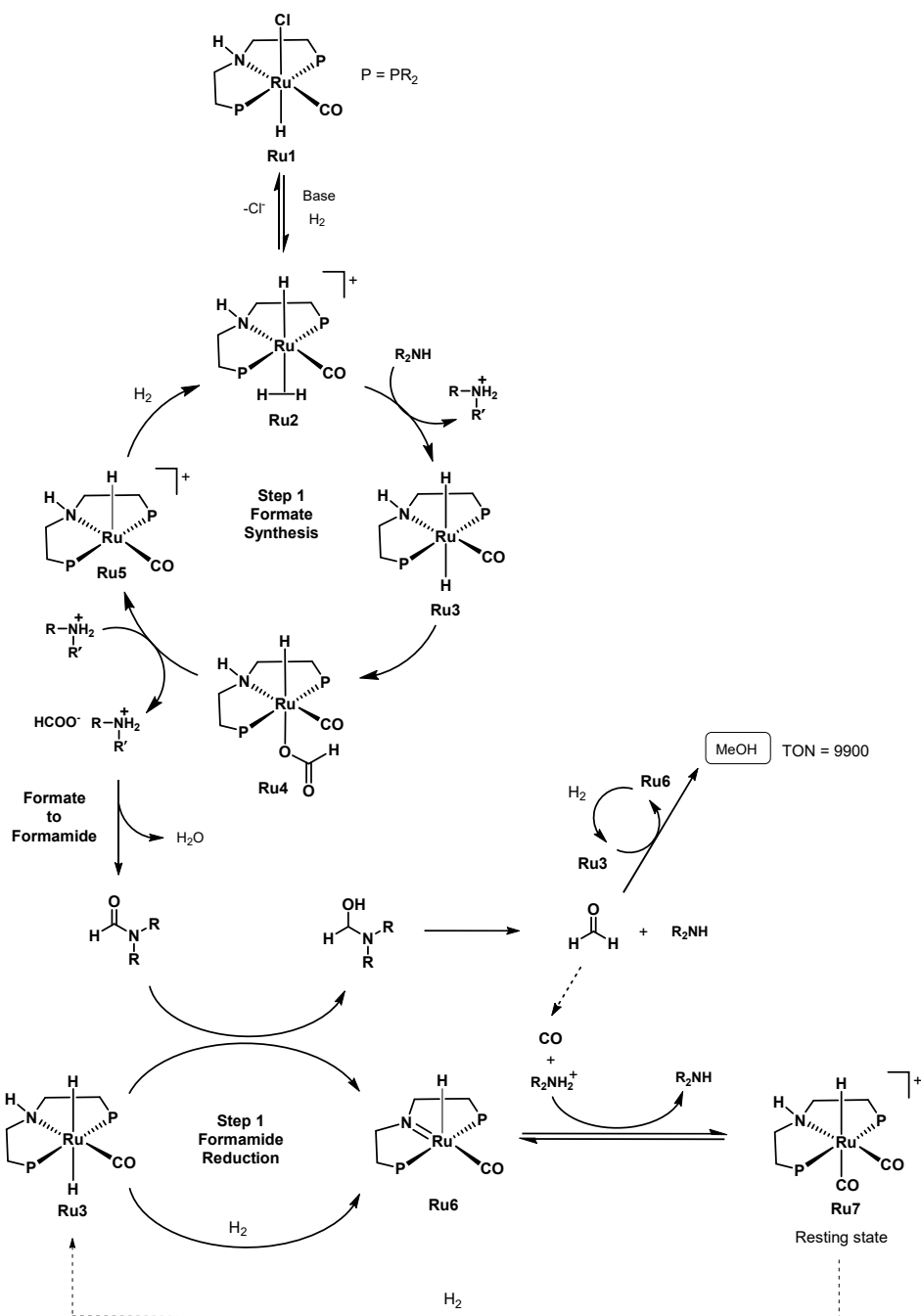
In 2018, Prakash showed another system for the integrative CO<sub>2</sub> capture (trapped in the form of carbamate and bicarbonate salts) followed by hydrogenation to methanol, using a biphasic 2-methyltetrahydrofuran (2-MTHF)/water solvent system, as shown in Scheme 45b [590]. The authors screened known PNP catalysts (**Ru-MACHO**, **Ru-MACHO-BH**, **10**, the Mn-PNP **25**, as well as the iron-PNP congener of **15** where HBH<sub>3</sub> is substituted with Br). Again, the commercially available **Ru-MACHO-BH** was found to be the most active, in combination with PEHA. After 11 mmol of CO<sub>2</sub> was trapped in 0.79 g of PEHA, the system afforded 95% yield of methanol by applying 50 μmol of catalyst in 2-MTHF at 70 bar H<sub>2</sub> at 145 °C for 72 h (TON = 208). Importantly, the biphasic solvent system allows recycling the catalyst, as well as the amine; after the reaction, the amine stays in the bottom aqueous solution, whereas the catalyst remains in the top organic layer. After extracting the methanol, both the amine and catalyst could be reused for three consecutive runs, retaining 90% of the activity in methanol production.

The year after, another approach was proposed by the same author, using amines immobilized onto a solid-silica support as CO<sub>2</sub> capturing agent for the hydrogenation to methanol [591]. The covalently bonded solid-supported amines (SSAs) showed good recyclability properties for CO<sub>2</sub> absorption/desorption, as well as easy separation from the reaction media by simple filtration. The catalyst could be also effectively recycled by vacuum evaporation of the solvent and methanol. One more time, **Ru-MACHO-BH** performed best among the screened Ru- and Mn-PNP catalysts, albeit with lower yields and turnovers compared with the previous reported results. 40 μmol of the catalyst under the reaction conditions in Scheme 46, afforded a yield of ≈5% in methanol after 2 cycles, with a TON of 90 in the first hydrogenation reaction.

Recently, Prakash also investigated the mechanism of ruthenium PNP-catalyzed amine-assisted hydrogenation of CO<sub>2</sub> to methanol [592]. As shown before, **Ru-MACHO** and **Ru-MACHO-BH** are the best catalysts for the transformation, with (di/poly)amines acting as effective reusable additives. In this work, TONs up to 1050 were achieved using PEHA, 10 mmol of **Ru-MACHO-BH**<sub>3</sub> as catalyst, K<sub>3</sub>PO<sub>4</sub> as base, in triglyme, under CO<sub>2</sub>/3H<sub>2</sub> (75 bar), and at 145 °C for 40 h. A long-term reaction was carried out using **Ru-MACHO-BH**<sub>3</sub> and PEHA and the catalyst was active for >10 days and TON of 9900 was achieved. The authors also provided mechanistic insight by means of NMR and ATR-IR spectroscopy techniques, as well as single-crystal X-ray diffraction analysis. The proposed catalytic cycle for methanol production through formamide is depicted in Scheme 47; the authors showed a deactivation pathway that leads to the formation of a dicarbonyl complex of **Ru-MACHO**. Under reaction conditions, in the presence of H<sub>2</sub>, the resting state is converted back to the active specie by CO dissociation and it was found to selectively catalyze the hydrogenation of the in situ formed formamides resulting in high methanol yields.



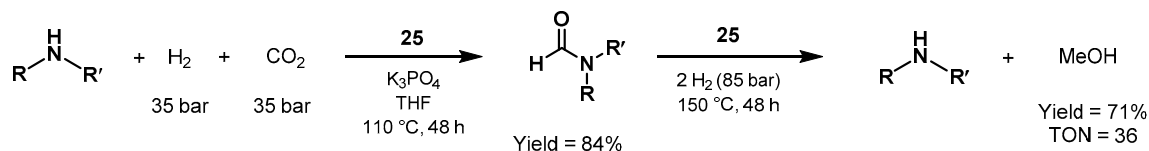
**Scheme 46.**  $\text{CO}_2$  hydrogenation to methanol using **Ru-MACHO-BH** and silica-supported amines as capturing agents proposed by Prakash [591].



**Scheme 47.** Proposed catalytic cycle for amine-assisted  $\text{CO}_2$  hydrogenation to methanol showed by Prakash [592].

In the last five years, several groups performed studies on the mechanism of CO<sub>2</sub> hydrogenation involving pincer-type catalysis. Pathak studied the base-free CO<sub>2</sub> hydrogenation employing a series of aliphatic Mn-PNP complexes using density functional theory (DFT) calculations [593]. The results suggested that the aliphatic amido PNP complex promotes the heterolytic H<sub>2</sub> cleavage and a proton transfer mechanism, contrarily to other CO<sub>2</sub> hydrogenation pathways promoted by base. Pincer ligands containing  $\sigma$ -donor and  $\pi$ -acceptor functionalities were investigated to explore the steric and electronic effects on the rate-determining step. It was found that both  $\sigma$ -donor, as well as  $\pi$ -acceptor ligands have a pronounced effect on the catalytic activity; in particular, the authors concluded that  $\sigma$ -donor ligands induce hydride transfer mechanism, while  $\pi$ -acceptor ligands promote the heterolytic H<sub>2</sub> cleavage. The same author reported theoretical studies using DFT and microkinetic modelling to study the mechanism of Mn-PNP-catalyzed CO<sub>2</sub> hydrogenation to methanol in the presence of morpholine as a co-catalyst via formamide intermediate [594]. The amidation step increases the overall rate of the reaction, while the *N*-formylmorpholine hydrogenation step could follow two different competitive pathways, both of them showing similar reaction energy barriers for the hydrogenation step.

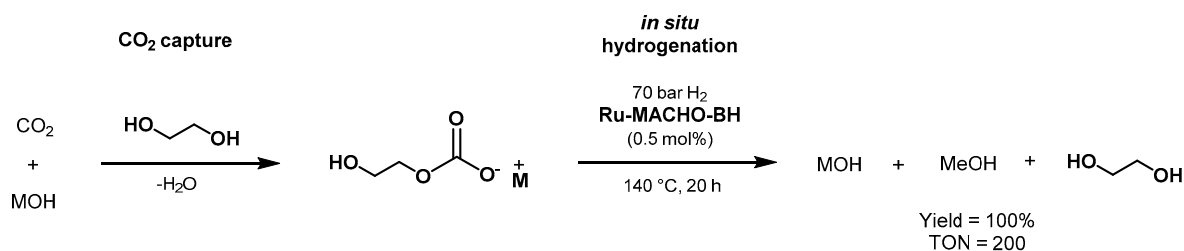
The Mn-PNP pincer complex **25** was employed by Prakash for the hydrogenation of CO<sub>2</sub> to methanol in a sequential two-step approach [595]. The first step involves the *N*-formylation of an amine resulting in the corresponding formamide, which is further hydrogenated to methanol regenerating the initial amine. The first step was carried out by applying a 1:1 pressure of CO<sub>2</sub>:H<sub>2</sub> (60 bar), at 110 °C, for 24 h, in the presence of THF as solvent and K<sub>3</sub>PO<sub>4</sub> as base. In the second step, the 1:1 gas mixture was replaced with 80 bar H<sub>2</sub> pressure, at 80 °C, for 36 h. After optimization, the authors proposed a scale up of the process using 0.1 mol% of catalyst **25** combined with benzylamine as trapping agent; the first reduction step afforded 84% yield in formamide, corresponding to a TON of 840. Later, the hydrogenation step was performed under 85 bar of hydrogen, affording 71% yield in methanol with a TON of 36 (Scheme 48).



**Scheme 48.** CO<sub>2</sub> hydrogenation to methanol promoted by the Mn-PNP complex **25** reported by Prakash [595].

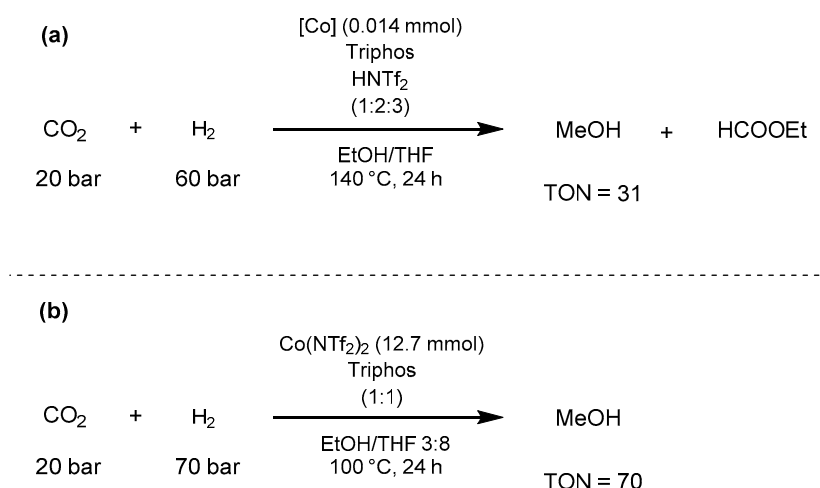
Based on a different approach, Prakash proposed this year the first example of hydroxide-based CO<sub>2</sub> capture from air, followed by hydrogenation to methanol [596]. CO<sub>2</sub> was successfully captured in ethylene glycol in the presence of hydroxide bases (NaOH or KOH) simply by stirring at room temperature for 3 h. The obtained bicarbonate and formate salts were later hydrogenated to methanol with high yields in an integrated one-pot system, as depicted in Scheme 49. Under optimized conditions, 0.5 mol% of **Ru-MACHO-BH** hydrogenated the bicarbonate species to methanol at 140 °C under 70 bar of H<sub>2</sub>, resulting in 100% yield of methanol after 20 h, with TON of 200. The formed methanol can be easily separated by distillation, with contemporary hydroxide base regeneration. Finally, the authors proposed a one-pot method for direct CO<sub>2</sub> capture from ambient air and direct methanol production; the system afforded 100% yield of MeOH after 72 h with the reaction conditions shown in Scheme 49. Considering the surprising capture efficacy as well as stability of the hydroxide bases, the authors postulated that the hydroxide-based system might be superior to the alternative amine routes for a scalable process.





**Scheme 49.** Hydroxide-based CO<sub>2</sub> capture and subsequent hydrogenation proposed by Prakash [596].

In 2017, Beller reported an efficient cobalt catalyst for the production of methanol from CO<sub>2</sub> [597]. The authors started their investigation based on the Co(BF<sub>4</sub>)<sub>2</sub>/Triphos catalyst proposed by de Bruin for the hydrogenation of esters and carboxylic acids [598]. In this work, the active catalytic specie is formed in situ from either [Co(acac)<sub>3</sub>], Co(OAc)<sub>2</sub>·4H<sub>2</sub>O, or Co(BF<sub>4</sub>)<sub>2</sub>·6H<sub>2</sub>O, in the presence of the Triphos ligand and HNTf<sub>2</sub>. It was found that a 1:3 relationship between [Co]/[HNTf<sub>2</sub>] and two equivalents of Triphos with respect to cobalt, afforded the highest activity. The highest TON of 31 was obtained using [Co(acac)<sub>3</sub>] as the metal precursor, with the reaction conditions shown in Scheme 50a. The system was later optimized in 2019 [599]; the previous reported results could be improved by either using modified Triphos ligands, as well as by replacing Co(acac)<sub>2</sub> with Co(NTf<sub>2</sub>)<sub>2</sub>. After screening of a range of ligands and additives, the authors proposed a new system that is additive free and notably, active below 100 °C (Scheme 50b).



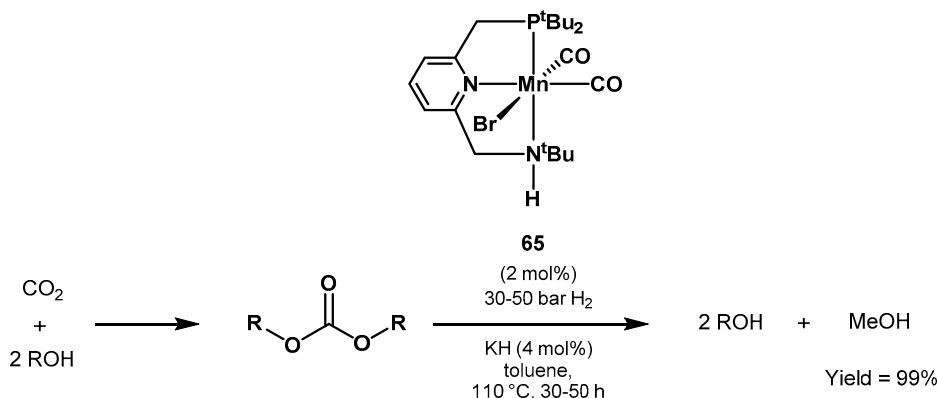
**Scheme 50.** In situ formed Co-PPP catalysts for carbon dioxide hydrogenation developed by Beller [597,599]:

(a) First generation systems formed by various Co precursor and Triphos ligand, and (b) second generation using Co(NTf<sub>2</sub>)<sub>2</sub> in combination with Triphos.

In 2017, Klankermayer demonstrated the efficient conversion of carbon dioxide to dialkoxymethane ethers catalyzed by a combination of Co(BF<sub>4</sub>)<sub>2</sub>, the Triphos ligand and HNTf<sub>2</sub> as a co-catalyst. The system was optimized for both the transformation of CO<sub>2</sub> to dimethoxymethane (DMM), as well as for the hydrogenation of CO<sub>2</sub> to alkoxy formates (AF) and dialkoxymethane ethers (DAM) in the presence of selected alcohols [600].

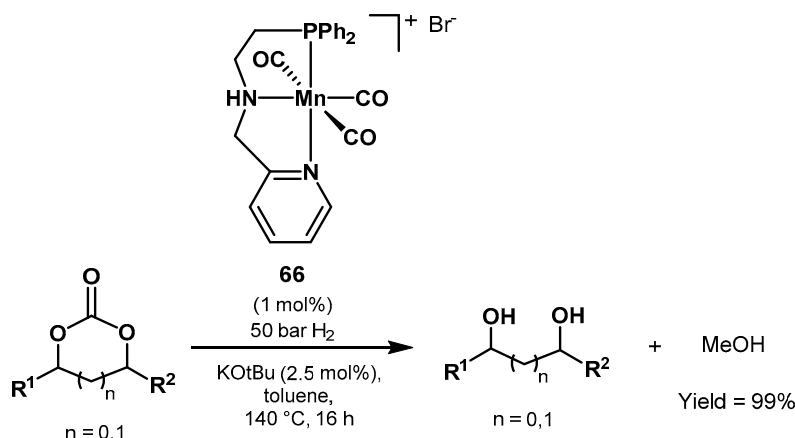
In 2018, Milstein showed the hydrogenation of organic carbonates to methanol and alcohols catalyzed by a manganese PNP complex [601]. The catalyst precursor **65** is activated in situ by catalytic amount of base, while the active amido form performs also in the absence of base. The authors demonstrated the efficient hydrogenation of a wide range of symmetrical and unsymmetrical acyclic carbonates and cyclic carbonates, which was possible to convert to methanol and two equivalents of the corresponding alcohols in high to excellent yields (62–99%), as shown in Scheme 51. In addition, the hydrogenation of poly(propylene carbonate) was also investigated as a route for the treatment of

waste plastics. Under the same reaction conditions, catalyst **65** afforded methanol and propylenediol in 59% and 68% yields, respectively, with propylene carbonate as a by-product.



**Scheme 51.** Hydrogenation of carbonates to methanol and alcohols proposed by Milstein [601].

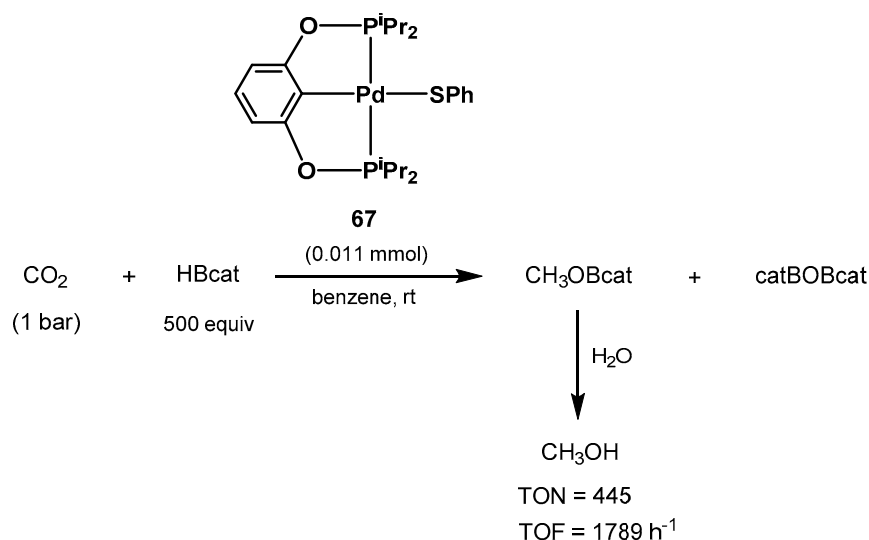
The same transformation was reported by Cavallo, El-Sepelgy and Rueping using the PNN manganese pincer complex **66** [602]. Several cyclic organic carbonates were successfully hydrogenated to methanol and valuable polyols under the reaction conditions shown in Scheme 52.



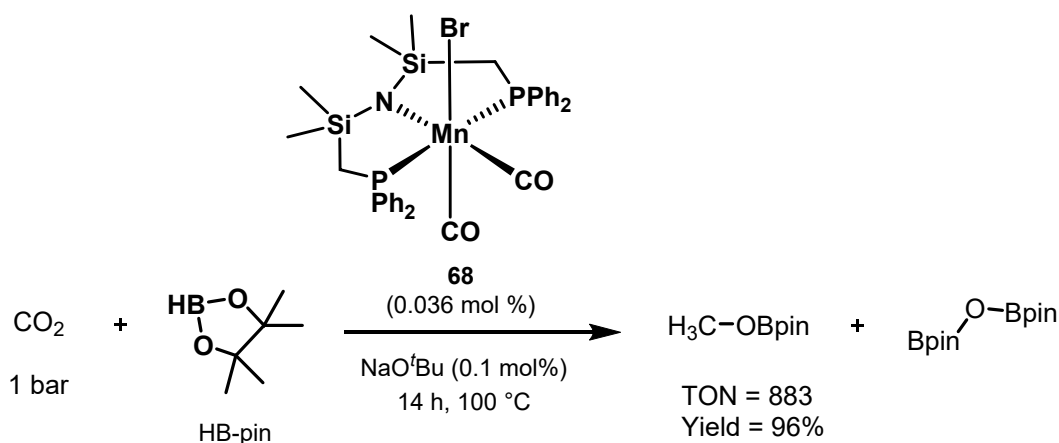
**Scheme 52.** Manganese-PNN complex **66** catalyzes the hydrogenation of organic carbonates to methanol and polyols as showed by Cavallo, El-Sepelgy, and Rueping [602].

In 2016, Zhang, Chen, and Guan explored the use of bis(phosphinite) pincer ligated Pd thiolate complexes for the hydrogenation of CO<sub>2</sub> [603]. Catecholborane was used to trap CO<sub>2</sub> at room temperature with 1 bar of CO<sub>2</sub>, using catalyst **67** (Scheme 53). A TOF of 1789 h<sup>−1</sup> and a TON of 445 were achieved with this method, being one of the most active systems to date reported for the homogeneous catalytic reduction of CO<sub>2</sub> to methanol or its derivative under mild reaction conditions.

Leitner reported the manganese pincer complex **68** for the reduction of CO<sub>2</sub> and other carbonyl groups using pinacolborane [604]. The system operates using reasonable low catalyst loadings and under solvent-less conditions. The best result was achieved using 0.036 mol% of catalyst **68** and NaOtBu at 100 °C resulting in 96% yield and a TON of 883 after 14 h (Scheme 54). In addition, several cyclic and linear carbonates could be quantitatively converted into the corresponding boronate esters and protected methanol in yields exceeding 95%.



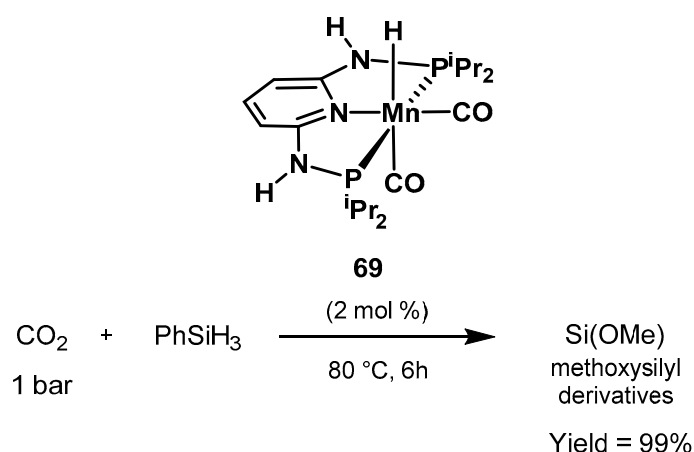
**Scheme 53.** Catalytic reduction of CO<sub>2</sub> to CH<sub>3</sub>OBcat catalyzed by PCP pincer ligated Pd thiolate complexes reported by Zhang, Chen, and Guan [603].



**Scheme 54.** Leitner's hydroboration of CO<sub>2</sub> using the manganese complex **68** as catalyst [604].

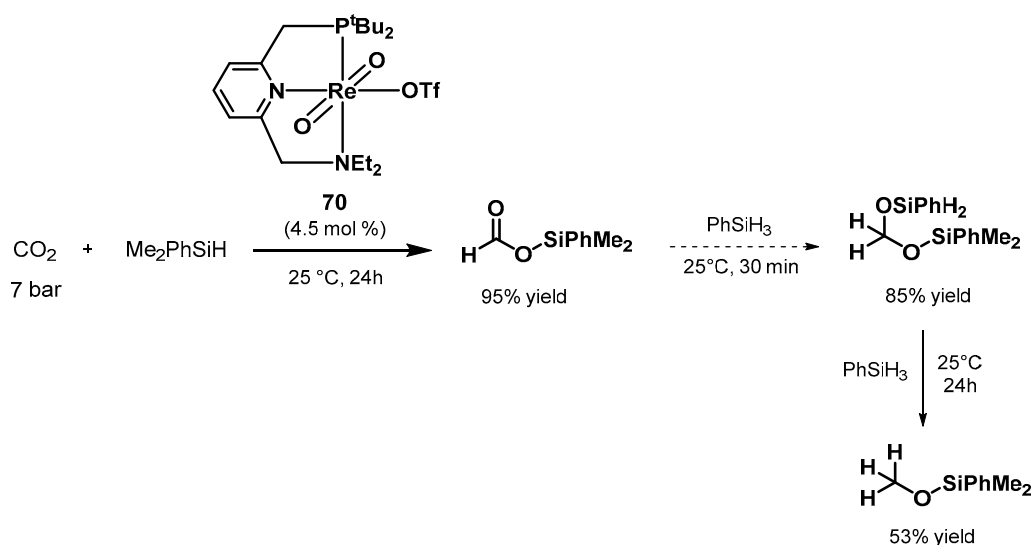
Another method for the capture of CO<sub>2</sub> is its reduction in the presence of silanes, with the formation of strong Si-O bonds as the driving force promoting the transformation. The hydrosilylation of CO<sub>2</sub> has gained much attention in the past decades, with several homogeneous systems reported to catalyze the conversion of carbon dioxide to silyl formates [605–607], as well as to the methoxysilyl derivatives [608–610]. With regard to pincer complexes, important results were achieved in 2010 by Chirik with a Co-PNP complex [611], as well as by Guan using a Ni-PCP catalyst [612].

Gonsalvi and Kirchner showed the Mn(I)-PNP complex **63** as an active catalyst for the selective and efficient reduction of CO<sub>2</sub> to MeOH in the presence of hydrosilanes [613]. The reaction was performed applying 0.014 mmol of the catalyst (10 mol% catalyst to CO<sub>2</sub> and 2 mol% catalyst to Si-H bonds) under mild conditions (80 °C, 1 bar CO<sub>2</sub>), in the presence of 5 equivalents of PhSiH<sub>3</sub> and DMSO as solvent (Scheme 55). It was possible to achieve 99% yield of methanol, in the form of Si(OMe) derivatives, after 6 h.



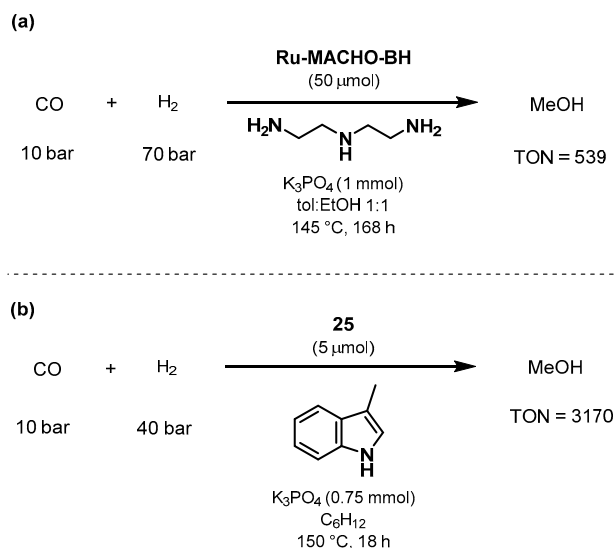
**Scheme 55.** Hydrosilylation of  $\text{CO}_2$  to methoxisilyl derivatives catalyzed by the Mn-PNP **68** reported by Gonsalvi and Kirchner [613].

Abu-Omar developed a method for carbon dioxide reduction into silyl-protected methanol in the presence of an oxo-rhenium PNN pincer complex (Scheme 56) [614]. The reaction employs catalyst **70** (4.5 mol%) with  $\text{Me}_2\text{PhSiH}$  and  $\text{CO}_2$  (7 bar), in DCM, at  $25^\circ\text{C}$  to promote the addition of Si-H to  $\text{Re}=\text{O}$  bond affording a complex capable of reducing  $\text{CO}_2$  into a silyl formate (95% yield). After 24 h, the silyl formate was reduced to silyl methanol with 53% yield.



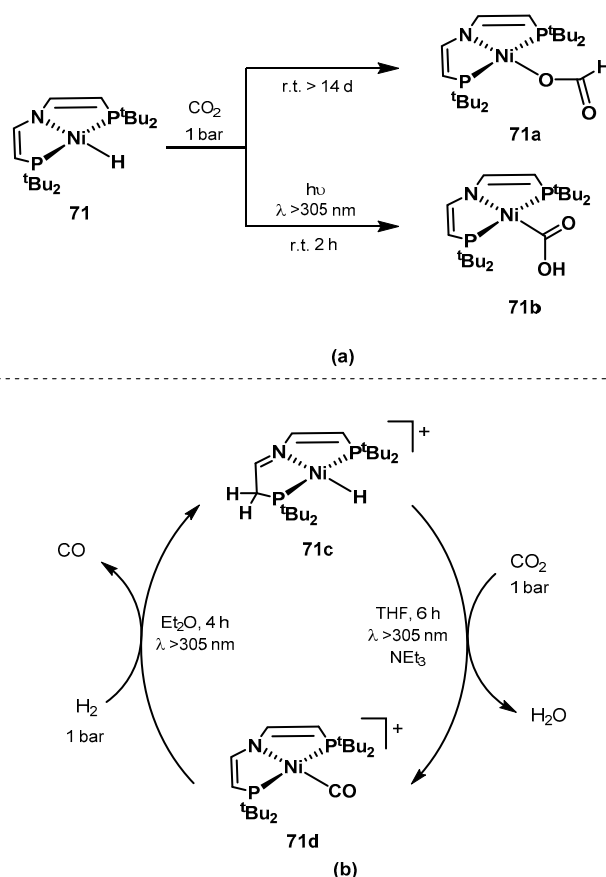
**Scheme 56.** Abu-Omar's  $\text{CO}_2$  reduction to silyl-protected methanol catalyzed by the oxo-rhenium PNN pincer complex **70** [614].

In 2019, Beller and Checinski reported the manganese pincer complex **25** as suitable catalyst also for carbon monoxide hydrogenation to methanol at mild conditions, in the presence of either pyrroles, indoles, or carbazoles as promoter [615]. The reaction performed at  $150^\circ\text{C}$  for 18 h under 1 bar of CO and 40 bar of  $\text{H}_2$ , using  $5\ \mu\text{mol}$  of catalyst **25**,  $0.75\ \text{mmol}$  of  $\text{K}_3\text{PO}_4$  as base, and benzene as solvent. This resulted in the formation of methanol with high selectivity and turnover numbers up to 3170. Simultaneously, Prakash reported the same transformation proceeding via formamide catalyzed by **Ru-MACHO-BH** [616]. Both catalysts show promising robustness and tolerance to CO. Similarities and differences between the two proposed catalytic systems for CO hydrogenation can be found in Scheme 57; it is possible to observe how the method proposed by Beller is superior in terms of hydrogen pressure, catalyst loading, as well as reaction time.



**Scheme 57.** CO hydrogenation to methanol proposed by (a) Prakash and (b) Beller [615,616].

In 2018, Schneider proposed a reverse water-gas-shift reaction (WGS) promoted by a nickel pincer complex at ambient reaction conditions [617]. The authors proposed a novel mechanism for CO<sub>2</sub> activation, opposed to the kinetically favored insertion into the catalyst M-H bonds providing formates (Scheme 58a). Under photochemical conditions, the selective formation of the metallacarboxylate was observed [618], consisting in the first step of the proposed WGS, followed by water elimination, CO release, and heterolytic H<sub>2</sub> activation to restore the active hydride specie (Scheme 58b).



**Scheme 58.** Water-gas-shift (WGS) reaction of CO<sub>2</sub> to CO and water with a nickel PNP pincer complex proposed by Schneider [617]: (a) Reactivity of 71 with CO<sub>2</sub> and (b) proposed mechanism.

The iridium-based complexes **72** and **73** reported by Milstein (Figure 5) showed good activity for the reversible activation of CO<sub>2</sub> [619]. Complex **72** is dearomatized at room temperature and reacts with CO<sub>2</sub> in THF or benzene affording two isomers, one where the hydride is trans to the bonded oxygen from CO<sub>2</sub>, and a second isomer where the hydride is trans to the pincer ligand. On the contrary, complex **73** reacts with CO<sub>2</sub> at room temperature in the presence of THF, affording only one isomer. The reaction is highly solvent dependent. Under similar conditions, using benzene as solvent, the authors observed a mixture of unidentified products. However, the addition of CO<sub>2</sub> to a pre-heated benzene solution containing **73** at 80 °C resulted in full conversion.

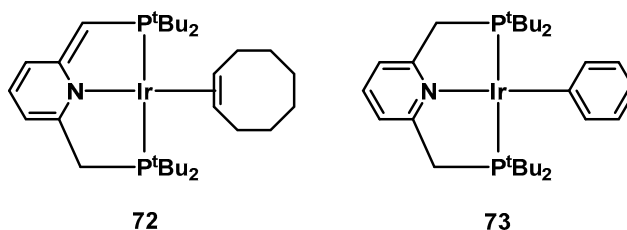
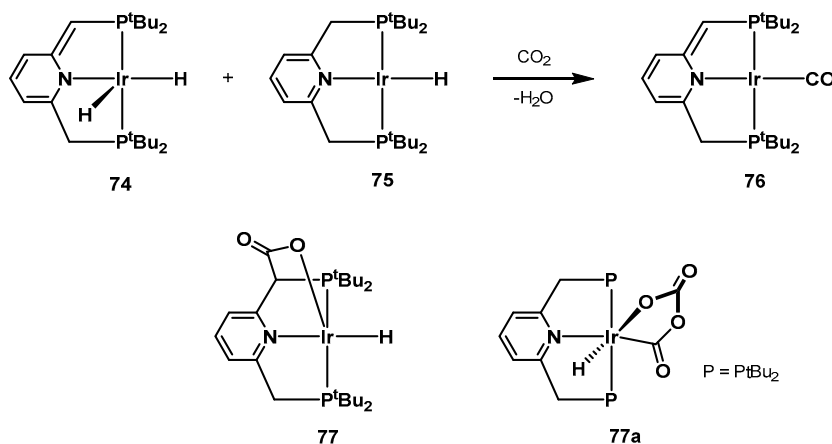


Figure 5. Iridium-based complexes **72** and **73** synthesized by Milstein [619].

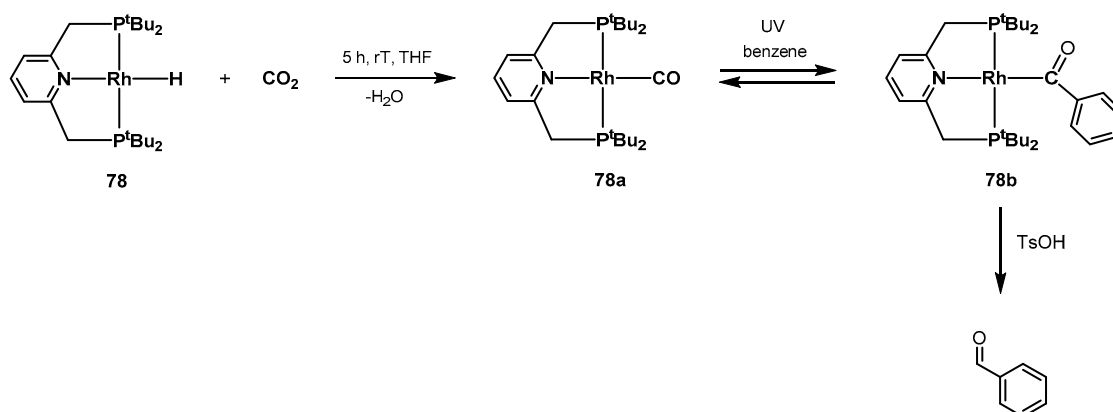
The same group showed a stoichiometric CO<sub>2</sub> reductive cleavage to CO and water promoted by a mixture of the two complexes **74** and **75** via metal-ligand cooperation (Scheme 59) [620]. It was suggested that a proton is transferred from the ligand to the activated CO<sub>2</sub> resulting in its cleavage. A reversible 1,3 addition of CO<sub>2</sub> to the benzylic position was also showed by the studies revealing that complex **77** is the kinetic product. Together with the observed, rare example of di-CO<sub>2</sub> metallocycle complex **77a**, both of them are reversibly formed and do not participate in the formation of **76**. The reaction of **74** and **75** with CO results in the formation of dihydrogen and **76**.



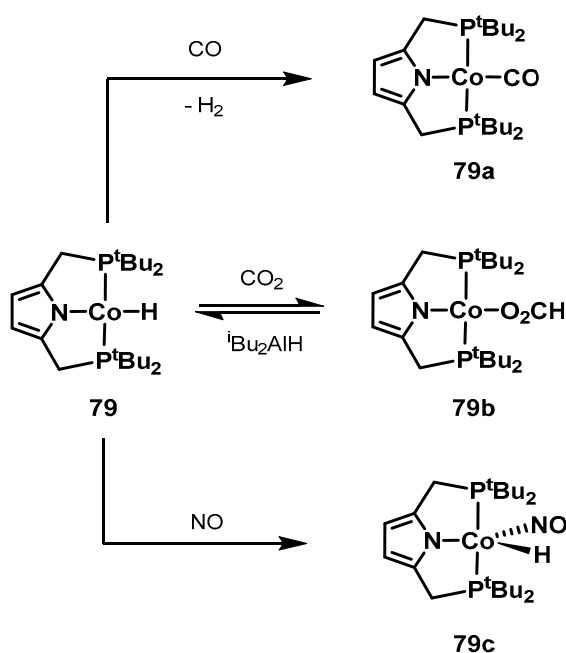
Scheme 59. Reactivity of **74** and **75** with CO<sub>2</sub> showed by Milstein [620].

Milstein also reported that the Rh(I)-PNP pincer complex **78** promotes the splitting of CO<sub>2</sub> leading to the Rh(I) carbonyl complex **78a** that by UV irradiation activates a C-H bond in benzene, followed by the protonation of the benzoyl complex **78b** resulting in a benzaldehyde molecule (Scheme 60) [621].

The reactivity between a square-planar Co(II)-hydrido-PNP complex and small molecules such as CO<sub>2</sub> and CO was investigated by Tonzetich in 2018 [622]. Complex **79** demonstrated a facile migratory insertion of CO<sub>2</sub> producing the formate complex **79b**. The complex was also reacted with nitric oxide, providing the first example of cobalt nitrosyl-hydride complex (Scheme 61).



**Scheme 60.** CO<sub>2</sub> cleavage and photocarbonylation of benzene reported by Milstein [621].



**Scheme 61.** Square planar Co(II)-hydrido-PNP complex **79** and its reactivity with small molecules showed by Tonzetich in 2018 [622].

### 3.1.3. CO<sub>2</sub> Hydrogenation to Formate Salts

Several groups explored the homogeneous hydrogenation of CO<sub>2</sub> to give basic formate salts, which can be later acidified to provide formic acid. Various combination of ruthenium complexes bearing phosphine ligands were found to be active in this transformation [623–625]. Important milestones were achieved by Jessop, with Ru-P(Me<sub>3</sub>)<sub>3</sub> catalysts [560,562], Zhang with Ru-P(Ph<sub>3</sub>)<sub>3</sub> species [626], Leitner with the meta-trisulfonated triphenylphosphine ligand (TPPMS) [627], as well as Beller, using [RuCl<sub>2</sub>(benzene)]<sub>2</sub> in combination with the phosphorous ligand bis(diphenylphosphino)methane (DPPM) [628]. In addition, the hydrogenation of bicarbonates (used as CO<sub>2</sub>-trapping agents) as an indirect route to provide formates has also been investigated by many groups [629–631]. Important advances in this regard have been achieved by Beller and Laurenczy using again [RuCl<sub>2</sub>(benzene)]<sub>2</sub> and DPPM [632,633], resulting in a formate yield of 61%, and a TON = 2,793 after 20 h at 100 °C in the presence of 50 bar of hydrogen and 35 bar of CO<sub>2</sub> in a sodium bicarbonate solution.

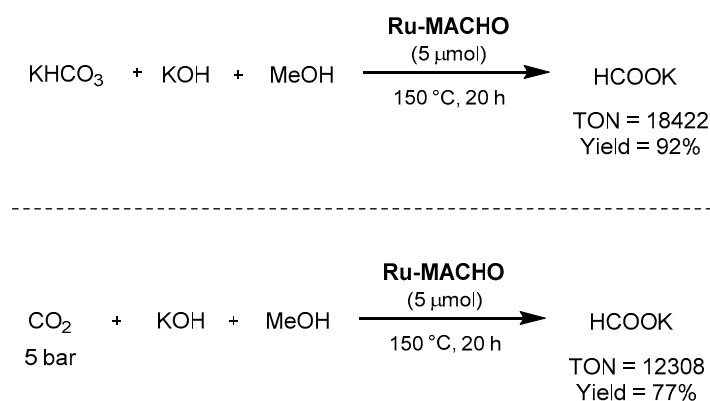
In 2012, the same group showed that not only ruthenium, but also iron and cobalt catalysts are highly active for the hydrogenation of bicarbonates to give formates. In the presence of an iron(II)-fluoro-tris(2-(diphenylphosphino)phenyl)phosphino]tetrafluoroborate complex, obtained



in situ from  $\text{Fe}(\text{BF}_4)_2 \cdot 6\text{H}_2\text{O}$  and tris(2-(diarylphosphino)aryl)phosphine, the hydrogenation of bicarbonates afforded  $\text{TON} > 7500$  and  $\text{TOF} > 750$ , with 77% yield of sodium formate under 60 bar of hydrogen in methanol at  $100^\circ\text{C}$  [634]. The hydrogenation of  $\text{CO}_2$  to formic acid in the presence of methanol and amines was also investigated, resulting in a mixture of formic acid and methyl formate, albeit with only 15% of carbon dioxide conversion.

Using the same approach, the hydrogenation of bicarbonate and carbon dioxide was also demonstrated using an in situ formed cobalt complex [635]. By simply applying 0.028 mol of  $\text{Co}(\text{BF}_4)_2 \cdot 6\text{H}_2\text{O}$ , in the presence of 1 equivalent of the Tetraphos ligand  $\text{PP}_3$  ( $\text{P}(\text{CH}_2\text{CH}_2\text{PPh}_2)_3$ ), under 1:1 60 bar of  $\text{H}_2/\text{CO}_2$  at  $80^\circ\text{C}$ , it was possible to obtain 94% yield of sodium formate, with a TON of 645 after 20 h.

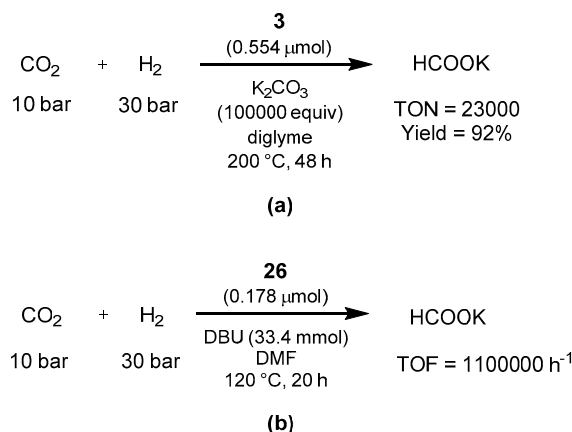
Regarding the use of pincer complexes, Beller employed in 2014 **Ru-MACHO** as the catalyst for the combined methanol dehydrogenation and bicarbonate hydrogenation, as well as for the synthesis of potassium formate from carbon dioxide, potassium hydroxide, and methanol [636]. In the first transformation, the reaction afforded excellent TON ( $>18,000$ ), TOF ( $>1300\text{ h}^{-1}$ ), as well as yield (92% of potassium formate), as shown in Scheme 62. Under the same reaction conditions, with 5 bar of carbon dioxide, the reaction afforded a formate yield of 77%, with a TON of 12308.



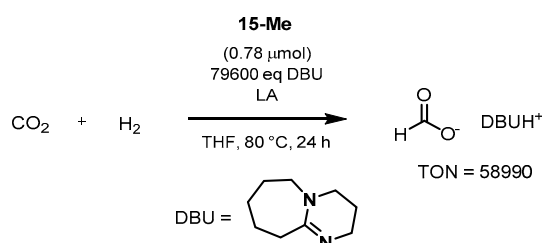
**Scheme 62.** **Ru-MACHO**-catalyzed hydrogenation of bicarbonate and  $\text{CO}_2$  to formate showed by Beller [636].

Sanford showed in 2013 that the Milstein PNN catalyst **3** efficiently catalyze the hydrogenation of  $\text{CO}_2$  to formate in the presence of potassium carbonate as base (Scheme 63a) [637]. In addition, the authors performed stoichiometric studies of various organometallic intermediates, showing that the reaction proceeds with a classic ligand-based aromatization/dearomatization pathway. The year after, Pidko showed that another Milstein catalyst, the PNP-pincer **26**, is able to perform the same transformation [638]. With the reaction conditions shown in Scheme 63b, the hydrogenation of  $\text{CO}_2$  proceeds in the presence of DBU as base, showing activity already at  $65^\circ\text{C}$  and a TOF of  $1,100,000\text{ h}^{-1}$  at  $120^\circ\text{C}$  (Scheme 63b). Importantly for an energetic cycle point of view, catalyst **26** is very active in the reverse formic acid dehydrogenation as well, affording high turnover numbers (1063000) in  $\text{DMF}/\text{NEt}_3$ .

In 2014, Hazari and Schneider demonstrated Fe-PNP complexes as catalysts with a Lewis acid as co-catalyst for the dehydrogenation of formic acid (see Section 2.2.2) [389]. One year later, the hydrogenation of  $\text{CO}_2$  catalyzed by the same system was demonstrated by Hazari and Bernskoetter [639]. The catalytic activities of both  $\text{Fe-PN}^{\text{HP}}$  and  $\text{Fe-PN}^{\text{MeP}}$  complexes were investigated in the study. Both of them demonstrated better results in the presence of co-catalytic amounts of a Lewis acid. The reactions were carried out under 70 bar of  $\text{CO}_2/\text{H}_2$  (1:1), 79,600 equivalents of DBU to the catalyst, LiOTf as additive (DBU/LiOTf 5:1), THF as solvent, and at  $80^\circ\text{C}$  for 24 h. After optimization,  $0.3\text{ } \mu\text{mol}$  of catalysts **15-Me** afforded the best turnover number of 58,990 and 74% yield (Scheme 64). Quantitative yields were afforded when increasing the catalyst loading to  $0.78\text{ } \mu\text{mol}$ .

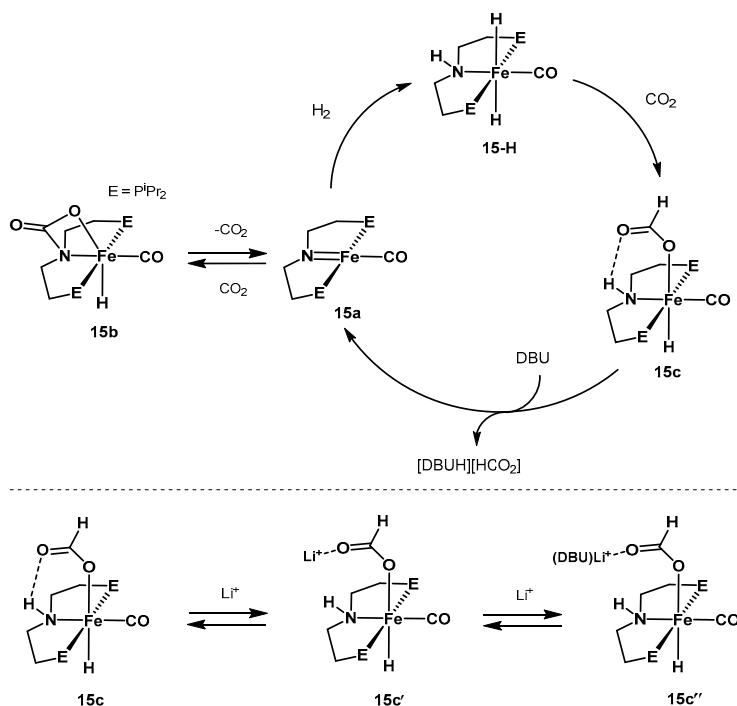


**Scheme 63.** Hydrogenation of CO<sub>2</sub> to formate using Milstein's catalysts **3** (a) and **26** (b) as reported by Sanford [637] and Pidko [638].



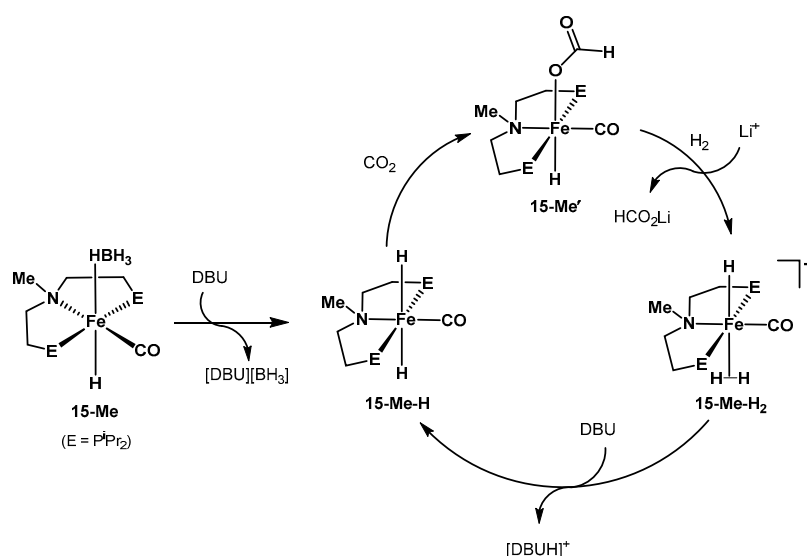
**Scheme 64.** Hazari and Schneider's CO<sub>2</sub> hydrogenation catalyzed by **15-Me** [639].

In catalytic systems containing a secondary amine ligand, studies via NMR analysis suggested that the key role of the Lewis acid is the weakening of the stability of the hydrogen bond between N-H and Fe-O<sub>2</sub>CH moieties in **15c** (Scheme 65).



**Scheme 65.** Proposed mechanism for (<sup>R</sup>PNP)Fe(H)COLi<sup>+</sup> catalyzed CO<sub>2</sub> hydrogenation and activation of HCO<sub>2</sub>-1a by Li<sup>+</sup> and DBU as showed by Hazari and Schneider [639].

On the other hand, in the presence of tertiary amine ligand systems, the authors showed that  $(iPrPN^{Me}P)Fe(H)CO(BH_4)$  is activated by DBU to produce the complex  $(iPrPN^{Me}P)Fe(H)_2CO$  which rapidly captures  $CO_2$  (Scheme 66). Here, the role of the Lewis acid consists in promoting the dihydrogen substitution on the formate complex, generating a transient cationic iron(II) dihydrogen intermediate. DBU deprotonates the dihydrogen complex resulting in the regeneration of  $(iPrPN^{Me}P)Fe(H)_2CO$ . The proposed pathway is believed to improve the reaction rate resulting in turnover frequencies as high as  $20,000\ h^{-1}$ . In addition, the authors reported kinetic studies on the influence of solvent and Lewis acid on the insertion of  $CO_2$  metal hydrides. Small and highly charged Lewis acids such as  $Li^+$  provide stabilization of the incipient negative charge on the carboxylate group, hence of the rate-determining step, as long as it is not sequestered by the solvent via  $O\cdots LA^+$  interactions.

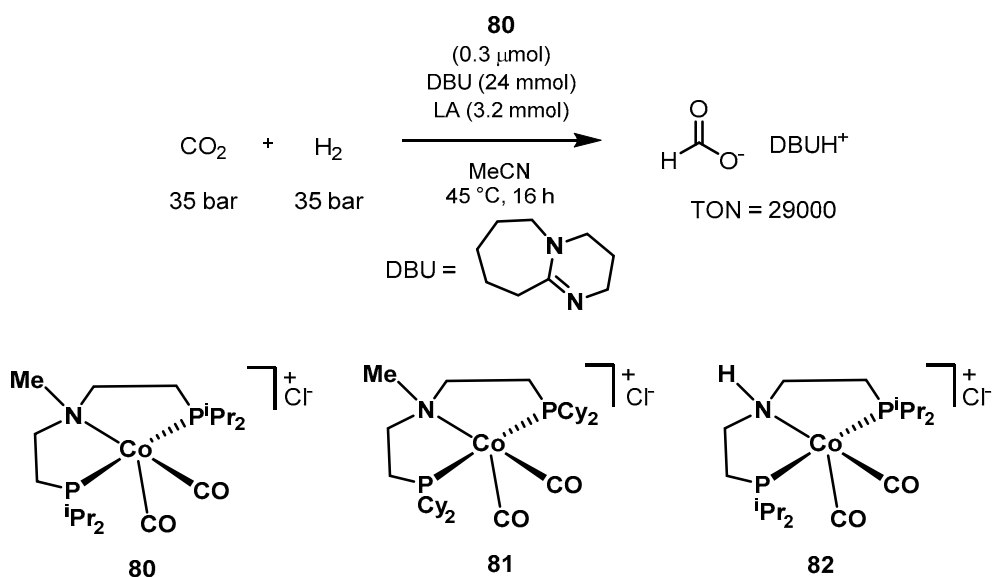


**Scheme 66.** Proposed pathway for catalytic  $CO_2$  hydrogenation using  $(iPrPN^{Me}P)Fe(H)CO(BH_4)$  reported by Hazari and Schneider [639].

In 2016, a comprehensive overview of the state-of-the-art for  $CO_2$  hydrogenation, as well as formic acid/methanol dehydrogenation using first-row metal complexes, was published by Bernskoetter and Hazari [640]. The authors provide comparisons between selected iron and cobalt pincers with known Ru-PNP catalysts, and investigate the role of Lewis acid additives in the improvement of these promising base metal catalysts.

The same year, Bernskoetter showed the synthesis, as well as crystallographic characterization, of cobalt(I)-PNP complexes derived from the pincer ligand  $Me-N[CH_2CH_2(P^iPr)_2]$  [641]. The new complexes showed in this work performed better than previously reported  $P^{Me}NP$  cobalt pincer catalysts for the hydrogenation of  $CO_2$  to formate. When  $0.3\ \mu mol$  of complex  $[(iPrPNP)Co(CO)_2]^+$  **80** was paired with  $3.2\ mmol$  of the Lewis acidic additive  $LiOTf$ ,  $2.4\ mmol$  of DBU as the base, under  $70\ bar$  of  $1:1\ CO_2/H_2$  at  $45\ ^\circ C$ , a TON near 30,000 and a TOF of  $5700\ h^{-1}$  were afforded after 16 h (Scheme 67).

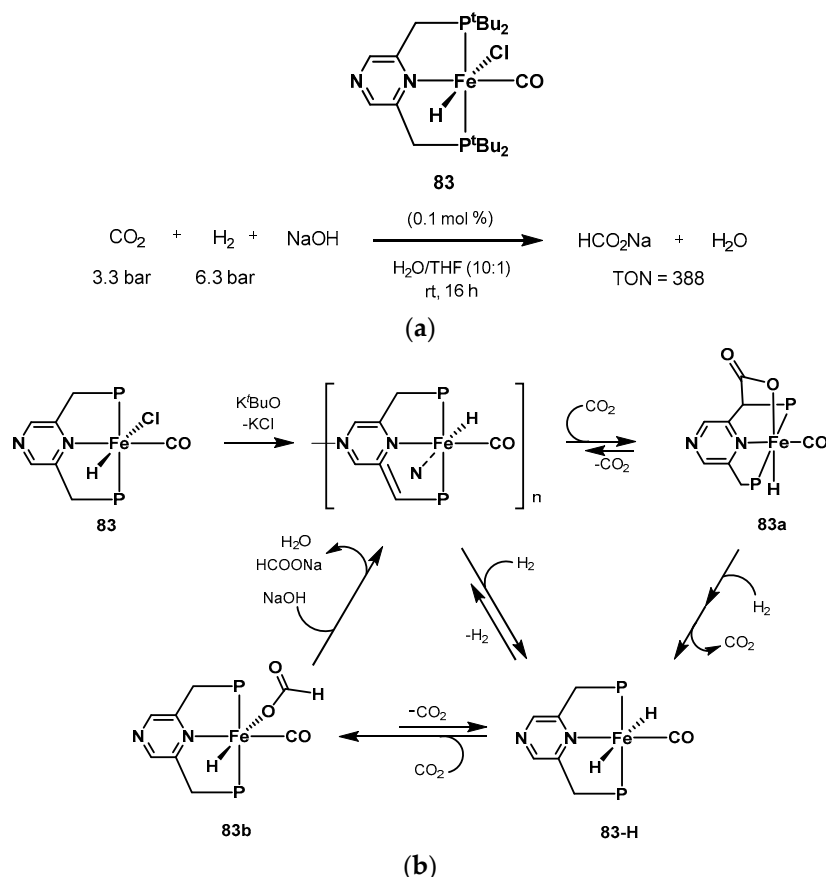
Bernskoetter further investigated the influence of various bifunctional PNP pincer ligands within the same class of low-valent cobalt complexes [642]. Cobalt(I) precatalysts containing tertiary amine ligand showed better activity, as well as improved stability, than those bearing the secondary amine pincer ligand. In this report, the reactions were performed using the same conditions, as shown in Scheme 67. Catalyst **80** achieved a TON of 29,000, while catalyst **81** and **82** achieved TONs of 24,000 and 450, respectively.



**Scheme 67.** Co-PNP complexes tested by Bernskoetter for CO<sub>2</sub> hydrogenation to formate with Lewis acid additives [641,642].

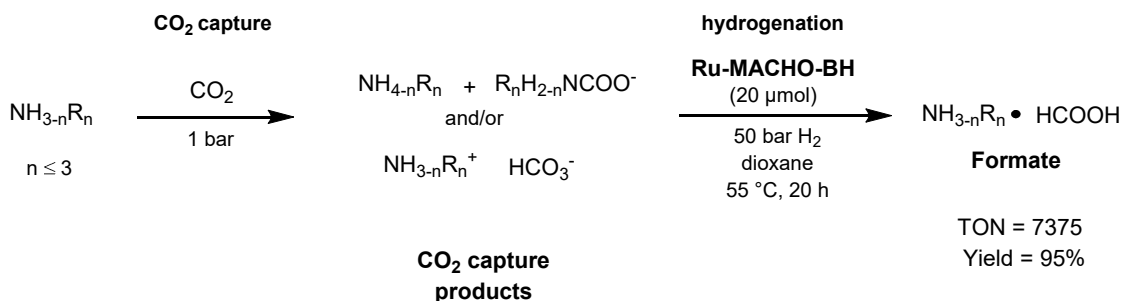
Later, Milstein developed Fe-PNP complexes based on the pyrazine backbone (PNzP) [643]. In a similar fashion as the pyridine congener, the PNzP ligand promotes the metal-ligand cooperation by aromatization/dearomatization of the pyrazine ring. Under basic conditions, complex **83** (0.1 mol%) catalyzes the hydrogenation of CO<sub>2</sub> (3.3 bar) to formate salts at low H<sub>2</sub> pressure (6.3 bar) and temperature (55 °C) (Scheme 68a). However, only moderate TON values (up to 388) were obtained. The authors proposed a catalytic cycle for the reaction based on observations obtained with NMR spectroscopy as well as X-ray diffraction. At first, one of the pincer arms is deprotonated to generate a stable dearomatized compound. The so-formed complex reacts with CO<sub>2</sub> and H<sub>2</sub> to afford compounds **83a** and **83-H**, respectively. **83a** reacts with H<sub>2</sub> by formal substitution of CO<sub>2</sub>, leading to compound **83-H**. CO<sub>2</sub> is inserted to **83-H** into the hydride-iron bond generating the formate complex **83b**. In the presence of base, **83b** produces the dearomatized complex that reacts with H<sub>2</sub> regenerating the cycle (Scheme 68b).

Gonsalvi and Kirchner reported Fe(II)-hydrido carbonyl complexes supported by PNP ligands with *N*-H or *N*-Me spacers as catalysts for CO<sub>2</sub> and NaHCO<sub>3</sub> hydrogenation to sodium formate in protic solvents and in the presence of base [644]. Studies showed that catalyst **29** can work as a bifunctional catalyst in which the *N*-H spacer promotes metal-ligand cooperation. In contrary, the *N*-Me spacer of complex **29-Me** prevents that possibility. Moreover, the authors speculate that the presence of a labile bromide as well as the strongly  $\sigma$ -basic H and  $\pi$ -acidic CO ligands might be ideal for catalytic CO<sub>2</sub> hydrogenation reactions. The hydrogenation of NaHCO<sub>3</sub> was catalyzed by **29** (0.05 and 0.005 mol%) under 90 bar of H<sub>2</sub> at 80 °C, and after 24 h of reaction TONs of 1964 (98% yield) and 4560 (23% yield) were achieved, respectively. The use of THF inhibited the reaction suggesting that the use of protic solvents stabilizes the reaction intermediates through hydrogen bonding. The hydrogenation of CO<sub>2</sub> catalyzed by 0.08 mol% of **29** under 80 bar pressure at 80 °C in H<sub>2</sub>O/THF proceeded in basic conditions (12.5 mmol NaOH) and resulted in TONs up to 1220 with 98% of yield. The use of NaOH in H<sub>2</sub>O/THF in this reaction was fundamental since changing to other bases and solvents resulted in no activity or low conversions. Applying 0.01 mol% of **29-Me**, DBU as base and EtOH as solvent at 80 °C, the reaction afforded 98% yield in sodium formate, corresponding to a TON of 9840. With lower catalyst loading (0.005 mol% of **29-Me**) a TON of 10,275 was achieved, albeit with only 21% yield of formate.



**Scheme 68.** (a) Hydrogenation of CO<sub>2</sub> catalyzed by **83** and (b) the proposed mechanism for hydrogenation of CO<sub>2</sub> reported by Milstein [643].

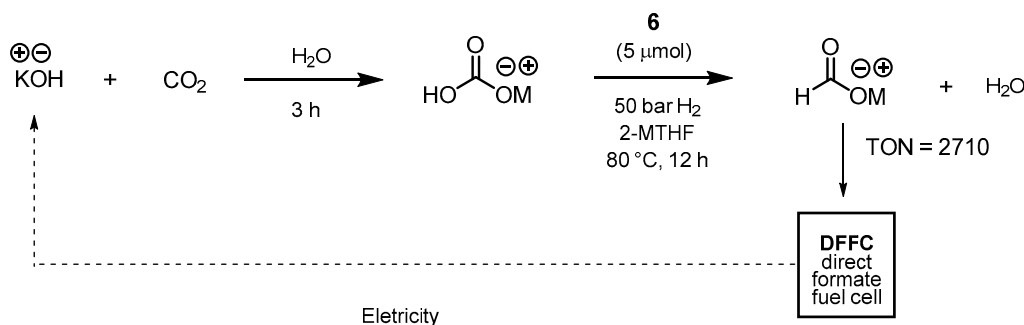
Prakash explored a green and direct procedure for CO<sub>2</sub> capture and its transformation to formate using known Ru- and Fe-PNP pincer complexes without the need of an excess of base [645]. Superbases, such as tetramethylguanidine (TMG), as additives showed the best results for the combined CO<sub>2</sub> capture (15.6 mmol) followed by hydrogenation in aqueous media using 2 μmol of **Ru-MACHO-BH** and 50 bar of H<sub>2</sub> at 55 °C for 20 h in dioxane/water (Scheme 69). It was found that other substrates, such as bicarbonate/carbonates and carbamates, could be converted into formate as well. The catalyst recyclability showed a TON for formate of 7375 in five consecutive hydrogenation steps of 5 h each, by reusing the same organic layer containing the catalyst and with no decrease of the catalytic activity (formate yield = 95%).



**Scheme 69.** CO<sub>2</sub> capture and hydrogenation to formate catalyzed by **Ru-MACHO-BH** reported by Prakash [645].

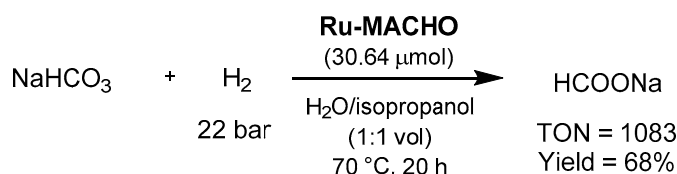
Based on the same approach using hydroxides shown in Section 3.1.2 for the production of methanol, Prakash proposed in 2018 a neutral CO<sub>2</sub> capture and hydrogenation to formate cycle at

low temperatures, with contemporary regeneration of the hydroxide base [646]. Among the screened bases, NaOH, KOH, and CsOH performed best, with the formation of HCOOK being the fastest and completed within 30 min. After the capture of 13.6 mmol of CO<sub>2</sub>, the reaction afforded a TON of 2710 and TOF of 5420 h<sup>-1</sup> using KOH, catalyst **6**, 2-MTHF as the organic solvent, H<sub>2</sub> (50 bar), and at 80 °C (Scheme 70). The obtained formate solution was directly used without any purification in a formate fuel cell, producing electricity with consequent base regeneration, providing a carbon-neutral energy production cycle. The biphasic H<sub>2</sub>O/2-MTHF system has again a positive impact on the recycling of the catalyst and the hydroxide base; catalyst **6** retained similar catalytic activity even after five cycles, affording over 90% formate yield in each cycle.



**Scheme 70.** Capture and hydrogenation of CO<sub>2</sub> combined with a direct formate fuel cell by Prakash [646].

The same year, Treigerman showed a hydrogen storage system based on aqueous sodium bicarbonate and the ruthenium PNP catalyst **Ru-MACHO** (Scheme 71) [647]. The hydrogen charge is performed under mild reaction conditions (70 °C and 20 bar H<sub>2</sub>) in isopropanol/water to afford sodium formate, which can be subsequently decomposed to release hydrogen and recycled sodium bicarbonate. **Ru-MACHO** shows again promising recyclability properties, retaining its activity through numerous cycles of the hydrogenations. Simply adding sodium bicarbonate and heating to 70 °C, a TON > 610 was measured in each cycle.



**Scheme 71.** Hydrogenation of sodium bicarbonate to sodium formate catalyzed by **Ru-MACHO** reported by Treigerman [647].

In 2017, Peng and Zhang reported the syntheses and characterizations of [RuCl(L1)MeCN]<sub>2</sub>]Cl **84** and [RuCl(L2)MeCN]<sub>2</sub>]Cl **85** (Figure 6) as suitable catalysts for the hydrogenation of CO<sub>2</sub> and bicarbonates to formate salts [648]. Complex **84** (0.1 mol%) showed a good activity and achieved 34% yield (based on NaOH) with a TON of 407 under 30 bar of H<sub>2</sub> and 15 bar of CO<sub>2</sub>, using 60 mmol of NaOH and THF/H<sub>2</sub>O (1:1) at 130 °C for 24 h. The investigations for the hydrogenation of sodium bicarbonate to sodium formate using **86** (0.05 mol%) showed yield of 77% and TON of 1530 under 30 bar of H<sub>2</sub>, using THF/H<sub>2</sub>O (1:1) at 130 °C for 24 h.

Kirchner and Gonsalvi reported in 2017 the use of Mn(I) pincer complexes for CO<sub>2</sub> hydrogenation to formate [649]. In this example, the hydride Mn(I) catalyst [Mn(<sup>i</sup>PrPNP<sup>NH</sup>)(H)(CO)<sub>2</sub>] **69** was employed and showed higher stability and activity than its Fe(II) analogue. Thus, using 10 μmol of catalyst **69**, at 80 °C, for 24 h, and 80 bar total pressure (1:1 H<sub>2</sub>/CO<sub>2</sub>) in THF/H<sub>2</sub>O, and in the presence of DBU as base and LiOTf as the co-catalyst, TONs up to 10,000 and yield up to >99% were achieved (Scheme 72). Decreasing the catalyst loading to 0.002 mol%, resulted in TONs up to 30,000. Importantly, the system

is active already at room temperature, and remains active for up to 48 h (TON = 26,600) with an average TOF of approximately  $550 \text{ h}^{-1}$  indicating a constant rate of reaction.

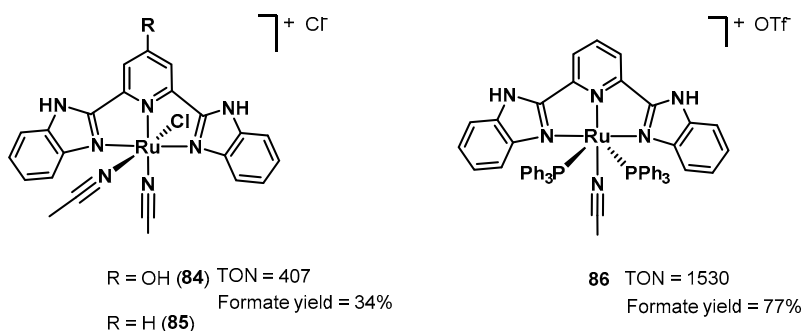
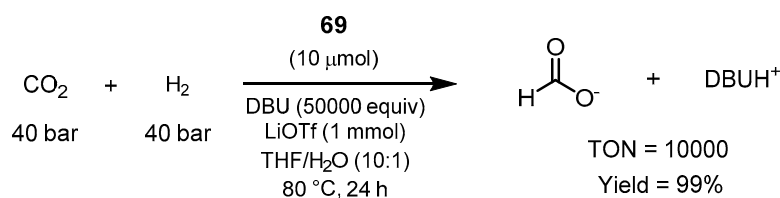
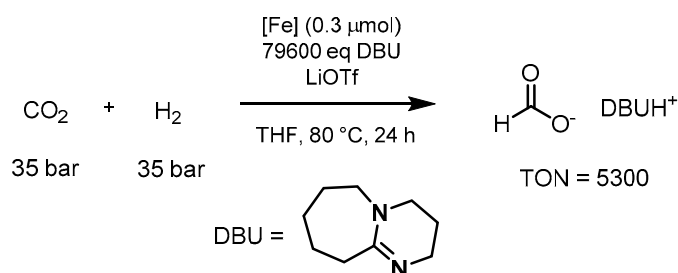


**Figure 6.** Ru-NNN pincer complexes synthesized and characterized by Peng and Zhang [648].



**Scheme 72.**  $\text{CO}_2$  hydrogenation to formate catalyzed by Mn complex **69** reported by Kirchner and Gonsalvi [649].

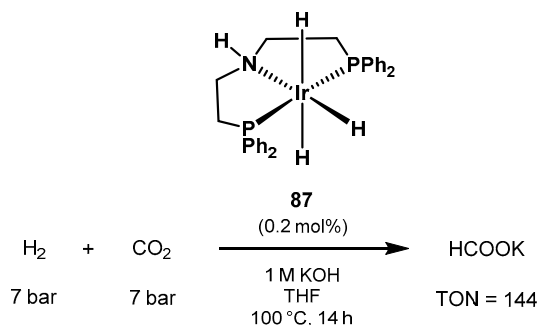
As discussed before (see Section 2.2.2), Bernskoetter and Hazari reported the synthesis of various iron-PNP complexes with ancillary isonitrile ligands and demonstrated their activity through formic acid dehydrogenation [405], as well as  $\text{CO}_2$  hydrogenation to formate salts [406]. The reaction using 0.3  $\mu\text{mol}$  of the catalyst **43a** (containing the isonitrile group  $\text{C}\equiv\text{NR}$ , with  $\text{R} = 2,6\text{-dimethylphenyl}$ ), DBU as base, LiOTf as co-catalyst (7.5:1 DBU/LiOTf), THF, at 80  $^\circ\text{C}$  for 24 h achieved a TON of 613. The second-generation isonitrile catalysts, with the methylated amino arm of the PNP pincer, showed better performance, with catalyst **43c** resulting in TON of 5300 under the same reaction conditions (Scheme 73).



**Scheme 73.**  $\text{CO}_2$  hydrogenation catalyzed by Fe-PNP isonitrile complexes proposed by Bernskoetter and Hazari [405,406].

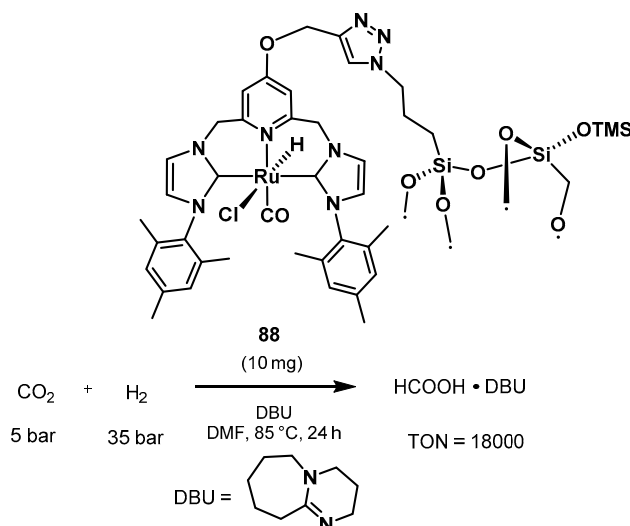
In 2019, Jagirdar showed the iridium trihydride complex  $[\text{IrH}_3(\text{PN}^{\text{H}}\text{P})]$  **87** (Scheme 74) as an active catalyst for the hydrogenation of  $\text{CO}_2$  to formate [650]. The reaction was carried out in aqueous 1 M KOH solution, with 0.2 mol% of **87**, at 14 bar of  $\text{H}_2$  and  $\text{CO}_2$  (1:1). A TON of 144 was afforded at 100  $^\circ\text{C}$  for 14 h or 25  $^\circ\text{C}$  for 19 h. The highest TOF of  $47 \text{ h}^{-1}$  was obtained at 80  $^\circ\text{C}$ .





**Scheme 74.** Ir-PNP catalyst **87** reported by Jagirdar for CO<sub>2</sub> hydrogenation to formate.

Recently, Copéret demonstrated the synthesis of an immobilized lutidine-derived pincer type *N*-heterocyclic carbene ruthenium on a highly ordered silica-based material [651]. Complex **88** was used as catalyst for CO<sub>2</sub> hydrogenation into the corresponding formic acid-base adduct affording a TON of 18,000 in 24 h (Scheme 75). It was demonstrated that the method improves the stability of the catalyst compared to the homogeneous analogue, which afforded a TON of 9250 after 24 h under the same reaction conditions.



**Scheme 75.** Catalyst **88** immobilized on silica material for the hydrogenation of carbon dioxide to formate salts showed by Copéret [651].

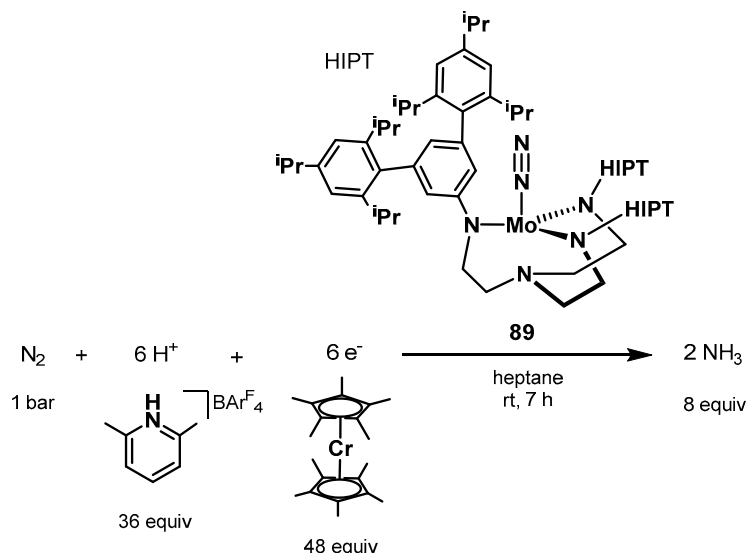
### 3.2. Nitrogen Fixation

The homogeneously catalyzed production of ammonia has remained challenging for a long time, and relatively unexplored; in this regard, Minter, Janik, Renner, and Greenlee recently reviewed the reduction of dinitrogen into ammonia by means of both heterogeneous and homogeneous catalysis [652]. Homogeneous pincer-type catalysis offers the possibility to perform nitrogen fixation under mild reaction conditions albeit significant further improvements are required to reach acceptable industrial relevance. Already in 2007, Leitner explored the potential of pincer complexes of Fe, Ru, and Os as active species for the production of ammonia from N<sub>2</sub> and H<sub>2</sub> [653]. Tucek [654], Nishibayashi [655–658], Fryzuk [659], and many other authors have reviewed this topic in depth [660–667], with pincer-type ligation being widely employed in the proposed methods.

Back in 1965, the first dinitrogen complex was synthesized by Allen and Senoff [668]; since this report, many studies have focused on the synthesis of novel transition metal dinitrogen complexes and their reactivity with dinitrogen with the purpose of finding alternative approaches for a greener nitrogen fixation process. Several homogeneous systems have been explored for this transformation [669–678],

inspired by the biological nitrogen fixation performed by the active Fe/Mo site of nitrogenase [679,680]. In addition, various works have covered the photochemical activation of molecular nitrogen [681–688].

Only in 2003, Schrock developed the first homogeneously catalyzed production of ammonia using transition metal-nitrogen complexes [689,690]. Eight equivalents of ammonia per catalyst were produced when dinitrogen reacted with a reductant and a proton source at room temperature under 1 bar of  $N_2$  and in the presence of the molybdenum-dinitrogen complex **89** bearing a triamide-monoamine tetradentate ligand (Scheme 76). The mechanism of the reaction was elucidated through isolation of key intermediates; however, they were unsuccessful in improving the catalytic activity of the system.

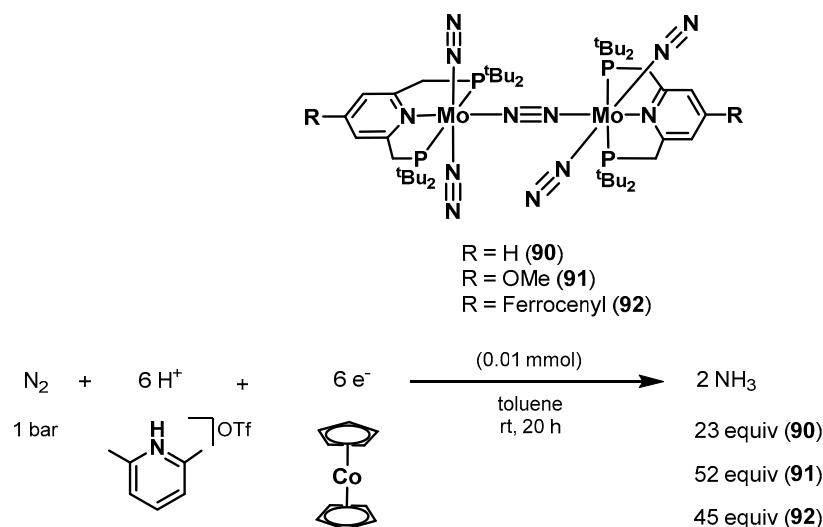


**Scheme 76.** First example of homogeneous ammonia production by Schrock [690].

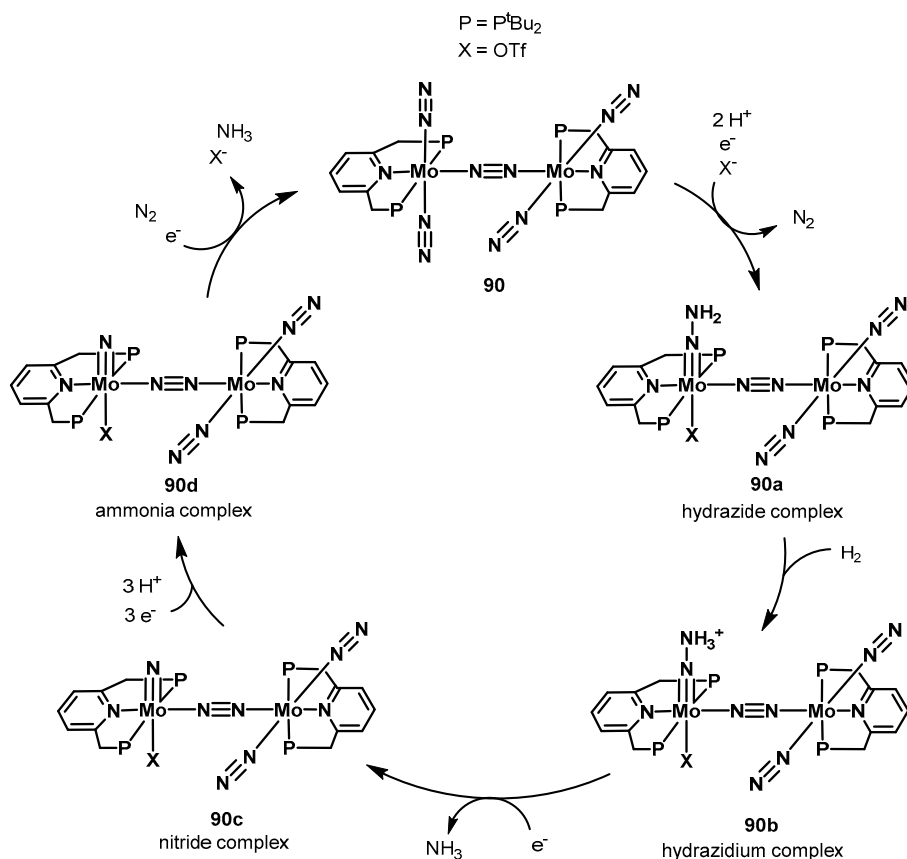
In 2011, Nishibayashi showed the molybdenum PNP pincer complex **90** for the second example of catalytic production of ammonia from dinitrogen at ambient conditions [691]. By applying 0.01 mmol of catalyst **90**, 216 equivalents of  $[LuH]OTf$  as the proton source, and 288 equivalents of cobaltocene as electrons donor, it was possible to obtain 23 equivalents of ammonia (12 per molybdenum atom) at room temperature (Scheme 77). The mechanistic cycle was elucidated in 2014 in collaboration with Yoshizawa and shown in Scheme 78 [692]. It was shown that the complex maintains a dinuclear character in solution as opposed to the hypothesis that dinitrogen bridges dissociate to the corresponding mononuclear complexes; in case of PNP pincer ligation, the dinuclear specie catalyzes the protonation of the terminal dinitrogen, which is the first step of the catalytic cycle.

In a following paper from 2014, Nishibayashi demonstrated that the catalytic activity can be almost doubled with the introduction of electron-donating groups such as methyl and methoxy groups onto the pyridine ring of the PNP pincer ligand [693]. As shown in Scheme 77, catalyst **91** afforded up to 52 equivalents of ammonia, with 360 equivalents of  $CoCp$  and 480 equivalents of  $[LuH]OTf$  under 1 bar  $N_2$  at room temperature after 20 h.

The same group later reported the synthesis of other molybdenum-dinitrogen complexes bearing different redox-active substituent on the PNP pincer ligand, with the aim of promoting the reduction step of the transformation [694,695]. The catalysts were then tested for the synthesis of ammonia from molecular dinitrogen. The reactions were performed under 1 bar of  $N_2$  with 0.01 mmol of catalyst, toluene as solvent, at room temperature, for 20 h, and with 288 equivalents of  $[LuH]OTf$  and 216 equivalents of  $CoCp_2$ . The complexes containing ferrocene as a redox-active moiety in the pyridine ring of the PNP ligand showed higher activity for ammonia production, up to 45 equivalents using catalyst **92** (Scheme 77). Electrochemical and theoretical studies showed that the interaction between the Fe atom of the ferrocene moiety and the Mo atom of the catalyst might be fundamental to achieve high catalytic activities.



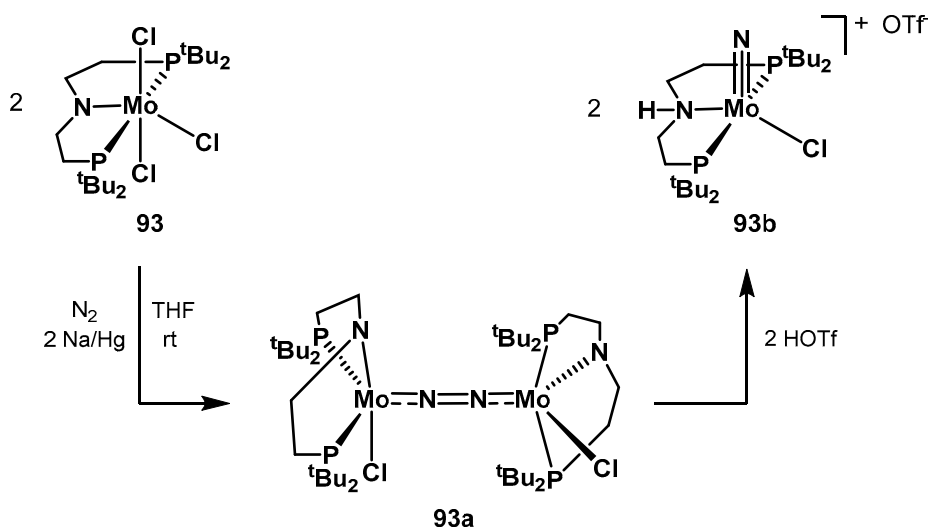
**Scheme 77.** Molybdenum-catalyzed ammonia production developed by Nishibayashi [691,693–695].



**Scheme 78.** Catalytic cycle for the dinitrogen-bridged catalyst 90 proposed by the groups of Yoshizawa and Nishibayashi [692].

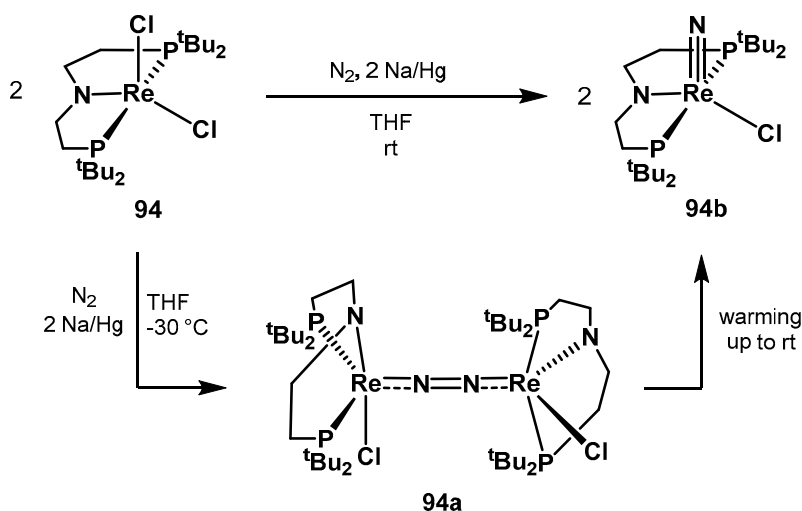
In 2017, Schneider reviewed in depth the mechanism of  $\text{N}_2$  bond activation catalyzed by mid to late transition metal complexes [696]. The same author reported the molybdenum complex 93 and demonstrated the nitrogen activation following the procedure shown in Scheme 79 [697]. The reaction proceeds by reduction of 93 and formation of the diatomic species 93a, which later undergoes protonation in Brønsted acid conditions, resulting in the formation of two corresponding nitrides (93b) and formal dinitrogen cleavage. The authors investigated the mechanism of the reaction in depth by means of DFT calculations, NMR spectroscopy, cyclic voltammetry, MO theory, as well as

X-ray diffraction analysis in order to elucidate the unexpected protonation step as the driving force to nitrogen splitting.



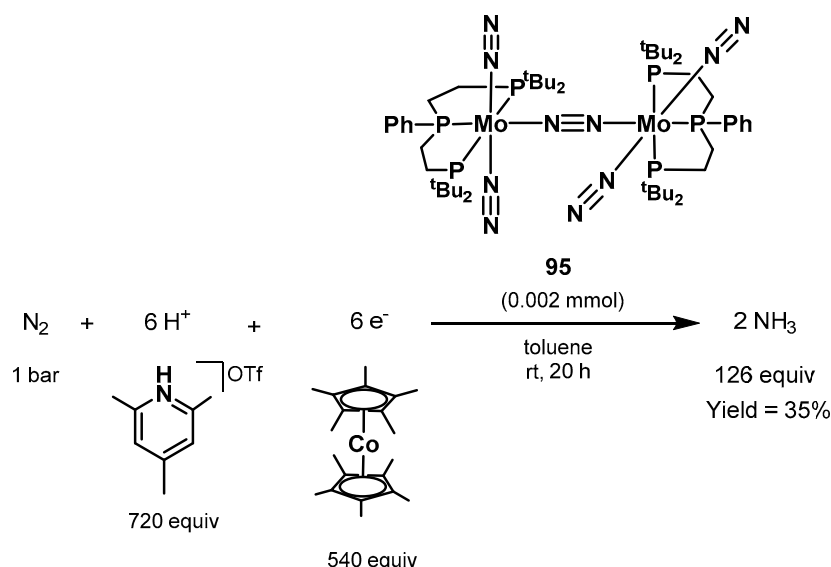
**Scheme 79.** Molybdenum complex proposed by Schneider for catalytic  $N_2$  splitting [697].

In 2018, the same author performed a systematic investigation on the mechanism of both chemical and electrochemical  $N_2$  splitting, using the rhenium system reported in 2014 [698], and shown in Scheme 80, as an archetypal pincer halide precursor for  $N_2$  cleavage [699]. By means of electrochemical data and computational studies, the authors elucidated the rhenium-catalyzed  $N_2$  activation, up to the final splitting step. The reaction proceeds through formation of the dinuclear species **94a**, which undergoes N-N bond cleavage resulting in two rhenium nitrido complexes. A comproportionation between  $Re^I/Re^{III}$  states was found to be the driving force of the electrochemical splitting, while a  $Ru^{II}$  specie represents the binding state of nitrogen and at the same time cause of the main deactivation pathways. In another work, Schneider reported an innovative approach for the synthesis of acetonitrile using dinitrogen and ethyl triflate catalyzed by complex **94** [700]. The authors demonstrated the feasibility of the catalytic cycle by means of  $^{15}N$ -labeled samples with consequent production of  $^{15}N$ -labeled acetonitrile, accompanied with efficient recovery of the rhenium catalyst. The work offers new insights on the possibility of forming C-N triple bonds after  $N_2$  splitting, expanding the possible applications derived from  $N_2$  splitting to organic transformations.



**Scheme 80.** First example of rhenium-catalyzed ammonia production developed by Schneider [699].

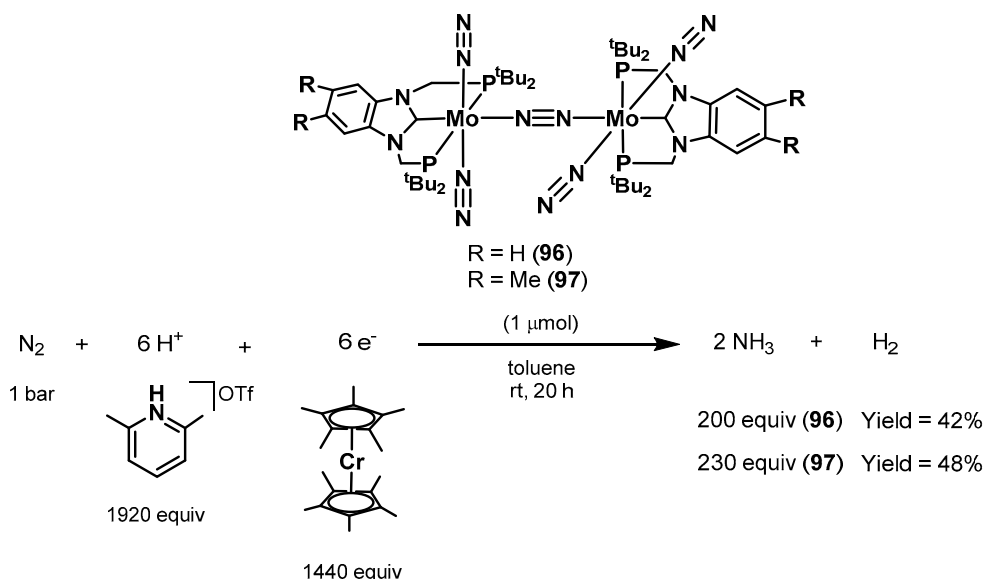
With the purpose of increasing the stability of the first generation Mo-PNP catalyst, Nishibayashi showed new dinitrogen-bridged PPP pincer catalysts for nitrogen fixation [701]. The authors tested new alternatives for the pincer moiety after noticing how the deactivation of the catalyst in the previous reported works was mainly due to the dissociation of the PNP ligand, observed in solution at completed reaction. Using the Mo-PPP catalyst **95**, it was possible to increase the ammonia production up to 126 equivalents, with the reaction conditions showed in Scheme 81. This result represents an improvement with respect to the first Nishibayashi catalyst **90** with five times higher activity.



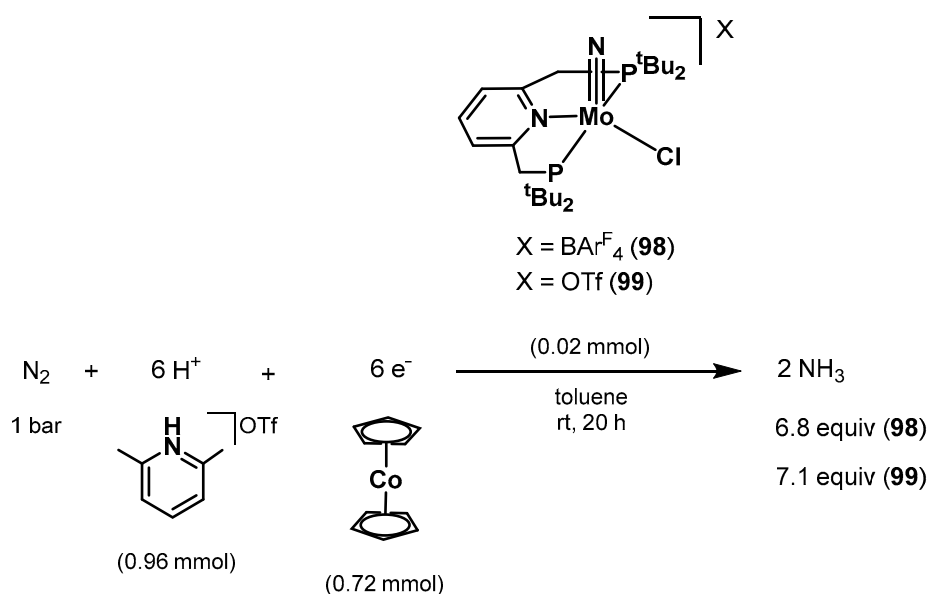
**Scheme 81.** Mo-PPP dinitrogen complex **95** developed by Nishibayashi [701].

In 2017, the same author reported remarkable activities toward nitrogen fixation by new molybdenum complexes bearing NHC-based PCP-pincer ligands [702]. Both catalysts **96** and **97** resulted in improved catalytic activity; the reaction afforded 200 and 230 equivalents of ammonia using **96** and **97**, respectively. The yield of ammonia was 48% with **97** and 42% with **96**, with yields in  $\text{H}_2$  of 18% and 14% (based on  $\text{CoCp}^*$ ), respectively (Scheme 82). The authors postulated that the higher performance of **97** is given by an increased back donating ability of the molybdenum centers in the presence of two methyl groups to the benzimidazol-2-ylidene skeleton of the PCP ligand, resulting in enhanced activation of the terminal dinitrogen ligands compared to the previously shown complexes. In addition, the authors performed stability tests in order to compare the first generation Mo-PNP complex **90** with the new PCP ligand synthesized in this study. In this report, the PCP ligand was not observed in solution after the reaction, indicating a higher resistance to dissociation, and the residual presence of the active species. Indeed, after the first 47 equivalents of  $\text{NH}_3$  produced, with complex **96** it was possible to feed the reaction adding more  $\text{CoCp}^*$  and  $[\text{LuH}]\text{OTf}$  resulting in further 69 equivalents of ammonia produced after two extra hours. Encouraged by these findings, the authors reported the synthesis of the PCP ligand on larger scale, as well as its consequent complexation with rhodium, nickel, and iridium accompanied by X-ray crystal structure analysis of the obtained complexes [703].

Nishibayashi also showed novel synthesis procedures for the preparation of new molybdenum(V)-nitride complexes as suitable catalysts for nitrogen fixation [704]. In this report, the reaction was performed under ambient reaction temperatures, using toluene as solvent, 0.020 mmol of the catalyst,  $[\text{LuH}]\text{OTf}$  (0.96 mmol) as proton source, and  $\text{CoCp}_2$  (0.72 mmol) as reductant. The use of **98** and **99** afforded the best results among the prepared catalysts, yielding 6.8 and 7.1 equivalents of  $\text{NH}_3$ , respectively (Scheme 83).



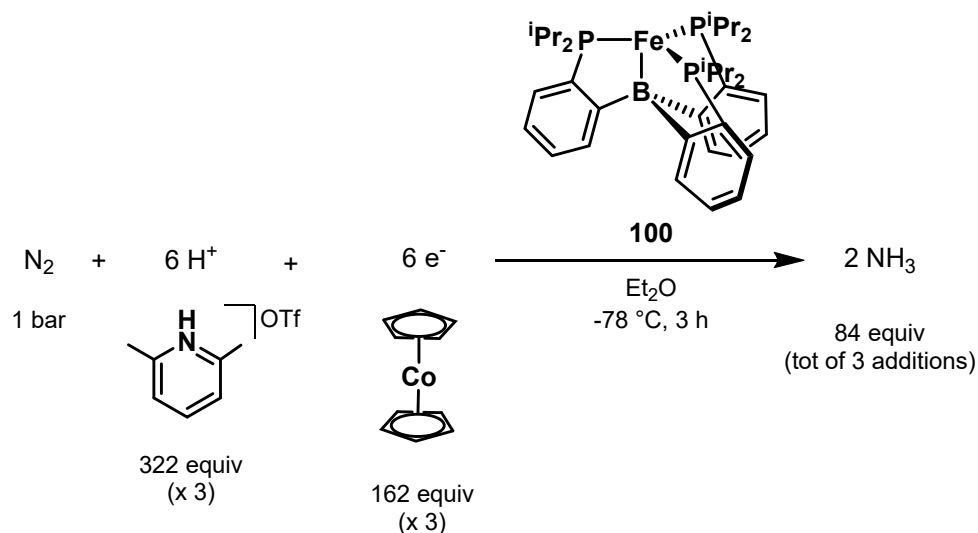
**Scheme 82.** Mo-PCP dinitrogen-bridged catalysts developed by Nishibayashi [702].



**Scheme 83.** Catalytic reduction of dinitrogen into ammonia by molybdenum-nitride complexes reported by Nishibayashi [704].

Nishibayashi suggested that in the homogeneous catalytic systems based on the molybdenum complexes showed previously, the bimetallic structure facilitates the dinitrogen conversion into ammonia in comparison to the corresponding monometallic complexes, because of the through-bond interactions between the two metal centers [692]. Tian investigated the chain-like extended models of Nishibayashi's catalyst by computational studies [705]. The effect of the dimension and the types of bridging ligands on the catalytic activities over nitrogen fixation were examined in the study. Polynuclear chains bearing four ([Mo]<sub>4</sub>) increased the catalytic activity when compared to the mono and bimetallic species, and carbide showed to be a more effective bridging ligand than N<sub>2</sub> regarding electronic charges dispersion between metal atoms, hence favoring the resulting catalytic cycle. The authors concluded that catalytic systems for the conversion of N<sub>2</sub> into NH<sub>3</sub> become more efficient with the extension of the polynuclear chain up to a proper size, combined with a suitable bridging ligand to facilitate charge dispersion between the metal centers.

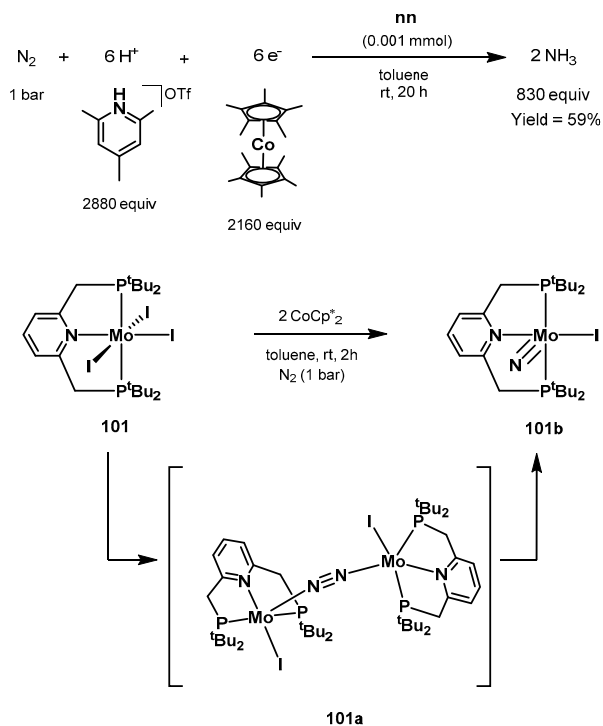
Inspired by the naturally occurring nitrogen fixation by nitrogenase, Peters investigated in 2013 the ammonia fixation by synthesizing an iron model complex able to produce 7 equivalents of ammonia per catalyst [706]. In 2017 and 2018, an improved catalytic activity was reported by Peters; following the same approach, using the  $P_3^BFe$  catalyst **100** showed in Scheme 84 it was possible to achieve  $NH_3$  efficiently and with high turnover numbers [707,708]. The reactions were performed using  $CoCp_2$  (54 equivalents) as reductant and  $[Ph_2NH_2]OTf$  (108 equivalents) as the acid, in  $Et_2O$  as solvent, at  $-78\text{ }^\circ\text{C}$ , and for 3 h yielding up to 72% (for  $e^-$  delivery) and 13 equivalents of  $NH_3$  per Fe site. In another experiment, with increased amount of additives, it was possible to achieve a TON of 84 after two further additions of fresh reductant and acid after cooling the mixture to  $-196\text{ }^\circ\text{C}$  (Scheme 84). Freeze-quench Mössbauer spectroscopy under reaction conditions offered insights on the rate of the key step, as well as the formation of a borohydrido-hydrido complex as a resting state. In addition, the prospect of a proton-coupled electron transfer (PCET) under catalytic conditions was further supported by theoretical and experimental studies, demonstrating plausible explanations for the increased efficiency observed.



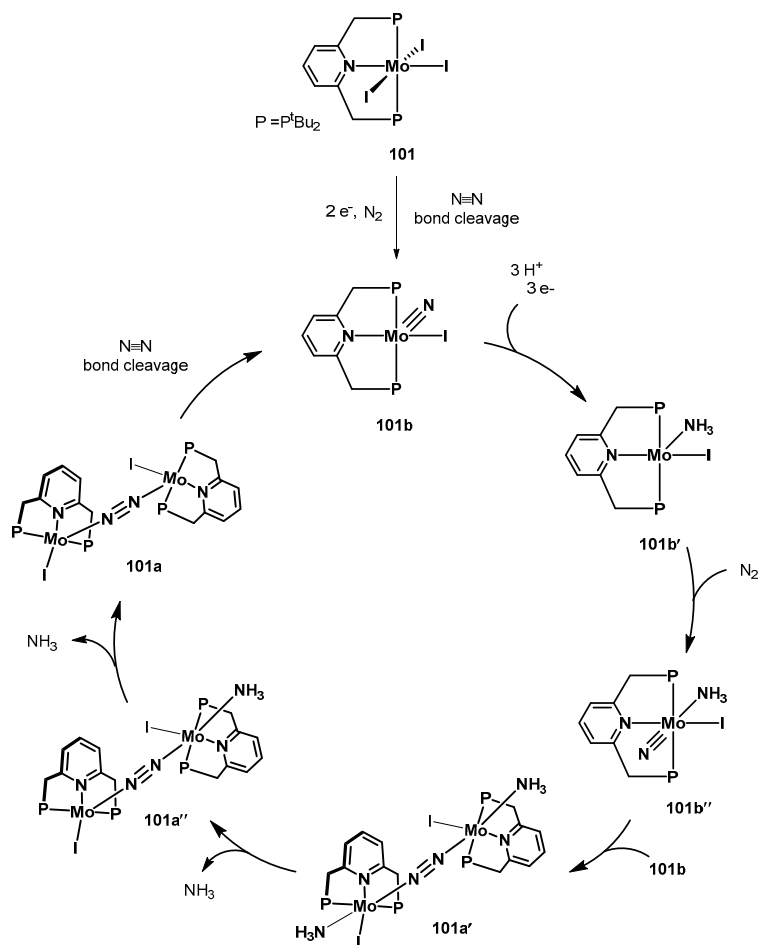
**Scheme 84.** Iron-catalyzed ammonia production developed by Peters using catalyst **100** [707].

In 2017, Nishibayashi reported the highest catalytic activity for nitrogen fixation using a molybdenum-iodide complex bearing a PNP pincer ligand [709]. The reaction performed under ambient reaction conditions, using 1 bar of  $N_2$ , 0.48 mmol of  $[Ph_2NH_2]OTf$  as proton source, in toluene, and using  $CoCp^*_2$  (0.36 mmol) as reductant and 0.001 mmol of Mo catalysts for 20 h afforded up to 830 equivalents of  $NH_3$  (415 equivalents of ammonia per Mo), as showed in Scheme 85. The generation of a dinitrogen-bridged di-molybdenum-iodide complex in the reaction is responsible for the higher activity due the direct cleavage of the nitrogen triple bond of the bridging ligand in the core (Scheme 85). Curiously, when a stoichiometric amount of iodine was added to the dinitrogen-bridged molybdenum complex **90**, the catalyst showed high catalytic activity, comparable to that of complex **101** and nitride complex **101b**. It was demonstrated that the ammonia is produced by the mononuclear nitride complex **101b**, thus encouraging further studies that resulted in the formulation of the new catalytic cycle depicted in Scheme 86 [709].



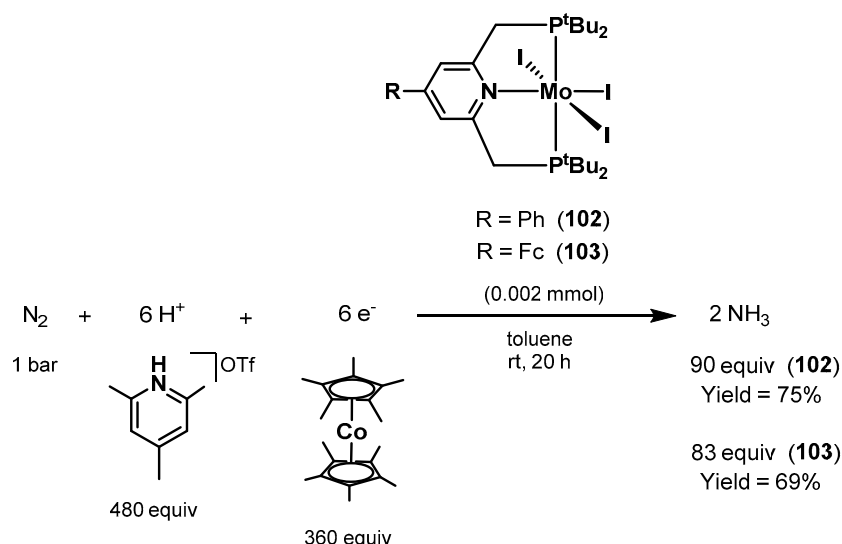


**Scheme 85.** Molybdenum-iodide complex **101** and conversion to **101b** by generation of the dinitrogen-bridged species **101a** showed by Nishibayashi [709].



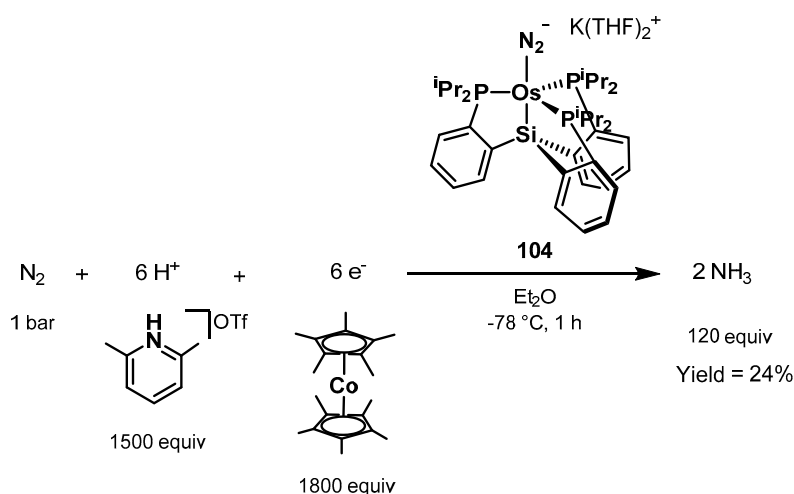
**Scheme 86.** Proposed catalytic cycle using the nitride complex **101** reported by Nishibayashi [709].

In 2019, Nishibayashi showed the synthesis of new molybdenum triiodide complexes bearing various substituents on the pyridine moiety of the PNP pincer ligand [710]. It was found that the catalytic activity toward nitrogen fixation increases with the introduction of Ph and Fc groups at the 4-position of the pyridine ring because of the electron withdrawing- and redox properties of the so-formed ligands. This observation is in contrast with the experimental results obtained with the afore-mentioned di-nuclear molybdenum species [693]. The work also confirms the preference of molybdenum systems for iodide ligands, performing better than the bromide or chloride congeners. The catalytic activity of the two selected complexes is shown in Scheme 87.



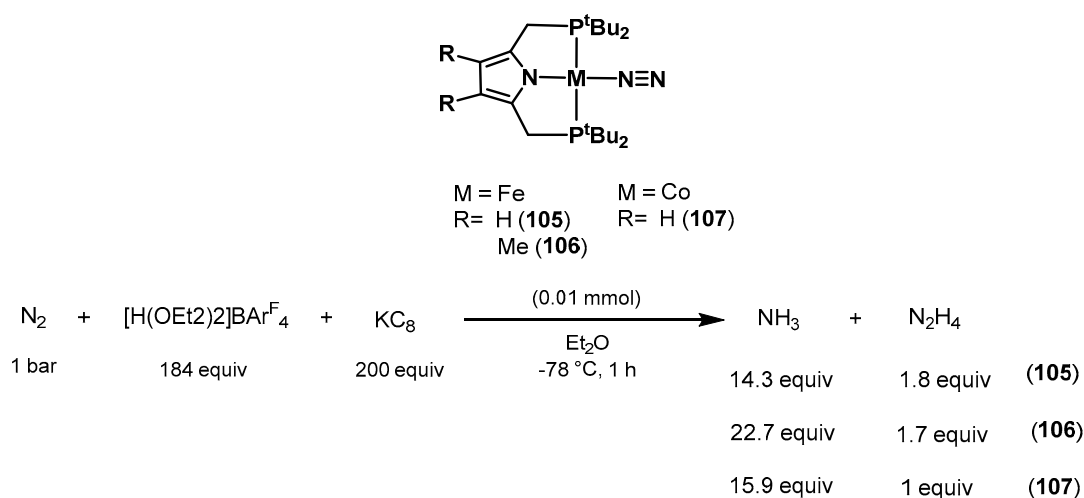
**Scheme 87.** Molybdenum triiodide complexes bearing various substituted PNP pincer ligands reported by Nishibayashi [710].

Peters also continued his studies on the topic and reported in 2017 an improved catalytic ammonia production employing new ruthenium and osmium complexes [711]. While the ruthenium catalysts tested in the study were found to be poorly active (4.3 equivalents of ammonia produced), using osmium catalyst **104** for the reaction afforded up to 120 equivalents of ammonia with high loadings of CoCp<sub>2</sub> and [HNPh<sub>2</sub>]OTf as reductant and proton source, respectively (Scheme 88). In 2015, Peters explored the same transformation using a cobalt congener of catalyst **104**, which performed scarcely in ammonia production resulting in only 2.4 equivalents of NH<sub>3</sub> [712].



**Scheme 88.** Osmium-catalyzed nitrogen fixation developed by Peters [711].

After the preliminary works by Peters, Nishibayashi explored the reactivity of iron metal complexes for nitrogen fixation as well, reporting the synthesis of Fe, Mo, and Cr azaferrocene-based PNP-type pincer ligands [695]. In 2017, Nishibayashi proposed iron–dinitrogen complexes bearing an anionic PNP pincer ligand for the catalytic nitrogen fixation producing ammonia and hydrazine [713]. 1 atm of molecular dinitrogen,  $\text{KC}_8$  (40 equivalents) as reductant,  $[\text{H}(\text{OEt}_2)_2]\text{Bar}^{\text{F}}_4$  (38 equivalents) as proton source, 0.010 mmol of catalyst,  $\text{Et}_2\text{O}$  or THF as solvent, and at  $-78^\circ\text{C}$  for 1 h were used as conditions for the conversion to ammonia and hydrazine up to 14.3 equivalents and 1.8 equivalents respectively. The best result was obtained using catalyst **105** (Scheme 89). Later, the authors succeeded in improving the catalytic activity of this family of catalysts by proposing a new complex bearing the anionic methyl-substituted pyrrole-bases PNP ligand [714]. As shown in Scheme 89, catalyst **106** afforded 22.7 equivalents of ammonia per catalyst under the same reaction conditions.

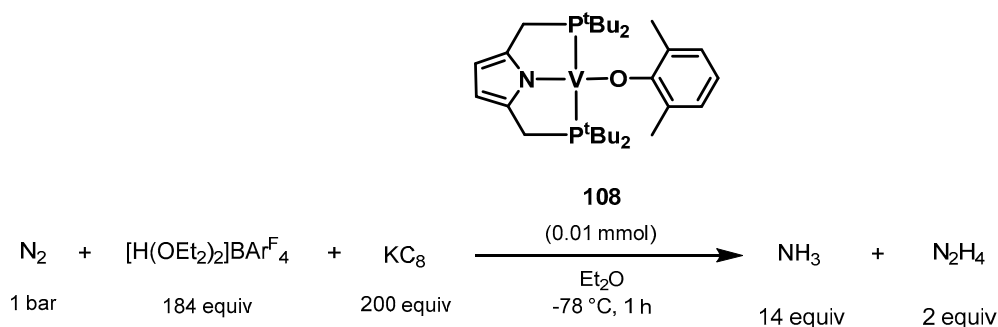


**Scheme 89.** Nitrogen fixation catalyzed by iron- and cobalt-PNP complexes by Nishibayashi [713–715].

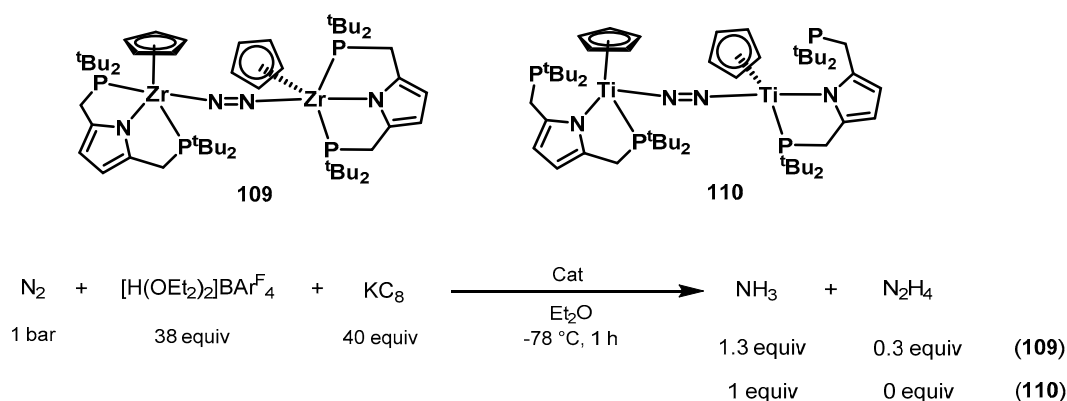
In addition to iron, Nishibayashi also showed the first successful example of cobalt-catalyzed nitrogen fixation [715]. Catalyst **107** showed catalytic activity similar to its iron congener, affording 15.9 equivalents of ammonia under the same reaction conditions (Scheme 89). Interestingly, when a cobalt catalyst bearing a PBP ligand was employed in the transformation, only 0.4 equivalents of ammonia were produced, indicating a relevant contribution of the PNP ligand to the catalytic activity.

In 2018, Nishibayashi designed and prepared novel vanadium complexes containing anionic pyrrole-based PNP pincer complex and aryloxy ligands, and tested them in the direct conversion of molecular dinitrogen into ammonia and hydrazine [716]. The reaction was performed using 200 equivalents of  $\text{KC}_8$  as reductant, 184 equivalents of  $[\text{H}(\text{OEt}_2)_2]\text{Bar}^{\text{F}}_4$  as proton source,  $\text{Et}_2\text{O}$  as solvent, at  $-78^\circ\text{C}$  for 1 h. The reaction afforded up to 14 equivalents of ammonia and 2 equivalents of hydrazine when a mixture of catalyst **108** was employed (Scheme 90). Remarkably, this work represents the first example of vanadium-catalyzed nitrogen fixation, a step toward the understanding of the reaction mechanism involving the FeV nitrogenase active site. In addition, the authors synthesized the dinitrogen-bridged version of **108**, which afforded 4.6 equivalents of  $\text{NH}_3$  per vanadium.

Contemporarily, the same author also explored the synthesis of novel dinitrogen-bridged species, reporting a new class of dinitrogen-bridged di-titanium and di-zirconium complexes with anionic pyrrole-based PNP pincer complexes for the conversion of dinitrogen into ammonia and hydrazine [717]. The best result was achieved using a mixture of catalyst **109**, with 40 equivalents of  $\text{KC}_8$  as reductant, 38 equivalents of  $[\text{H}(\text{OEt}_2)_2][\text{Bar}^{\text{F}}_4]$  as proton source,  $\text{Et}_2\text{O}$  as solvent, and at  $-78^\circ\text{C}$  for 1 h yielding up to 1.3 equivalents of ammonia and 0.31 equivalents of hydrazine (Scheme 91). Under the same reaction conditions, catalyst **110** afforded 1 equivalent of ammonia, with no hydrazine.

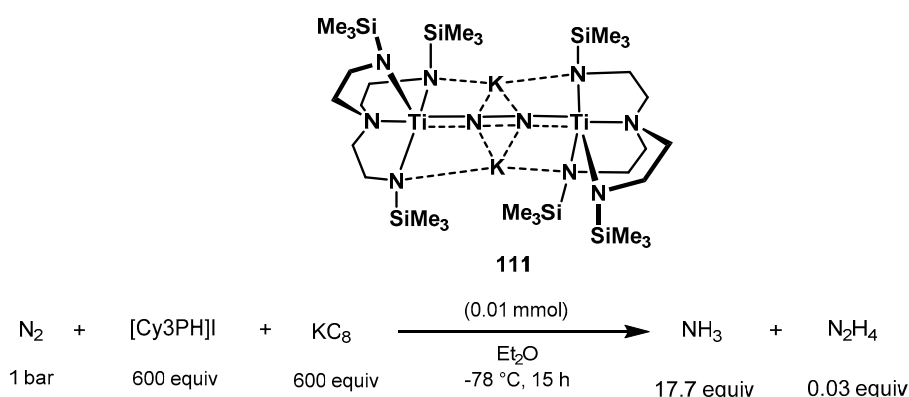


**Scheme 90.** Vanadium PNP complex for dinitrogen conversion into ammonia and hydrazine reported by Nishibayashi [716].



**Scheme 91.** Dinitrogen-bridged di-titanium and di-zirconium complexes bearing pyrrole-based anionic PNP pincer ligands synthesized by Nishibayashi [717].

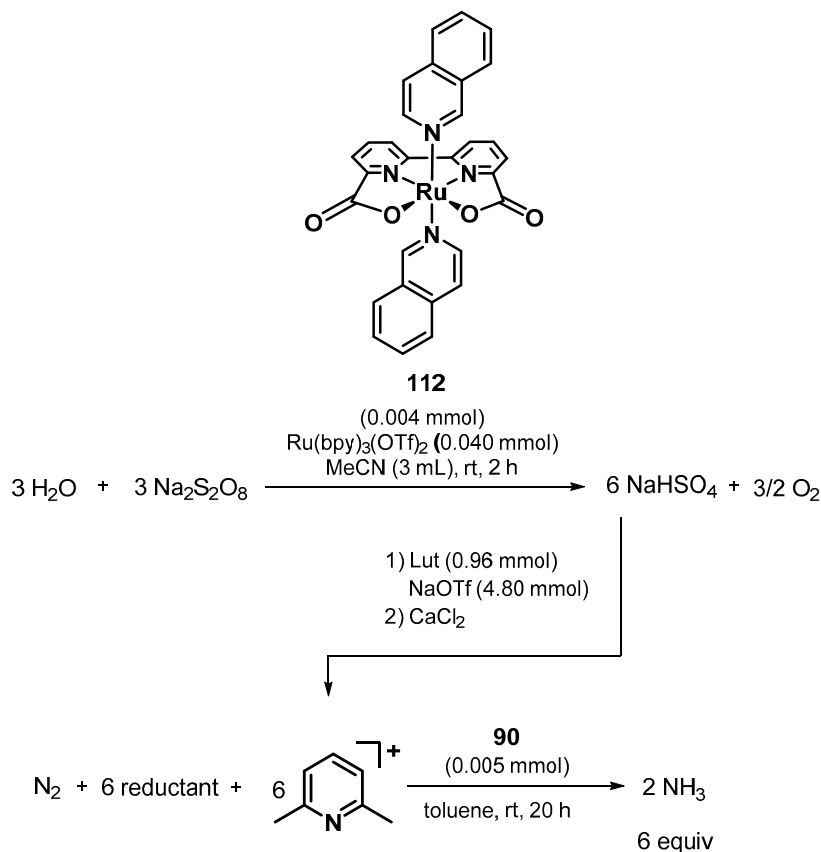
Improved results using a di-titanium species have been achieved by Liddle using catalyst 111 [718]. After screening reaction conditions and additives, the reaction afforded up to 9 equivalents of ammonia per titanium atom using  $[\text{Cy}_3\text{PH}]\text{I}$  as proton source and  $\text{KC}_8$  as reductant, notably with higher selectivity and only traces of hydrazine as the co-product (Scheme 92).



**Scheme 92.** Di-titanium catalyst 111 reported by Liddle for nitrogen fixation [718].

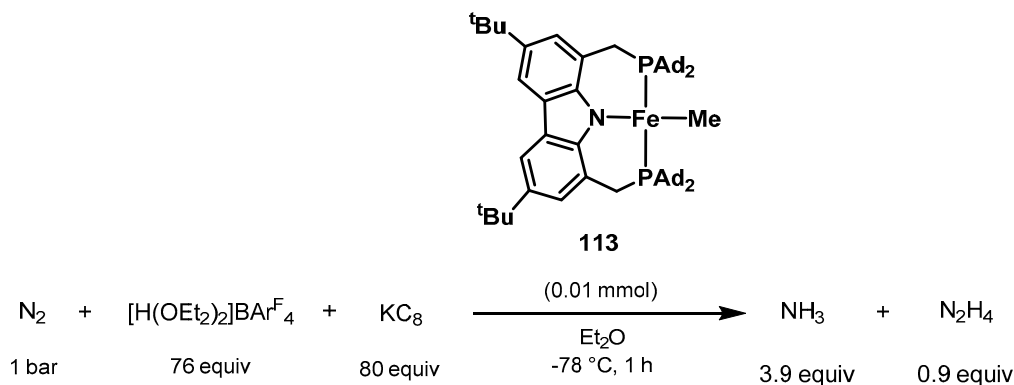
Nishibayashi also showed an example of nitrogen fixation using a proton source obtained in situ by means of a ruthenium-catalyzed oxidation of water promoted by a photosensitizer (Scheme 93) [719]. In the proposed method, the oxidation of water occurs using  $\text{Na}_2\text{S}_2\text{O}_8$  as a sacrificial oxidizing agent, a suitable ruthenium catalyst for water oxidation (**112**) and  $\text{Ru}(\text{bpy})_3(\text{OTf})_2$  ( $\text{bpy} = 2,2'$ -bipyridine) as the photosensitizer. After 2 h of irradiation of visible light at room temperature, the reaction afforded 99%

conversion into  $O_2$ . 2,6-Lutidine and sodium trifluoromethanesulfonate (NaOTf) were added to the reaction in order to obtain  $[LutH]^+$  to be used in the following step;  $CoCp_2$  was used as the reducing agent to promote the conversion of dinitrogen gas into in the presence of catalyst **90** (0.005 mmol) under ambient reaction conditions, resulting in a total of 6 equivalents of ammonia released.



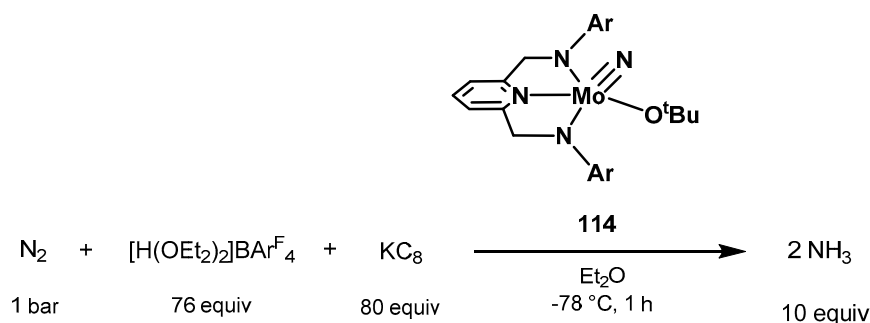
**Scheme 93.** Nishibayashi's catalytic reduction of dinitrogen into ammonia using an in situ proton source and catalyzed by the molybdenum complex **90** [719].

Nishibayashi reported the synthesis of a range of iron-methyl complexes containing anionic carbazole PNP ligands [720]. Bulkier substituents such as adamantyl groups at the phosphorus atoms showed better catalytic activity toward nitrogen fixation. The reaction using catalyst **113**, 1 bar of  $N_2$ , 80 equivalents of  $KC_8$  as reductant, 76 equivalents of  $[H(OEt_2)_2]BAr_4^F$  as proton source, in  $Et_2O$ , at  $-78^\circ C$  afforded up to 4.8 equivalents of fixed nitrogen as a mixture of ammonia and hydrazine after 1 h (Scheme 94).



**Scheme 94.** Nitrogen fixation catalyzed by the iron PNP complex **113** proposed by Nishibayashi [720].

In 2017, Schrock reported the synthesis and the catalytic activity of the  $[\text{Ar}_2\text{N}_3]\text{Mo}(\text{OtBu})$  complex **114** as catalyst for the reduction of dinitrogen to ammonia [721]. The reactions were performed in a mixture of **114** in diethyl ether as solvent, 108 equivalents of  $\text{CoCp}^*_2$  as reductant, 120 equivalents of  $[\text{Ph}_2\text{NH}]\text{OTf}$  as proton source, at temperatures between  $-78^\circ\text{C}$  and  $22^\circ\text{C}$ , achieving up to 10 equivalents of  $\text{NH}_3$  per Mo atom, as depicted in Scheme 95. The authors were not able to demonstrate whereas the *t*Bu group remain intact during the catalytic cycle, or if it is transformed into an OH or an oxo ligand after protonation from  $[\text{Ph}_2\text{NH}]\text{OTf}$ .



**Scheme 95.** Dinitrogen conversion into ammonia catalyzed by the Mo-NNN complex **114** showed by Schrock [721].

Szymczak studied the incorporation of two 9-borabicyclo[3.3.1]-nonyl substituents within the secondary coordination sphere of the Fe(II)-NNN pincer complex **115** [722]. The inserted groups act as a Lewis acidic site and allow the coordination of one or two equivalents of hydrazine, as well as stabilization of Fe-NH<sub>2</sub> intermediates (**116** in Figure 7). Later, by addition of  $[\text{HNEt}_3][\text{Cl}]$ , a species with two molecules of ammonia bound to the boron groups was isolated and characterized by single-crystal diffraction studies. Finally, the release of ammonia is achieved with contemporary coordination of a new molecule of hydrazine.

Holland and Mayer studied the protonation, and subsequent reduction of the ruthenium and iridium pincer complexes **117a** and **117b** to investigate their reactivity toward the activation of dinitrogen [723]. The stretching frequencies of  $\text{N}_2$  in the complexes **117a** and **117b** showed little activation of the dinitrogen ligand. Later, by means of NMR spectroscopy and cyclic voltammetry, the authors tested the reactivity of the prepared catalysts, however with no positive results in terms of catalytic ammonia production. The protonation, which is a fundamental step in the electrochemical reduction of dinitrogen, results in the formation of cationic metal-hydrides that lose  $\text{N}_2$  preventing any further functionalization. Reduction of the metal-hydride with  $\text{CoCp}_2^*$  also results in fast disproportionation to Ir(II) species, preventing any nitrogen coordination at room temperature (Scheme 96).

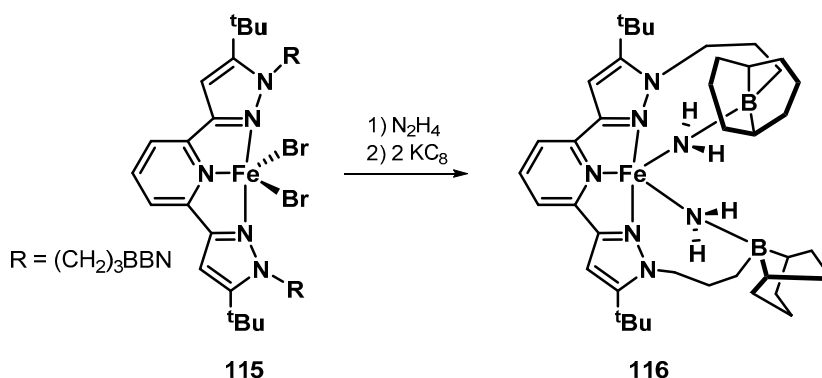
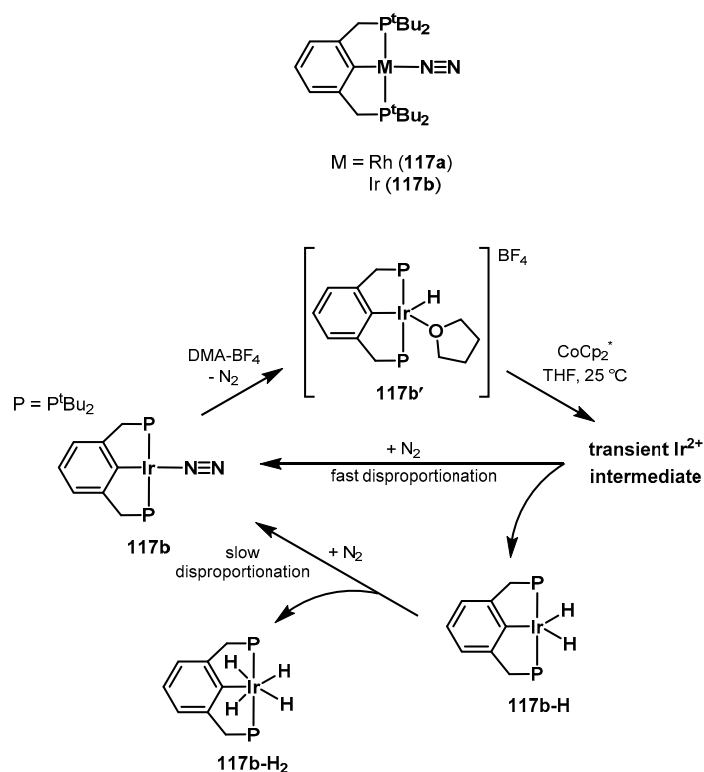
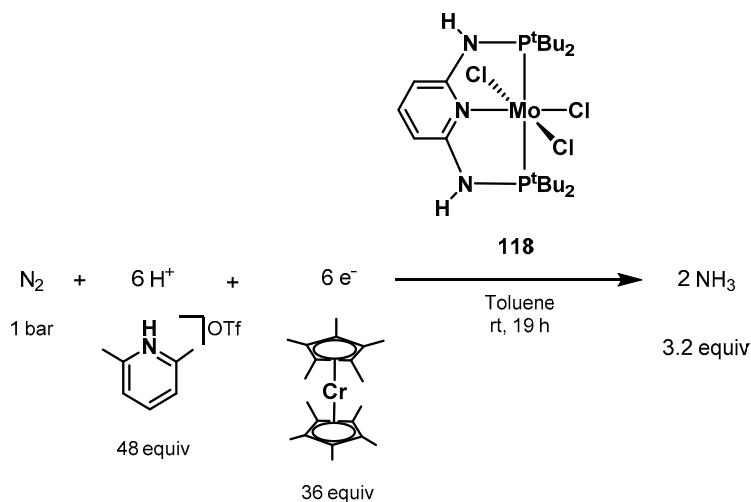


**Figure 7.** Szymczak's Fe(II)-NNN pincer complex **115** coordinates one to two equivalents of hydrazine [722].



**Scheme 96.** Ruthenium and iridium PCP pincer complexes tested by Holland and Mayer and reactivity of complex **117b** in the presence of proton source and reducing agents [723].

Tuczek reported in 2018 new molybdenum complexes bearing a  $\text{PN}^3\text{P}$  pincer ligand with various substituents on both metal center and pincer arms [724]. The authors investigated the reactivity with  $\text{N}_2$  through the formation of dinitrogen-bridged species based on the classic Nishibayashi Mo-PNP catalysts showed before. It was found that the nature of the substituents has a strong influence on the reactivity toward dinitrogen; the reaction performed with 48 equivalents of [LutH]OTf and 36 equivalents of  $\text{CrCp}_2^*$  afforded poor catalytic activity with most of the tested catalyst candidates. Only when 0.01 mmol of complex **118** were applied, it was possible to achieve 3.12 equivalents of ammonia per catalyst (Scheme 97).

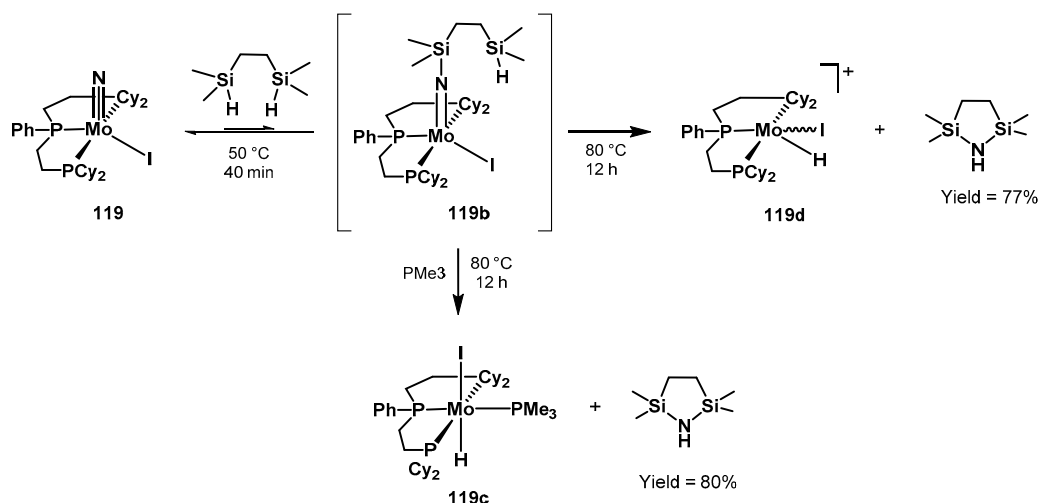


**Scheme 97.** Catalytic ammonia production catalyzed by complex **118** as showed by Tuczek [724].



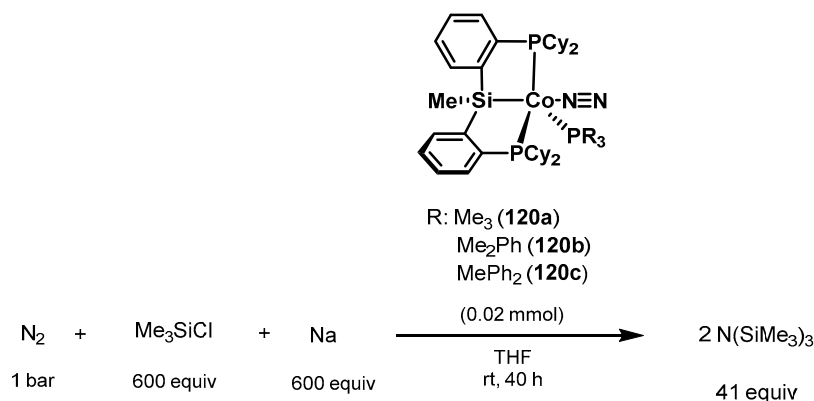
Dinitrogen can be also reduced and trapped into in the form of silylamines, from which ammonia can be easily released after hydrolysis. Preliminary studies on the topic date back to 1972 with the work of Shiina [725], and later Hidai in 1989 [726]. Many other reports explored the transformation up to recent days using molybdenum [727], iron [728,729], vanadium [730], titanium [731,732], as well as cobalt homogeneous catalysts [733–737]. A comprehensive review from Nishibayashi recently covered the catalytic silylation of dinitrogen into silylamines as precursors for ammonia production [738].

With regard to the most recent publications involving pincer ligation, Mézailles reported in 2016 the Mo-PPP complex **119** for the reduction of ammonia to silylamines in the presence of silanes [739]. Similar to the previously showed species, catalyst **119** can be obtained starting from a chlorido precursor through formation of a dinitrogen-bridged species, followed by nitrogen splitting and formation of the nitrido species. Catalyst **119** is then able to react with the bis-silane under mild reaction conditions, resulting in high yields of the corresponding amine (Scheme 98). However, the authors could not achieve the final reduction step from Mo(II) to Mo(I) to regenerate the dinitrogen-bridged specie from **119d**, required to finish a catalytic cycle.



**Scheme 98.** Catalytic silylation of dinitrogen to silylamine proposed by Mézailles [739].

In 2017, Nishibayashi designed and prepared iron and cobalt-dinitrogen complexes containing a PSiP ligand, and tested them as catalysts for the transformation of dinitrogen gas into silylamine [740]. 1 bar of molecular dinitrogen, 600 equivalents of Na as reductant, MeSiCl (600 equivalents) as silylating reagent in THF at room temperature for 40 h yielded up to 41 equivalents of NH<sub>3</sub> when employing 0.020 mmol of catalyst **120c** (Scheme 99).



**Scheme 99.** Cobalt-catalyzed silylation of N<sub>2</sub> reported by Nishibayashi [740].

### 3.3. Valorization of Biomass-Derived Compounds

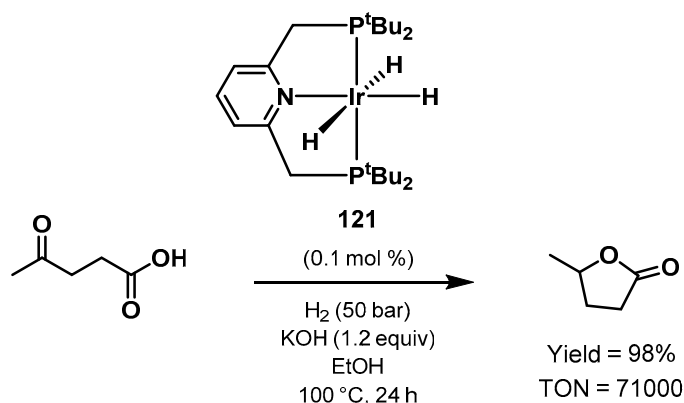
Catalytic hydrogenation is a powerful tool for the valorization of biomass-derived compounds into valuable fuels and bulk chemicals for the industry, such as monomers for polymer production, bio-fuels, and additives [741–750]. Among the others, levulinic acid (LA) and  $\gamma$ -valerolactone (GVL) can be readily obtained from biomass by acid treatment of sugar monomers, such as glucose, fructose, and sucrose, representing versatile platform molecules for the bulk industry [751–759], as highlighted by Horvath in 2008 [760]. The use of pincer complexes for this type of transformations is relatively new, but again showing promising performances and allowing the useful hydrogenation of esters, carboxylic acids and aldehydes at mild reaction conditions [761,762].

Various groups reported the use of ruthenium precursors in the presence of different ligands for the hydrogenation of biogenic acids to useful building blocks [763–767]. However, most of the reports use high temperatures (>200 °C) and strong acidic conditions to achieve acceptable yields. Important results using Ru/Triphos combinations were achieved by Leitner [577,768–771], as well as by Beller [772–774] for the hydrogenation of several bio substrates. Milstein employed catalyst **24-H** for the efficient hydrogenation of cyclic di-esters, e.g., biomass-derived glycolide and lactide, to 1,2-diols [775].

The hydrogenation of levulinic acid has been reported by Leitner and Klankermayer [768], Fu [776], and Fischmeister [777], using iridium complexes, as well as by Garcia, who reported the precatalyst [(dtbpe)PdCl<sub>2</sub>] (dtbpe = 1,2-(bis-di-tert-butylphosphino)ethane) to efficiently catalyze LA hydrogenation, as well as formic acid dehydrogenation to CO<sub>2</sub> and H<sub>2</sub> [778].

In 2015, Singh showed the conversion of several biomass-derived substrates, such as furfural, 5-hydroxymethylfurfural (HMF), and 5-methylfurfural (5-MF), into levulinic acid and diketones, 1-hydroxyhexane-2,5-dione (1-HHD), 3-hydroxyhexane-2,5-dione (3-HHD), and hexane-2,5-dione (2,5-HD) [779]. The reaction proceeds in the presence of formic acid and it is highly dependent on the choice of the ligand, as well as formic acid concentration, reaction temperature and time. The authors screened different Ru(II)-arene catalysts bearing ethylenediamine-based bidentate ligands. Applying 5 mol% of the catalyst, in water at 100 °C, various substrates were quantitatively converted into the corresponding ring-opened products.

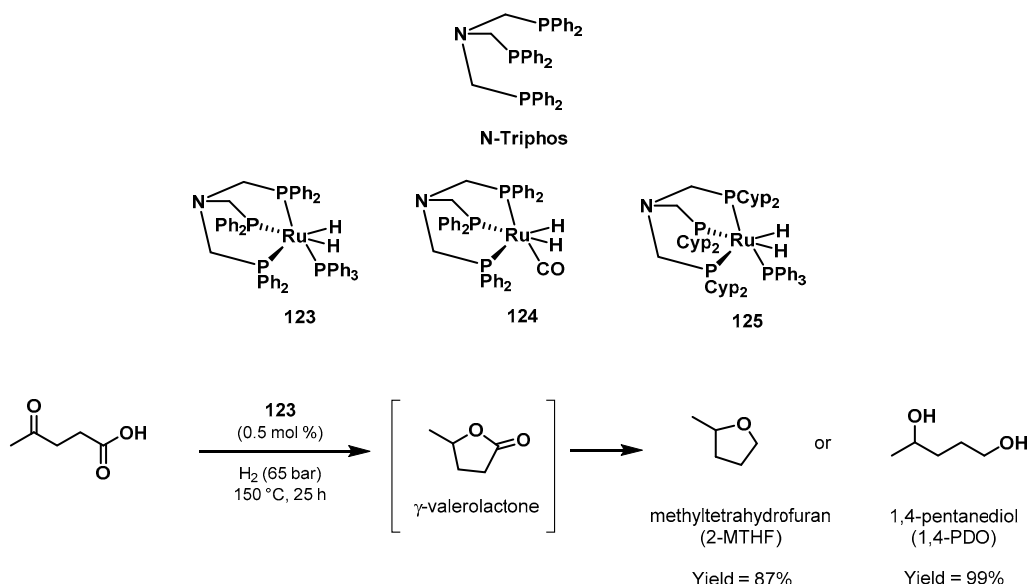
With regard to pincer complexes, in 2012 Zhou used the trihydride iridium complex **121** for the hydrogenation of levulinic acid to  $\gamma$ -valerolactone (Scheme 100) [780]. In this sense, Chen used in 2015 density functional theory (DFT) calculations to investigate the mechanism of this transformation catalyzed by Ir-PNP complexes [781].



**Scheme 100.** Iridium-catalyzed hydrogenation of levulinic acid to  $\gamma$ -valerolactone proposed by Zhou [780].

Long and Miller reported the efficient conversion of levulinic acid to either 1,4-pentandiol (PDO) or 2-methyltetrahydrofuran (2-MTHF) using ruthenium complexes bearing a modified Triphos ligand with a nitrogen central atom (Scheme 101) [782]. Catalyst **123** performed best in both transformations,

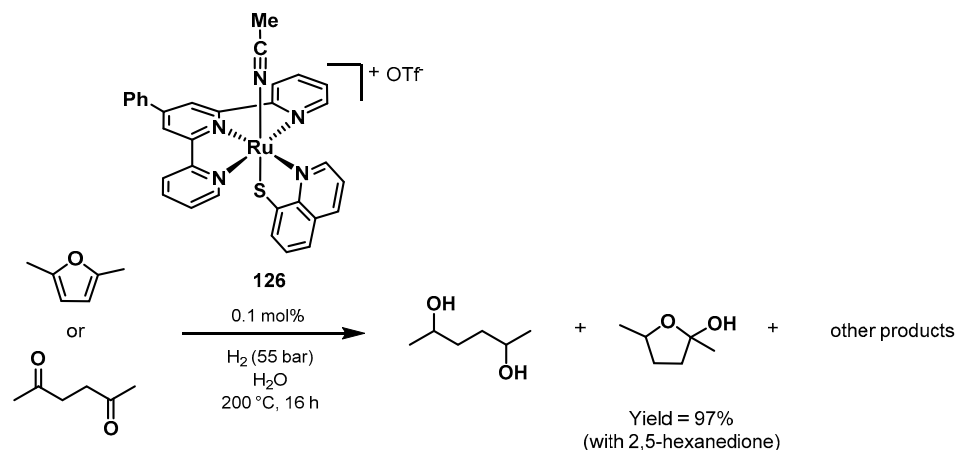
affording quantitative yields in PDO and 2-MTHF. The active species was formed in situ with 0.5 mol% of  $[\text{Ru}(\text{acac})_3]$  as the metal precursor, 1.0 mol% of N-Triphos, under 65 bar of hydrogen, with no solvent at 150 °C for 25 h. The reaction with these conditions afforded 99% yield of PDO (with 1% of  $\gamma$ -valerolactone). When 5 mol% of  $\text{HN}(\text{Tf}_2)$  was added as additive, and THF as solvent, the selectivity of the reaction changed dramatically, resulting in 87% yield in 2-MTHF and 10% in  $\gamma$ -valerolactone.



**Scheme 101.** Hydrogenation of levulinic acid into 1,4-pentandiol (PDO) and 2-methyltetrahydrofuran (2-MTHF) showed by Long and Miller [782].

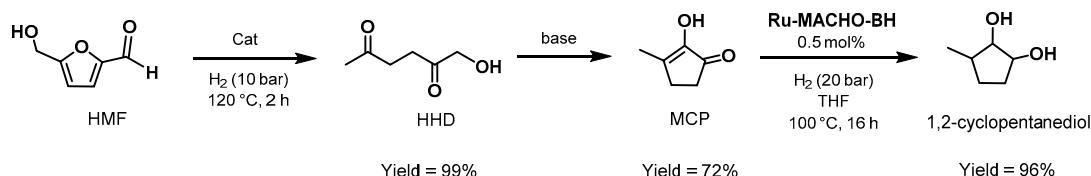
The year after, Deng and Palkovits showed the same transformations using Ru precursors and a modified version of N-Triphos, where an ethylene linker was substituted in one of the arms [783]. The reactions were performed in THF, with 1.5 equivalents of the novel ligand, 70 bar  $\text{H}_2$ , 160 °C, for 18 h. The selectivity was found to be highly dependent on the ruthenium precursor used (0.2 mol% Ru loading); when using  $[\text{Ru}(\text{acac})_3]$  as in the previous study by Miller, the reaction afforded 33% yield of GVL and 66% yield of PDO. Surprisingly, both  $[\text{Ru}(\text{acac})_3]$  and  $\text{RuH}_2(\text{PPh}_3)_4$  produced 99% and 95% yield in GVL respectively, when no ligand was added to the reaction mixture, while in the presence of the ethylated N-Triphos ligand,  $\text{RuH}_2(\text{PPh}_3)_4$  afforded 98% yield in PDO. With different combination of a Ru precursor and the new ligand, the authors successfully hydrogenated a series of biogenic acids; among other substrates, fumaric-, succinic-, itaconic-, and maleic acid were converted in high yields into the corresponding lactones at 170 °C and 70 bar  $\text{H}_2$  in 48 h.

In 2015, Schlaf showed the synthesis of various ruthenium pincer complexes in the form of  $[(40\text{-Ph-terpy})(\text{bipy})\text{Ru}(\text{L})](\text{OTf})_n$  and  $[(40\text{-Ph-terpy})(\text{quS})\text{Ru}(\text{L})](\text{OTf})_n$  ( $n = 0$  or 1 depending on the charge of L, L = labile ligand, e.g.,  $\text{H}_2\text{O}$ ,  $\text{CH}_3\text{CN}$  or  $\text{OTf}$ , bipy = 2,20-bipyridine, quS = quinoline-8-thiolate)) [784]. The authors tested the prepared complexes for the hydrogenation of the biomass derived substrates 2,5-DMF (2,5-dimethylfuran), obtainable from 5-hydroxymethylfurfural, and 2,5-hexanedione, the hydrolysis product of 2,5-dimethylfuran. The reactions were carried out in aqueous acidic medium and temperature between 175 and 225 °C, using complex **126** as the catalyst. It was possible to afford yields of hydrogenated products up to 97% (using 2,5-hexanedione) and 66% using 2,5-DMF. The yield in 2,5-hexanediol was 82% and 78% starting from 2,5-hexanedione and 2,5-dimethylfuran, respectively (Scheme 102).



**Scheme 102.** Water and high temperature stable hydrogenation pincer catalyst for biomass-derived substrates developed by Schlaf [784].

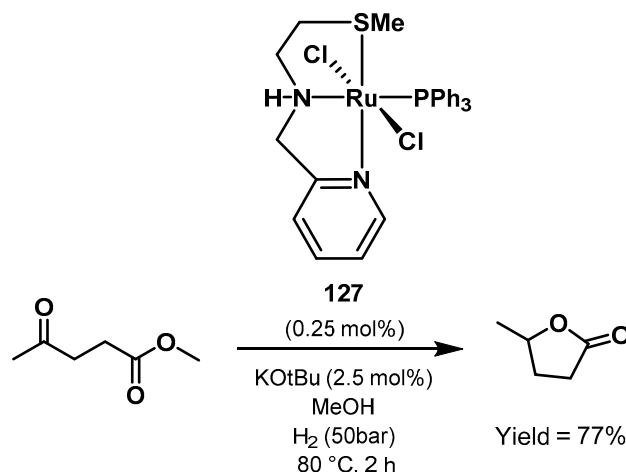
In 2018, de Vries reported a method for the transformation of HMF into 2-hydroxy-3-methylcyclopent-2-enone (MCP) using Ir and Ru complexes as catalysts [785]. The strategy involved the intramolecular aldol condensation of 1-hydroxyhexane-2,5-dione (HHD), as depicted in Scheme 99. The only pincer complex tested in this transformation was **Ru-MACHO-BH**, which afforded 93% of conversion of HMF with 0.5 mol% catalyst loading, 10 bar of  $\text{H}_2$  in water at 120 °C, however with only 5% yield of 1-hydroxyhexane-2,5-dione. On the contrary, when the authors explored the hydrogenation of MCP into valuable chemicals, **Ru-MACHO-BH** afforded full conversion of MCP into 3-Methyl-1,2-cyclopentanediol, which was isolated in 96% yield as a mixture of diastereomers after 16 h (Scheme 103). Recently, de Vries has reviewed the state-of-the-art of relevant sustainable transformations of 5-hydroxymethylfurfural involving 1-hydroxyhexane-2,5-dione as a key intermediate [786].



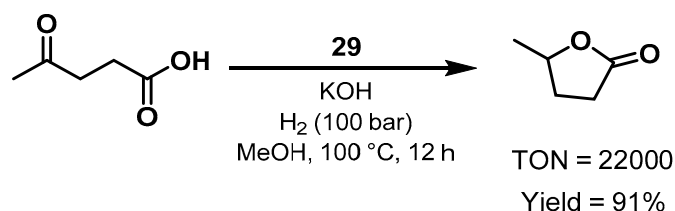
**Scheme 103.** Conversion of HMF to higher-value products showed by de Vries [785].

The same author also reported that the Ru-NNS complex **127** showed in Scheme 104 catalyzes the selective hydrogenation of methyl levulinate into  $\gamma$ -valerolactone [787]. The reaction was performed in methanol, with 0.25 mol% of **127**, 2.5 mol% of KOtBu, under 50 bar of  $\text{H}_2$  at 80 °C, affording 77% yield after 2 h (Scheme 104). In the same work, the authors explored the hydrogenation of a wide series of saturated- as well as  $\alpha,\beta$ -unsaturated esters. It was possible to hydrogenate  $\gamma$ -valerolactone affording the ring-opened product 1,4-pentanediol in 92% yield using 0.25 mol% of catalyst **127**, 2.5 mol% of KOtBu, under 60 bar of hydrogen, at 80 °C after 2 h.

In 2019, Song showed the hydrogenation of levulinic acid and methyl levulinate into  $\gamma$ -valerolactone catalyzed by the iron pincer complex **29** [788]. High TON and TOF up to respectively 23,000 and 1917  $\text{h}^{-1}$  could be achieved for the hydrogenation of levulinic acid. The best results were obtained using 0.002 mol% of catalyst **29** in the presence of methanol as solvent, 1 equivalent of KOH, under 100 bar, at 100 °C for 12 h (Scheme 105). The use of  $\text{H}_2\text{O}$  as solvent was also possible and afforded TON of 22,500 and TOF of 1875  $\text{h}^{-1}$ . When methyl levulinate was used under similar conditions,  $\gamma$ -valerolactone was obtained with TON up to 22,000 and TOF of 1833  $\text{h}^{-1}$ . With higher catalyst loading (10 mol%) it was possible to afford 91% and 81% yield in GVL from levulinic acid and methyl levulinate respectively. The authors also explored the dehydration of several carbohydrates to afford LA, which was subsequently converted into GVL in high yields.

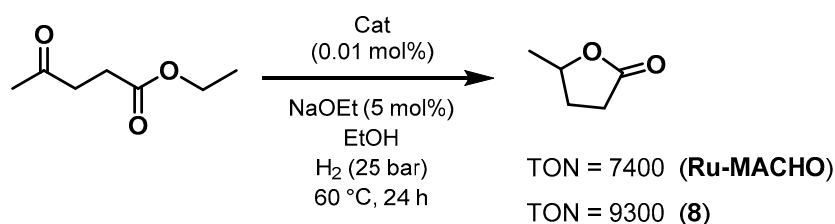


**Scheme 104.** Hydrogenation of methyl levulinate catalyzed by Ru-SNN catalyst **127** showed by de Vries [787].



**Scheme 105.** Hydrogenation of levulinic acid and methyl levulinate into  $\gamma$ -valerolactone showed by Song [788].

Recently, our group in collaboration with Paixão have demonstrated the efficient hydrogenation of alkyl levulinates to  $\gamma$ -valerolactone catalyzed by either ruthenium or iridium PNP catalysts, in the presence of small amount of base additive, and at low temperature and H<sub>2</sub> pressure [789]. Both catalysts **Ru-MACHO** and **8** (Scheme 2) were found to be active in the conversion of both methyl as well as ethyl levulinate into  $\gamma$ -valerolactone, without the need of solvent and also in large scale reactions. The hydrogenation of ethyl levulinate was carried out using 0.01 mol% of catalyst at 60 °C and under 20 bar of hydrogen. Turnover numbers of 7400 and 9300 were obtained using **Ru-MACHO** and **8**, respectively (Scheme 106). In addition, a scale-up experiment was performed with a combination of mild reaction conditions and low catalyst loading; whereas **Ru-MACHO** was found to be practically inactive under the same reaction conditions, 0.050 mol% (500 ppm) of **8** led to full conversion after 72 h at 25 °C (TON = 2000) using ethanol as alcohol additive. Full conversion was also obtained for methyl levulinate under the same conditions, but with methanol as the alcoholic additive. Finally, a recycling experiments was performed using 0.5 mol% of **Ru-MACHO**; four consecutive additions of ethyl levulinate every 20 h showed full conversion in each run without detectable deactivation of the catalyst. Catalyst **8** was found to be inactive under the recycling conditions.

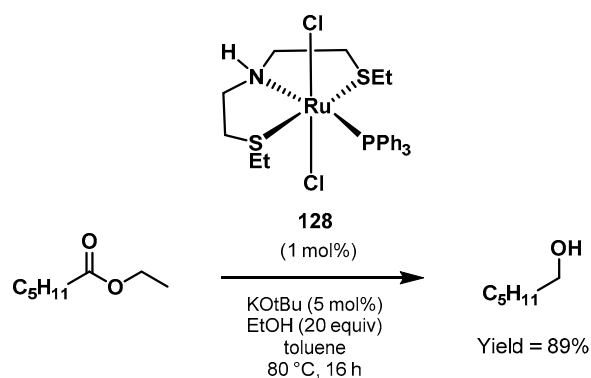


**Scheme 106.** Catalytic hydrogenation of ethyl levulinate to  $\gamma$ -valerolactone catalyzed by Ru- and Ir-PNP complexes at mild reaction conditions showed by Paixão and Nielsen [789].

### 3.4. Transfer Hydrogenation

Transfer hydrogenation reactions represent an elegant, sustainable strategy for the obtainment of molecules of higher complexity. The process does not require stoichiometric amount of additives and thus does not necessarily produce waste. In this transformation, hydrogen is inserted onto a molecule from an organic hydrogen source without the presence of hazardous H<sub>2</sub> gas. The hydrogen donors are usually easily accessible and inexpensive, such as isopropanol, methanol, formic acid, and ethanol, of which particularly the latter two are readily obtainable from renewable sources. Possibilities and applications offered by homogeneous transfer hydrogenation have been reviewed recently by Kempe [790], Corma-Sabater [791], as well as Kayaki [792], while Morris investigated the mechanism of transfer hydrogenation catalyzed by iron-group hydrides [793]. Milstein [56,64], as well as Noyori [794–797], provided fundamental milestones, dramatically expanding the scope of substrates for transfer hydrogenation and coupling reactions using homogeneous catalysis, including pincer complexes. In 2008, Grützmacher reported the first efficient transfer hydrogenation with ethanol as the hydrogen source [798]. By applying an air-sensitive rhodium complex bearing a bis(5-H-dibenzocyclohepten-5-yl)amine ligand, they could reach 98% conversion of different ketones at mild temperatures. Since then, several reports have covered the topic [799–805], using also isopropanol [806], formic acid [807], as well as glycerol [808] as the hydrogen sources. Metal pincer complexes have appeared as suitable catalysts for this type of transformations as well [116,809–813].

With regard to the past five years, Khaskin explored in 2016 the use of the Gusev SNS catalyst, known for the hydrogenation of esters [40], for an unprecedented metathesis pathway coupled with transfer hydrogenation in the presence of ethanol [814]. The authors explored the reaction of ethyl hexanoate in the presence of **Ru-MACHO**, which afforded a statistical equilibrium of products confirming the metathesis pathway. Later, the authors screened the Gusev complexes **13** and **128**, with **128** being the most efficient in producing metathesis products, with 99% selectivity after 16 h at 80 °C in toluene, using 0.02 mol% of catalyst loading and 5 mol% KO<sup>t</sup>Bu. The scope was extended to alkyl, aryl, and mixed alkyl-aryl esters that were all efficiently scrambled using 0.2 mol% catalyst loading. Finally, with optimized conditions, the authors explored the selective transfer hydrogenation of ethyl hexanoate using ethanol as hydrogen source; by increasing the catalyst loading to 1 mol%, in the presence of 20 equivalents of ethanol, it was possible to afford 89% yield in hexanol (Scheme 107).



**Scheme 107.** Transfer hydrogenation of esters proposed by Khaskin in 2016 [814].

Thiel showed in 2018 an environmentally benign method for the hydrogenation of ketones, aldehydes and imines using ethanol as the hydrogen source, in combination with the ruthenium(II) pincer complex **129** in Figure 8 [815]. The catalyst is stable against moisture and oxygen, and allowed a wide scope of substrates; with 0.1 mol% as the catalyst loading, with 7.5 mol% KOH, in EtOH, it was possible to convert several phenyl ketones and aldehydes into the corresponding alcohols with >99% yields after 45 min, in some cases already after 15 min, at 40 °C. It was found that a rapid removal of acetic aldehyde under a constant N<sub>2</sub> flow is fundamental to push the equilibrium for high conversions.



However, it was not possible to hydrogenate olefins and heteroaromatic compounds with neither ethanol nor isopropanol as the hydrogen donors.

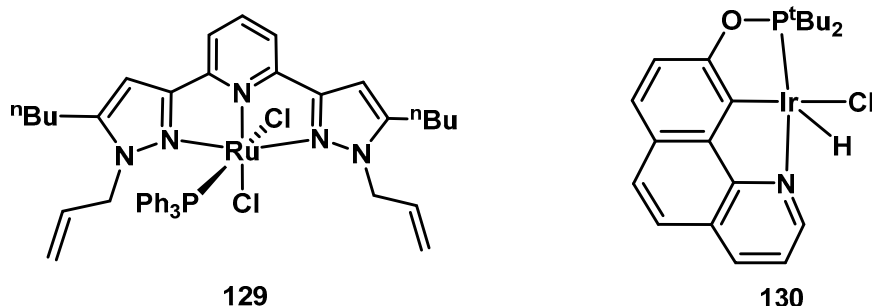


**Figure 8.** Ruthenium and iridium pincer catalysts reported by Thiel [815] and Huang [816] to catalyze transfer hydrogenations in the presence of ethanol.

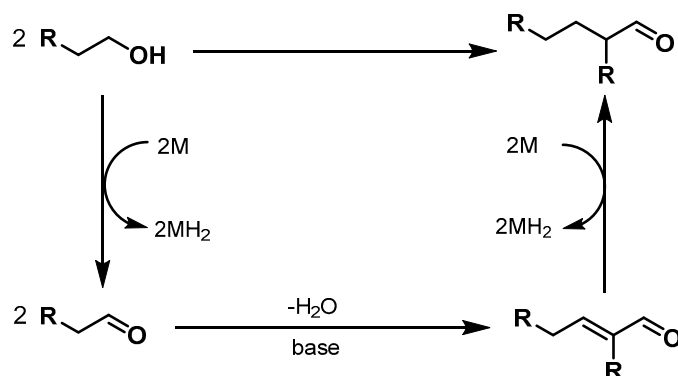
The same year, Huang reported the transfer hydrogenation of alkenes catalyzed by the iridium-NCP pincer complex **130** containing a rigid benzoquinoline backbone in the presence of ethanol [816]. The authors explored the conversion of a wide range of substrates, from substituted alkyl alkenes and aryl alkenes, to electron-rich/deficient olefins, *O*- and *N*-heteroarenes, as well as internal alkynes. The optimization was performed using cyclooctene and 1-octene as substrates; applying 1 mol% catalyst loading, yields >99% were achieved of the hydrogenated products, with 2.2 mol% of NaOtBu in ethanol, at 30 °C after 12 h. The rapid conversion of acetaldehyde, formed as the first EtOH dehydrogenation product, into ethyl acetate eliminates the possibility of catalyst poisoning by the iridium-mediated decarbonylation of the aldehyde.

In 2019, de Vries employed the iron-PNP catalyst **15** for the transfer hydrogenation of esters using ethanol as the hydrogen source [817]. The authors were able to hydrogenate more than 20 different substrates in good to excellent yields, including aromatic- and aliphatic esters and lactones. The initial screening was performed using methyl benzoate as the substrate, 5 mol% of **15** at 100 °C; after 24 h, 88% yield of benzyl alcohol was obtained. The authors also explored the use of different hydrogen sources, with isopropanol and butanol resulting in high conversion but lower selectivity in the desired product, whereas MeOH was found to poison the system. The optimized conditions were 5 mol% of catalyst, 96 equivalents of ethanol, at 100 °C for 24 h; with this protocol, the authors carried out the transfer hydrogenation of a series of relevant substrates, e.g., the bio-derived methyl oleate and  $\alpha$ -Angelica lactone. In addition, methyl levulinate was successfully converted into 1,4-pentanediol (PDO) in a single step. Remarkably, the system is also active for the depolymerization of polyester to the diols, expanding the applicability of this protocol to the recycling of plastics as well. Notably, the same transformation for polyesters reduction was reported in 2013 by Robertson using Milstein's catalyst **4** [818].

### Ethanol Upgrading

One of the most appealing processes in sustainable chemistry is the upgrading of (bio)-ethanol into useful fuels and fuel additives [819–821]. The Guerbet reaction is a process enabling the formation of C-C bonds starting from simple alcohols. In this transformation, the alcoholic substrate is dehydrogenated to form an aldehyde, which undergoes aldol condensation before the product is finally hydrogenated resulting in a higher alcohol (Scheme 108) [822]. Ethanol is currently produced from crops and used as fuel [823–825], albeit with only 70% of the energy density stored in gasoline. On the contrary, butanol presents several advantages, e.g., it has an energy density closer to that of gasoline (90%), is non-corrosive, immiscible with water and can be blended with gasoline at concentrations up to 16% [826–828]. Butanol is currently produced by bacterial fermentation of starch and sugars in the A.B.E. process [829], producing a mixture of acetone, butanol, and ethanol, while poor selectivity, separation issues, as well as low conversion and yield usually affect the Guerbet pathway [830].

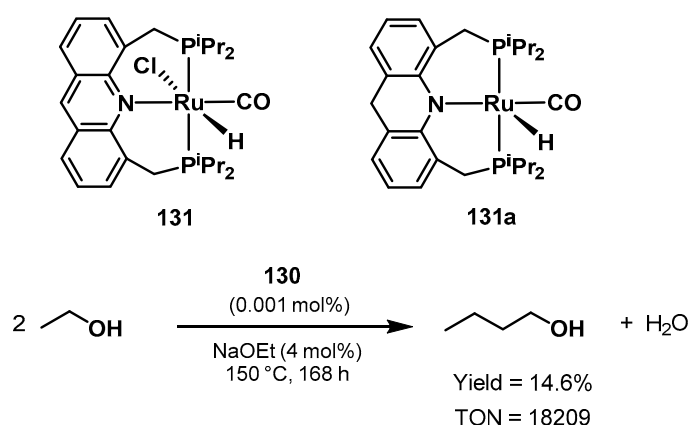




Scheme 108. Guerbet reaction.

The upgrading of ethanol results in 1-butanol and other C4/C6 products and isomers. Most of them are considered valuable bio-fuel, fuel additives, or monomers for bio-polymers. The reaction presents some drawbacks especially regarding the selectivity. *N*-butanol can undergo dehydrogenation reactions resulting in even higher alcohols and other side products. In addition, the high loading of base required, often promotes competitive reactions resulting in the formation of inactive carbonates. Research has focused on catalyst design as well as reaction conditions optimization to achieve acceptable yields and selectivity of 1-butanol.

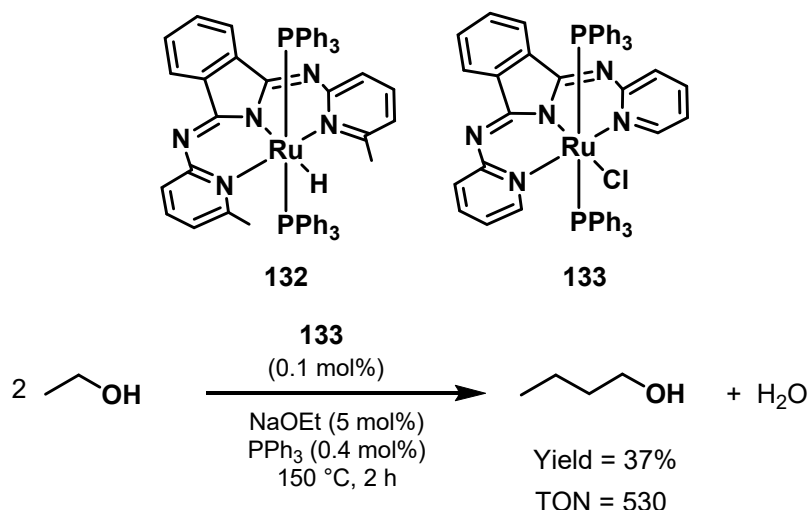
In 2016, Milstein reported a very efficient ruthenium pincer complex catalyst for ethanol upgrading [831]. The reaction performed using 0.02 mol% of catalyst **131** in Scheme 109, EtONa (4 mol%), at 150 °C for 16 h produced the highest conversion of ethanol (66.9%) affording up to 38.4% yield in butanol. Lowering of the catalyst loading to 0.001 mol% afforded the record TON of 18,209 with 14.6% yield and 86% selectivity. Mechanistic studies and isolation of reaction intermediates led to the conclusion that the active species is the dearomatized complex **131a**, which is formed after activation by base. The major deactivation pathway is believed to occur through reaction of the formed water with ethanol and base, resulting in the formation of inactive NaOAc. In addition, the authors also explored the possibility to produce longer chain alcohols from ethanol; with a base loading of 20 mol%, it was possible to produce higher alcohols reaching a record conversion of 73.4%, with 37.6% selectivity to C6 and C8 alcohols.



Scheme 109. Ru-PNP catalyst for ethanol upgrading developed by Milstein [831].

The same year, Szymczak proposed an air-stable Ru-NNN catalyst for the upgrading of ethanol to 1-butanol [832]. The catalyst is a modification of a previously reported catalyst (**132** in Scheme 110) found to be active in the reversible transformation between ketones and alcohols via hydrogenation and acceptorless dehydrogenation reactions [833]. The authors also carried out mechanistic studies supported by kinetic and isotopic labeling studies, proposing an inner-sphere mechanism with a  $\beta$ -H

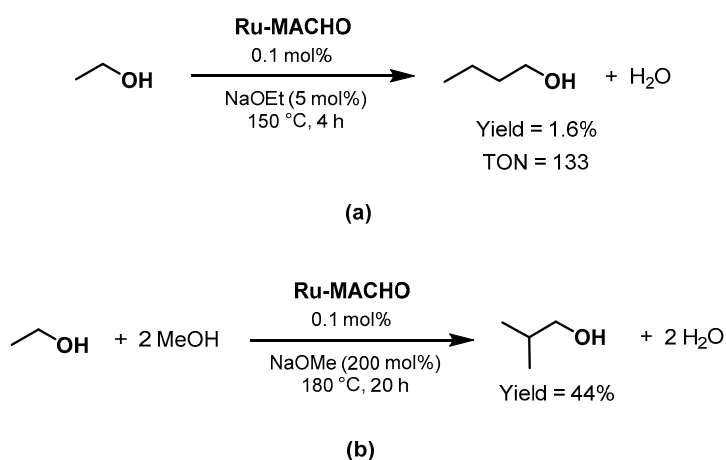
elimination as the turnover-limiting step in the dehydrogenation of alcohols using catalyst **132** [834]. In this report, catalyst **133** was used for the catalytic upgrading of ethanol achieving 37% yield of 1-butanol with 78% selectivity after 2 h at 150 °C. The addition of 0.4 mol% of PPh<sub>3</sub> prevents phosphine dissociation, as well as the competitive EtOH decarbonylation pathway. After optimization, the catalyst **133** resulted in a TON of 530 and a TOF of 265 h<sup>-1</sup> with the reaction conditions shown in Scheme 110.



**Scheme 110.** Ru-NNN complexes synthesized by Szymczak and ethanol upgrading using catalyst **133** [832,833].

In 2015, Wass showed the catalytic upgrading of ethanol using different ruthenium precursors in combination with various ligands, as well as the PNP complex **Ru-MACHO** [835]. With the reaction conditions showed in Scheme 111a, **Ru-MACHO** afforded 13.3% conversion and 12.4% selectivity in 1-butanol. The best result was obtained employing [RuCl<sub>2</sub>(η<sup>6</sup>-p-cymene)]<sub>2</sub> and the bidentate ligand 2-(diphenylphosphino)ethylamine, with 90% selectivity and 31% conversion.

In another work, high selectivity toward isobutanol was obtained using different combinations of ruthenium precursors and PP and PN bidentate ligands [836]. The catalyst bearing the 1,1-bis(diphenylphosphino)methane as ligand, with 200 mol% of base loading (NaOMe), 0.1 mol% of methanol, at 180 °C, afforded 75% conversion of ethanol with 99% selectivity to isobutanol and only traces of *n*-propanol and *n*-butanol.

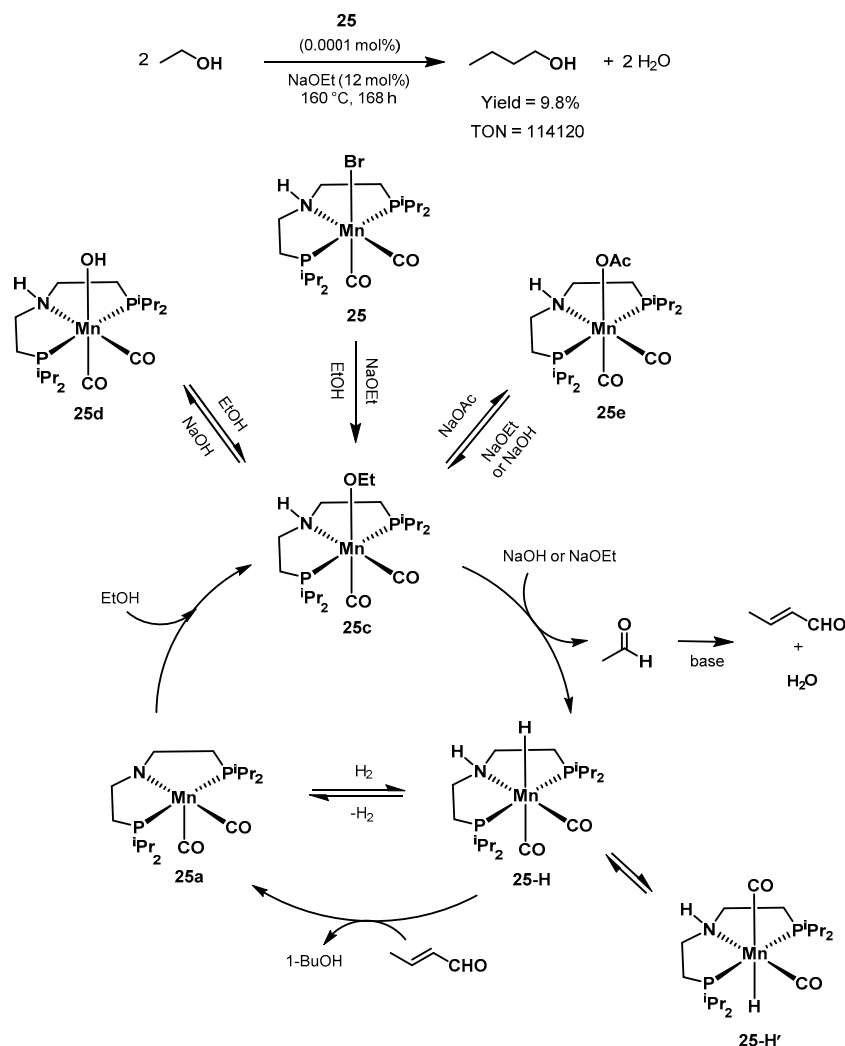


**Scheme 111.** Ethanol upgrading to (a) 1-butanol and (b) to isobutanol proposed by Wass [835,837].

In 2017, the same author tested the catalyst precursors *trans*-[RuCl<sub>2</sub>(dppm)<sub>2</sub>], [RuCl<sub>2</sub>(dppea)<sub>2</sub>], as well as **Ru-MACHO** for the upgrading of ethanol to isobutanol [837]. The pre-catalyst

*trans*-[RuCl<sub>2</sub>(dppm)<sub>2</sub>] was shown to be the most active in the presence of water, yielding 36% of isobutanol, at 78% selectivity from an aqueous ethanol/methanol mixture with water concentrations typical of that of a crude fermentation broth. In addition, the catalyst allows to perform the reaction using hydroxide instead of alkoxide bases. The use of H<sub>2</sub>O/NaOH with **Ru-MACHO** led to deactivation of the catalytic system and formation of carbonate and formate salts. However, in the presence of NaOMe and without water, **Ru-MACHO** afforded 44% yield in isobutanol with 89% selectivity under the reaction conditions shown in Scheme 111b. The superior activity of *trans*-[RuCl<sub>2</sub>(dppm)<sub>2</sub>] is explained by the superior water tolerance compared to the other PN and PNP complexes tested in the work.

The same year, Liu showed the first example, and state-of-the-art, of ethanol upgrading into 1-butanol using a homogeneous non-noble-metal catalyst [838]. The manganese pincer complex **25** resulted in the extraordinary TON of 114,120 and TOF of 3078 h<sup>−1</sup> with 92% selectivity and 9.8% yield of 1-butanol at 160 °C for 168 h (Scheme 112). Increasing the catalyst loading to 0.02 mol% under the same reaction conditions resulted in 14.5% yield in 1-butanol with 82% selectivity and a TON of 1031. The group also performed mechanistic studies using controlled experiments with reaction intermediates, NMR spectroscopy and single crystal X-Ray crystallography to investigate the role of the N-H/N-Me moiety of the PNP pincer ligand. The proposed catalytic cycle is depicted in Scheme 112.



**Scheme 112.** Proposed catalytic cycle of complex **25** for the Guerbet reaction of ethanol to butanol proposed by Liu [838].

In 2018, Jones screened several Mn-PNP complexes of the same family as catalysts for the Guerbet reaction [839]. The chosen Mn-Br(CO)<sub>2</sub>-PNP complexes bearing different substituents on the phosphorous atoms were all found to catalyze the transformation, with catalyst **25** performing best; *N*-butanol could be obtained in 31% yield using 0.5 mol% of **25**, NaOEt, at 150 °C for 48 h. High loading of the base (25 mol%) was required to maintain the catalytic activity. The water formed during the reaction promotes the major deactivation pathways.

#### 4. Conclusions

In conclusion, we covered the main advances of the last five years in relevant sustainable chemical transformations catalyzed by pincer complexes. Dehydrogenation and hydrogenation reactions, together with valorization of biomass-derived compounds are the main processes where sustainability is predominant. In particular, efficient and continuous hydrogen release from LOHCs, as well as CO<sub>2</sub> capture and hydrogenation are the main areas of interest in a hydrogen economy perspective, with methanol, formic acid, and its derivatives as the most studied alternatives. Homogeneous N<sub>2</sub> hydrogenation provides a clean, atom-efficient route for the synthesis of ammonia. Pincer complexes also catalyze the upgrading of ethanol into bio-fuels and the hydrogenation of biomass-derived compounds into high-value molecules.

Low catalyst loading, high selectivity, and mild reaction conditions are the main advantages of pincer-type catalysis. The applied pincer complexes show outstanding performance and promising potential for optimization. The long-term stability of the developed catalytic systems, as well as the use of expensive, rare metals are the main drawbacks that need optimization. More robust, possibly air- and moisture-stable catalysts are highly desirable to extend the lifetime and practical applicability of these otherwise promising catalysts. Remarkably, cheap and abundant first-row transition metals show very promising activity, potentially further increasing the sustainability of this versatile family of catalytic systems.

Pincer complexes have showed great reliability and flexibility for a plethora of sustainable chemical processes. Ligand design and the expanding use of first-row metals offer numerous possibilities for further optimization. Many groups are working extensively on the topic to find efficient, novel chemical and energy production routes and provide the society with sustainable solutions.

**Funding:** This research was funded by VILLUM FONDEN, grant number 19049, and by INDEPENDENT RESEARCH FUND DENMARK, grant number 8022-00330B.

**Conflicts of Interest:** The authors declare no conflict of interest.

#### References

1. Anastas, P.T.; Warner, J.C. *Green Chemistry: Theory and Practice 2000*; Oxford University Press: New York, NY, USA, 1998; p. 1546.
2. Grützmacher, H. Cooperating Ligands in Catalysis. *Angew. Chem. Int. Ed.* **2008**, *47*, 1814–1818. [[CrossRef](#)]
3. Askevold, B.; Roesky, H.W.; Schneider, S. Learning from the Neighbors: Improving Homogeneous Catalysts with Functional Ligands Motivated by Heterogeneous and Biocatalysis. *ChemCatChem* **2012**, *4*, 307–320. [[CrossRef](#)]
4. Lawrence, M.A.W.; Green, K.A.; Nelson, P.N.; Lorraine, S.C. Review: Pincer ligands—Tunable, versatile and applicable. *Polyhedron* **2018**, *143*, 11–27. [[CrossRef](#)]
5. Morales-Morales, D. *Pincer Compounds: Chemistry and Applications*; Elsevier: Amsterdam, The Netherlands, 2018; ISBN 9780128129326.
6. Morales-Morales, D.; Jensen, C. *The Chemistry of Pincer Compounds*; Elsevier: Amsterdam, The Netherlands, 2007; ISBN 9780444531384.
7. Moulton, B.C.J.; Shaw, B.L. *1020 J.C.S.; Dalton*: New York, NY, USA, 1975; pp. 1020–1024.
8. Liu, C.-C.; Liu, Q.-L.; Wu, Z.-Y.; Chen, Y.-C.; Xie, H.-J.; Lei, Q.-F.; Fang, W.-J. Mechanistic insights into small molecule activation induced by ligand cooperativity in PCcarbeneP nickel pincer complexes: A quantum chemistry study. *J. Mol. Model.* **2015**, *21*, 242. [[CrossRef](#)]

9. Zhao, S.; Wu, J.; Chen, W. Organometallic chemistry of bis (N-heterocyclic carbene) ligands containing a heteroarene spacer. *J. Organomet. Chem.* **2017**, *848*, 249–280. [[CrossRef](#)]
10. Pugh, D.; Danopoulos, A.A. Metal complexes with ‘pincer’-type ligands incorporating N-heterocyclic carbene functionalities. *Coord. Chem. Rev.* **2007**, *251*, 610–641. [[CrossRef](#)]
11. Mejuto, C.; García-Eleno, M.A.; Guisado-Barrios, G.; Spasyuk, D.; Gusev, D.; Peris, E. Ruthenium complexes with an N-heterocyclic carbene NNC-pincer ligand: Preparation and catalytic properties. *Org. Chem. Front.* **2015**, *2*, 936–941. [[CrossRef](#)]
12. Jiang, Y.; Gendy, C.; Roesler, R. Nickel, Ruthenium, and Rhodium NCN-Pincer Complexes Featuring a Six-Membered N-Heterocyclic Carbene Central Moiety and Pyridyl Pendant Arms. *Organometallics* **2018**, *37*, 1123–1132. [[CrossRef](#)]
13. Sung, S.; Wang, Q.; Krämer, T.; Young, R.D. Synthesis and reactivity of a PCcarbeneP cobalt (i) complex: The missing link in the cobalt PXP pincer series (X = B, C, N). *Chem. Sci.* **2018**, *9*, 8234–8241. [[CrossRef](#)] [[PubMed](#)]
14. Prokopchuk, D.E.; Tsui, B.T.H.; Lough, A.J.; Morris, R.H. Intramolecular C-H/O-H bond cleavage with water and alcohol using a phosphine-free ruthenium carbene NCN Pincer Complex. *Chem. A Eur. J.* **2014**, *20*, 16960–16968. [[CrossRef](#)] [[PubMed](#)]
15. Shimoyama, Y.; Ishizuka, T.; Kotani, H.; Kojima, T. Ruthenium (II) Complexes Having a Pincer-Type Ligand with Two N-Heterocyclic Carbene Moieties. *Z. Fur. Anorg. Und. Allg. Chem.* **2018**, *644*, 611–615. [[CrossRef](#)]
16. Charra, V.; de Frémont, P.; Braunstein, P. Multidentate N-heterocyclic carbene complexes of the 3d metals: Synthesis, structure, reactivity and catalysis. *Coord. Chem. Rev.* **2017**, *341*, 53–176. [[CrossRef](#)]
17. Andrew, R.E.; González-Sebastián, L.; Chaplin, A.B. NHC-based pincer ligands: Carbenes with a bite. *Dalt. Trans.* **2016**, *45*, 1299–1305. [[CrossRef](#)] [[PubMed](#)]
18. Cheng, J.; Wang, L.; Wang, P.; Deng, L. High-Oxidation-State 3d Metal (Ti-Cu) Complexes with N-Heterocyclic Carbene Ligation. *Chem. Rev.* **2018**, *118*, 9930–9987. [[CrossRef](#)] [[PubMed](#)]
19. Liddle, S.T.; Mills, D.P.; Wooles, A.J. Early metal bis (phosphorus-stabilised) carbene chemistry. *Chem. Soc. Rev.* **2011**, *40*, 2164–2176. [[CrossRef](#)] [[PubMed](#)]
20. Zhang, D.; Zi, G. N-heterocyclic carbene (NHC) complexes of group 4 transition metals. *Chem. Soc. Rev.* **2015**, *44*, 1898–1921. [[CrossRef](#)]
21. Polukeev, A.V.; Wendt, O.F. Cyclohexane-Based Phosphinite Iridium Pincer Complexes: Synthesis, Characterization, Carbene Formation, and Catalytic Activity in Dehydrogenation Reactions. *Organometallics* **2017**, *36*, 639–649. [[CrossRef](#)]
22. Gu, S.; Chen, C.; Qiu, H.; Chen, W. Potentially Hemilabile N-Heterocyclic Carbene Palladium Complexes: Synthesis and Catalytic Applications. *Curr. Org. Chem.* **2011**, *15*, 3291–3308. [[CrossRef](#)]
23. Peris, E.; Crabtree, R.H. Recent homogeneous catalytic applications of chelate and pincer N-heterocyclic carbenes. *Coord. Chem. Rev.* **2004**, *248*, 2239–2246. [[CrossRef](#)]
24. Li, H.; Zheng, B.; Huang, K.W. A new class of PN3-pincer ligands for metal-ligand cooperative catalysis. *Coord. Chem. Rev.* **2015**, *293–294*, 116–138. [[CrossRef](#)]
25. Kisala, J.; Ruman, T. Pincer Complexes Based on Phosphinoaminopyridines: Synthesis, Structural Characterization and Catalytic Applications. *Curr. Org. Chem.* **2011**, *15*, 3486–3502. [[CrossRef](#)]
26. Benito-Garagorri, D.; Kirchner, K. Modularly designed transition metal PNP and PCP pincer complexes based on aminophosphines: Synthesis and catalytic applications. *Acc. Chem. Res.* **2008**, *41*, 201–213. [[CrossRef](#)] [[PubMed](#)]
27. Deolka, S.; Tarannam, N.; Fayzullin, R.R.; Kozuch, S.; Khaskin, E. Unusual rearrangement of modified PNP ligand based Ru complexes relevant to alcohol dehydrogenation catalysis. *Chem. Commun.* **2019**, *55*, 11350–11353. [[CrossRef](#)]
28. Henrion, M.; Roisnel, T.; Couturier, J.L.; Dubois, J.L.; Sortais, J.B.; Darcel, C.; Carpentier, J.F. Ruthenium complexes bearing amino-bis (phosphinite) or amino-bis (aminophosphine) ligands: Application in catalytic ester hydrogenation. *Mol. Catal.* **2017**, *432*, 15–22. [[CrossRef](#)]
29. Yao, C.; Chakraborty, P.; Aresu, E.; Li, H.; Guan, C.; Zhou, C.; Liang, L.C.; Huang, K.W. Monomeric nickel hydroxide stabilized by a sterically demanding phosphorus-nitrogen PN3P-pincer ligand: Synthesis, reactivity and catalysis. *Dalt. Trans.* **2018**, *47*, 16057–16065. [[CrossRef](#)]
30. Gradiski, M.V.; Tsui, B.T.H.; Lough, A.J.; Morris, R.H. PNN’ & P 2 NN’ ligands via reductive amination with phosphine aldehydes: Synthesis and base-metal coordination chemistry. *Dalt. Trans.* **2019**, *48*, 2150–2159.

31. Kim, Y.; Lee, J.; Son, Y.-H.; Choi, S.-U.; Alam, M.; Park, S. Novel nickel(II), palladium(II), and platinum(II) complexes having a pyrrolyl-iminophosphine (PNN) pincer: Synthesis, crystal structures, and cytotoxic activity. *J. Inorg. Biochem.* **2020**, *205*, 111015. [\[CrossRef\]](#)
32. Adams, G.M.; Weller, A.S. POP-type ligands: Variable coordination and hemilabile behaviour. *Coord. Chem. Rev.* **2018**, *355*, 150–172. [\[CrossRef\]](#)
33. Leis, W.; Mayer, H.A.; Kaska, W.C. Cycloheptatrienyl, alkyl and aryl PCP-pincer complexes: Ligand backbone effects and metal reactivity. *Coord. Chem. Rev.* **2008**, *252*, 1787–1797. [\[CrossRef\]](#)
34. Morales-Morales, D. Recent Applications of Phosphinite POCOP Pincer Complexes towards Organic Transformations. *Mini. Rev. Org. Chem.* **2008**, *5*, 141–152. [\[CrossRef\]](#)
35. Gelman, D.; Romm, R. PC( $sp^3$ )P Transition Metal Pincer Complexes: Properties and Catalytic Applications. In *Topics in Organometallic Chemistry*; Springer: Berlin, Germany, 2013; pp. 289–317. ISBN 9783642310805.
36. Leforestier, B.; Gyton, M.R.; Chaplin, A.B. Synthesis and group 9 complexes of macrocyclic PCP and POCOP pincer ligands. *Dalt. Trans.* **2020**, *49*, 2087–2101. [\[CrossRef\]](#)
37. Jensen, C.M. Iridium PCP pincer complexes: Highly active and robust catalysts for novel homogeneous aliphatic dehydrogenations. *Chem. Commun.* **1999**, *3*, 2443–2449. [\[CrossRef\]](#)
38. Barrett, B.J.; Iluc, V.M. Coordination of a Hemilabile Pincer Ligand with an Olefinic Backbone to Mid-to-Late Transition Metals. *Inorg. Chem.* **2014**, *53*, 7248–7259. [\[CrossRef\]](#)
39. Schörgenhumer, J.; Zimmermann, A.; Waser, M. SNS-Ligands for Ru-Catalyzed Homogeneous Hydrogenation and Dehydrogenation Reactions. *Org. Process Res. Dev.* **2018**, *22*, 862–870. [\[CrossRef\]](#)
40. Spasyuk, D.; Smith, S.; Gusev, D.G. Replacing Phosphorus with Sulfur for the Efficient Hydrogenation of Esters. *Angew. Chem. Int. Ed.* **2013**, *52*, 2538–2542. [\[CrossRef\]](#)
41. Valdés, H.; González-Sebastián, L.; Morales-Morales, D. Aromatic para-functionalized NCN pincer compounds. *J. Organomet. Chem.* **2017**, *845*, 229–257. [\[CrossRef\]](#)
42. Fernández-Alvarez, F.J.; Lalrempuia, R.; Oro, L.A. Monoanionic NSiN-type ligands in transition metal coordination chemistry and catalysis. *Coord. Chem. Rev.* **2017**, *350*, 49–60. [\[CrossRef\]](#)
43. Garbe, S.; Krause, M.; Klimpel, A.; Neundorff, I.; Lippmann, P.; Ott, I.; Brünink, D.; Strassert, C.A.; Doltsinis, N.L.; Klein, A. Cyclometalated Pt Complexes of CNC Pincer Ligands: Luminescence and Cytotoxic Evaluation. *Organometallics* **2020**, *39*, 746–756. [\[CrossRef\]](#)
44. Ruan, J.; Wang, D.; Vedernikov, A.N.  $\text{CH}_3\text{-X}$  Reductive Elimination Reactivity of  $\text{Pt}^{\text{IV}}\text{Me}$  Complexes Supported by a Sulfonated CNN Pincer Ligand ( $\text{X} = \text{OH}, \text{CF}_3\text{CO}_2, \text{PhNMe}_2^+$ ). *Organometallics* **2020**, *39*, 142–152. [\[CrossRef\]](#)
45. Heidebrecht, J.; Gendy, C.; Gelfand, B.S.; Roesler, R. Water-soluble NNN-pincer complexes of cobalt, nickel and palladium: Solid-state structures and catalytic activity. *Polyhedron* **2018**, *143*, 138–143. [\[CrossRef\]](#)
46. Kozlov, V.A.; Aleksanyan, D.V.; Vasilév, A.A.; Odinets, I.L. Thiophosphoryl-, thiophosphoryloxy-, and thiophosphorylamino-benzene derivatives as novel classes of hybrid pincer ligands. *Phosphorus Sulfur Silicon Relat. Elem.* **2011**, *186*, 626–637. [\[CrossRef\]](#)
47. Al-Noaimi, M.; Awwadi, F.F.; Talib, W.H.; Atia, S.; Hammud, H.H. Cis and trans- palladium (II) complexes derived from SNN amidrazon pincer ligand: Synthesis, crystal structures and biological evaluation. *J. Mol. Struct.* **2019**, *1197*, 282–291. [\[CrossRef\]](#)
48. Okamoto, K.; Kuwabara, J.; Kanbara, T. Secondary Thioamides as Multidentate Ligands for Functional Metal Complexes. *Chem. Lett.* **2015**, *44*, 102–110. [\[CrossRef\]](#)
49. Simon, M.; Breher, F. Multidentate silyl ligands in transition metal chemistry. *Dalt. Trans.* **2017**, *46*, 7976–7997. [\[CrossRef\]](#)
50. Zhou, Y.P.; Mo, Z.; Luecke, M.P.; Driess, M. Stereoselective Transfer Semi-Hydrogenation of Alkynes to E-Olefins with N-Heterocyclic Silylene–Manganese Catalysts. *Chem. A Eur. J.* **2018**, *24*, 4780–4784. [\[CrossRef\]](#)
51. Kumar, A.; Rao, G.K.; Saleem, F.; Singh, A.K. Organoselenium ligands in catalysis. *Dalt. Trans.* **2012**, *41*, 11949–11977. [\[CrossRef\]](#)
52. Sharma, K.N.; Satrawala, N.; Srivastava, A.K.; Ali, M.; Joshi, R.K. Palladium (ii) ligated with a selenated (Se, CNHC, N-) -type pincer ligand: An efficient catalyst for Mizoroki-Heck and Suzuki-Miyaura coupling in water. *Org. Biomol. Chem.* **2019**, *17*, 8969–8976. [\[CrossRef\]](#)
53. Kameo, H.; Nakazawa, H. Recent developments in the coordination chemistry of multidentate ligands featuring a boron moiety. *Chem. Asian J.* **2013**, *8*, 1720–1734. [\[CrossRef\]](#)



54. Yamashita, M. The Organometallic Chemistry of Boron-Containing Pincer Ligands based on Diazaboroles and Carboranes. *Bull. Chem. Soc. Jpn.* **2016**, *89*, 269–281. [\[CrossRef\]](#)
55. Balakrishna, M.S. Unusual and rare pincer ligands: Synthesis, metallation, reactivity and catalytic studies. *Polyhedron* **2018**, *143*, 2–10. [\[CrossRef\]](#)
56. Van Der Boom, M.E.; Milstein, D. Cyclometalated phosphine-based pincer complexes: Mechanistic insight in catalysis, coordination, and bond activation. *Chem. Rev.* **2003**, *103*, 1759–1792. [\[CrossRef\]](#) [\[PubMed\]](#)
57. Peris, E.; Crabtree, R.H. Key factors in pincer ligand design. *Chem. Soc. Rev.* **2018**, *47*, 1959–1968. [\[CrossRef\]](#) [\[PubMed\]](#)
58. Toda, T.; Suzuki, S.; Kuwata, S. Metallo-supramolecular assembly of protic pincer-type complexes: Encapsulation of dinitrogen and carbon disulfide into a multiproton-responsive diruthenium cage. *Chem. Commun.* **2019**, *55*, 1028–1031. [\[CrossRef\]](#)
59. Nelson, D.J.; Nolan, S.P. Hydroxide complexes of the late transition metals: Organometallic chemistry and catalysis. *Coord. Chem. Rev.* **2017**, *353*, 278–294. [\[CrossRef\]](#)
60. Maser, L.; Vondung, L.; Langer, R. The ABC in pincer chemistry—From amine- to borylene- and carbon-based pincer-ligands. *Polyhedron* **2018**, *143*, 28–42. [\[CrossRef\]](#)
61. Gusev, D.G.; Madott, M.; Dolgushin, F.M.; Lyssenko, K.A.; Antipin, M.Y. Agostic bonding in pincer complexes of ruthenium. *Organometallics* **2000**, *19*, 1734–1739. [\[CrossRef\]](#)
62. Annibale, V.T.; Song, D. Multidentate actor ligands as versatile platforms for small molecule activation and catalysis. *RSC Adv.* **2013**, *3*, 11432–11449. [\[CrossRef\]](#)
63. Ananthnag, G.S.; Shetti, V.S. Synthesis, structure and catalysis of organometallic porphyrin-pincer hybrids: A review. *Dalt. Trans.* **2017**, *46*, 14062–14082. [\[CrossRef\]](#)
64. Gunanathan, C.; Milstein, D. Bond Activation and Catalysis by Ruthenium Pincer Complexes. *Chem. Rev.* **2014**, *114*, 12024–12087. [\[CrossRef\]](#)
65. Younus, H.A.; Ahmad, N.; Su, W.; Verpoort, F. Ruthenium pincer complexes: Ligand design and complex synthesis. *Coord. Chem. Rev.* **2014**, *276*, 112–152. [\[CrossRef\]](#)
66. Younus, H.A.; Su, W.; Ahmad, N.; Chen, S.; Verpoort, F. Ruthenium pincer complexes: Synthesis and catalytic applications. *Adv. Synth. Catal.* **2015**, *357*, 283–330. [\[CrossRef\]](#)
67. Werkmeister, S.; Junge, K.; Beller, M. Catalytic hydrogenation of carboxylic acid esters, amides, and nitriles with homogeneous catalysts. *Org. Process Res. Dev.* **2014**, *18*, 289–302. [\[CrossRef\]](#)
68. Gusev, D.G.; Lough, A.J. Experimental and computational study of pincer complexes of ruthenium with Py, CO, and N<sub>2</sub> ligands. *Organometallics* **2002**, *21*, 5091–5099. [\[CrossRef\]](#)
69. Gusev, D.G.; Dolgushin, F.M.; Antipin, M.Y. Hydride, borohydride, and dinitrogen pincer complexes of ruthenium. *Organometallics* **2000**, *19*, 3429–3434. [\[CrossRef\]](#)
70. Abbel, R.; Abdur-Rashid, K.; Faatz, M.; Hadzovic, A.; Lough, A.J.; Morris, R.H. A succession of isomers of ruthenium dihydride complexes. Which one is the ketone hydrogenation catalyst? *J. Am. Chem. Soc.* **2005**, *127*, 1870–1882. [\[CrossRef\]](#)
71. Bruneau, C.; Dixneuf, P.H. *Ruthenium in Catalysis*; Springer: Berlin, Germany, 2014; ISBN 9783319084817.
72. Dub, P.A.; Ikariya, T. Quantum chemical calculations with the inclusion of nonspecific and specific solvation: Asymmetric transfer hydrogenation with bifunctional ruthenium catalysts. *J. Am. Chem. Soc.* **2013**, *135*, 2604–2619. [\[CrossRef\]](#)
73. Bertoli, M.; Choualeb, A.; Lough, A.J.; Moore, B.; Spasyuk, D.; Gusev, D.G. Osmium and ruthenium catalysts for dehydrogenation of alcohols. *Organometallics* **2011**, *30*, 3479–3482. [\[CrossRef\]](#)
74. Chelucci, G.; Baldino, S.; Baratta, W. Recent advances in osmium-catalyzed hydrogenation and dehydrogenation reactions. *Acc. Chem. Res.* **2015**, *48*, 363–379. [\[CrossRef\]](#)
75. Bertoli, M.; Choualeb, A.; Gusev, D.G.; Lough, A.J.; Major, Q.; Moore, B. PNP pincer osmium polyhydrides for catalytic dehydrogenation of primary alcohols. *Dalt. Trans.* **2011**, *40*, 8941. [\[CrossRef\]](#)
76. Gusev, D.G.; Lough, A.J.; Double, C.-H. activation on osmium and ruthenium centers: Carbene vs olefin products. *Organometallics* **2002**, *21*, 2601–2603. [\[CrossRef\]](#)
77. Choi, J.; MacArthur, A.H.R.; Brookhart, M.; Goldman, A.S. Dehydrogenation and Related Reactions Catalyzed by Iridium Pincer Complexes. *Chem. Rev.* **2011**, *111*, 1761–1779. [\[CrossRef\]](#)
78. Choualeb, A.; Lough, A.J.; Gusev, D.G. Hemilabile pincer-type hydride complexes of iridium. *Organometallics* **2007**, *26*, 5224–5229. [\[CrossRef\]](#)



79. Clarke, Z.E.; Maragh, P.T.; Dasgupta, T.P.; Gusev, D.G.; Lough, A.J.; Abdur-Rashid, K. A family of active iridium catalysts for transfer hydrogenation of ketones. *Organometallics* **2006**, *25*, 4113–4117. [\[CrossRef\]](#)
80. Meiners, J.; Scheibel, M.G.; Lemée-Cailleau, M.H.; Mason, S.A.; Boeddinghaus, M.B.; Fässler, T.F.; Herdtweck, E.; Khusniyarov, M.M.; Schneider, S. Square-planar iridium (II) and iridium (III) amido complexes stabilized by a PNP pincer ligand. *Angew. Chem. Int. Ed.* **2011**, *50*, 8184–8187. [\[CrossRef\]](#)
81. Goldberg, J.M.; Wong, G.W.; Brastow, K.E.; Kaminsky, W.; Goldberg, K.I.; Heinekey, D.M. The Importance of Steric Factors in Iridium Pincer Complexes. *Organometallics* **2015**, *34*, 753–762. [\[CrossRef\]](#)
82. Scheibel, M.G.; Wu, Y.; Stückl, A.C.; Krause, L.; Carl, E.; Stalke, D.; De Bruin, B.; Schneider, S. Synthesis and reactivity of a transient, terminal nitrido complex of rhodium. *J. Am. Chem. Soc.* **2013**, *135*, 17719–17722. [\[CrossRef\]](#)
83. Sundermann, A.; Uzan, O.; Milstein, D.; Martin, J.M.L. Selective C-C vs C-H bond activation by rhodium (I) PCP pincer complexes. A computational study. *J. Am. Chem. Soc.* **2000**, *122*, 7095–7104. [\[CrossRef\]](#)
84. Urgoitia, G.; Galdón, G.; Churrua, F.; SanMartin, R.; Herrero, M.T.; Domínguez, E. Aerobic oxidation of secondary benzyl alcohols catalyzed by phosphinite-based palladium pincer complexes. *Environ. Chem. Lett.* **2018**, *16*, 1101–1108. [\[CrossRef\]](#)
85. Albrecht, M.; Van Koten, G. Platinum group organometallics based on “pincer” complexes: Sensors, switches, and catalysts. *Angew. Chem. Int. Ed.* **2001**, *40*, 3750–3781. [\[CrossRef\]](#)
86. Selander, N.; Szabó, K.J. Catalysis by palladium pincer complexes. *Chem. Rev.* **2011**, *111*, 2048–2076. [\[CrossRef\]](#)
87. González-Sebastián, L.; Morales-Morales, D. Cross-coupling reactions catalysed by palladium pincer complexes. A review of recent advances. *J. Organomet. Chem.* **2019**, *893*, 39–51. [\[CrossRef\]](#)
88. Esteruelas, M.A.; López, A.M.; Oliván, M. Polyhydrides of Platinum Group Metals: Nonclassical Interactions and  $\sigma$ -Bond Activation Reactions. *Chem. Rev.* **2016**, *116*, 8770–8847. [\[CrossRef\]](#)
89. Therrien, J.A.; Wolf, M.O.; Patrick, B.O. Synthesis and comparison of nickel, palladium, and platinum bis (N-heterocyclic carbene) pincer complexes for electrocatalytic CO<sub>2</sub> reduction. *Dalt. Trans.* **2018**, *47*, 1827–1840. [\[CrossRef\]](#)
90. Bauer, G.; Hu, X. Recent developments of iron pincer complexes for catalytic applications. *Inorg. Chem. Front.* **2016**, *3*, 741–765. [\[CrossRef\]](#)
91. Dai, H.; Guan, H. Iron Dihydride Complexes: Synthesis, Reactivity, and Catalytic Applications. *Isr. J. Chem.* **2017**, *57*, 1170–1203. [\[CrossRef\]](#)
92. Bhattacharya, P.; Guan, H. Synthesis and catalytic applications of iron pincer complexes. *Comments Inorg. Chem.* **2011**, *32*, 88–112. [\[CrossRef\]](#)
93. Balaraman, E.; Nandakumar, A.; Jaiswal, G.; Sahoo, M.K. Iron-catalyzed dehydrogenation reactions and their applications in sustainable energy and catalysis. *Catal. Sci. Technol.* **2017**, *7*, 3177–3195. [\[CrossRef\]](#)
94. Benito-Garagorri, D.; Puchberger, M.; Mereiter, K.; Kirchner, K. Stereospecific and reversible CO binding at iron pincer complexes. *Angew. Chem. Int. Ed.* **2008**, *47*, 9142–9145. [\[CrossRef\]](#)
95. Junge, K.; Schröder, K.; Beller, M. Homogeneous catalysis using iron complexes: Recent developments in selective reductions. *Chem. Commun.* **2011**, *47*, 4849. [\[CrossRef\]](#)
96. Bernskoetter, W.H.; Hazari, N. Hydrogenation and dehydrogenation reactions catalyzed by iron pincer compounds. In *Pincer Compounds*; Elsevier Inc.: Amsterdam, The Netherlands, 2018; ISBN 9780128129326.
97. Rohit, K.R.; Radhika, S.; Saranya, S.; Anilkumar, G. Manganese-Catalysed Dehydrogenative Coupling—An Overview. *Adv. Synth. Catal.* **2020**, *362*, 1602–1650. [\[CrossRef\]](#)
98. Waiba, S.; Maji, B. Manganese Catalyzed Acceptorless Dehydrogenative Coupling Reactions. *ChemCatChem* **2019**, *12*, 1891–1902. [\[CrossRef\]](#)
99. Maji, B.; Barman, M.K. Recent Developments of Manganese Complexes for Catalytic Hydrogenation and Dehydrogenation Reactions. *Synthesis* **2017**, *49*, 3377–3393. [\[CrossRef\]](#)
100. Garbe, M.; Junge, K.; Beller, M. Homogeneous Catalysis by Manganese-Based Pincer Complexes. *Eur. J. Org. Chem.* **2017**, *2017*, 4344–4362. [\[CrossRef\]](#)
101. Eberhardt, N.A.; Guan, H. Nickel Hydride Complexes. *Chem. Rev.* **2016**, *116*, 8373–8426. [\[CrossRef\]](#)
102. Gafurov, Z.N.; Kagilev, A.A.; Kantyukov, A.O.; Balabaev, A.A.; Sinyashin, O.G.; Yakhvarov, D.G. Classification and synthesis of nickel pincer complexes. *Russ. Chem. Bull.* **2018**, *67*, 385–394. [\[CrossRef\]](#)
103. Klein, A.; Sandleben, A.; Vogt, N. Synthesis, Structure and Reactivity of Cyclometalated Nickel (II) Complexes: A Review and Perspective. *Proc. Natl. Acad. Sci. India Sect. A Phys. Sci.* **2016**, *86*, 533–549. [\[CrossRef\]](#)

104. Gutsulyak, D.V.; Piers, W.E.; Borau-Garcia, J.; Parvez, M. Activation of water, ammonia, and other small molecules by PC carbeneP nickel pincer complexes. *J. Am. Chem. Soc.* **2013**, *135*, 11776–11779. [\[CrossRef\]](#)
105. LaPierre, E.A.; Clapson, M.L.; Piers, W.E.; Maron, L.; Spasyuk, D.M.; Gendy, C. Oxygen Atom Transfer to Cationic PCNi(II) Complexes Using Amine-N-Oxides. *Inorg. Chem.* **2018**, *57*, 495–506. [\[CrossRef\]](#)
106. Chapman, G.; Nicholas, K.M. Vanadium-catalyzed deoxydehydration of glycols. *Chem. Commun.* **2013**, *49*, 8199. [\[CrossRef\]](#)
107. Gopaladasu, T.V.; Nicholas, K.M. Carbon Monoxide (CO)- and Hydrogen-Driven, Vanadium-Catalyzed Deoxydehydration of Glycols. *ACS Catal.* **2016**, *6*, 1901–1904. [\[CrossRef\]](#)
108. Hanson, S.K.; Baker, R.T.; Gordon, J.C.; Scott, B.L.; Thorn, D.L. Aerobic Oxidation of Lignin Models Using a Base Metal Vanadium Catalyst. *Inorg. Chem.* **2010**, *49*, 5611–5618. [\[CrossRef\]](#) [\[PubMed\]](#)
109. Junge, K.; Papa, V.; Beller, M. Cobalt–Pincer Complexes in Catalysis. *Chem. A Eur. J.* **2019**, *25*, 122–143. [\[CrossRef\]](#) [\[PubMed\]](#)
110. Liu, W.; Sahoo, B.; Junge, K.; Beller, M. Cobalt Complexes as an Emerging Class of Catalysts for Homogeneous Hydrogenations. *Acc. Chem. Res.* **2018**, *51*, 1858–1869. [\[CrossRef\]](#) [\[PubMed\]](#)
111. Ai, W.; Zhong, R.; Liu, X.; Liu, Q. Hydride Transfer Reactions Catalyzed by Cobalt Complexes. *Chem. Rev.* **2019**, *119*, 2876–2953. [\[CrossRef\]](#) [\[PubMed\]](#)
112. Lagaditis, P.O.; Schluschaß, B.; Demeshko, S.; Würtele, C.; Schneider, S. Square-Planar Cobalt (III) Pincer Complex. *Inorg. Chem.* **2016**, *55*, 4529–4536. [\[CrossRef\]](#)
113. Midya, S.P.; Pitchaimani, J.; Landge, V.G.; Madhu, V.; Balaraman, E. Direct access to: N -alkylated amines and imines via acceptorless dehydrogenative coupling catalyzed by a cobalt (ii)-NNN pincer complex. *Catal. Sci. Technol.* **2018**, *8*, 3469–3473. [\[CrossRef\]](#)
114. Ge, H.; Jing, Y.; Yang, X. Computational Design of Cobalt Catalysts for Hydrogenation of Carbon Dioxide and Dehydrogenation of Formic Acid. *Inorg. Chem.* **2016**, *55*, 12179–12184. [\[CrossRef\]](#)
115. Gorgas, N.; Kirchner, K. Isoelectronic Manganese and Iron Hydrogenation/Dehydrogenation Catalysts: Similarities and Divergences. *Acc. Chem. Res.* **2018**, *51*, 1558–1569. [\[CrossRef\]](#)
116. Reed-Berendt, B.G.; Polidano, K.; Morrill, L.C. Recent advances in homogeneous borrowing hydrogen catalysis using earth-abundant first row transition metals. *Org. Biomol. Chem.* **2019**, *17*, 1595–1607. [\[CrossRef\]](#)
117. Anastas, P.T.; Zimmerman, J.B. The periodic table of the elements of green and sustainable chemistry. *Green Chem.* **2019**, 6545–6566. [\[CrossRef\]](#)
118. Kallmeier, F.; Kempe, R. Manganese Complexes for (De) Hydrogenation Catalysis: A Comparison to Cobalt and Iron Catalysts. *Angew. Chem. Int. Ed.* **2018**, *57*, 46–60. [\[CrossRef\]](#) [\[PubMed\]](#)
119. Nguyen, D.H.; Morin, Y.; Zhang, L.; Trivelli, X.; Capet, F.; Paul, S.; Desset, S.; Dumeignil, F.; Gauvin, R.M. Oxidative Transformations of Biosourced Alcohols Catalyzed by Earth-Abundant Transition Metals. *ChemCatChem* **2017**, *9*, 2652–2660. [\[CrossRef\]](#)
120. Mukherjee, A.; Milstein, D. Homogeneous Catalysis by Cobalt and Manganese Pincer Complexes. *ACS Catal.* **2018**, *8*, 11435–11469. [\[CrossRef\]](#)
121. Zell, T.; Langer, R. From Ruthenium to Iron and Manganese—A Mechanistic View on Challenges and Design Principles of Base-Metal Hydrogenation Catalysts. *ChemCatChem* **2018**, *10*, 1930–1940. [\[CrossRef\]](#)
122. Filonenko, G.A.; Van Putten, R.; Hensen, E.J.M.; Pidko, E.A. Catalytic (de) hydrogenation promoted by non-precious metals-Co, Fe and Mn: Recent advances in an emerging field. *Chem. Soc. Rev.* **2018**, *47*, 1459–1483. [\[CrossRef\]](#) [\[PubMed\]](#)
123. Alig, L.; Fritz, M.; Schneider, S. First-Row Transition Metal (De) Hydrogenation Catalysis Based on Functional Pincer Ligands. *Chem. Rev.* **2019**, *119*, 2681–2751. [\[CrossRef\]](#)
124. Zhang, Z.; Butt, N.A.; Zhou, M.; Liu, D.; Zhang, W. Asymmetric Transfer and Pressure Hydrogenation with Earth-Abundant Transition Metal Catalysts. *Chin. J. Chem.* **2018**, *36*, 443–454. [\[CrossRef\]](#)
125. Riisager, A.; Fehrmann, R.; Haumann, M.; Wasserscheid, P. Supported Ionic Liquid Phase (SILP) catalysis: An innovative concept for homogeneous catalysis in continuous fixed-bed reactors. *Eur. J. Inorg. Chem.* **2006**, 695–706. [\[CrossRef\]](#)
126. Selvam, T.; MacHoke, A.; Schwieger, W. Supported ionic liquids on non-porous and porous inorganic materials-A topical review. *Appl. Catal. A Gen.* **2012**, 445–446, 92–101. [\[CrossRef\]](#)

127. Brünig, J.; Csendes, Z.; Weber, S.; Gorgas, N.; Bittner, R.W.; Limbeck, A.; Bica, K.; Hoffmann, H.; Kirchner, K. Chemoselective Supported Ionic-Liquid-Phase (SILP) Aldehyde Hydrogenation Catalyzed by an Fe(II) PNP Pincer Complex. *ACS Catal.* **2018**, *8*, 1048–1051. [\[CrossRef\]](#)
128. Castro-Amoedo, R.; Csendes, Z.; Brünig, J.; Sauer, M.; Foelske-Schmitz, A.; Yigit, N.; Rupprechter, G.; Gupta, T.; Martins, A.M.; Bica, K.; et al. Carbon-based SILP catalysis for the selective hydrogenation of aldehydes using a well-defined Fe(ii) PNP complex. *Catal. Sci. Technol.* **2018**, *8*, 4812–4820. [\[CrossRef\]](#)
129. Sheludko, B.; Cunningham, M.T.; Goldman, A.S.; Celik, F.E. Continuous-Flow Alkane Dehydrogenation by Supported Pincer-Ligated Iridium Catalysts at Elevated Temperatures. *ACS Catal.* **2018**, *8*, 7828–7841. [\[CrossRef\]](#)
130. Barman, M.K.; Waiba, S.; Maji, B. Manganese-Catalyzed Direct Olefination via an Acceptorless Dehydrogenative Coupling of Methyl Heteroarenes with Primary Alcohols. *Synlett* **2019**, *30*, 12–20.
131. Thiagarajan, S.; Gunanathan, C. Ruthenium-Catalyzed  $\alpha$ -Olefination of Nitriles Using Secondary Alcohols. *ACS Catal.* **2018**, *8*, 2473–2478. [\[CrossRef\]](#)
132. Zhang, G.; Irrgang, T.; Dietel, T.; Kallmeier, F.; Kempe, R. Manganese-Catalyzed Dehydrogenative Alkylation or  $\alpha$ -Olefination of Alkyl-Substituted N-Heteroarenes with Alcohols. *Angew. Chem. Int. Ed.* **2018**, *57*, 9131–9135. [\[CrossRef\]](#) [\[PubMed\]](#)
133. Bauer, E.B.; Andavan, G.T.S.; Hollis, T.K.; Rubio, R.J.; Cho, J.; Kuchenbeiser, G.R.; Helgert, T.R.; Letko, C.S.; Tham, F.S. Air- and water-stable catalysts for hydroamination/cyclization. Synthesis and application of CCC-NHC pincer complexes of Rh and Ir. *Org. Lett.* **2008**, *10*, 1175–1178. [\[CrossRef\]](#) [\[PubMed\]](#)
134. Cho, J.; Hollis, T.K.; Valente, E.J.; Trate, J.M. CCC-N-heterocyclic carbene pincer complexes: Synthesis, characterization and hydroamination activity of a hafnium complex. *J. Organomet. Chem.* **2011**, *696*, 373–377. [\[CrossRef\]](#)
135. Castonguay, A.; Spasyuk, D.M.; Madern, N.; Beauchamp, A.L.; Zargarian, D. Regioselective hydroamination of acrylonitrile catalyzed by cationic pincer complexes of nickel (II). *Organometallics* **2009**, *28*, 2134–2141. [\[CrossRef\]](#)
136. Takaya, J.; Iwasawa, N. Hydrocarboxylation of allenes with CO<sub>2</sub> catalyzed by silyl pincer-type palladium complex. *J. Am. Chem. Soc.* **2008**, *130*, 15254–15255. [\[CrossRef\]](#)
137. Serra, D.; Cao, P.; Cabrera, J.; Padilla, R.; Rominger, F.; Limbach, M. Development of platinum (II) and -(IV) CNC pincer complexes and their application in a hydrovinylation reaction. *Organometallics* **2011**, *30*, 1885–1895. [\[CrossRef\]](#)
138. Mastalir, M.; Pittenauer, E.; Allmaier, G.; Kirchner, K. Manganese-Catalyzed Aminomethylation of Aromatic Compounds with Methanol as a Sustainable C1 Building Block. *J. Am. Chem. Soc.* **2017**, *139*, 8812–8815. [\[CrossRef\]](#)
139. Zhang, Y.; Fang, H.; Yao, W.; Leng, X.; Huang, Z. Synthesis of Pincer Hydrido Ruthenium Olefin Complexes for Catalytic Alkane Dehydrogenation. *Organometallics* **2016**, *35*, 181–188. [\[CrossRef\]](#)
140. Kumar, A.; Bhatti, T.M.; Goldman, A.S. Dehydrogenation of Alkanes and Aliphatic Groups by Pincer-Ligated Metal Complexes. *Chem. Rev.* **2017**, *117*, 12357–12384. [\[CrossRef\]](#) [\[PubMed\]](#)
141. Das, K.; Kumar, A. *Alkane Dehydrogenation Reactions Catalyzed by Pincer-Metal Complexes*, 1st ed.; Elsevier Inc.: Amsterdam, The Netherlands, 2019; ISBN 9780128171172.
142. Renkema, K.B.; Kissin, Y.V.; Goldman, A.S. Mechanism of alkane transfer-dehydrogenation catalyzed by a pincer-ligated iridium complex. *J. Am. Chem. Soc.* **2003**, *125*, 7770–7771. [\[CrossRef\]](#) [\[PubMed\]](#)
143. Zhu, K.; Achord, P.D.; Zhang, X.; Krogh-Jespersen, K.; Goldman, A.S. Highly effective pincer-ligated iridium catalysts for alkane dehydrogenation. DFT calculations of relevant thermodynamic, kinetic, and spectroscopic properties. *J. Am. Chem. Soc.* **2004**, *126*, 13044–13053. [\[CrossRef\]](#) [\[PubMed\]](#)
144. Göttker-Schnetmann, I.; White, P.; Brookhart, M. Iridium Bis (phosphinite) p-XPCP Pincer Complexes: Highly Active Catalysts for the Transfer Dehydrogenation of Alkanes. *J. Am. Chem. Soc.* **2004**, *126*, 1804–1811. [\[CrossRef\]](#) [\[PubMed\]](#)
145. Nawara-Hultzs, A.J.; Hackenberg, J.D.; Punji, B.; Supplee, C.; Emge, T.J.; Bailey, B.C.; Schrock, R.R.; Brookhart, M.; Goldman, A.S. Rational design of highly active “hybrid” phosphine-phosphinite pincer iridium catalysts for alkane metathesis. *ACS Catal.* **2013**, *3*, 2505–2514. [\[CrossRef\]](#)
146. Chakraborty, S.; Gellrich, U.; Diskin-Posner, Y.; Leitun, G.; Avram, L.; Milstein, D. Manganese-Catalyzed N-Formylation of Amines by Methanol Liberating H<sub>2</sub>: A Catalytic and Mechanistic Study. *Angew. Chem.* **2017**, *129*, 4293–4297. [\[CrossRef\]](#)

147. Daw, P.; Chakraborty, S.; Leitus, G.; Diskin-Posner, Y.; Ben-David, Y.; Milstein, D. Selective N-Formylation of Amines with H<sub>2</sub> and CO<sub>2</sub> Catalyzed by Cobalt Pincer Complexes. *ACS Catal.* **2017**, *7*, 2500–2504. [[CrossRef](#)]
148. El-Sepelgy, O.; Matador, E.; Brzozowska, A.; Rueping, M. C-Alkylation of Secondary Alcohols by Primary Alcohols through Manganese-Catalyzed Double Hydrogen Autotransfer. *ChemSusChem* **2019**, *12*, 3099–3102. [[CrossRef](#)]
149. Freitag, F.; Irrgang, T.; Kempe, R. Cobalt-Catalyzed Alkylation of Secondary Alcohols with Primary Alcohols via Borrowing Hydrogen/Hydrogen Autotransfer. *Chem. A Eur. J.* **2017**, *23*, 12110–12113. [[CrossRef](#)] [[PubMed](#)]
150. Barman, M.K.; Jana, A.; Maji, B. Phosphine-Free NNN-Manganese Complex Catalyzed  $\alpha$ -Alkylation of Ketones with Primary Alcohols and Friedländer Quinoline Synthesis. *Adv. Synth. Catal.* **2018**, *360*, 3233–3238. [[CrossRef](#)]
151. Peña-López, M.; Piehl, P.; Elangovan, S.; Neumann, H.; Beller, M. Manganese-Catalyzed Hydrogen-Autotransfer C–C Bond Formation:  $\alpha$ -Alkylation of Ketones with Primary Alcohols. *Angew. Chem. Int. Ed.* **2016**, *55*, 14967–14971. [[CrossRef](#)] [[PubMed](#)]
152. Elangovan, S.; Neumann, J.; Sortais, J.B.; Junge, K.; Darcel, C.; Beller, M. Efficient and selective N-alkylation of amines with alcohols catalysed by manganese pincer complexes. *Nat. Commun.* **2016**, *7*, 1–8. [[CrossRef](#)] [[PubMed](#)]
153. Mastalir, M.; Tomsu, G.; Pittenauer, E.; Allmaier, G.; Kirchner, K. Co(II) PCP Pincer Complexes as Catalysts for the Alkylation of Aromatic Amines with Primary Alcohols. *Org. Lett.* **2016**, *18*, 3462–3465. [[CrossRef](#)] [[PubMed](#)]
154. Rösler, S.; Ertl, M.; Irrgang, T.; Kempe, R. Cobalt-Catalyzed Alkylation of Aromatic Amines by Alcohols. *Angew. Chem. Int. Ed.* **2015**, *54*, 15046–15050. [[CrossRef](#)]
155. Mastalir, M.; Stöger, B.; Pittenauer, E.; Puchberger, M.; Allmaier, G.; Kirchner, K. Air Stable Iron(II) PNP Pincer Complexes as Efficient Catalysts for the Selective Alkylation of Amines with Alcohols. *Adv. Synth. Catal.* **2016**, *358*, 3824–3831. [[CrossRef](#)]
156. Homberg, L.; Roller, A.; Hultsch, K.C. A Highly Active PN 3 Manganese Pincer Complex Performing N-Alkylation of Amines under Mild Conditions. *Org. Lett.* **2019**, *21*, 3142–3147. [[CrossRef](#)]
157. Landge, V.G.; Mondal, A.; Kumar, V.; Nandakumar, A.; Balaraman, E. Manganese catalyzed N-alkylation of anilines with alcohols: Ligand enabled selectivity. *Org. Biomol. Chem.* **2018**, *16*, 8175–8180. [[CrossRef](#)]
158. Li, J.; Lutz, M.; Klein Gebbink, R.J.M. *N,N,O*-Coordinated tricarbonylrhenium precatalysts for the aerobic deoxydehydration of diols and polyols. *Catal. Sci. Technol.* **2020**, *10*, 3782–3788. [[CrossRef](#)]
159. Siu, T.C.; Silva, I.; Lunn, M.J.; John, A. Influence of the pendant arm in deoxydehydration catalyzed by dioxomolybdenum complexes supported by amine bisphenolate ligands. *New J. Chem.* **2020**, *44*, 9933–9941. [[CrossRef](#)]
160. Petersen, A.R.; Fristrup, P. New Motifs in Deoxydehydration: Beyond the Realms of Rhenium. *Chem. A Eur. J.* **2017**, *23*, 10235–10243. [[CrossRef](#)] [[PubMed](#)]
161. Tshibalonza, N.N.; Monbaliu, J.-C.M. The deoxydehydration (DODH) reaction: A versatile technology for accessing olefins from bio-based polyols. *Green Chem.* **2020**. [[CrossRef](#)]
162. Chen, F.; Wang, N.; Lei, H.; Guo, D.; Liu, H.; Zhang, Z.; Zhang, W.; Lai, W.; Cao, R. Electrocatalytic Water Oxidation by a Water-Soluble Copper(II) Complex with a Copper-Bound Carbonate Group Acting as a Potential Proton Shuttle. *Inorg. Chem.* **2017**, *56*, 13368–13375. [[CrossRef](#)] [[PubMed](#)]
163. Lant, H.M.C.; Michaelos, T.K.; Sharninghausen, L.S.; Mercado, B.Q.; Crabtree, R.H.; Brudvig, G.W. *N,N,O* Pincer Ligand with a Deprotonatable Site That Promotes Redox-Leveling, High Mn Oxidation States, and a Mn<sub>2</sub>O<sub>2</sub> Dimer Competent for Catalytic Oxygen Evolution. *Eur. J. Inorg. Chem.* **2019**, *2019*, 2115–2123. [[CrossRef](#)]
164. Kohl, S.W.; Weiner, L.; Schwartsburd, L.; Konstantinovski, L.; Shimon, L.J.W.; Ben-David, Y.; Iron, M.A.; Milstein, D. Consecutive Thermal H<sub>2</sub> and Light-Induced O<sub>2</sub> Evolution from Water Promoted by a Metal Complex. *Science* **2009**, *324*, 74–77. [[CrossRef](#)]
165. Sandhya, K.S.; Suresh, C.H. Water splitting promoted by a ruthenium(II) PNN complex: An alternate pathway through a dihydrogen complex for hydrogen production. *Organometallics* **2011**, *30*, 3888–3891. [[CrossRef](#)]
166. Sandhya, K.S.; Suresh, C.H. DFT study on the mechanism of water-assisted dihydrogen elimination in group 6 octahedral metal hydride complexes. *Dalt. Trans.* **2012**, *41*, 11018–11025. [[CrossRef](#)]



167. Sandhya, K.S.; Remya, G.S.; Suresh, C.H. Pincer Ligand Modifications to Tune the Activation Barrier for H<sub>2</sub> Elimination in Water Splitting Milstein Catalyst. *Inorg. Chem.* **2015**, *54*, 11150–11156. [\[CrossRef\]](#)
168. Ma, C.; Piccinin, S.; Fabris, S. Reaction mechanisms of water splitting and H<sub>2</sub> evolution by a Ru(II)-pincer complex identified with Ab initio metadynamics simulations. *ACS Catal.* **2012**, *2*, 1500–1506. [\[CrossRef\]](#)
169. Yang, X.; Hall, M.B. Mechanism of water splitting and oxygen-oxygen bond formation by a mononuclear ruthenium complex. *J. Am. Chem. Soc.* **2010**, *132*, 120–130. [\[CrossRef\]](#) [\[PubMed\]](#)
170. Nielsen, M. Catalyst Kinetics and Stability in Homogeneous Alcohol Acceptorless Dehydrogenation. In *Advanced Chemical Kinetics*; InTech: London, UK, 2018; Chapter 6; ISBN 978-953-51-3816-7.
171. Nielsen, M. Hydrogen production by homogeneous catalysis: Alcohol acceptorless dehydrogenation. In *Hydrogen Production and Remediation of Carbon and Pollutants*; Springer: Basel, Switzerland, 2015; Chapter 1; ISBN 9783319193755.
172. Valdés, H.; García-Eleno, M.A.; Canseco-Gonzalez, D.; Morales-Morales, D. Recent Advances in Catalysis with Transition-Metal Pincer Compounds. *ChemCatChem* **2018**, *10*, 3136–3172. [\[CrossRef\]](#)
173. Shende, V.S.; Saptal, V.B.; Bhanage, B.M. Recent Advances Utilized in the Recycling of Homogeneous Catalysis. *Chem. Rec.* **2019**, *19*, 2022–2043. [\[CrossRef\]](#) [\[PubMed\]](#)
174. Dixneuf, P.H. *Organometallics for Green Catalysis*; Springer: Basel, Switzerland, 2019; ISBN 9783030109547.
175. Werkmeister, S.; Neumann, J.; Junge, K.; Beller, M. Pincer-Type Complexes for Catalytic (De) Hydrogenation and Transfer (De) Hydrogenation Reactions: Recent Progress. *Chem. A Eur. J.* **2015**, *21*, 12226–12250. [\[CrossRef\]](#)
176. Crabtree, R.H. Homogeneous Transition Metal Catalysis of Acceptorless Dehydrogenative Alcohol Oxidation: Applications in Hydrogen Storage and to Heterocycle Synthesis. *Chem. Rev.* **2017**, *117*, 9228–9246. [\[CrossRef\]](#)
177. Gunanathan, C.; Milstein, D. Applications of Acceptorless Dehydrogenation and Related Transformations in Chemical Synthesis. *Science* **2013**, *341*, 1229712. [\[CrossRef\]](#)
178. Spasyuk, D.; Smith, S.; Gusev, D.G. From esters to alcohols and back with ruthenium and osmium catalysts. *Angew. Chem. Int. Ed.* **2012**, *51*, 2772–2775. [\[CrossRef\]](#)
179. Spasyuk, D.; Gusev, D.G. Acceptorless dehydrogenative coupling of ethanol and hydrogenation of esters and imines. *Organometallics* **2012**, *31*, 5239–5242. [\[CrossRef\]](#)
180. Nielsen, M.; Junge, H.; Kammer, A.; Beller, M. Towards a green process for bulk-scale synthesis of ethyl acetate: Efficient acceptorless dehydrogenation of ethanol. *Angew. Chem. Int. Ed.* **2012**, *51*, 5711–5713. [\[CrossRef\]](#)
181. Sponholz, P.; Mellmann, D.; Cordes, C.; Alsabeh, P.G.; Li, B.; Li, Y.; Nielsen, M.; Junge, H.; Dixneuf, P.; Beller, M. Efficient and Selective Hydrogen Generation from Bioethanol using Ruthenium Pincer-type Complexes. *ChemSusChem* **2014**, *7*, 2419–2422. [\[CrossRef\]](#)
182. Li, Y.; Sponholz, P.; Nielsen, M.; Junge, H.; Beller, M. Iridium-catalyzed hydrogen production from monosaccharides, disaccharide, cellulose, and lignocellulose. *ChemSusChem* **2015**, *8*, 804–808. [\[CrossRef\]](#)
183. Nguyen, D.H.; Trivelli, X.; Capet, F.; Swesi, Y.; Favre-Régouillon, A.; Vanoye, L.; Dumeignil, F.; Gauvin, R.M. Deeper Mechanistic Insight into Ru Pincer-Mediated Acceptorless Dehydrogenative Coupling of Alcohols: Exchanges, Intermediates, and Deactivation Species. *ACS Catal.* **2018**, *8*, 4719–4734. [\[CrossRef\]](#)
184. Pandey, P.; Dutta, I.; Bera, J.K. Acceptorless Alcohol Dehydrogenation: A Mechanistic Perspective. *Proc. Natl. Acad. Sci. India Sect. A Phys. Sci.* **2016**, *86*, 561–579. [\[CrossRef\]](#)
185. Anaby, A.; Schelwies, M.; Schwaben, J.; Rominger, F.; Hashmi, A.S.K.; Schaub, T. Study of Precatalyst Degradation Leading to the Discovery of a New Ru<sup>0</sup> Precatalyst for Hydrogenation and Dehydrogenation. *Organometallics* **2018**, *37*, 2193–2201. [\[CrossRef\]](#)
186. Dub, P.A.; Gordon, J.C. The mechanism of enantioselective ketone reduction with Noyori and Noyori-Ikariya bifunctional catalysts. *Dalt. Trans.* **2016**, *45*, 6756–6781. [\[CrossRef\]](#) [\[PubMed\]](#)
187. Remya, G.S.; Suresh, C.H. Hydrogen elimination reactivity of ruthenium pincer hydride complexes: A DFT study. *New J. Chem.* **2019**, *43*, 14634–14642. [\[CrossRef\]](#)
188. Handgraaf, J.-W.; Meijer, E.J. Realistic Modeling of Ruthenium-Catalyzed Transfer Hydrogenation. *J. Am. Chem. Soc.* **2007**, *129*, 3099–3103. [\[CrossRef\]](#)
189. Hou, C.; Zhang, Z.; Zhao, C.; Ke, Z. DFT Study of Acceptorless Alcohol Dehydrogenation Mediated by Ruthenium Pincer Complexes: Ligand Tautomerization Governing Metal Ligand Cooperation. *Inorg. Chem.* **2016**, *55*, 6539–6551. [\[CrossRef\]](#)

190. Awasthi, M.K.; Singh, S.K. Ruthenium Catalyzed Dehydrogenation of Alcohols and Mechanistic Study. *Inorg. Chem.* **2019**, *58*, 14912–14923. [\[CrossRef\]](#)
191. Chen, X.; Yang, X. Mechanistic Insights and Computational Design of Transition-Metal Catalysts for Hydrogenation and Dehydrogenation Reactions. *Chem. Rec.* **2016**, *16*, 2364–2378. [\[CrossRef\]](#)
192. Tao, J.; Wen, L.; Lv, X.; Qi, Y.; Yin, H. Ruthenium(II)-PNN pincer complex catalyzed dehydrogenation of benzyl alcohol to ester: A DFT study. *J. Mol. Struct.* **2016**, *1110*, 24–31. [\[CrossRef\]](#)
193. Ji, M.; Dong, C.; Yang, X. Density functional theory prediction of cobalt pincer complexes for catalytic dehydrogenation of ethanol. *J. Coord. Chem.* **2016**, *69*, 1380–1387. [\[CrossRef\]](#)
194. Dub, P.A.; Gordon, J.C. Metal-ligand bifunctional catalysis: The “Accepted” mechanism, the issue of concertedness, and the function of the ligand in catalytic cycles involving hydrogen atoms. *ACS Catal.* **2017**, *7*, 6635–6655. [\[CrossRef\]](#)
195. Vicent, C.; Gusev, D.G. ESI-MS Insights into Acceptorless Dehydrogenative Coupling of Alcohols. *ACS Catal.* **2016**, *6*, 3301–3309. [\[CrossRef\]](#)
196. Dub, P.A.; Gordon, J.C. The role of the metal-bound N–H functionality in Noyori-type molecular catalysts. *Nat. Rev. Chem.* **2018**, *2*, 396–408. [\[CrossRef\]](#)
197. Schneider, S.; Meiners, J.; Askevold, B. Cooperative aliphatic PNP amido pincer ligands-versatile building blocks for coordination chemistry and catalysis. *Eur. J. Inorg. Chem.* **2012**, 412–429. [\[CrossRef\]](#)
198. Charman, H.B. Hydride transfer reactions catalysed by metal complexes. *J. Chem. Soc. B Phys. Org.* **1967**, *36*, 629–632. [\[CrossRef\]](#)
199. Morton, D.; Cole-Hamilton, D.J. ChemInform Abstract: Molecular Hydrogen Complexes in Catalysis: Highly Efficient Hydrogen Production from Alcoholic Substrates Catalyzed by Ruthenium Complexes. *ChemInform* **2016**, *20*, 1154–1156. [\[CrossRef\]](#)
200. Morton, D.; Cole-Hamilton, D.J.; Schofield, J.A.; Pryce, R.J. Rapid thermal hydrogen production from 2,3-butanediol catalyzed by homogeneous rhodium catalysis. *Polyhedron* **1987**, *6*, 2187–2189. [\[CrossRef\]](#)
201. Dobson, A.; Robinson, S.D. Catalytic dehydrogenation of primary and secondary alcohols by Ru(OCOFCF<sub>3</sub>)<sub>2</sub>(CO)(PPh<sub>3</sub>)<sub>2</sub>. *J. Organomet. Chem.* **1975**, *87*, 52–53. [\[CrossRef\]](#)
202. Dobson, A.; Robinson, S.D. Complexes of the Platinum Metals. 7. Homogeneous Ruthenium and Osmium Catalysts for the Dehydrogenation of Primary and Secondary Alcohols. *Inorg. Chem.* **1977**, *16*, 137–142. [\[CrossRef\]](#)
203. Zhang, J.; Gandelman, M.; Shimon, L.J.W.; Rozenberg, H.; Milstein, D. Electron-rich, bulky ruthenium PNP-type complexes. Acceptorless catalytic alcohol dehydrogenation. *Organometallics* **2004**, *23*, 4026–4033. [\[CrossRef\]](#)
204. Zhang, J.; Leitun, G.; Ben-David, Y.; Milstein, D. Facile conversion of alcohols into esters and dihydrogen catalyzed by new ruthenium complexes. *J. Am. Chem. Soc.* **2005**, *127*, 10840–10841. [\[CrossRef\]](#) [\[PubMed\]](#)
205. Milstein, D. Discovery of environmentally benign catalytic reactions of alcohols catalyzed by pyridine-based pincer Ru complexes, based on metal-ligand cooperation. *Top. Catal.* **2010**, *53*, 915–923. [\[CrossRef\]](#)
206. Gunanathan, C.; Milstein, D. Metal-ligand cooperation by aromatization-dearomatization: A new paradigm in bond activation and “green” catalysis. *Acc. Chem. Res.* **2011**, *44*, 588–602. [\[CrossRef\]](#)
207. Milstein, D. Metal-ligand cooperation by aromatization-dearomatization as a tool in single bond activation. *Phil. Trans. R. Soc. A* **2015**, *373*, 20140189. [\[CrossRef\]](#)
208. Khusnutdinova, J.R.; Milstein, D. Metal-Ligand Cooperation. *Angew. Chem. Int. Ed.* **2015**, *54*, 12236–12273. [\[CrossRef\]](#)
209. Zell, T.; Milstein, D. Hydrogenation and Dehydrogenation Iron Pincer Catalysts Capable of Metal–Ligand Cooperation by Aromatization/Deaeromatization. *Acc. Chem. Res.* **2015**, *48*, 1979–1994. [\[CrossRef\]](#)
210. Hale, L.V.A.; Szymczak, N.K. Hydrogen Transfer Catalysis beyond the Primary Coordination Sphere. *ACS Catal.* **2018**, *8*, 6446–6461. [\[CrossRef\]](#)
211. Gelman, D.; Musa, S. Coordination Versatility of sp<sup>3</sup>-Hybridized Pincer Ligands toward Ligand–Metal Cooperative Catalysis. *ACS Catal.* **2012**, *2*, 2456–2466. [\[CrossRef\]](#)
212. Dub, P.A.; Ikariya, T. Catalytic Reductive Transformations of Carboxylic and Carbonic Acid Derivatives Using Molecular Hydrogen. *ACS Catal.* **2012**, *2*, 1718–1741. [\[CrossRef\]](#)
213. Eisenstein, O.; Crabtree, R.H. Outer sphere hydrogenation catalysis. *New J. Chem.* **2013**, *37*, 21–27. [\[CrossRef\]](#)
214. Yang, X. Hydrogenation of carbon dioxide catalyzed by PNP pincer iridium, iron, and cobalt complexes: A computational design of base metal catalysts. *ACS Catal.* **2011**, *1*, 849–854. [\[CrossRef\]](#)

215. Hasanayn, F.; Baroudi, A.; Bengali, A.A.; Goldman, A.S. Hydrogenation of dimethyl carbonate to methanol by trans-[Ru(H)<sub>2</sub>(PNN)(CO)] catalysts: DFT evidence for ion-pair-mediated metathesis paths for C-OME bond cleavage. *Organometallics* **2013**, *32*, 6969–6985. [\[CrossRef\]](#)
216. Li, H.; Hall, M.B. Computational mechanistic studies on reactions of transition metal complexes with noninnocent pincer ligands: Aromatization-dearomatization or not. *ACS Catal.* **2015**, *5*, 1895–1913. [\[CrossRef\]](#)
217. Gusev, D.G. Revised Mechanisms of the Catalytic Alcohol Dehydrogenation and Ester Reduction with the Milstein PNN Complex of Ruthenium. *Organometallics* **2020**, *39*, 258–270. [\[CrossRef\]](#)
218. Junge, H.; Beller, M. Ruthenium-catalyzed generation of hydrogen from iso-propanol. *Tetrahedron Lett.* **2005**, *46*, 1031–1034. [\[CrossRef\]](#)
219. Nielsen, M.; Kammer, A.; Cozzula, D.; Junge, H.; Gladiali, S.; Beller, M. Efficient hydrogen production from alcohols under mild reaction conditions. *Angew. Chem. Int. Ed.* **2011**, *50*, 9593–9597. [\[CrossRef\]](#)
220. Kuriyama, W.; Matsumoto, T.; Ogata, O.; Ino, Y.; Aoki, K.; Tanaka, S.; Ishida, K.; Kobayashi, T.; Sayo, N.; Saito, T. Catalytic hydrogenation of esters. Development of an efficient catalyst and processes for synthesising (*R*)-1,2-propanediol and 2-(*l*-Menthoxo)ethanol. *Org. Process Res. Dev.* **2012**, *16*, 166–171. [\[CrossRef\]](#)
221. Gunanathan, C.; Ben-David, Y.; Milstein, D. Direct Synthesis of Amides from Alcohols and Amines with Liberation of H<sub>2</sub>. *Science* **2007**, *317*, 790–792. [\[CrossRef\]](#)
222. Kumar, A.; Espinosa-Jalapa, N.A.; Leitus, G.; Diskin-Posner, Y.; Avram, L.; Milstein, D. Direct Synthesis of Amides by Dehydrogenative Coupling of Amines with either Alcohols or Esters: Manganese Pincer Complex as Catalyst. *Angew. Chem. Int. Ed.* **2017**, *56*, 14992–14996. [\[CrossRef\]](#) [\[PubMed\]](#)
223. Gusev, D.G. Rethinking the dehydrogenative amide synthesis. *ACS Catal.* **2017**, *7*, 6656–6662. [\[CrossRef\]](#)
224. Schley, N.D.; Dobereiner, G.E.; Crabtree, R.H. Oxidative synthesis of amides and pyrroles via dehydrogenative alcohol oxidation by ruthenium diphosphine diamine complexes. *Organometallics* **2011**, *30*, 4174–4179. [\[CrossRef\]](#)
225. Lane, E.M.; Uttley, K.B.; Hazari, N.; Bernskoetter, W. Iron-Catalyzed Amide Formation from the Dehydrogenative Coupling of Alcohols and Secondary Amines. *Organometallics* **2017**, *36*, 2020–2025. [\[CrossRef\]](#)
226. Esteruelas, M.A.; Honczek, N.; Oliván, M.; Oñate, E.; Valencia, M. Direct access to pop-type osmium(II) and osmium(IV) complexes: Osmium a promising alternative to ruthenium for the synthesis of imines from alcohols and amines. *Organometallics* **2011**, *30*, 2468–2471. [\[CrossRef\]](#)
227. Fertig, R.; Irrgang, T.; Freitag, F.; Zander, J.; Kempe, R. Manganese-Catalyzed and Base-Switchable Synthesis of Amines or Imines via Borrowing Hydrogen or Dehydrogenative Condensation. *ACS Catal.* **2018**, *8*, 8525–8530. [\[CrossRef\]](#)
228. Mastalir, M.; Glatz, M.; Gorgas, N.; Stöger, B.; Pittenauer, E.; Allmaier, G.; Veiros, L.F.; Kirchner, K. Divergent Coupling of Alcohols and Amines Catalyzed by Isoelectronic Hydride Mn and Fe PNP Pincer Complexes. *Chem. A Eur. J.* **2016**, *22*, 12316–12320. [\[CrossRef\]](#)
229. Borghs, J.C.; Azofra, L.M.; Biberger, T.; Linnenberg, O.; Cavallo, L.; Rueping, M.; El-Sepelgy, O. Manganese-Catalyzed Multicomponent Synthesis of Pyrroles through Acceptorless Dehydrogenation Hydrogen Autotransfer Catalysis: Experiment and Computation. *ChemSusChem* **2019**, *12*, 3083–3088. [\[CrossRef\]](#)
230. Gnanaprakasam, B.; Balaraman, E.; Gunanathan, C.; Milstein, D. Synthesis of polyamides from diols and diamines with liberation of H<sub>2</sub>. *J. Polym. Sci. Part A Polym. Chem.* **2012**, *50*, 1755–1765. [\[CrossRef\]](#)
231. Michlik, S.; Kempe, R. A sustainable catalytic pyrrole synthesis. *Nat. Chem.* **2013**, *5*, 140–144. [\[CrossRef\]](#)
232. Srimani, D.; Ben-David, Y.; Milstein, D. Direct Synthesis of Pyrroles by Dehydrogenative Coupling of  $\beta$ -Aminoalcohols with Secondary Alcohols Catalyzed by Ruthenium Pincer Complexes. *Angew. Chem.* **2013**, *125*, 4104–4107. [\[CrossRef\]](#)
233. Daw, P.; Chakraborty, S.; Garg, J.A.; Ben-David, Y.; Milstein, D. Direct Synthesis of Pyrroles by Dehydrogenative Coupling of Diols and Amines Catalyzed by Cobalt Pincer Complexes. *Angew. Chem. Int. Ed.* **2016**, *55*, 14373–14377. [\[CrossRef\]](#) [\[PubMed\]](#)
234. Midya, S.P.; Landge, V.G.; Sahoo, M.K.; Rana, J.; Balaraman, E. Cobalt-catalyzed acceptorless dehydrogenative coupling of aminoalcohols with alcohols: Direct access to pyrrole, pyridine and pyrazine derivatives. *Chem. Commun.* **2017**, *54*, 90–93. [\[CrossRef\]](#)

235. Borghs, J.C.; Lebedev, Y.; Rueping, M.; El-Sepelgy, O. Sustainable Manganese-Catalyzed Solvent-Free Synthesis of Pyrroles from 1,4-Diols and Primary Amines. *Org. Lett.* **2019**, *21*, 70–74. [\[CrossRef\]](#) [\[PubMed\]](#)
236. Michlik, S.; Kempe, R. Regioselectively functionalized pyridines from sustainable resources. *Angew. Chem. Int. Ed.* **2013**, *52*, 6326–6329. [\[CrossRef\]](#) [\[PubMed\]](#)
237. Gnanaprakasam, B.; Balaraman, E.; Ben-David, Y.; Milstein, D. Synthesis of peptides and pyrazines from  $\beta$ -amino alcohols through extrusion of  $H_2$  catalyzed by ruthenium pincer complexes: Ligand-controlled selectivity. *Angew. Chem. Int. Ed.* **2011**, *50*, 12240–12244. [\[CrossRef\]](#)
238. Daw, P.; Kumar, A.; Espinosa-Jalapa, N.A.; Diskin-Posner, Y.; Ben-David, Y.; Milstein, D. Synthesis of Pyrazines and Quinoxalines via Acceptorless Dehydrogenative Coupling Routes Catalyzed by Manganese Pincer Complexes. *ACS Catal.* **2018**, *8*, 7734–7741. [\[CrossRef\]](#) [\[PubMed\]](#)
239. Das, K.; Mondal, A.; Srimani, D. Phosphine free Mn-complex catalysed dehydrogenative C-C and C-heteroatom bond formation: A sustainable approach to synthesize quinoxaline, pyrazine, benzothiazole and quinoline derivatives. *Chem. Commun.* **2018**, *54*, 10582–10585. [\[CrossRef\]](#)
240. Deibl, N.; Kempe, R. Manganese-Catalyzed Multicomponent Synthesis of Pyrimidines from Alcohols and Amidines. *Angew. Chem. Int. Ed.* **2017**, *56*, 1663–1666. [\[CrossRef\]](#)
241. Das, U.K.; Ben-David, Y.; Diskin-Posner, Y.; Milstein, D. N-Substituted Hydrazones by Manganese-Catalyzed Coupling of Alcohols with Hydrazine: Borrowing Hydrogen and Acceptorless Dehydrogenation in One System. *Angew. Chem. Int. Ed.* **2018**, *57*, 2179–2182. [\[CrossRef\]](#)
242. Mastalir, M.; Glatz, M.; Pittenauer, E.; Allmaier, G.; Kirchner, K. Sustainable Synthesis of Quinolines and Pyrimidines Catalyzed by Manganese PNP Pincer Complexes. *J. Am. Chem. Soc.* **2016**, *138*, 15543–15546. [\[CrossRef\]](#) [\[PubMed\]](#)
243. Chakraborty, S.; Leitus, G.; Milstein, D. Iron-Catalyzed Mild and Selective Hydrogenative Cross-Coupling of Nitriles and Amines to Form Secondary Aldimines. *Angew. Chem.* **2017**, *129*, 2106–2110. [\[CrossRef\]](#)
244. Mukherjee, A.; Nerush, A.; Leitus, G.; Shimon, L.J.W.; Ben David, Y.; Espinosa Jalapa, N.A.; Milstein, D. Manganese-Catalyzed Environmentally Benign Dehydrogenative Coupling of Alcohols and Amines to Form Aldimines and  $H_2$ : A Catalytic and Mechanistic Study. *J. Am. Chem. Soc.* **2016**, *138*, 4298–4301. [\[CrossRef\]](#) [\[PubMed\]](#)
245. Dai, Z.; Luo, Q.; Meng, X.; Li, R.; Zhang, J.; Peng, T. Ru(II) complexes bearing 2,6-bis(benzimidazole-2-yl)pyridine ligands: A new class of catalysts for efficient dehydrogenation of primary alcohols to carboxylic acids and  $H_2$  in the alcohol/CsOH system. *J. Organomet. Chem.* **2017**, *830*, 11–18. [\[CrossRef\]](#)
246. Zhang, L.; Nguyen, D.H.; Raffa, G.; Trivelli, X.; Capet, F.; Desset, S.; Paul, S.; Dumeignil, F.; Gauvin, R.M. Catalytic Conversion of Alcohols into Carboxylic Acid Salts in Water: Scope, Recycling, and Mechanistic Insights. *ChemSusChem* **2016**, *9*, 1413–1423. [\[CrossRef\]](#)
247. Luo, Q.; Dai, Z.; Luo, Q.; Jiang, H.; Li, H.; Zhang, J.; Peng, T. Ni(II)-N'NN' pincer complexes catalyzed dehydrogenation of primary alcohols to carboxylic acids and  $H_2$  accompanied by alcohol etherification. *Catal. Sci. Technol.* **2017**, *7*, 2506–2511.
248. Shao, Z.; Wang, Y.; Liu, Y.; Wang, Q.; Fu, X.; Liu, Q. A general and efficient Mn-catalyzed acceptorless dehydrogenative coupling of alcohols with hydroxides into carboxylates. *Org. Chem. Front.* **2018**, *5*, 1248–1256. [\[CrossRef\]](#)
249. Bhatia, A.; Muthaiah, S. Well-Defined Ruthenium Complex for Acceptorless Alcohol Dehydrogenation in Aqueous Medium. *ChemistrySelect* **2018**, *3*, 3737–3741. [\[CrossRef\]](#)
250. Huang, F.; Liu, Z.; Yu, Z. C-alkylation of ketones and related compounds by alcohols: Transition-metal-catalyzed dehydrogenation. *Angew. Chem. Int. Ed.* **2016**. [\[CrossRef\]](#)
251. Wang, Z.; Pan, B.; Liu, Q.; Yue, E.; Solan, G.A.; Ma, Y.; Sun, W.H. Efficient acceptorless dehydrogenation of secondary alcohols to ketones mediated by a PNN-Ru(II) catalyst. *Catal. Sci. Technol.* **2017**, *7*, 1654–1661. [\[CrossRef\]](#)
252. Zhang, L.; Raffa, G.; Nguyen, D.H.; Swesi, Y.; Corbel-Demailly, L.; Capet, F.; Trivelli, X.; Desset, S.; Paul, S.; Paul, J.F.; et al. Acceptorless dehydrogenative coupling of alcohols catalysed by ruthenium PNP complexes: Influence of catalyst structure and of hydrogen mass transfer. *J. Catal.* **2016**, *340*, 331–343. [\[CrossRef\]](#)
253. Srimani, D.; Balaraman, E.; Gnanaprakasam, B.; Ben-David, Y.; Milstein, D. Ruthenium pincer-catalyzed cross-dehydrogenative coupling of primary alcohols with secondary alcohols under neutral conditions. *Adv. Synth. Catal.* **2012**, *354*, 2403–2406. [\[CrossRef\]](#)



254. De Boer, S.Y.; Korstanje, T.J.; La Rooij, S.R.; Kox, R.; Reek, J.N.H.; Van Der Vlugt, J.I. Ruthenium PNN(O) Complexes: Cooperative Reactivity and Application as Catalysts for Acceptorless Dehydrogenative Coupling Reactions. *Organometallics* **2017**, *36*, 1541–1549. [\[CrossRef\]](#) [\[PubMed\]](#)
255. Nguyen, D.H.; Trivelli, X.; Capet, F.; Paul, J.F.; Dumeignil, F.; Gauvin, R.M. Manganese Pincer Complexes for the Base-Free, Acceptorless Dehydrogenative Coupling of Alcohols to Esters: Development, Scope, and Understanding. *ACS Catal.* **2017**, *7*, 2022–2032. [\[CrossRef\]](#)
256. Das, U.K.; Ben-David, Y.; Leitun, G.; Diskin-Posner, Y.; Milstein, D. Dehydrogenative Cross-Coupling of Primary Alcohols to Form Cross-Esters Catalyzed by a Manganese Pincer Complex. *ACS Catal.* **2019**, *9*, 479–484. [\[CrossRef\]](#)
257. Gunanathan, C.; Shimon, L.J.W.; Milstein, D. Direct conversion of alcohols to acetals and H<sub>2</sub> catalyzed by an acridine-based ruthenium pincer complex. *J. Am. Chem. Soc.* **2009**, *131*, 3146–3147. [\[CrossRef\]](#)
258. Das, U.K.; Chakraborty, S.; Diskin-Posner, Y.; Milstein, D. Direct Conversion of Alcohols into Alkenes by Dehydrogenative Coupling with Hydrazine/Hydrazone Catalyzed by Manganese. *Angew. Chem.* **2018**, *130*, 13632–13636. [\[CrossRef\]](#)
259. Musa, S.; Shaposhnikov, I.; Cohen, S.; Gelman, D. Ligand-metal cooperation in pcppincer complexes: Rational design and catalytic activity in acceptorless dehydrogenation of alcohols. *Angew. Chem. Int. Ed.* **2011**, *50*, 3533–3537. [\[CrossRef\]](#)
260. Peña-López, M.; Neumann, H.; Beller, M. Iron(II) Pincer-Catalyzed Synthesis of Lactones and Lactams through a Versatile Dehydrogenative Domino Sequence. *ChemCatChem* **2015**, *7*, 865–871. [\[CrossRef\]](#)
261. Zhao, J.; Hartwig, J.F. Acceptorless, Neat, Ruthenium-Catalyzed Dehydrogenative Cyclization of Diols to Lactones. *Organometallics* **2005**, *24*, 2441–2446. [\[CrossRef\]](#)
262. Chase, P.A.; Gossage, R.A.; Van Koten, G. Modern organometallic multidentate ligand design strategies: The birth of the privileged “pincer” ligand platform. In *The Privileged Pincer-Metal Platform: Coordination Chemistry & Applications*; Springer: Basel, Switzerland, 2015; ISBN 9783319229270.
263. Van Koten, G.; Gossage, R.A. *The Privileged Pincer-Metal Platform: Coordination Chemistry & Applications*; Springer: Basel, Switzerland, 2015; ISBN 9783319229270.
264. Van Koten, G. *Organometallic Pincer Chemistry*; van Koten, G., Milstein, D., Eds.; Topics in Organometallic Chemistry; Springer: Berlin/Heidelberg, Germany, 2013; ISBN 978-3-642-31080-5.
265. Szabó, K.J.; Wendt, O.F. *Pincer and Pincer-Type Complexes: Applications in Organic Synthesis and Catalysis*; Wiley-VCH: Weinheim, Germany, 2014; ISBN 9783527681303.
266. van Koten, G. Pincer ligands as powerful tools for catalysis in organic synthesis. *J. Organomet. Chem.* **2013**, *730*, 156–164. [\[CrossRef\]](#)
267. Niermann, M.; Beckendorff, A.; Kaltschmitt, M.; Bonhoff, K. Liquid Organic Hydrogen Carrier (LOHC)—Assessment based on chemical and economic properties. *Int. J. Hydrog. Energy* **2019**, *44*, 6631–6654. [\[CrossRef\]](#)
268. Zhu, Q.-L.; Xu, Q. Liquid organic and inorganic chemical hydrides for high-capacity hydrogen storage. *Energy Environ. Sci.* **2015**, *8*, 478–512. [\[CrossRef\]](#)
269. Biniwale, R.B.; Rayalu, S.; Devotta, S.; Ichikawa, M. Chemical hydrides: A solution to high capacity hydrogen storage and supply. *Int. J. Hydrog. Energy* **2008**, *33*, 360–365. [\[CrossRef\]](#)
270. Di Profio, P.; Arca, S.; Rossi, F.; Filippini, M. Comparison of hydrogen hydrates with existing hydrogen storage technologies: Energetic and economic evaluations. *Int. J. Hydrog. Energy* **2009**, *34*, 9173–9180. [\[CrossRef\]](#)
271. Sotoodeh, F.; Huber, B.J.M.; Smith, K.J. Dehydrogenation kinetics and catalysis of organic heteroaromatics for hydrogen storage. *Int. J. Hydrog. Energy* **2012**, *37*, 2715–2722. [\[CrossRef\]](#)
272. Züttel, A. Materials for hydrogen storage. *Mater. Today* **2003**, *6*, 24–33. [\[CrossRef\]](#)
273. He, T.; Pei, Q.; Chen, P. Liquid organic hydrogen carriers. *J. Energy Chem.* **2015**, *24*, 587–594. [\[CrossRef\]](#)
274. Preuster, P.; Papp, C.; Wasserscheid, P. Liquid organic hydrogen carriers (LOHCs): Toward a hydrogen-free hydrogen economy. *Acc. Chem. Res.* **2017**, *50*, 74–85. [\[CrossRef\]](#)
275. Stark, K.; Emelyanenko, V.N.; Zhabina, A.A.; Varfolomeev, M.A.; Verevkin, S.P.; Müller, K.; Arlt, W. Liquid Organic Hydrogen Carriers: Thermophysical and Thermochemical Studies of Carbazole Partly and Fully Hydrogenated Derivatives. *Ind. Eng. Chem. Res.* **2015**, *54*, 7953–7966. [\[CrossRef\]](#)

276. Müller, K.; Stark, K.; Emelyanenko, V.N.; Varfolomeev, M.A.; Zaitsau, D.H.; Shoifet, E.; Schick, C.; Verevkin, S.P.; Arlt, W. Liquid Organic Hydrogen Carriers: Thermophysical and Thermochemical Studies of Benzyl- and Dibenzyl-toluene Derivatives. *Ind. Eng. Chem. Res.* **2015**, *54*, 7967–7976. [\[CrossRef\]](#)
277. Sotoodeh, F.; Smith, K.J. An overview of the kinetics and catalysis of hydrogen storage on organic liquids. *Can. J. Chem. Eng.* **2013**, *91*, 1477–1490. [\[CrossRef\]](#)
278. Sotoodeh, F.; Smith, K.J. Kinetics of hydrogen uptake and release from heteroaromatic compounds for hydrogen storage. *Ind. Eng. Chem. Res.* **2010**, *49*, 1018–1026. [\[CrossRef\]](#)
279. Müller, K.; Aslam, R.; Fischer, A.; Stark, K.; Wasserscheid, P.; Arlt, W. Experimental assessment of the degree of hydrogen loading for the dibenzyl toluene based LOHC system. *Int. J. Hydrog. Energy* **2016**, *41*, 22097–22103. [\[CrossRef\]](#)
280. He, T.; Pachfule, P.; Wu, H.; Xu, Q.; Chen, P. Hydrogen carriers. *Nat. Rev. Mater.* **2016**, *1*, 16059. [\[CrossRef\]](#)
281. Müller, K.; Völkl, J.; Arlt, W. Thermodynamic Evaluation of Potential Organic Hydrogen Carriers. *Energy Technol.* **2013**, *1*, 20–24. [\[CrossRef\]](#)
282. Crabtree, R.H. Hydrogen storage in liquid organic heterocycles. *Energy Environ. Sci.* **2008**, *1*, 134. [\[CrossRef\]](#)
283. Markiewicz, M.; Zhang, Y.Q.; Bösmann, A.; Brückner, N.; Thöming, J.; Wasserscheid, P.; Stolte, S. Environmental and health impact assessment of Liquid Organic Hydrogen Carrier (LOHC) systems—Challenges and preliminary results. *Energy Environ. Sci.* **2015**, *8*, 1035–1045. [\[CrossRef\]](#)
284. Teichmann, D.; Arlt, W.; Wasserscheid, P.; Freymann, R. A future energy supply based on Liquid Organic Hydrogen Carriers (LOHC). *Energy Environ. Sci.* **2011**, *4*, 2767. [\[CrossRef\]](#)
285. Teichmann, D.; Stark, K.; Müller, K.; Zöttl, G.; Wasserscheid, P.; Arlt, W. Energy storage in residential and commercial buildings via Liquid Organic Hydrogen Carriers (LOHC). *Energy Environ. Sci.* **2012**, *5*, 9044. [\[CrossRef\]](#)
286. Teichmann, D.; Arlt, W.; Wasserscheid, P. Liquid Organic Hydrogen Carriers as an efficient vector for the transport and storage of renewable energy. *Int. J. Hydrog. Energy* **2012**, *37*, 18118–18132. [\[CrossRef\]](#)
287. Ahmed, A.; Al-Amin, A.Q.; Ambrose, A.F.; Saidur, R. Hydrogen fuel and transport system: A sustainable and environmental future. *Int. J. Hydrog. Energy* **2016**, *41*, 1369–1380. [\[CrossRef\]](#)
288. Eypasch, M.; Schimpe, M.; Kanwar, A.; Hartmann, T.; Herzog, S.; Frank, T.; Hamacher, T. Model-based techno-economic evaluation of an electricity storage system based on Liquid Organic Hydrogen Carriers. *Appl. Energy* **2017**, *185*, 320–330. [\[CrossRef\]](#)
289. Johnson, T.C.; Morris, D.J.; Wills, M. Hydrogen generation from formic acid and alcohols using homogeneous catalysts. *Chem. Soc. Rev.* **2010**, *39*, 81–88. [\[CrossRef\]](#)
290. Friedrich, A.; Schneider, S. Acceptorless dehydrogenation of alcohols: Perspectives for synthesis and H<sub>2</sub> storage. *ChemCatChem* **2009**, *1*, 72–73. [\[CrossRef\]](#)
291. Trincado, M.; Banerjee, D.; Grützmacher, H. Molecular catalysts for hydrogen production from alcohols. *Energy Environ. Sci.* **2014**, *7*, 2464–2503. [\[CrossRef\]](#)
292. Campos, J. Dehydrogenation of alcohols and polyols from a hydrogen production perspective. *Phys. Sci. Rev.* **2018**, *3*, 1–25.
293. Shimabayashi, T.; Fujita, K. Ichi Metal-catalyzed hydrogenation and dehydrogenation reactions for efficient hydrogen storage. *Tetrahedron* **2020**, *76*, 130946. [\[CrossRef\]](#)
294. Onishi, N.; Laurenczy, G.; Beller, M.; Himeda, Y. Recent progress for reversible homogeneous catalytic hydrogen storage in formic acid and in methanol. *Coord. Chem. Rev.* **2018**, *373*, 317–332. [\[CrossRef\]](#)
295. Sordakis, K.; Tang, C.; Vogt, L.K.; Junge, H.; Dyson, P.J.; Beller, M.; Laurenczy, G. Homogeneous Catalysis for Sustainable Hydrogen Storage in Formic Acid and Alcohols. *Chem. Rev.* **2018**, *118*, 372–433. [\[CrossRef\]](#)
296. Trincado, M.; Grützmacher, H.; Precht, M.H.G. CO<sub>2</sub>-based hydrogen storage—Hydrogen generation from formaldehyde/water. *Phys. Sci. Rev.* **2018**, *3*, 1–19.
297. Langer, R.; Thomas, Z.; Schaub, T. CO<sub>2</sub>-based hydrogen storage: CO<sub>2</sub> hydrogenation to formic acid, formaldehyde and methanol. *Phys. Sci. Rev.* **2018**, *3*, 1–14.
298. Boddien, A.; Gärtner, F.; Nielsen, M.; Losse, S.; Junge, H. *Hydrogen Generation from Formic Acid and Alcohols*; Elsevier: Amsterdam, The Netherlands, 2013; Volume 6, pp. 587–603. ISBN 9780080965291.
299. Enthaler, S.; von Langermann, J.; Schmidt, T. Carbon dioxide and formic acid—The couple for environmental-friendly hydrogen storage? *Energy Environ. Sci.* **2010**, *3*, 1207. [\[CrossRef\]](#)
300. Eppinger, J.; Huang, K.W. Formic Acid as a Hydrogen Energy Carrier. *ACS Energy Lett.* **2017**, *2*, 188–195. [\[CrossRef\]](#)

301. Olah, G.A.; Goeppert, A.; Prakash, G.K.S. The “Methanol Economy”: General Aspects. In *Beyond Oil and Gas*; Wiley: Weinheim, Germany, 2018.
302. Olah, G.A. After oil and gas: Methanol economy. *Catal. Lett.* **2004**, *93*, 1–2. [[CrossRef](#)]
303. Stephan, D.W. A step closer to a methanol economy. *Nature* **2013**, *495*, 54–55. [[CrossRef](#)]
304. Salvi, B.L.; Subramanian, K.A.; Panwar, N.L. Alternative fuels for transportation vehicles: A technical review. *Renew. Sustain. Energy Rev.* **2013**, *25*, 404–419. [[CrossRef](#)]
305. Piola, L.; Fernández-Salas, J.A.; Nahra, F.; Poater, A.; Cavallo, L.; Nolan, S.P. Ruthenium-catalysed decomposition of formic acid: Fuel cell and catalytic applications. *Mol. Catal.* **2017**, *440*, 184–189. [[CrossRef](#)]
306. Muradov, N.; Veziroglu, T. “Green” path from fossil-based to hydrogen economy: An overview of carbon-neutral technologies. *Int. J. Hydrog. Energy* **2008**, *33*, 6804–6839. [[CrossRef](#)]
307. Olah, G.A.; Prakash, G.K.S.; Goeppert, A. Anthropogenic Chemical Carbon Cycle for a Sustainable Future. *J. Am. Chem. Soc.* **2011**, *133*, 12881–12898. [[CrossRef](#)]
308. Fu, H.C.; You, F.; Li, H.R.; He, L.N. CO<sub>2</sub> Capture and in situ Catalytic Transformation. *Front. Chem.* **2019**, *7*, 1–15. [[CrossRef](#)]
309. Artz, J.; Müller, T.E.; Thenert, K.; Kleinekorte, J.; Meys, R.; Sternberg, A.; Bardow, A.; Leitner, W. Sustainable Conversion of Carbon Dioxide: An Integrated Review of Catalysis and Life Cycle Assessment. *Chem. Rev.* **2018**, *118*, 434–504. [[CrossRef](#)] [[PubMed](#)]
310. Klankermayer, J.; Wesselbaum, S.; Beydoun, K.; Leitner, W. Selective Catalytic Synthesis Using the Combination of Carbon Dioxide and Hydrogen: Catalytic Chess at the Interface of Energy and Chemistry. *Angew. Chem. Int. Ed.* **2016**, *55*, 7296–7343. [[CrossRef](#)] [[PubMed](#)]
311. Langer, R.; Thomas, Z.; Suárez, A. Hydrogenation of carbonyl compounds of relevance to hydrogen storage in alcohols. *Phys. Sci. Rev.* **2018**, *3*, 1–31.
312. Song, C. Global challenges and strategies for control, conversion and utilization of CO<sub>2</sub> for sustainable development involving energy, catalysis, adsorption and chemical processing. *Catal. Today* **2006**, *115*, 2–32. [[CrossRef](#)]
313. Rumayor, M.; Dominguez-Ramos, A.; Irabien, A. Formic Acid manufacture: Carbon dioxide utilization alternatives. *Appl. Sci.* **2018**, *8*, 1–12. [[CrossRef](#)]
314. Obama, B. The irreversible momentum of clean energy. *Science* **2017**, *355*, 126–129. [[CrossRef](#)]
315. Li, Y.; Nielsen, M.; Li, B.; Dixneuf, P.H.; Junge, H.; Beller, M. Ruthenium-catalyzed hydrogen generation from glycerol and selective synthesis of lactic acid. *Green Chem.* **2015**, *17*, 193–198. [[CrossRef](#)]
316. Sharninghausen, L.S.; Mercado, B.Q.; Crabtree, R.H.; Hazari, N. Selective conversion of glycerol to lactic acid with iron pincer precatalysts. *Chem. Commun.* **2015**, *51*, 16201–16204. [[CrossRef](#)]
317. Chakraborty, S.; Lagaditis, P.O.; Förster, M.; Bielinski, E.A.; Hazari, N.; Holthausen, M.C.; Jones, W.D.; Schneider, S. Well-Defined Iron Catalysts for the Acceptorless Reversible Dehydrogenation-Hydrogenation of Alcohols and Ketones. *ACS Catal.* **2014**, *4*, 3994–4003. [[CrossRef](#)]
318. Lane, E.M.; Hazari, N.; Bernskoetter, W.H. Iron-catalyzed urea synthesis: Dehydrogenative coupling of methanol and amines. *Chem. Sci.* **2018**, *9*, 4003–4008. [[CrossRef](#)] [[PubMed](#)]
319. Xie, Y.; Hu, P.; Ben-David, Y.; Milstein, D. A Reversible Liquid Organic Hydrogen Carrier System Based on Methanol-Ethylenediamine and Ethylene Urea. *Angew. Chem. Int. Ed.* **2019**, *58*, 5105–5109. [[CrossRef](#)] [[PubMed](#)]
320. Alberico, E.; Nielsen, M. Towards a methanol economy based on homogeneous catalysis: Methanol to H<sub>2</sub> and CO<sub>2</sub> to methanol. *Chem. Commun.* **2015**, *51*, 6714–6725. [[CrossRef](#)] [[PubMed](#)]
321. Kothandaraman, J.; Kar, S.; Goeppert, A.; Sen, R.; Prakash, G.K.S. Advances in Homogeneous Catalysis for Low Temperature Methanol Reforming in the Context of the Methanol Economy. *Top. Catal.* **2018**, *61*, 542–559. [[CrossRef](#)]
322. Simon Araya, S.; Liso, V.; Cui, X.; Li, N.; Zhu, J.; Sahlin, S.L.; Jensen, S.H.; Nielsen, M.P.; Kær, S.K. A Review of the Methanol Economy: The Fuel Cell Route. *Energies* **2020**, *13*, 596. [[CrossRef](#)]
323. Cortright, R.D.; Davda, R.R.; Dumesic, J.A. Hydrogen from catalytic reforming of biomass-derived hydrocarbons in liquid water. In *Materials for Sustainable Energy*; Macmillan Publishers Ltd.: London, UK, 2010; pp. 289–292.
324. Shabaker, J. Aqueous-phase reforming of methanol and ethylene glycol over alumina-supported platinum catalysts. *J. Catal.* **2003**, *215*, 344–352. [[CrossRef](#)]

325. Navarro, R.M.; Peña, M.A.; Fierro, J.L.G. Hydrogen Production Reactions from Carbon Feedstocks: Fossil Fuels and Biomass. *Chem. Rev.* **2007**, *107*, 3952–3991. [\[CrossRef\]](#)
326. Palo, D.R.; Dagle, R.A.; Holladay, J.D. Methanol Steam Reforming for Hydrogen Production. *Chem. Rev.* **2007**, *107*, 3992–4021. [\[CrossRef\]](#) [\[PubMed\]](#)
327. Sá, S.; Silva, H.; Brandão, L.; Sousa, J.M.; Mendes, A. Catalysts for methanol steam reforming—A review. *Appl. Catal. B Environ.* **2010**, *99*, 43–57. [\[CrossRef\]](#)
328. Iulianelli, A.; Ribeiro, P.; Mendes, A.; Basile, A. Methanol steam reforming for hydrogen generation via conventional and membrane reactors: A review. *Renew. Sustain. Energy Rev.* **2014**, *29*, 355–368. [\[CrossRef\]](#)
329. Nielsen, M.; Alberico, E.; Baumann, W.; Drexler, H.J.; Junge, H.; Gladiali, S.; Beller, M. Low-temperature aqueous-phase methanol dehydrogenation to hydrogen and carbon dioxide. *Nature* **2013**, *495*, 85–89. [\[CrossRef\]](#) [\[PubMed\]](#)
330. Rodríguez-Lugo, R.E.; Trincado, M.; Vogt, M.; Tewes, F.; Santiso-Quinones, G.; Grützmacher, H. A homogeneous transition metal complex for clean hydrogen production from methanol—Water mixtures. *Nat. Chem.* **2013**, *5*, 342–347. [\[CrossRef\]](#)
331. Fujita, K.; Kawahara, R.; Aikawa, T.; Yamaguchi, R. Hydrogen Production from a Methanol-Water Solution Catalyzed by an Anionic Iridium Complex Bearing a Functional Bipyridonate Ligand under Weakly Basic Conditions. *Angew. Chem. Int. Ed.* **2015**, *54*, 9057–9060. [\[CrossRef\]](#)
332. Alberico, E.; Sponholz, P.; Cordes, C.; Nielsen, M.; Drexler, H.J.; Baumann, W.; Junge, H.; Beller, M. Selective hydrogen production from methanol with a defined Iron pincer catalyst under mild conditions. *Angew. Chem. Int. Ed.* **2013**, *52*, 14162–14166. [\[CrossRef\]](#) [\[PubMed\]](#)
333. Hu, P.; Diskin-Posner, Y.; Ben-David, Y.; Milstein, D. Reusable homogeneous catalytic system for hydrogen production from methanol and water. *ACS Catal.* **2014**, *4*, 2649–2652. [\[CrossRef\]](#)
334. Monney, A.; Barsch, E.; Sponholz, P.; Junge, H.; Ludwig, R.; Beller, M. Base-free hydrogen generation from methanol using a bi-catalytic system. *Chem. Commun.* **2014**, *50*, 707–709. [\[CrossRef\]](#) [\[PubMed\]](#)
335. Agapova, A.; Junge, H.; Beller, M. Developing Bimetallic Cascade Reactions: Ruthenium-catalyzed Hydrogen Generation from Methanol. *Chem. A Eur. J.* **2019**, *25*, 9345–9349. [\[CrossRef\]](#) [\[PubMed\]](#)
336. Bielinski, E.A.; Förster, M.; Zhang, Y.; Bernskoetter, W.H.; Hazari, N.; Holthausen, M.C. Base-Free Methanol Dehydrogenation Using a Pincer-Supported Iron Compound and Lewis Acid Co-catalyst. *ACS Catal.* **2015**, *5*, 2404–2415. [\[CrossRef\]](#)
337. Alberico, E.; Lennox, A.J.J.; Vogt, L.K.; Jiao, H.; Baumann, W.; Drexler, H.J.; Nielsen, M.; Spannenberg, A.; Checinski, M.P.; Junge, H.; et al. Unravelling the Mechanism of Basic Aqueous Methanol Dehydrogenation Catalyzed by Ru-PNP Pincer Complexes. *J. Am. Chem. Soc.* **2016**, *138*, 14890–14904. [\[CrossRef\]](#)
338. Pinggen, D.; Choi, J.-H.; Allen, H.; Murray, G.; Ganji, P.; van Leeuwen, P.W.N.M.; Precht, M.H.G.; Vogt, D. Amide versus amine ligand paradigm in the direct amination of alcohols with Ru-PNP complexes. *Catal. Sci. Technol.* **2018**, *8*, 3969–3976. [\[CrossRef\]](#)
339. Dub, P.A.; Scott, B.L.; Gordon, J.C. Why does alkylation of the N-H functionality within M/NH bifunctional Noyori-type catalysts lead to turnover? *J. Am. Chem. Soc.* **2017**, *139*, 1245–1260. [\[CrossRef\]](#)
340. Choi, J.H.; Heim, L.E.; Ahrens, M.; Precht, M.H.G. Selective conversion of alcohols in water to carboxylic acids by in situ generated ruthenium trans dihydrido carbonyl PNP complexes. *Dalt. Trans.* **2014**, *43*, 17248–17254. [\[CrossRef\]](#)
341. Wei, Z.; De Aguirre, A.; Junge, K.; Beller, M.; Jiao, H. Exploring the mechanisms of aqueous methanol dehydrogenation catalyzed by defined PNP Mn and Re pincer complexes under base-free as well as strong base conditions. *Catal. Sci. Technol.* **2018**, *8*, 3649–3665. [\[CrossRef\]](#)
342. Jiang, Y.Y.; Xu, Z.Y.; Yu, H.Z.; Fu, Y. A self-catalytic role of methanol in PNP-Ru pincer complex catalysed dehydrogenation. *Sci. China Chem.* **2016**, *59*, 724–729. [\[CrossRef\]](#)
343. Lei, M.; Pan, Y.; Ma, X. The nature of hydrogen production from aqueous-phase methanol dehydrogenation with ruthenium pincer complexes under mild conditions. *Eur. J. Inorg. Chem.* **2015**, *2015*, 794–803. [\[CrossRef\]](#)
344. Yang, X. Mechanistic insights into ruthenium-catalyzed production of H<sub>2</sub> and CO<sub>2</sub> from methanol and water: A DFT study. *ACS Catal.* **2014**, *4*, 1129–1133. [\[CrossRef\]](#)
345. Strobel, V.; Schuster, J.J.; Braeuer, A.S.; Vogt, L.K.; Junge, H.; Haumann, M. Shining light on low-temperature methanol aqueous-phase reforming using homogeneous Ru-pincer complexes—operando Raman-GC studies. *React. Chem. Eng.* **2017**, *2*, 390–396. [\[CrossRef\]](#)



346. Andérez-Fernández, M.; Vogt, L.K.; Fischer, S.; Zhou, W.; Jiao, H.; Garbe, M.; Elangovan, S.; Junge, K.; Junge, H.; Ludwig, R.; et al. A Stable Manganese Pincer Catalyst for the Selective Dehydrogenation of Methanol. *Angew. Chem. Int. Ed.* **2017**, *56*, 559–562. [\[CrossRef\]](#) [\[PubMed\]](#)
347. Prichatz, C.; Alberico, E.; Baumann, W.; Junge, H.; Beller, M. Iridium–PNP Pincer Complexes for Methanol Dehydrogenation at Low Base Concentration. *ChemCatChem* **2017**, *9*, 1891–1896. [\[CrossRef\]](#)
348. Agapova, A.; Alberico, E.; Kammer, A.; Junge, H.; Beller, M. Catalytic Dehydrogenation of Formic Acid with Ruthenium–PNP–Pincer Complexes: Comparing N-Methylated and NH-Ligands. *ChemCatChem* **2019**, *11*, 1910–1914. [\[CrossRef\]](#)
349. Schwarz, C.H.; Agapova, A.; Junge, H.; Haumann, M. Immobilization of a selective Ru-pincer complex for low temperature methanol reforming—Material and process improvements. *Catal. Today* **2020**, *342*, 178–186. [\[CrossRef\]](#)
350. Laurenczy, G.; Dyson, P.J. Homogeneous Catalytic Dehydrogenation of Formic Acid: Progress towards a Hydrogen-Based Economy. *J. Braz. Chem. Soc.* **2014**, *25*, 2157–2163. [\[CrossRef\]](#)
351. Treigerman, Z.; Sasson, Y. Further Observations on the Mechanism of Formic Acid Decomposition by Homogeneous Ruthenium Catalyst. *ChemistrySelect* **2017**, *2*, 5816–5823. [\[CrossRef\]](#)
352. Müller, K.; Brooks, K.; Autrey, T. Hydrogen Storage in Formic Acid: A Comparison of Process Options. *Energy Fuels* **2017**, *31*, 12603–12611. [\[CrossRef\]](#)
353. Mellmann, D.; Sponholz, P.; Junge, H.; Beller, M. Formic acid as a hydrogen storage material—development of homogeneous catalysts for selective hydrogen release. *Chem. Soc. Rev.* **2016**, *45*, 3954–3988. [\[CrossRef\]](#) [\[PubMed\]](#)
354. Guan, C.; Pan, Y.; Zhang, T.; Ajitha, M.J.; Huang, K.W. An Update on Formic Acid Dehydrogenation by Homogeneous Catalysis. *Chem. Asian J.* **2020**, *15*, 937–946. [\[CrossRef\]](#) [\[PubMed\]](#)
355. Enthaler, S.; Loges, B. The Rise of the Iron Age in Hydrogen Evolution? *ChemCatChem* **2012**, *4*, 323–325. [\[CrossRef\]](#)
356. Grasemann, M.; Laurenczy, G. Formic acid as a hydrogen source—Recent developments and future trends. *Energy Environ. Sci.* **2012**, *5*, 8171. [\[CrossRef\]](#)
357. Fukuzumi, S.; Yamada, Y.; Suenobu, T.; Ohkubo, K.; Kotani, H. Catalytic mechanisms of hydrogen evolution with homogeneous and heterogeneous catalysts. *Energy Environ. Sci.* **2011**, *4*, 2754. [\[CrossRef\]](#)
358. Loges, B.; Boddien, A.; Gärtner, F.; Junge, H.; Beller, M. Catalytic Generation of Hydrogen from Formic acid and its Derivatives: Useful Hydrogen Storage Materials. *Top. Catal.* **2010**, *53*, 902–914. [\[CrossRef\]](#)
359. Fukuzumi, S. Bioinspired Energy Conversion Systems for Hydrogen Production and Storage. *Eur. J. Inorg. Chem.* **2008**, *2008*, 1351–1362. [\[CrossRef\]](#)
360. Scotti, N.; Psaro, R.; Ravasio, N.; Zaccheria, F. A new Cu-based system for formic acid dehydrogenation. *RSC Adv.* **2014**, *4*, 61514–61517. [\[CrossRef\]](#)
361. Enthaler, S.; Brück, A.; Kammer, A.; Junge, H.; Irran, E.; Güllak, S. Exploring the reactivity of nickel pincer complexes in the decomposition of formic acid to CO<sub>2</sub>/H<sub>2</sub> and the hydrogenation of NaHCO<sub>3</sub> to HCOONa. *ChemCatChem* **2015**, *7*, 65–69. [\[CrossRef\]](#)
362. Jiang, K.; Xu, K.; Zou, S.; Cai, W.-B. B-Doped Pd Catalyst: Boosting Room-Temperature Hydrogen Production from Formic Acid–Formate Solutions. *J. Am. Chem. Soc.* **2014**, *136*, 4861–4864. [\[CrossRef\]](#) [\[PubMed\]](#)
363. Wang, W.-H.; Ertem, M.Z.; Xu, S.; Onishi, N.; Manaka, Y.; Suna, Y.; Kambayashi, H.; Muckerman, J.T.; Fujita, E.; Himeda, Y. Highly Robust Hydrogen Generation by Bioinspired Ir Complexes for Dehydrogenation of Formic Acid in Water: Experimental and Theoretical Mechanistic Investigations at Different pH. *ACS Catal.* **2015**, *5*, 5496–5504. [\[CrossRef\]](#)
364. Guerriero, A.; Bricout, H.; Sordakis, K.; Peruzzini, M.; Monflier, E.; Hapiot, F.; Laurenczy, G.; Gonsalvi, L. Hydrogen Production by Selective Dehydrogenation of HCOOH Catalyzed by Ru-Biaryl Sulfonated Phosphines in Aqueous Solution. *ACS Catal.* **2014**, *4*, 3002–3012. [\[CrossRef\]](#)
365. Oldenhof, S.; De Bruin, B.; Lutz, M.; Siegler, M.A.; Patureau, F.W.; Van Der Lugt, J.I.; Reek, J.N.H. Base-free production of H<sub>2</sub> by dehydrogenation of formic acid using an iridium-bisMETAMORPhos complex. *Chem. A Eur. J.* **2013**, *19*, 11507–11511. [\[CrossRef\]](#) [\[PubMed\]](#)
366. Tedsree, K.; Li, T.; Jones, S.; Chan, C.W.A.; Yu, K.M.K.; Bagot, P.A.J.; Marquis, E.A.; Smith, G.D.W.; Tsang, S.C.E. Hydrogen production from formic acid decomposition at room temperature using a Ag-Pd core-shell nanocatalyst. *Nat. Nanotechnol.* **2011**, *6*, 302–307. [\[CrossRef\]](#) [\[PubMed\]](#)

367. Boddien, A.; Loges, B.; Junge, H.; Gärtner, F.; Noyes, J.R.; Beller, M. Continuous hydrogen generation from formic acid: Highly active and stable ruthenium catalysts. *Adv. Synth. Catal.* **2009**, *351*, 2517–2520. [[CrossRef](#)]
368. Fellay, C.; Dyson, P.J.; Laurenczy, G. A viable hydrogen-storage system based on selective formic acid decomposition with a ruthenium catalyst. *Angew. Chem. Int. Ed.* **2008**, *47*, 3966–3968. [[CrossRef](#)] [[PubMed](#)]
369. Loges, B.; Boddien, A.; Junge, H.; Beller, M. Controlled generation of hydrogen from formic acid amine adducts at room temperature and application in H<sub>2</sub>/O<sub>2</sub> fuel cells. *Angew. Chem. Int. Ed.* **2008**, *47*, 3962–3965. [[CrossRef](#)] [[PubMed](#)]
370. Czaun, M.; Goepfert, A.; May, R.; Haiges, R.; Prakash, G.K.S.; Olah, G.A. Hydrogen Generation from Formic Acid Decomposition by Ruthenium Carbonyl Complexes. Tetra-ruthenium Dodecacarbonyl Tetrahydride as an Active Intermediate. *ChemSusChem* **2011**, *4*, 1241–1248. [[CrossRef](#)]
371. Fukuzumi, S.; Kobayashi, T.; Suenobu, T. Efficient Catalytic Decomposition of Formic Acid for the Selective Generation of H<sub>2</sub> and H/D Exchange with a Water-Soluble Rhodium Complex in Aqueous Solution. *ChemSusChem* **2008**, *1*, 827–834. [[CrossRef](#)]
372. Onishi, M. Decomposition of formic acid catalyzed by hydrido (phosphonite) cobalt (I) under photoirradiation. *J. Mol. Catal.* **1993**, *80*, 145–149. [[CrossRef](#)]
373. Zhou, X.; Huang, Y.; Xing, W.; Liu, C.; Liao, J.; Lu, T. High-quality hydrogen from the catalyzed decomposition of formic acid by Pd–Au/C and Pd–Ag/C. *Chem. Commun.* **2008**, 3540. [[CrossRef](#)] [[PubMed](#)]
374. Sponholz, P.; Mellmann, D.; Junge, H.; Beller, M. Towards a Practical Setup for Hydrogen Production from Formic Acid. *ChemSusChem* **2013**, *6*, 1172–1176. [[CrossRef](#)]
375. Loges, B.; Boddien, A.; Junge, H.; Noyes, J.R.; Baumann, W.; Beller, M. Hydrogen generation: Catalytic acceleration and control by light. *Chem. Commun.* **2009**, *28*, 4185. [[CrossRef](#)]
376. Fukuzumi, S.; Kobayashi, T.; Suenobu, T. Unusually Large Tunneling Effect on Highly Efficient Generation of Hydrogen and Hydrogen Isotopes in pH-Selective Decomposition of Formic Acid Catalyzed by a Heterodinuclear Iridium–Ruthenium Complex in Water. *J. Am. Chem. Soc.* **2010**, *132*, 1496–1497. [[CrossRef](#)] [[PubMed](#)]
377. Himeda, Y. Highly efficient hydrogen evolution by decomposition of formic acid using an iridium catalyst with 4,4′-dihydroxy-2,2′-bipyridine. *Green Chem.* **2009**, *11*, 2018. [[CrossRef](#)]
378. Tanaka, R.; Yamashita, M.; Chung, L.W.; Morokuma, K.; Nozaki, K. Mechanistic Studies on the Reversible Hydrogenation of Carbon Dioxide Catalyzed by an Ir-PNP Complex. *Organometallics* **2011**, *30*, 6742–6750. [[CrossRef](#)]
379. Gu, X.; Lu, Z.-H.; Jiang, H.-L.; Akita, T.; Xu, Q. Synergistic Catalysis of Metal–Organic Framework-Immobilized Au–Pd Nanoparticles in Dehydrogenation of Formic Acid for Chemical Hydrogen Storage. *J. Am. Chem. Soc.* **2011**, *133*, 11822–11825. [[CrossRef](#)]
380. Bi, Q.-Y.; Du, X.-L.; Liu, Y.-M.; Cao, Y.; He, H.-Y.; Fan, K.-N. Efficient Subnanometric Gold-Catalyzed Hydrogen Generation via Formic Acid Decomposition under Ambient Conditions. *J. Am. Chem. Soc.* **2012**, *134*, 8926–8933. [[CrossRef](#)]
381. Barnard, J.H.; Wang, C.; Berry, N.G.; Xiao, J. Long-range metal–ligand bifunctional catalysis: Cyclometallated iridium catalysts for the mild and rapid dehydrogenation of formic acid. *Chem. Sci.* **2013**, *4*, 1234. [[CrossRef](#)]
382. Boddien, A.; Jackstell, R.; Junge, H.; Spannenberg, A.; Baumann, W.; Ludwig, R.; Beller, M. Ortho-metalation of iron(0) tribenzylphosphine complexes: Homogeneous catalysts for the generation of hydrogen from formic acid. *Angew. Chem. Int. Ed.* **2010**, *49*, 8993–8996. [[CrossRef](#)] [[PubMed](#)]
383. Boddien, A.; Loges, B.; Gärtner, F.; Torborg, C.; Fumino, K.; Junge, H.; Ludwig, R.; Beller, M. Iron-catalyzed hydrogen production from formic acid. *J. Am. Chem. Soc.* **2010**, *132*, 8924–8934. [[CrossRef](#)] [[PubMed](#)]
384. Boddien, A.; Mellmann, D.; Gärtner, F.; Jackstell, R.; Junge, H.; Dyson, P.J.; Laurenczy, G.; Ludwig, R.; Beller, M. Efficient Dehydrogenation of Formic Acid Using an Iron Catalyst. *Science* **2011**, *333*, 1733–1736. [[CrossRef](#)] [[PubMed](#)]
385. Langer, R.; Iron, M.A.; Konstantinovski, L.; Diskin-Posner, Y.; Leituss, G.; Ben-David, Y.; Milstein, D. Iron borohydride pincer complexes for the efficient hydrogenation of ketones under mild, base-free conditions: Synthesis and mechanistic insight. *Chem. A Eur. J.* **2012**, *18*, 7196–7209. [[CrossRef](#)]
386. Zhang, J.; Leituss, G.; Ben-David, Y.; Milstein, D. Efficient homogeneous catalytic hydrogenation of esters to alcohols. *Angew. Chem. Int. Ed.* **2006**, *45*, 1113–1115. [[CrossRef](#)]

387. Langer, R.; Diskin-Posner, Y.; Leitun, G.; Shimon, L.J.W.; Ben-David, Y.; Milstein, D. Low-pressure hydrogenation of carbon dioxide catalyzed by an iron pincer complex exhibiting noble metal activity. *Angew. Chem. Int. Ed.* **2011**, *50*, 9948–9952. [[CrossRef](#)] [[PubMed](#)]
388. Zell, T.; Butschke, B.; Ben-David, Y.; Milstein, D. Efficient hydrogen liberation from formic acid catalyzed by a well-defined iron pincer complex under mild conditions. *Chem. A Eur. J.* **2013**, *19*, 8068–8072. [[CrossRef](#)]
389. Bielinski, E.A.; Lagaditis, P.O.; Zhang, Y.; Mercado, B.Q.; Würtele, C.; Bernskoetter, W.H.; Hazari, N.; Schneider, S. Lewis acid-assisted formic acid dehydrogenation using a pincer-supported iron catalyst. *J. Am. Chem. Soc.* **2014**, *136*, 10234–10237. [[CrossRef](#)] [[PubMed](#)]
390. Kothandaraman, J.; Czaun, M.; Goeppert, A.; Haiges, R.; Jones, J.P.; May, R.B.; Prakash, G.K.S.; Olah, G.A. Amine-free reversible hydrogen storage in formate salts catalyzed by ruthenium pincer complex without pH control or solvent change. *ChemSusChem* **2015**, *8*, 1442–1451. [[CrossRef](#)]
391. Mellone, I.; Gorgas, N.; Bertini, F.; Peruzzini, M.; Kirchner, K.; Gonsalvi, L. Selective Formic Acid Dehydrogenation Catalyzed by Fe-PNP Pincer Complexes Based on the 2,6-Diaminopyridine Scaffold. *Organometallics* **2016**, *35*, 3344–3349. [[CrossRef](#)]
392. Mellone, I.; Bertini, F.; Peruzzini, M.; Gonsalvi, L. An active, stable and recyclable Ru(II) tetraphosphine-based catalytic system for hydrogen production by selective formic acid dehydrogenation. *Catal. Sci. Technol.* **2016**, *6*, 6504–6512. [[CrossRef](#)]
393. Czaun, M.; Kothandaraman, J.; Goeppert, A.; Yang, B.; Greenberg, S.; May, R.B.; Olah, G.A.; Prakash, G.K.S. Iridium-Catalyzed Continuous Hydrogen Generation from Formic Acid and Its Subsequent Utilization in a Fuel Cell: Toward a Carbon Neutral Chemical Energy Storage. *ACS Catal.* **2016**, *6*, 7475–7484. [[CrossRef](#)]
394. Cohen, S.; Borin, V.; Schapiro, I.; Musa, S.; De-Botton, S.; Belkova, N.V.; Gelman, D. Ir(III)-PC(sp<sup>3</sup>)P Bifunctional Catalysts for Production of H<sub>2</sub> by Dehydrogenation of Formic Acid: Experimental and Theoretical Study. *ACS Catal.* **2017**, *7*, 8139–8146. [[CrossRef](#)]
395. Musa, S.; Fronton, S.; Vaccaro, L.; Gelman, D. Bifunctional ruthenium(II) PCP pincer complexes and their catalytic activity in acceptorless dehydrogenative reactions. *Organometallics* **2013**, *32*, 3069–3073. [[CrossRef](#)]
396. Musa, S.; Ghosh, A.; Vaccaro, L.; Ackermann, L.; Gelman, D. Efficient E-Selective Transfer Semihydrogenation of Alkynes by Means of Ligand-Metal Cooperating Ruthenium Catalyst. *Adv. Synth. Catal.* **2015**, *357*, 2351–2357. [[CrossRef](#)]
397. Esteruelas, M.A.; García-Yebra, C.; Martín, J.; Oñate, E. Dehydrogenation of Formic Acid Promoted by a Trihydride-Hydroxo-Osmium(IV) Complex: Kinetics and Mechanism. *ACS Catal.* **2018**, *8*, 11314–11323. [[CrossRef](#)]
398. Pan, Y.; Pan, C.L.; Zhang, Y.; Li, H.; Min, S.; Guo, X.; Zheng, B.; Chen, H.; Anders, A.; Lai, Z.; et al. Selective hydrogen generation from formic acid with well-defined complexes of ruthenium and phosphorus-nitrogen PN3-pincer ligand. *Chem. Asian J.* **2016**, *11*, 1357–1360. [[CrossRef](#)] [[PubMed](#)]
399. He, L.-P.; Chen, T.; Gong, D.; Lai, Z.; Huang, K.-W. Enhanced Reactivities toward Amines by Introducing an Imine Arm to the Pincer Ligand: Direct Coupling of Two Amines to Form an Imine Without Oxidant. *Organometallics* **2012**, *31*, 5208–5211. [[CrossRef](#)]
400. Chen, T.; Li, H.; Qu, S.; Zheng, B.; He, L.; Lai, Z.; Wang, Z.X.; Huang, K.W. Hydrogenation of esters catalyzed by ruthenium PN3-Pincer complexes containing an aminophosphine arm. *Organometallics* **2014**, *33*, 4152–4155. [[CrossRef](#)]
401. Min, S.; Rasul, S.; Li, H.; Grills, D.C.; Takanabe, K.; Li, L.J.; Huang, K.W. Electrocatalytic Reduction of Carbon Dioxide with a Well-Defined PN3-Ru Pincer Complex. *Chempluschem* **2016**, *81*, 166–171. [[CrossRef](#)]
402. Li, H.; Gonçalves, T.P.; Hu, J.; Zhao, Q.; Gong, D.; Lai, Z.; Wang, Z.; Zheng, J.; Huang, K.W. A Pseudodearomatized PN<sup>3</sup>P-Ni-H Complex as a Ligand and  $\sigma$ -Nucleophilic Catalyst. *J. Org. Chem.* **2018**, *83*, 14969–14977. [[CrossRef](#)] [[PubMed](#)]
403. Wang, X.; Ling, E.A.P.; Guan, C.; Zhang, Q.; Wu, W.; Liu, P.; Zheng, N.; Zhang, D.; Lopatin, S.; Lai, Z.; et al. Single-Site Ruthenium Pincer Complex Knitted into Porous Organic Polymers for Dehydrogenation of Formic Acid. *ChemSusChem* **2018**, *11*, 3591–3598. [[CrossRef](#)] [[PubMed](#)]
404. Nakahara, Y.; Toda, T.; Matsunami, A.; Kayaki, Y.; Kuwata, S. Protic NNN and NCN Pincer-Type Ruthenium Complexes Featuring (Trifluoromethyl) pyrazole Arms: Synthesis and Application to Catalytic Hydrogen Evolution from Formic Acid. *Chem. Asian J.* **2018**, *13*, 73–80. [[CrossRef](#)] [[PubMed](#)]



405. Curley, J.B.; Smith, N.E.; Bernskoetter, W.H.; Hazari, N.; Mercado, B.Q. Catalytic Formic Acid Dehydrogenation and CO<sub>2</sub> Hydrogenation Using Iron PNP Pincer Complexes with Isonitrile Ligands. *Organometallics* **2018**, *37*, 3846–3853. [\[CrossRef\]](#)
406. Smith, N.E.; Bernskoetter, W.H.; Hazari, N.; Mercado, B.Q. Synthesis and Catalytic Activity of PNP-Supported Iron Complexes with Ancillary Isonitrile Ligands. *Organometallics* **2017**, *36*, 3995–4004. [\[CrossRef\]](#)
407. Prichatz, C.; Trincado, M.; Tan, L.; Casas, F.; Kammer, A.; Junge, H.; Beller, M.; Grützmacher, H. Highly Efficient Base-Free Dehydrogenation of Formic Acid at Low Temperature. *ChemSusChem* **2018**, *11*, 3092–3095. [\[CrossRef\]](#) [\[PubMed\]](#)
408. Zhou, W.; Wei, Z.; Spannenberg, A.; Jiao, H.; Junge, K.; Junge, H.; Beller, M. Cobalt-Catalyzed Aqueous Dehydrogenation of Formic Acid. *Chem. A Eur. J.* **2019**, *25*, 8459–8464. [\[CrossRef\]](#)
409. Müller, K.; Stark, K.; Müller, B.; Arlt, W. Amine borane based hydrogen carriers: An evaluation. *Energy Fuels* **2012**, *26*, 3691–3696. [\[CrossRef\]](#)
410. Staubitz, A.; Robertson, A.P.M.; Manners, I. Ammonia-Borane and Related Compounds as Dihydrogen Sources. *Chem. Rev.* **2010**, *110*, 4079–4124. [\[CrossRef\]](#)
411. Staubitz, A.; Robertson, A.P.M.; Sloan, M.E.; Manners, I. Amine- and Phosphine-Borane Adducts: New Interest in Old Molecules. *Chem. Rev.* **2010**, *110*, 4023–4078. [\[CrossRef\]](#)
412. Pagano, J.K.; Stelmach, J.P.W.; Waterman, R. Cobalt-catalyzed ammonia borane dehydrocoupling and transfer hydrogenation under aerobic conditions. *Dalt. Trans.* **2015**, *44*, 12074–12077. [\[CrossRef\]](#) [\[PubMed\]](#)
413. Moury, R.; Demirci, U. Hydrazine Borane and Hydrazinidoboranes as Chemical Hydrogen Storage Materials. *Energies* **2015**, *8*, 3118–3141. [\[CrossRef\]](#)
414. Zhao, Q.; Li, J.; Hamilton, E.J.M.; Chen, X. The continuing story of the diammoniate of diborane. *J. Organomet. Chem.* **2015**, *798*, 24–29. [\[CrossRef\]](#)
415. Jepsen, L.H.; Ley, M.B.; Lee, Y.-S.; Cho, Y.W.; Dornheim, M.; Jensen, J.O.; Filinchuk, Y.; Jørgensen, J.E.; Besenbacher, F.; Jensen, T.R. Boron–nitrogen based hydrides and reactive composites for hydrogen storage. *Mater. Today* **2014**, *17*, 129–135. [\[CrossRef\]](#)
416. Chen, X.; Zhao, J.-C.; Shore, S.G. The Roles of Dihydrogen Bonds in Amine Borane Chemistry. *Acc. Chem. Res.* **2013**, *46*, 2666–2675. [\[CrossRef\]](#)
417. Stubbs, N.E.; Robertson, A.P.M.; Leita, E.M.; Manners, I. Amine–borane dehydrogenation chemistry: Metal-free hydrogen transfer, new catalysts and mechanisms, and the synthesis of polyaminoboranes. *J. Organomet. Chem.* **2013**, *730*, 84–89. [\[CrossRef\]](#)
418. Peng, B.; Chen, J. Ammonia borane as an efficient and lightweight hydrogen storage medium. *Energy Environ. Sci.* **2008**. [\[CrossRef\]](#)
419. Davis, B.L.; Dixon, D.A.; Garner, E.B.; Gordon, J.C.; Matus, M.H.; Scott, B.; Stephens, F.H. Efficient Regeneration of Partially Spent Ammonia Borane Fuel. *Angew. Chem. Int. Ed.* **2009**, *48*, 6812–6816. [\[CrossRef\]](#)
420. Sutton, A.D.; Burrell, A.K.; Dixon, D.A.; Garner, E.B.; Gordon, J.C.; Nakagawa, T.; Ott, K.C.; Robinson, J.P.; Vasiliu, M. Regeneration of Ammonia Borane Spent Fuel by Direct Reaction with Hydrazine and Liquid Ammonia. *Science* **2011**, *331*, 1426–1429. [\[CrossRef\]](#)
421. Reller, C.; Mertens, F.O.R.L. A Self-Contained Regeneration Scheme for Spent Ammonia Borane Based on the Catalytic Hydrodechlorination of BCl<sub>3</sub>. *Angew. Chem. Int. Ed.* **2012**, *51*, 11731–11735. [\[CrossRef\]](#)
422. Davis, B.L.; Rekken, B.D.; Michalczyk, R.; Garner, E.B., III; Dixon, D.A.; Kalviri, H.; Baker, R.T.; Thorn, D.L. Lewis base assisted B–H bond redistribution in borazine and polyborazylene. *Chem. Commun.* **2013**, *49*, 9095. [\[CrossRef\]](#) [\[PubMed\]](#)
423. Smythe, N.C.; Gordon, J.C. Ammonia Borane as a Hydrogen Carrier: Dehydrogenation and Regeneration. *Eur. J. Inorg. Chem.* **2010**, *2010*, 509–521. [\[CrossRef\]](#)
424. Keaton, R.J.; Blacquiere, J.M.; Baker, R.T. Base Metal Catalyzed Dehydrogenation of Ammonia–Borane for Chemical Hydrogen Storage. *J. Am. Chem. Soc.* **2007**, *129*, 1844–1845. [\[CrossRef\]](#) [\[PubMed\]](#)
425. Vance, J.R.; Robertson, A.P.M.; Lee, K.; Manners, I. Photoactivated, Iron-Catalyzed Dehydrocoupling of Amine-Borane Adducts: Formation of Boron-Nitrogen Oligomers and Polymers. *Chem. A Eur. J.* **2011**, *17*, 4099–4103. [\[CrossRef\]](#)

426. Baker, R.T.; Gordon, J.C.; Hamilton, C.W.; Henson, N.J.; Lin, P.-H.; Maguire, S.; Murugesu, M.; Scott, B.L.; Smythe, N.C. Iron Complex-Catalyzed Ammonia-Borane Dehydrogenation. A Potential Route toward B-N-Containing Polymer Motifs Using Earth-Abundant Metal Catalysts. *J. Am. Chem. Soc.* **2012**, *134*, 5598–5609. [\[CrossRef\]](#)
427. Duman, S.; Metin, Ö.; Özkaz, S. B-N Polymer Embedded Iron(0) Nanoparticles as Highly Active and Long Lived Catalyst in the Dehydrogenation of Ammonia Borane. *J. Nanosci. Nanotechnol.* **2013**, *13*, 4954–4961. [\[CrossRef\]](#)
428. Lichtenberg, C.; Adelhardt, M.; Gianetti, T.L.; Meyer, K.; de Bruin, B.; Grützmacher, H. Low-Valent Iron Mono-Diazadiene Compounds: Electronic Structure and Catalytic Application. *ACS Catal.* **2015**, *5*, 6230–6240. [\[CrossRef\]](#)
429. Kawano, Y.; Uruichi, M.; Shimoi, M.; Taki, S.; Kawaguchi, T.; Kakizawa, T.; Ogino, H. Dehydrocoupling reactions of borane-secondary and -primary amine adducts catalyzed by group-6 carbonyl complexes: Formation of aminoboranes and borazines. *J. Am. Chem. Soc.* **2009**, *131*, 14946–14957. [\[CrossRef\]](#)
430. Sloan, M.E.; Staubitz, A.; Clark, T.J.; Russell, C.A.; Lloyd-Jones, G.C.; Manners, I. Homogeneous Catalytic Dehydrocoupling/Dehydrogenation of Amine-Borane Adducts by Early Transition Metal, Group 4 Metallocene Complexes. *J. Am. Chem. Soc.* **2010**, *132*, 3831–3841. [\[CrossRef\]](#)
431. Sonnenberg, J.F.; Morris, R.H. Evidence for Iron Nanoparticles Catalyzing the Rapid Dehydrogenation of Ammonia-Borane. *ACS Catal.* **2013**, *3*, 1092–1102. [\[CrossRef\]](#)
432. Chaplin, A.B.; Weller, A.S. B-H activation at a rhodium(I) center: Isolation of a bimetallic complex relevant to the transition-metal-catalyzed dehydrocoupling of amine-boranes. *Angew. Chem. Int. Ed.* **2010**, *49*, 581–584. [\[CrossRef\]](#) [\[PubMed\]](#)
433. Blaquiere, N.; Diallo-Garcia, S.; Gorelsky, S.I.; Black, D.A.; Fagnou, K. Ruthenium-catalyzed dehydrogenation of ammonia boranes. *J. Am. Chem. Soc.* **2008**, *130*, 14034–14035. [\[CrossRef\]](#) [\[PubMed\]](#)
434. Bhattacharya, P.; Krause, J.A.; Guan, H. Mechanistic Studies of Ammonia Borane Dehydrogenation Catalyzed by Iron Pincer Complexes. *J. Am. Chem. Soc.* **2014**, *136*, 11153–11161. [\[CrossRef\]](#) [\[PubMed\]](#)
435. Buss, J.A.; Edouard, G.A.; Cheng, C.; Shi, J.; Agapie, T. Molybdenum Catalyzed Ammonia Borane Dehydrogenation: Oxidation State Specific Mechanisms. *J. Am. Chem. Soc.* **2014**, *136*, 11272–11275. [\[CrossRef\]](#)
436. Erickson, K.A.; Stelmach, J.P.W.; Mucha, N.T.; Waterman, R. Zirconium-Catalyzed Amine Borane Dehydrocoupling and Transfer Hydrogenation. *Organometallics* **2015**, *34*, 4693–4699. [\[CrossRef\]](#)
437. Lin, T.-P.; Peters, J.C. Boryl-Mediated Reversible H<sub>2</sub> Activation at Cobalt: Catalytic Hydrogenation, Dehydrogenation, and Transfer Hydrogenation. *J. Am. Chem. Soc.* **2013**, *135*, 15310–15313. [\[CrossRef\]](#)
438. Lichtenberg, C.; Viciu, L.; Adelhardt, M.; Sutter, J.; Meyer, K.; de Bruin, B.; Grützmacher, H. Low-Valent Iron(I) Amido Olefin Complexes as Promoters for Dehydrogenation Reactions. *Angew. Chem. Int. Ed.* **2015**, *54*, 5766–5771. [\[CrossRef\]](#)
439. Conley, B.L.; Guess, D.; Williams, T.J. A Robust, Air-Stable, Reusable Ruthenium Catalyst for Dehydrogenation of Ammonia Borane. *J. Am. Chem. Soc.* **2011**, *133*, 14212–14215. [\[CrossRef\]](#)
440. Zhang, X.; Kam, L.; Trerise, R.; Williams, T.J. Ruthenium-Catalyzed Ammonia Borane Dehydrogenation: Mechanism and Utility. *Acc. Chem. Res.* **2017**, *50*, 86–95. [\[CrossRef\]](#)
441. Rossin, A.; Peruzzini, M. Ammonia-Borane and Amine-Borane Dehydrogenation Mediated by Complex Metal Hydrides. *Chem. Rev.* **2016**, *116*, 8848–8872. [\[CrossRef\]](#)
442. Marziale, A.N.; Friedrich, A.; Klopsch, I.; Drees, M.; Celinski, V.R.; Schmedt Auf Der Günne, J.; Schneider, S. The mechanism of borane-amine dehydrocoupling with bifunctional ruthenium catalysts. *J. Am. Chem. Soc.* **2013**, *135*, 13342–13355. [\[CrossRef\]](#) [\[PubMed\]](#)
443. Glüer, A.; Förster, M.; Celinski, V.R.; Schmedt Auf Der Günne, J.; Holthausen, M.C.; Schneider, S. Highly Active Iron Catalyst for Ammonia Borane Dehydrocoupling at Room Temperature. *ACS Catal.* **2015**, *5*, 7214–7217. [\[CrossRef\]](#)
444. Johnson, H.C.; Hooper, T.N.; Weller, A.S. The Catalytic Dehydrocoupling of Amine-Boranes and Phosphine-Boranes. In *Topics in Organometallic Chemistry*; Springer: Basel, Switzerland, 2015; pp. 153–220.
445. Käß, M.; Friedrich, A.; Drees, M.; Schneider, S. Ruthenium complexes with cooperative PNP ligands: Bifunctional catalysts for the dehydrogenation of ammonia-borane. *Angew. Chem. Int. Ed.* **2009**, *48*, 905–907. [\[CrossRef\]](#) [\[PubMed\]](#)

446. Friedrich, A.; Drees, M.; Schneider, S. Ruthenium-catalyzed dimethylamineborane dehydrogenation: Stepwise metal-centered dehydrocyclization. *Chem. A Eur. J.* **2009**, *15*, 10339–10342. [\[CrossRef\]](#)
447. Han, D.; Joks, M.; Klahn, M.; Spannenberg, A.; Drexler, H.J.; Baumann, W.; Jiao, H.; Knitsch, R.; Hansen, M.R.; Eckert, H.; et al. Iridium(III) hydrido complexes for the catalytic dehydrogenation of hydrazine borane. *Dalt. Trans.* **2016**, *45*, 17697–17704. [\[CrossRef\]](#)
448. Brayton, D.F.; Jensen, C.M. Dehydrogenation of pyrrolidine based liquid organic hydrogen carriers by an iridium pincer catalyst, an isothermal kinetic study. *Int. J. Hydrog. Energy* **2015**, *40*, 16266–16270. [\[CrossRef\]](#)
449. Titova, E.M.; Osipova, E.S.; Pavlov, A.A.; Filippov, O.A.; Safronov, S.V.; Shubina, E.S.; Belkova, N.V. Mechanism of Dimethylamine-Borane Dehydrogenation Catalyzed by an Iridium(III) PCP-Pincer Complex. *ACS Catal.* **2017**, *7*, 2325–2333. [\[CrossRef\]](#)
450. Denney, M.C.; Pons, V.; Hebden, T.J.; Heinekey, D.M.; Goldberg, K.I. Efficient catalysis of ammonia borane dehydrogenation. *J. Am. Chem. Soc.* **2006**, *128*, 12048–12049. [\[CrossRef\]](#) [\[PubMed\]](#)
451. Esteruelas, M.A.; Nolis, P.; Oliván, M.; Oñate, E.; Vallribera, A.; Vélez, A. Ammonia Borane Dehydrogenation Promoted by a Pincer-Square-Planar Rhodium(I) Monohydride: A Stepwise Hydrogen Transfer from the Substrate to the Catalyst. *Inorg. Chem.* **2016**, *55*, 7176–7181. [\[CrossRef\]](#) [\[PubMed\]](#)
452. Kwan, E.H.; Ogawa, H.; Yamashita, M. A Highly Active PBP-Iridium Catalyst for the Dehydrogenation of Dimethylamine-Borane: Catalytic Performance and Mechanism. *ChemCatChem* **2017**, *9*, 2457–2462. [\[CrossRef\]](#)
453. Kwan, E.H.; Kawai, Y.J.; Kamakura, S.; Yamashita, M. A long-tethered (P-B-P)-pincer ligand: Synthesis, complexation, and application to catalytic dehydrogenation of alkanes. *Dalt. Trans.* **2016**, *45*, 15931–15941. [\[CrossRef\]](#) [\[PubMed\]](#)
454. Hu, P.; Ben-David, Y.; Milstein, D. Rechargeable hydrogen storage system based on the dehydrogenative coupling of ethylenediamine with ethanol. *Angew. Chem. Int. Ed.* **2016**, *55*, 1061–1064. [\[CrossRef\]](#) [\[PubMed\]](#)
455. Kothandaraman, J.; Kar, S.; Sen, R.; Goepfert, A.; Olah, G.A.; Prakash, G.K.S. Efficient Reversible Hydrogen Carrier System Based on Amine Reforming of Methanol. *J. Am. Chem. Soc.* **2017**, *139*, 2549–2552. [\[CrossRef\]](#) [\[PubMed\]](#)
456. Kim, S.H.; Hong, S.H. Ruthenium-Catalyzed Urea Synthesis Using Methanol as the C1 Source. *Org. Lett.* **2016**, *18*, 212–215. [\[CrossRef\]](#) [\[PubMed\]](#)
457. Baratta, W.; Ballico, M.; Chelucci, G.; Siega, K.; Rigo, P. Osmium(II) CNN pincer complexes as efficient catalysts for both asymmetric transfer and H<sub>2</sub> hydrogenation of ketones. *Angew. Chem. Int. Ed.* **2008**, *47*, 4362–4365. [\[CrossRef\]](#) [\[PubMed\]](#)
458. Abdur-Rashid, K.; Clapham, S.E.; Hadzovic, A.; Harvey, J.N.; Lough, A.J.; Morris, R.H. Mechanism of the hydrogenation of ketones catalyzed by trans-dihydrido(diamine)ruthenium(II) complexes. *J. Am. Chem. Soc.* **2002**, *124*, 15104–15118. [\[CrossRef\]](#)
459. Abdur-Rashid, K.; Faatz, M.; Lough, A.J.; Morris, R.H. Catalytic cycle for the asymmetric hydrogenation of prochiral ketones to chiral alcohols: Direct hydride and proton transfer from chiral catalysts trans-Ru(H)<sub>2</sub>(diphosphine)(diamine) to ketones and direct addition of dihydrogen to the resulting hydridoamid. *J. Am. Chem. Soc.* **2001**, *123*, 7473–7474. [\[CrossRef\]](#)
460. Rautenstrauch, V.; Hoang-Cong, X.; Churlaud, R.; Abdur-Rashid, K.; Morris, R.H. Hydrogenation versus Transfer Hydrogenation of Ketones: Two Established Ruthenium Systems Catalyze Both. *Chem. A Eur. J.* **2003**, *9*, 4954–4967. [\[CrossRef\]](#)
461. Raja, M.U.; Ramesh, R.; Ahn, K.H. Rhodium(III) NCN pincer complexes catalyzed transfer hydrogenation of ketones. *Tetrahedron Lett.* **2009**, *50*, 7014–7017. [\[CrossRef\]](#)
462. Hou, C.; Li, Y.; Zhao, C.; Ke, Z. A DFT study of Co(i) and Ni(ii) pincer complex-catalyzed hydrogenation of ketones: Intriguing mechanism dichotomy by ligand field variation. *Catal. Sci. Technol.* **2019**, *9*, 125–135. [\[CrossRef\]](#)
463. Filonenko, G.A.; Cosimi, E.; Lefort, L.; Conley, M.P.; Copéret, C.; Lutz, M.; Hensen, E.J.M.; Pidko, E.A. Lutidine-derived Ru-CNC hydrogenation pincer catalysts with versatile coordination properties. *ACS Catal.* **2014**, *4*, 2667–2671. [\[CrossRef\]](#)
464. Saudan, L.A.; Saudan, C.M.; Debieux, C.; Wyss, P. Dihydrogen reduction of carboxylic esters to alcohols under the catalysis of homogeneous ruthenium complexes: High efficiency and unprecedented chemoselectivity. *Angew. Chem. Int. Ed.* **2007**, *46*, 7473–7476. [\[CrossRef\]](#) [\[PubMed\]](#)

465. Yuwen, J.; Chakraborty, S.; Brennessel, W.W.; Jones, W.D. Additive-Free Cobalt-Catalyzed Hydrogenation of Esters to Alcohols. *ACS Catal.* **2017**, *7*, 3735–3740. [[CrossRef](#)]
466. Kim, D.; Le, L.; Drance, M.J.; Jensen, K.H.; Bogdanovski, K.; Cervarich, T.N.; Barnard, M.G.; Pudalov, N.J.; Knapp, S.M.M.; Chianese, A.R. Ester Hydrogenation Catalyzed by CNN-Pincer Complexes of Ruthenium. *Organometallics* **2016**, *35*, 982–989. [[CrossRef](#)]
467. Le, L.; Liu, J.; He, T.; Malek, J.C.; Cervarich, T.N.; Buttner, J.C.; Pham, J.; Keith, J.M.; Chianese, A.R. Unexpected CNN-to-CC Ligand Rearrangement in Pincer–Ruthenium Precatalysts Leads to a Base-Free Catalyst for Ester Hydrogenation. *Organometallics* **2019**, *38*, 3311–3321. [[CrossRef](#)]
468. Filonenko, G.A.; Aguila, M.J.B.; Schulpen, E.N.; Van Putten, R.; Wiecko, J.; Müller, C.; Lefort, L.; Hensen, E.J.M.; Pidko, E.A. Bis-N-heterocyclic Carbene Aminopincer Ligands Enable High Activity in Ru-Catalyzed Ester Hydrogenation. *J. Am. Chem. Soc.* **2015**, *137*, 7620–7623. [[CrossRef](#)]
469. He, T.; Buttner, J.C.; Reynolds, E.F.; Pham, J.; Malek, J.C.; Keith, J.M.; Chianese, A.R. Dehydroalkylative Activation of CNN- And PNN-Pincer Ruthenium Catalysts for Ester Hydrogenation. *J. Am. Chem. Soc.* **2019**, *141*, 17404–17413. [[CrossRef](#)]
470. Acosta-Ramirez, A.; Bertoli, M.; Gusev, D.G.; Schlaf, M. Homogeneous catalytic hydrogenation of long-chain esters by an osmium pincer complex and its potential application in the direct conversion of triglycerides into fatty alcohols. *Green Chem.* **2012**, *14*, 1178. [[CrossRef](#)]
471. Chakraborty, S.; Dai, H.; Bhattacharya, P.; Fairweather, N.T.; Gibson, M.S.; Krause, J.A.; Guan, H. Iron-Based Catalysts for the Hydrogenation of Esters to Alcohols. *J. Am. Chem. Soc.* **2014**, *136*, 7869–7872. [[CrossRef](#)]
472. Werkmeister, S.; Junge, K.; Wendt, B.; Alberico, E.; Jiao, H.; Baumann, W.; Junge, H.; Gallou, F.; Beller, M. Hydrogenation of esters to alcohols with a well-defined iron complex. *Angew. Chem. Int. Ed.* **2014**, *53*, 8722–8726. [[CrossRef](#)]
473. Sun, Y.; Koehler, C.; Tan, R.; Annibale, V.T.; Song, D. Ester hydrogenation catalyzed by Ru-CNN pincer complexes. *Chem. Commun.* **2011**, *47*, 8349–8351. [[CrossRef](#)]
474. Wang, Z.; Chen, X.; Liu, B.; Liu, Q.B.; Solan, G.A.; Yang, X.; Sun, W.H. Cooperative interplay between a flexible PNN-Ru(II) complex and a NaBH<sub>4</sub> additive in the efficient catalytic hydrogenation of esters. *Catal. Sci. Technol.* **2017**, *7*, 1297–1304. [[CrossRef](#)]
475. Yan, X.; Yang, X. Mechanistic insights into the iridium catalysed hydrogenation of ethyl acetate to ethanol: A DFT study. *Dalt. Trans.* **2018**. [[CrossRef](#)] [[PubMed](#)]
476. Spasyuk, D.; Vicent, C.; Gusev, D.G. Chemoselective hydrogenation of carbonyl compounds and acceptorless dehydrogenative coupling of alcohols. *J. Am. Chem. Soc.* **2015**, *137*, 3743–3746. [[CrossRef](#)] [[PubMed](#)]
477. Qu, S.; Dai, H.; Dang, Y.; Song, C.; Wang, Z.X.; Guan, H. Computational mechanistic study of Fe-catalyzed hydrogenation of esters to alcohols: Improving catalysis by accelerating precatalyst activation with a lewis base. *ACS Catal.* **2014**, *4*, 4377–4388. [[CrossRef](#)]
478. Wei, Z.; Jiao, H. *Bifunctional Aliphatic PNP Pincer Catalysts for Hydrogenation: Mechanisms and Scope*, 1st ed.; Elsevier: Amsterdam, The Netherlands, 2019; ISBN 9780128157282.
479. Hey, D.A.; Reich, R.M.; Baratta, W.; Kühn, F.E. Current advances on ruthenium(II) N-heterocyclic carbenes in hydrogenation reactions. *Coord. Chem. Rev.* **2018**, *374*, 114–132. [[CrossRef](#)]
480. Elangovan, S.; Topf, C.; Fischer, S.; Jiao, H.; Spannenberg, A.; Baumann, W.; Ludwig, R.; Junge, K.; Beller, M. Selective Catalytic Hydrogenations of Nitriles, Ketones, and Aldehydes by Well-Defined Manganese Pincer Complexes. *J. Am. Chem. Soc.* **2016**, *138*, 8809–8814. [[CrossRef](#)]
481. Schneck, F.; Assmann, M.; Balmer, M.; Harms, K.; Langer, R. Selective Hydrogenation of Amides to Amines and Alcohols Catalyzed by Improved Iron Pincer Complexes. *Organometallics* **2016**, *35*, 1931–1943. [[CrossRef](#)]
482. Artús Suárez, L.; Culakova, Z.; Balcells, D.; Bernskoetter, W.H.; Eisenstein, O.; Goldberg, K.I.; Hazari, N.; Tilset, M.; Nova, A. The Key Role of the Hemiaminal Intermediate in the Iron-Catalyzed Deaminative Hydrogenation of Amides. *ACS Catal.* **2018**, *8*, 8751–8762. [[CrossRef](#)]
483. Jayarathne, U.; Zhang, Y.; Hazari, N.; Bernskoetter, W.H. Selective Iron-Catalyzed Deaminative Hydrogenation of Amides. *Organometallics* **2017**, *36*, 409–416. [[CrossRef](#)]
484. Coetzee, J.; Dodds, D.L.; Klankermayer, J.; Brosinski, S.; Leitner, W.; Slawin, A.M.Z.; Cole-Hamilton, D.J. Homogeneous Catalytic Hydrogenation of Amides to Amines. *Chem. A Eur. J.* **2013**, *19*, 11039–11050. [[CrossRef](#)] [[PubMed](#)]
485. Núñez Magro, A.A.; Eastham, G.R.; Cole-Hamilton, D.J. The synthesis of amines by the homogeneous hydrogenation of secondary and primary amides. *Chem. Commun.* **2007**, *30*, 3154–3156. [[CrossRef](#)] [[PubMed](#)]



486. Hernández-Juárez, M.; Vaquero, M.; Álvarez, E.; Salazar, V.; Suárez, A. Hydrogenation of imines catalysed by ruthenium(II) complexes based on lutidine-derived CNC pincer ligands. *Dalt. Trans.* **2013**, *42*, 351–354. [[CrossRef](#)] [[PubMed](#)]
487. Hernández-Juárez, M.; López-Serrano, J.; Lara, P.; Morales-Cerón, J.P.; Vaquero, M.; Álvarez, E.; Salazar, V.; Suárez, A. Ruthenium(II) complexes containing lutidine-derived pincer CNC ligands: Synthesis, structure, and catalytic hydrogenation of C=N bonds. *Chem. A Eur. J.* **2015**, *21*, 7540–7555. [[CrossRef](#)]
488. Perera, F. Pollution from Fossil-Fuel Combustion is the Leading Environmental Threat to Global Pediatric Health and Equity: Solutions Exist. *Int. J. Environ. Res. Public Health* **2017**, *15*, 16. [[CrossRef](#)]
489. Butler, C. Climate Change, Health and Existential Risks to Civilization: A Comprehensive Review (1989–2013). *Int. J. Environ. Res. Public Health* **2018**, *15*, 2266. [[CrossRef](#)]
490. Diffenbaugh, N.S.; Singh, D.; Mankin, J.S.; Horton, D.E.; Swain, D.L.; Touma, D.; Charland, A.; Liu, Y.; Haugen, M.; Tsiang, M.; et al. Quantifying the influence of global warming on unprecedented extreme climate events. *Proc. Natl. Acad. Sci. USA* **2017**, *114*, 4881–4886. [[CrossRef](#)]
491. Haustein, K.; Allen, M.R.; Forster, P.M.; Otto, F.E.L.; Mitchell, D.M.; Matthews, H.D.; Frame, D.J. A real-time Global Warming Index. *Sci. Rep.* **2017**, *7*, 15417. [[CrossRef](#)]
492. Aresta, M. *Carbon Dioxide as Chemical Feedstock*; John Wiley & Sons: Hoboken, NJ, USA, 2010; ISBN 9783527324750.
493. Centi, G.; Perathoner, S. Opportunities and prospects in the chemical recycling of carbon dioxide to fuels. *Catal. Today* **2009**, *148*, 191–205. [[CrossRef](#)]
494. Gibson, D.H. The organometallic chemistry of carbon dioxide. *Chem. Rev.* **1996**, *96*, 2063–2095. [[CrossRef](#)]
495. Boot-Handford, M.E.; Abanades, J.C.; Anthony, E.J.; Blunt, M.J.; Brandani, S.; Mac Dowell, N.; Fernández, J.R.; Ferrari, M.-C.; Gross, R.; Hallett, J.P.; et al. Carbon capture and storage update. *Energy Environ. Sci.* **2014**, *7*, 130–189. [[CrossRef](#)]
496. Goeppert, A.; Czaun, M.; May, R.B.; Prakash, G.K.S.; Olah, G.A.; Narayanan, S.R. Carbon Dioxide Capture from the Air Using a Polyamine Based Regenerable Solid Adsorbent. *J. Am. Chem. Soc.* **2011**, *133*, 20164–20167. [[CrossRef](#)]
497. Gibbins, J.; Chalmers, H. Carbon capture and storage. *Energy Policy* **2008**, *36*, 4317–4322. [[CrossRef](#)]
498. Leung, D.Y.C.; Caramanna, G.; Maroto-Valer, M.M. An overview of current status of carbon dioxide capture and storage technologies. *Renew. Sustain. Energy Rev.* **2014**, *39*, 426–443. [[CrossRef](#)]
499. McCulloch, S.; Keeling, S.; Malischek, R.; Stanley, T. *20 Years of Carbon Capture and Storage*; OECD: Paris, France, 2016; ISBN 9789264267800.
500. Styring, P.; Jansen, D.; de Coninck, H.; Reith, H.; Armstrong, K. *Carbon Capture and Utilisation in the Green Economy*; Centre for Low Carbon Futures: New York, NY, USA, 2011.
501. de Coninck, H.; Benson, S.M. Carbon Dioxide Capture and Storage: Issues and Prospects. *Annu. Rev. Environ. Resour.* **2014**, *39*, 243–270. [[CrossRef](#)]
502. Goeppert, A.; Czaun, M.; Surya Prakash, G.K.; Olah, G.A. Air as the renewable carbon source of the future: An overview of CO<sub>2</sub> capture from the atmosphere. *Energy Environ. Sci.* **2012**, *5*, 7833. [[CrossRef](#)]
503. Cuéllar-Franca, R.M.; Azapagic, A. Carbon capture, storage and utilisation technologies: A critical analysis and comparison of their life cycle environmental impacts. *J. CO<sub>2</sub> Util.* **2015**, *9*, 82–102. [[CrossRef](#)]
504. Takht Ravanchi, M.; Sahebdehfar, S. Carbon dioxide capture and utilization in petrochemical industry: Potentials and challenges. *Appl. Petrochem. Res.* **2014**, *4*, 63–77. [[CrossRef](#)]
505. von der Assen, N.; Jung, J.; Bardow, A. Life-cycle assessment of carbon dioxide capture and utilization: Avoiding the pitfalls. *Energy Environ. Sci.* **2013**, *6*, 2721. [[CrossRef](#)]
506. Mac Dowell, N.; Fennell, P.S.; Shah, N.; Maitland, G.C. The role of CO<sub>2</sub> capture and utilization in mitigating climate change. *Nat. Clim. Chang.* **2017**, *7*, 243–249. [[CrossRef](#)]
507. Arakawa, H.; Aresta, M.; Armor, J.N.; Barteau, M.A.; Beckman, E.J.; Bell, A.T.; Bercaw, J.E.; Creutz, C.; Dinjus, E.; Dixon, D.A.; et al. Catalysis Research of Relevance to Carbon Management: Progress, Challenges, and Opportunities. *Chem. Rev.* **2001**, *101*, 953–996. [[CrossRef](#)]
508. Behr, A. Carbon Dioxide as an Alternative C1 Synthetic Unit: Activation by Transition-Metal Complexes. *Angew. Chem. Int. Ed. Engl.* **1988**, *27*, 661–678. [[CrossRef](#)]
509. Qiao, J.; Liu, Y.; Hong, F.; Zhang, J. A review of catalysts for the electroreduction of carbon dioxide to produce low-carbon fuels. *Chem. Soc. Rev.* **2014**, *43*, 631–675. [[CrossRef](#)] [[PubMed](#)]

510. Yin, X.; Moss, J.R. Recent developments in the activation of carbon dioxide by metal complexes. *Coord. Chem. Rev.* **1999**, *181*, 27–59. [\[CrossRef\]](#)
511. Sakakura, T.; Choi, J.-C.; Yasuda, H. Transformation of Carbon Dioxide. *Chem. Rev.* **2007**, *107*, 2365–2387. [\[CrossRef\]](#)
512. Peters, M.; Köhler, B.; Kuckshinrichs, W.; Leitner, W.; Markewitz, P.; Müller, T.E. Chemical Technologies for Exploiting and Recycling Carbon Dioxide into the Value Chain. *ChemSusChem* **2011**, *4*, 1216–1240. [\[CrossRef\]](#) [\[PubMed\]](#)
513. Aresta, M.; Dibenedetto, A. Utilisation of CO<sub>2</sub> as a chemical feedstock: Opportunities and challenges. *Dalt. Trans.* **2007**, 2975. [\[CrossRef\]](#)
514. Asinger, F. Methanol—Chemie und Energierohstoff. In *Methanol—Chem.-und Energierohstoff*; Springer: Berlin/Heidelberg, Germany, 1986.
515. Leitner, W. Carbon Dioxide as a Raw Material: The Synthesis of Formic Acid and Its Derivatives from CO<sub>2</sub>. *Angew. Chem. Int. Ed. Engl.* **1995**, *34*, 2207–2221. [\[CrossRef\]](#)
516. Leitner, W. The coordination chemistry of carbon dioxide and its relevance for catalysis: A critical survey. *Coord. Chem. Rev.* **1996**, *153*, 257–284. [\[CrossRef\]](#)
517. Jessop, P.G.; Ikariya, T.; Noyori, R. Homogeneous Hydrogenation of Carbon Dioxide. *Chem. Rev.* **1995**, *95*, 259–272. [\[CrossRef\]](#)
518. Olah, G.A.; Goeppert, A.; Prakash, G.K.S. Methanol-Based Chemicals, Synthetic Hydrocarbons and Materials. In *Beyond Oil and Gas: The Methanol Economy*; Wiley: Weinheim, Germany, 2009; pp. 375–386.
519. Goeppert, A.; Czaun, M.; Jones, J.-P.; Surya Prakash, G.K.; Olah, G.A. Recycling of carbon dioxide to methanol and derived products—Closing the loop. *Chem. Soc. Rev.* **2014**, *43*, 7995–8048. [\[CrossRef\]](#) [\[PubMed\]](#)
520. Olah, G.A. Towards Oil Independence Through Renewable Methanol Chemistry. *Angew. Chem. Int. Ed.* **2013**, *52*, 104–107. [\[CrossRef\]](#)
521. Malik, K.; Singh, S.; Basu, S.; Verma, A. Electrochemical reduction of CO<sub>2</sub> for synthesis of green fuel. *Wiley Interdiscip. Rev. Energy Environ.* **2017**, *6*, e244. [\[CrossRef\]](#)
522. Álvarez, A.; Bansode, A.; Urakawa, A.; Bavykina, A.V.; Wezendonk, T.A.; Makkee, M.; Gascon, J.; Kapteijn, F. Challenges in the Greener Production of Formates/Formic Acid, Methanol, and DME by Heterogeneously Catalyzed CO<sub>2</sub> Hydrogenation Processes. *Chem. Rev.* **2017**, *117*, 9804–9838. [\[CrossRef\]](#)
523. Behrens, M. Heterogeneous Catalysis of CO<sub>2</sub> Conversion to Methanol on Copper Surfaces. *Angew. Chem. Int. Ed.* **2014**, *53*, 12022–12024. [\[CrossRef\]](#)
524. Dang, S.; Yang, H.; Gao, P.; Wang, H.; Li, X.; Wei, W.; Sun, Y. A review of research progress on heterogeneous catalysts for methanol synthesis from carbon dioxide hydrogenation. *Catal. Today* **2019**, *330*, 61–75. [\[CrossRef\]](#)
525. Jessop, P.G. Homogeneous Hydrogenation of Carbon Dioxide. In *The Handbook of Homogeneous Hydrogenation*; WILEY-VCH: Weinheim, Germany, 2007; ISBN 9783527311613.
526. Wang, W.; Wang, S.; Ma, X.; Gong, J. Recent advances in catalytic hydrogenation of carbon dioxide. *Chem. Soc. Rev.* **2011**, *40*, 3703. [\[CrossRef\]](#) [\[PubMed\]](#)
527. Benson, E.E.; Kubiak, C.P.; Sathrum, A.J.; Smieja, J.M. Electrocatalytic and homogeneous approaches to conversion of CO<sub>2</sub> to liquid fuels. *Chem. Soc. Rev.* **2009**, *38*, 89–99. [\[CrossRef\]](#) [\[PubMed\]](#)
528. Sanz, S.; Azua, A.; Peris, E. '(η<sup>6</sup>-arene)Ru(bis-NHC)' complexes for the reduction of CO<sub>2</sub> to formate with hydrogen and by transfer hydrogenation with iPrOH. *Dalt. Trans.* **2010**, 39, 6339. [\[CrossRef\]](#) [\[PubMed\]](#)
529. Li, X.; He, X.; Liu, X.; He, L.N. Ruthenium-promoted reductive transformation of CO<sub>2</sub>. *Sci. China Chem.* **2017**, *60*, 841–852. [\[CrossRef\]](#)
530. Wiedner, E.S.; Linehan, J.C. Making a Splash in Homogeneous CO<sub>2</sub> Hydrogenation: Elucidating the Impact of Solvent on Catalytic Mechanisms. *Chem. A Eur. J.* **2018**, *24*, 16964–16971. [\[CrossRef\]](#)
531. Janes, T.; Yang, Y.; Song, D. Chemical reduction of CO<sub>2</sub> facilitated by C-nucleophiles. *Chem. Commun.* **2017**, 53, 11390–11398. [\[CrossRef\]](#) [\[PubMed\]](#)
532. Jiang, C.; Nichols, A.W.; Machan, C.W. A look at periodic trends in d-block molecular electrocatalysts for CO<sub>2</sub> reduction. *Dalt. Trans.* **2019**, 48, 9454–9468. [\[CrossRef\]](#)
533. Fernández-Alvarez, F.J.; Iglesias, M.; Oro, L.A.; Polo, V. CO<sub>2</sub> activation and catalysis driven by iridium complexes. *ChemCatChem* **2013**, *5*, 3481–3494. [\[CrossRef\]](#)
534. Kang, P.; Chen, Z.; Brookhart, M.; Meyer, T.J. Electrocatalytic Reduction of Carbon Dioxide: Let the Molecules Do the Work. *Top. Catal.* **2015**, *58*, 30–45. [\[CrossRef\]](#)

535. Jessop, P.G.; Joó, F.; Tai, C.-C. Recent advances in the homogeneous hydrogenation of carbon dioxide. *Coord. Chem. Rev.* **2004**, *248*, 2425–2442. [CrossRef]
536. Badiei, Y.M.; Wang, W.-H.; Hull, J.F.; Szalda, D.J.; Muckerman, J.T.; Himeda, Y.; Fujita, E. Cp\*Co(III) Catalysts with Proton-Responsive Ligands for Carbon Dioxide Hydrogenation in Aqueous Media. *Inorg. Chem.* **2013**, *52*, 12576–12586. [CrossRef] [PubMed]
537. Jeletic, M.S.; Mock, M.T.; Appel, A.M.; Linehan, J.C. A Cobalt-Based Catalyst for the Hydrogenation of CO<sub>2</sub> under Ambient Conditions. *J. Am. Chem. Soc.* **2013**, *135*, 11533–11536. [CrossRef] [PubMed]
538. Zhang, G.; Vasudevan, K.V.; Scott, B.L.; Hanson, S.K. Understanding the Mechanisms of Cobalt-Catalyzed Hydrogenation and Dehydrogenation Reactions. *J. Am. Chem. Soc.* **2013**, *135*, 8668–8681. [CrossRef] [PubMed]
539. Glüer, A.; Schneider, S. Iron catalyzed hydrogenation and electrochemical reduction of CO<sub>2</sub>: The role of functional ligands. *J. Organomet. Chem.* **2018**, *861*, 159–173. [CrossRef]
540. Jeletic, M.S.; Helm, M.L.; Hulley, E.B.; Mock, M.T.; Appel, A.M.; Linehan, J.C. A Cobalt Hydride Catalyst for the Hydrogenation of CO<sub>2</sub>: Pathways for Catalysis and Deactivation. *ACS Catal.* **2014**, *4*, 3755–3762. [CrossRef]
541. Jeletic, M.S.; Hulley, E.B.; Helm, M.L.; Mock, M.T.; Appel, A.M.; Wiedner, E.S.; Linehan, J.C. Understanding the Relationship Between Kinetics and Thermodynamics in CO<sub>2</sub> Hydrogenation Catalysis. *ACS Catal.* **2017**, *7*, 6008–6017. [CrossRef]
542. Shaffer, D.W.; Johnson, S.I.; Rheingold, A.L.; Ziller, J.W.; Goddard, W.A.; Nielsen, R.J.; Yang, J.Y. Reactivity of a Series of Isostructural Cobalt Pincer Complexes with CO<sub>2</sub>, CO, and H<sup>+</sup>. *Inorg. Chem.* **2014**, *53*, 13031–13041. [CrossRef] [PubMed]
543. Hojilla Atienza, C.C.; Milsmann, C.; Semproni, S.P.; Turner, Z.R.; Chirik, P.J. Reversible Carbon–Carbon Bond Formation Induced by Oxidation and Reduction at a Redox-Active Cobalt Complex. *Inorg. Chem.* **2013**, *52*, 5403–5417. [CrossRef] [PubMed]
544. Dubey, A.; Nencini, L.; Fayzullin, R.R.; Nervi, C.; Khusnutdinova, J.R. Bio-Inspired Mn(I) Complexes for the Hydrogenation of CO<sub>2</sub> to Formate and Formamide. *ACS Catal.* **2017**, *7*, 3864–3868. [CrossRef]
545. Jewess, M.; Crabtree, R.H. Electrocatalytic Nitrogen Fixation for Distributed Fertilizer Production? *ACS Sustain. Chem. Eng.* **2016**, *4*, 5855–5858. [CrossRef]
546. Liu, H. *Ammonia Synthesis Catalysts: Innovation and Practice*; World Scientific: Beijing, China, 2013; ISBN 9789814355780.
547. Jacobsen, C.J.H.; Dahl, S.; Clausen, B.S.; Bahn, S.; Logadottir, A.; Nørskov, J.K. Catalyst Design by Interpolation in the Periodic Table: Bimetallic Ammonia Synthesis Catalysts. *J. Am. Chem. Soc.* **2001**, *123*, 8404–8405. [CrossRef]
548. Liu, H. Ammonia synthesis catalyst 100 years: Practice, enlightenment and challenge. *Chinese J. Catal.* **2014**, *35*, 1619–1640. [CrossRef]
549. Levi, P.G.; Cullen, J.M. Mapping Global Flows of Chemicals: From Fossil Fuel Feedstocks to Chemical Products. *Environ. Sci. Technol.* **2018**, *52*, 1725–1734. [CrossRef]
550. Canfield, D.E.; Glazer, A.N.; Falkowski, P.G. The Evolution and Future of Earth’s Nitrogen Cycle. *Science* **2010**, *330*, 192–196. [CrossRef]
551. Galloway, J.N.; Townsend, A.R.; Erismann, J.W.; Bekunda, M.; Cai, Z.; Freney, J.R.; Martinelli, L.A.; Seitzinger, S.P.; Sutton, M.A. Transformation of the Nitrogen Cycle: Recent Trends, Questions, and Potential Solutions. *Science* **2008**, *320*, 889–892. [CrossRef]
552. Gruber, N.; Galloway, J.N. An Earth-system perspective of the global nitrogen cycle. *Nature* **2008**, *451*, 293–296. [CrossRef]
553. U.S. Geological Survey. *Mineral Commodity Summaries*; U.S. Geological Survey: Reston, VA, USA, 2020; ISBN 9781411343627.
554. Lipman, T.; Shah, N. Ammonia as an Alternative Energy Storage Medium for Hydrogen Fuel Cells: Scientific and Technical Review for Near-Term Stationary Power Demonstration Projects, Final Report. *Inst. Transp. Stud. Res. Rep. Work. Pap. Proc.* 2007. Available online: <https://escholarship.org/uc/item/7z69v4wp> (accessed on 9 July 2020).
555. Lan, R.; Irvine, J.T.S.; Tao, S. Ammonia and related chemicals as potential indirect hydrogen storage materials. *Int. J. Hydrog. Energy* **2012**, *37*, 1482–1494. [CrossRef]
556. Lan, R.; Tao, S. Ammonia as a Suitable Fuel for Fuel Cells. *Front. Energy Res.* **2014**, *2*, 1–4. [CrossRef]



557. Federsel, C.; Jackstell, R.; Beller, M. State-of-the-art catalysts for hydrogenation of carbon dioxide. *Angew. Chem. Int. Ed.* **2010**, *49*, 6254–6257. [[CrossRef](#)] [[PubMed](#)]
558. Kar, S.; Goeppert, A.; Prakash, G.K.S. Integrated CO<sub>2</sub> Capture and Conversion to Formate and Methanol: Connecting Two Threads. *Acc. Chem. Res.* **2019**, *52*, 2892–2903. [[CrossRef](#)]
559. Kar, S.; Kothandaraman, J.; Goeppert, A.; Prakash, G.K.S. Advances in catalytic homogeneous hydrogenation of carbon dioxide to methanol. *J. CO<sub>2</sub> Util.* **2018**, *23*, 212–218. [[CrossRef](#)]
560. Munshi, P.; Main, A.D.; Linehan, J.C.; Tai, C.C.; Jessop, P.G. Hydrogenation of carbon dioxide catalyzed by ruthenium trimethylphosphine complexes: The accelerating effect of certain alcohols and amines. *J. Am. Chem. Soc.* **2002**, *124*, 7963–7971. [[CrossRef](#)]
561. Urakawa, A.; Jutz, F.; Laurenczy, G.; Baiker, A. Carbon dioxide hydrogenation catalyzed by a ruthenium dihydride: A DFT and high-pressure spectroscopic investigation. *Chem. A Eur. J.* **2007**, *13*, 3886–3899. [[CrossRef](#)]
562. Jessop, P.G.; Hsiao, Y.; Ikariya, T.; Noyori, R. Homogeneous Catalysis in Supercritical Fluids: Hydrogenation of Supercritical Carbon Dioxide to Formic Acid, Alkyl Formates, and Formamides. *J. Am. Chem. Soc.* **1996**, *118*, 344–355. [[CrossRef](#)]
563. Jessop, P.G.; Ikariya, T.; Noyori, R. Homogeneous catalytic hydrogenation of supercritical carbon dioxide. *Nature* **1994**, *368*, 231–233. [[CrossRef](#)]
564. Graf, E.; Leitner, W. Direct formation of formic acid from carbon dioxide and dihydrogen using the [(Rh(cod)Cl)<sub>2</sub>]-Ph<sub>2</sub>P(CH<sub>2</sub>)<sub>4</sub>PPh<sub>2</sub> catalyst system. *J. Chem. Soc., Chem. Commun.* **1992**, 623–624. [[CrossRef](#)]
565. Gassner, F.; Leitner, W. Hydrogenation of carbon dioxide to formic acid using water-soluble rhodium catalysts. *J. Chem. Soc. Chem. Commun.* **1993**, 1465. [[CrossRef](#)]
566. Angermund, K.; Baumann, W.; Dinjus, E.; Fornika, R.; Görls, H.; Kessler, M.; Krüger, C.; Leitner, W.; Lutz, F. Complexes [(P2)Rh(hfacac)] as Model Compounds for the Fragment [(P2)Rh] and as Highly Active Catalysts for CO<sub>2</sub> Hydrogenation: The Accessible Molecular Surface (AMS) Model as an Approach to Quantifying the Intrinsic Steric Properties of Chelating Ligands i. *Chem. A Eur. J.* **1997**, *3*, 755–764. [[CrossRef](#)]
567. Himeda, Y.; Onozawa-Komatsuzaki, N.; Sugihara, H.; Kasuga, K. Simultaneous tuning of activity and water solubility of complex catalysts by acid-base equilibrium of ligands for conversion of carbon dioxide. *Organometallics* **2007**, *26*, 702–712. [[CrossRef](#)]
568. Tanaka, R.; Yamashita, M.; Nozaki, K. Catalytic Hydrogenation of Carbon Dioxide Using Ir(III)-Pincer Complexes RID E-4607-2010 RID E-8779-2010. *J. Am. Chem. Soc.* **2009**, *131*, 14168–14169. [[CrossRef](#)] [[PubMed](#)]
569. Schmeier, T.J.; Dobereiner, G.E.; Crabtree, R.H.; Hazari, N. Secondary coordination sphere interactions facilitate the insertion step in an iridium(III) CO<sub>2</sub> reduction catalyst. *J. Am. Chem. Soc.* **2011**, *133*, 9274–9277. [[CrossRef](#)]
570. Federsel, C.; Boddien, A.; Jackstell, R.; Jennerjahn, R.; Dyson, P.J.; Scopelliti, R.; Laurenczy, G.; Beller, M. A well-defined iron catalyst for the reduction of bicarbonates and carbon dioxide to formates, alkyl formates, and formamides. *Angew. Chem. Int. Ed.* **2010**, *49*, 9777–9780. [[CrossRef](#)]
571. Balaraman, E.; Gunanathan, C.; Zhang, J.; Shimon, L.J.W.; Milstein, D. Efficient hydrogenation of organic carbonates, carbamates and formates indicates alternative routes to methanol based on CO<sub>2</sub> and CO. *Nat. Chem.* **2011**, *3*, 609–614. [[CrossRef](#)] [[PubMed](#)]
572. Huff, C.A.; Sanford, M.S. Cascade catalysis for the homogeneous hydrogenation of CO<sub>2</sub> to methanol. *J. Am. Chem. Soc.* **2011**, *133*, 18122–18125. [[CrossRef](#)]
573. Balaraman, E.; Ben-David, Y.; Milstein, D. Unprecedented catalytic hydrogenation of urea derivatives to amines and methanol. *Angew. Chem. Int. Ed.* **2011**, *50*, 11702–11705. [[CrossRef](#)] [[PubMed](#)]
574. Ostapowicz, T.G.; Hölscher, M.; Leitner, W. CO<sub>2</sub> insertion into metal-carbon bonds: A computational study of RhI pincer complexes. *Chem. A Eur. J.* **2011**, *17*, 10329–10338. [[CrossRef](#)]
575. Ostapowicz, T.G.; Schmitz, M.; Krystof, M.; Klankermayer, J.; Leitner, W. Carbon dioxide as a C1 building block for the formation of carboxylic acids by formal catalytic hydrocarboxylation. *Angew. Chem. Int. Ed.* **2013**, *52*, 12119–12123. [[CrossRef](#)]
576. Wesselbaum, S.; Vom Stein, T.; Klankermayer, J.; Leitner, W. Hydrogenation of carbon dioxide to methanol by using a homogeneous ruthenium-phosphine catalyst. *Angew. Chem. Int. Ed.* **2012**, *51*, 7499–7502. [[CrossRef](#)] [[PubMed](#)]

577. Geilen, F.M.A.; Engendahl, B.; Hölscher, M.; Klankermayer, J.; Leitner, W. Selective Homogeneous Hydrogenation of Biogenic Carboxylic Acids with [Ru(TriPhos)H] <sup>+</sup>: A Mechanistic Study. *J. Am. Chem. Soc.* **2011**, *133*, 14349–14358. [CrossRef] [PubMed]
578. Wesselbaum, S.; Moha, V.; Meuresch, M.; Brosinski, S.; Thenert, K.M.; Kothe, J.; vom Stein, T.; Englert, U.; Hölscher, M.; Klankermayer, J.; et al. Hydrogenation of carbon dioxide to methanol using a homogeneous ruthenium-Triphos catalyst: From mechanistic investigations to multiphase catalysis. *Chem. Sci.* **2015**, *6*, 693–704. [CrossRef]
579. Beydoun, K.; Vom Stein, T.; Klankermayer, J.; Leitner, W. Ruthenium-catalyzed direct methylation of primary and secondary aromatic amines using carbon dioxide and molecular hydrogen. *Angew. Chem. Int. Ed.* **2013**, *52*, 9554–9557. [CrossRef]
580. Kang, P.; Cheng, C.; Chen, Z.; Schauer, C.K.; Meyer, T.J.; Brookhart, M. Selective electrocatalytic reduction of CO<sub>2</sub> to formate by water-stable iridium dihydride pincer complexes. *J. Am. Chem. Soc.* **2012**, *134*, 5500–5503. [CrossRef]
581. Osadchuk, I.; Tamm, T.; Ahlquist, M.S.G. Reduced State of Iridium PCP Pincer Complexes in Electrochemical CO<sub>2</sub> Hydrogenation. *ACS Catal.* **2016**, *6*, 3834–3839. [CrossRef]
582. Elmas, S.; Subhani, M.A.; Vogt, H.; Leitner, W.; Müller, T.E. Facile insertion of CO<sub>2</sub> into metal-phenoxide bonds. *Green Chem.* **2013**, *15*, 1356–1360. [CrossRef]
583. Vogt, M.; Rivada-Wheeler, O.; Iron, M.A.; Leitner, G.; Diskin-Posner, Y.; Shimon, L.J.W.; Ben-David, Y.; Milstein, D. Anionic nickel(II) complexes with doubly deprotonated PNP pincer-type ligands and their reactivity toward CO<sub>2</sub>. *Organometallics* **2013**, *32*, 300–308. [CrossRef]
584. Hull, J.F.; Himeda, Y.; Wang, W.-H.; Hashiguchi, B.; Periana, R.; Szalda, D.J.; Muckerman, J.T.; Fujita, E. Reversible hydrogen storage using CO<sub>2</sub> and a proton-switchable iridium catalyst in aqueous media under mild temperatures and pressures. *Nat. Chem.* **2012**, *4*, 383–388. [CrossRef] [PubMed]
585. Sordakis, K.; Tsurusaki, A.; Iguchi, M.; Kawanami, H.; Himeda, Y.; Laurenczy, G. Carbon Dioxide to Methanol: The Aqueous Catalytic Way at Room Temperature. *Chem. A Eur. J.* **2016**, *22*, 15605–15608. [CrossRef] [PubMed]
586. Rezayee, N.M.; Huff, C.A.; Sanford, M.S. Tandem amine and ruthenium-catalyzed hydrogenation of CO<sub>2</sub> to methanol. *J. Am. Chem. Soc.* **2015**, *137*, 1028–1031. [CrossRef] [PubMed]
587. Khusnutdinova, J.R.; Garg, J.A.; Milstein, D. Combining Low-Pressure CO<sub>2</sub> Capture and Hydrogenation to Form Methanol. *ACS Catal.* **2015**, *5*, 2416–2422. [CrossRef]
588. Shao, R.; Stangeland, A. Amines Used in CO<sub>2</sub> Capture-Health and Environmental Impacts. Bellona Found. Norway, Oslo. 2009. Available online: [https://network.bellona.org/content/uploads/sites/3/fil\\_Bellona\\_report\\_September\\_2009\\_-\\_Amines\\_used\\_in\\_CO2\\_capture.pdf](https://network.bellona.org/content/uploads/sites/3/fil_Bellona_report_September_2009_-_Amines_used_in_CO2_capture.pdf) (accessed on 9 July 2020).
589. Kothandaraman, J.; Goeppert, A.; Czaun, M.; Olah, G.A.; Prakash, G.K.S. Conversion of CO<sub>2</sub> from Air into Methanol Using a Polyamine and a Homogeneous Ruthenium Catalyst. *J. Am. Chem. Soc.* **2016**, *138*, 778–781. [CrossRef]
590. Kar, S.; Sen, R.; Goeppert, A.; Prakash, G.K.S. Integrative CO<sub>2</sub> Capture and hydrogenation to methanol with reusable catalyst and amine: Toward a carbon neutral methanol economy. *J. Am. Chem. Soc.* **2018**, *140*, 1580–1583. [CrossRef]
591. Kar, S.; Goeppert, A.; Prakash, G.K.S. Combined CO<sub>2</sub> Capture and Hydrogenation to Methanol: Amine Immobilization Enables Easy Recycling of Active Elements. *ChemSusChem* **2019**, *12*, 3172–3177. [CrossRef]
592. Kar, S.; Sen, R.; Kothandaraman, J.; Goeppert, A.; Chowdhury, R.; Munoz, S.B.; Haiges, R.; Prakash, G.K.S. Mechanistic Insights into Ruthenium-Pincer-Catalyzed Amine-Assisted Homogeneous Hydrogenation of CO<sub>2</sub> to Methanol. *J. Am. Chem. Soc.* **2019**, *141*, 3160–3170. [CrossRef]
593. Rawat, K.S.; Pathak, B. Aliphatic Mn-PNP complexes for the CO<sub>2</sub> hydrogenation reaction: A base free mechanism. *Catal. Sci. Technol.* **2017**, *7*, 3234–3242. [CrossRef]
594. Mandal, S.C.; Rawat, K.S.; Nandi, S.; Pathak, B. Theoretical insights into CO<sub>2</sub> hydrogenation to methanol by a Mn-PNP complex. *Catal. Sci. Technol.* **2019**, *9*, 1867–1878. [CrossRef]
595. Kar, S.; Goeppert, A.; Kothandaraman, J.; Prakash, G.K.S. Manganese-Catalyzed Sequential Hydrogenation of CO<sub>2</sub> to Methanol via Formamide. *ACS Catal.* **2017**, *7*, 6347–6351. [CrossRef]
596. Sen, R.; Goeppert, A.; Kar, S.; Prakash, G.K.S. Hydroxide Based Integrated CO<sub>2</sub> Capture from Air and Conversion to Methanol. *J. Am. Chem. Soc.* **2020**, *142*, 4544–4549. [CrossRef] [PubMed]

597. Schneidewind, J.; Adam, R.; Baumann, W.; Jackstell, R.; Beller, M. Low-Temperature Hydrogenation of Carbon Dioxide to Methanol with a Homogeneous Cobalt Catalyst. *Angew. Chem. Int. Ed.* **2017**, *56*, 1890–1893. [[CrossRef](#)] [[PubMed](#)]
598. Korstanje, T.J.; Ivar van der Vlugt, J.; Elsevier, C.J.; de Bruin, B. Hydrogenation of carboxylic acids with a homogeneous cobalt catalyst. *Science* **2015**, *350*, 298–302. [[CrossRef](#)]
599. Scharnagl, F.K.; Hertrich, M.F.; Neitzel, G.; Jackstell, R.; Beller, M. Homogeneous Catalytic Hydrogenation of CO<sub>2</sub> to Methanol—Improvements with Tailored Ligands. *Adv. Synth. Catal.* **2019**, *361*, 374–379.
600. Schieweck, B.G.; Klankermayer, J. Tailor-made Molecular Cobalt Catalyst System for the Selective Transformation of Carbon Dioxide to Dialkoxymethane Ethers. *Angew. Chem. Int. Ed.* **2017**, *56*, 10854–10857. [[CrossRef](#)]
601. Kumar, A.; Janes, T.; Espinosa-Jalapa, N.A.; Milstein, D. Manganese Catalyzed Hydrogenation of Organic Carbonates to Methanol and Alcohols. *Angew. Chem. Int. Ed.* **2018**, *57*, 12076–12080. [[CrossRef](#)] [[PubMed](#)]
602. Zubar, V.; Lebedev, Y.; Azofra, L.M.; Cavallo, L.; El-Sepelgy, O.; Rueping, M. Hydrogenation of CO<sub>2</sub>-Derived Carbonates and Polycarbonates to Methanol and Diols by Metal–Ligand Cooperative Manganese Catalysis. *Angew. Chem. Int. Ed.* **2018**, *57*, 13439–13443. [[CrossRef](#)] [[PubMed](#)]
603. Ma, Q.Q.; Liu, T.; Li, S.; Zhang, J.; Chen, X.; Guan, H. Highly efficient reduction of carbon dioxide with a borane catalyzed by bis(phosphinite) pincer ligated palladium thiolate complexes. *Chem. Commun.* **2016**, *52*, 14262–14265. [[CrossRef](#)]
604. Erken, C.; Kaithal, A.; Sen, S.; Weyhermüller, T.; Hölscher, M.; Werlé, C.; Leitner, W. Manganese-catalyzed hydroboration of carbon dioxide and other challenging carbonyl groups. *Nat. Commun.* **2018**, *9*, 1–9. [[CrossRef](#)]
605. Motokura, K.; Kashiwame, D.; Takahashi, N.; Miyaji, A.; Baba, T. Highly Active and Selective Catalysis of Copper Diphosphine Complexes for the Transformation of Carbon Dioxide into Silyl Formate. *Chem. A Eur. J.* **2013**, *19*, 10030–10037. [[CrossRef](#)]
606. Rit, A.; Zanardi, A.; Spaniol, T.P.; Maron, L.; Okuda, J. A Cationic Zinc Hydride Cluster Stabilized by an N-Heterocyclic Carbene: Synthesis, Reactivity, and Hydrosilylation Catalysis. *Angew. Chem. Int. Ed.* **2014**, *53*, 13273–13277. [[CrossRef](#)]
607. Tüchler, M.; Gärtner, L.; Fischer, S.; Boese, A.D.; Belaj, F.; Mösch-Zanetti, N.C. Efficient CO<sub>2</sub> Insertion and Reduction Catalyzed by a Terminal Zinc Hydride Complex. *Angew. Chem. Int. Ed.* **2018**, *57*, 6906–6909. [[CrossRef](#)]
608. Eisenschmid, T.C.; Eisenberg, R. The iridium complex catalyzed reduction of carbon dioxide to methoxide by alkylsilanes. *Organometallics* **1989**, *8*, 1822–1824. [[CrossRef](#)]
609. Riduan, S.N.; Zhang, Y.; Ying, J.Y. Conversion of Carbon Dioxide into Methanol with Silanes over N-Heterocyclic Carbene Catalysts. *Angew. Chem. Int. Ed.* **2009**, *48*, 3322–3325. [[CrossRef](#)]
610. Metsänen, T.T.; Oestreich, M. Temperature-Dependent Chemoselective Hydrosilylation of Carbon Dioxide to Formaldehyde or Methanol Oxidation State. *Organometallics* **2015**, *34*, 543–546. [[CrossRef](#)]
611. Scheuermann, M.L.; Semproni, S.P.; Pappas, I.; Chirik, P.J. Carbon dioxide hydrosilylation promoted by cobalt pincer complexes. *Inorg. Chem.* **2014**, *53*, 9463–9465. [[CrossRef](#)] [[PubMed](#)]
612. Huang, F.; Zhang, C.; Jiang, J.; Wang, Z.-X.; Guan, H. How Does the Nickel Pincer Complex Catalyze the Conversion of CO<sub>2</sub> to a Methanol Derivative? A Computational Mechanistic Study. *Inorg. Chem.* **2011**, *50*, 3816–3825. [[CrossRef](#)] [[PubMed](#)]
613. Bertini, F.; Glatz, M.; Stöger, B.; Peruzzini, M.; Veiros, L.F.; Kirchner, K.; Gonsalvi, L. Carbon Dioxide Reduction to Methanol Catalyzed by Mn(I) PNP Pincer Complexes under Mild Reaction Conditions. *ACS Catal.* **2019**, *9*, 632–639. [[CrossRef](#)]
614. Mazzotta, M.G.; Xiong, M.; Abu-Omar, M.M. Carbon Dioxide Reduction to Silyl-Protected Methanol Catalyzed by an Oxorhenium Pincer PNN Complex. *Organometallics* **2017**, *36*, 1688–1691. [[CrossRef](#)]
615. Ryabchuk, P.; Stier, K.; Junge, K.; Checinski, M.P.; Beller, M. Molecularly Defined Manganese Catalyst for Low-Temperature Hydrogenation of Carbon Monoxide to Methanol. *J. Am. Chem. Soc.* **2019**, *141*, 16923–16929. [[CrossRef](#)]
616. Kar, S.; Goepfert, A.; Prakash, G.K.S. Catalytic Homogeneous Hydrogenation of CO to Methanol via Formamide. *J. Am. Chem. Soc.* **2019**, *141*, 12518–12521. [[CrossRef](#)]

617. Schneck, F.; Schendzielorz, F.; Hatami, N.; Finger, M.; Würtele, C.; Schneider, S. Photochemically Driven Reverse Water-Gas Shift at Ambient Conditions mediated by a Nickel Pincer Complex. *Angew. Chem. Int. Ed.* **2018**, *57*, 14482–14487. [\[CrossRef\]](#)
618. Schneck, F.; Ahrens, J.; Finger, M.; Stüchl, A.C.; Würtele, C.; Schwarzer, D.; Schneider, S. The elusive abnormal CO<sub>2</sub> insertion enabled by metal-ligand cooperative photochemical selectivity inversion. *Nat. Commun.* **2018**, *9*, 1–8. [\[CrossRef\]](#)
619. Feller, M.; Ben-Ari, E.; Diskin-Posner, Y.; Milstein, D. CO<sub>2</sub> activation by metal–ligand-cooperation mediated by iridium pincer complexes. *J. Coord. Chem.* **2018**, *71*, 1679–1689. [\[CrossRef\]](#)
620. Feller, M.; Gellrich, U.; Anaby, A.; Diskin-Posner, Y.; Milstein, D. Reductive Cleavage of CO<sub>2</sub> by Metal-Ligand-Cooperation Mediated by an Iridium Pincer Complex. *J. Am. Chem. Soc.* **2016**, *138*, 6445–6454. [\[CrossRef\]](#) [\[PubMed\]](#)
621. Anaby, A.; Feller, M.; Ben-David, Y.; Leitun, G.; Diskin-Posner, Y.; Shimon, L.J.W.; Milstein, D. Bottom-Up Construction of a CO<sub>2</sub>-Based Cycle for the Photocarbonylation of Benzene, Promoted by a Rhodium(I) Pincer Complex. *J. Am. Chem. Soc.* **2016**, *138*, 9941–9950. [\[CrossRef\]](#)
622. Krishnan, V.M.; Arman, H.D.; Tonzetich, Z.J. Preparation and reactivity of a square-planar PNP cobalt(II)-hydrido complex: Isolation of the first {Co-NO} 8 -hydride. *Dalt. Trans.* **2018**, *47*, 1435–1441. [\[CrossRef\]](#) [\[PubMed\]](#)
623. Muller, K.; Sun, Y.; Heimermann, A.; Menges, F.; Niedner-Schatteburg, G.; van Wüllen, C.; Thiel, W.R. Structure-Reactivity Relationships in the Hydrogenation of Carbon Dioxide with Ruthenium Complexes Bearing Pyridinylazolato Ligands. *Chem. A Eur. J.* **2013**, *19*, 7825–7834. [\[CrossRef\]](#)
624. Thai, T.-T.; Therrien, B.; Süß-Fink, G. Arene ruthenium oxinato complexes: Synthesis, molecular structure and catalytic activity for the hydrogenation of carbon dioxide in aqueous solution. *J. Organomet. Chem.* **2009**, *694*, 3973–3981. [\[CrossRef\]](#)
625. Gao, Y.; Kuncheria, J.K.; Jenkins, H.A.; Puddephatt, R.J.; Yap, G.P.A. The interconversion of formic acid and hydrogen/carbon dioxide using a binuclear ruthenium complex catalyst. *J. Chem. Soc. Dalt. Trans.* **2000**, 3212–3217. [\[CrossRef\]](#)
626. Zhang, J.Z.; Li, Z.; Wang, H.; Wang, C.Y. Homogeneous catalytic synthesis of formic acid (salts) by hydrogenation of CO<sub>2</sub> with H<sub>2</sub> in the presence of ruthenium species. *J. Mol. Catal. A Chem.* **1996**, *112*, 9–14. [\[CrossRef\]](#)
627. Wesselbaum, S.; Hintermair, U.; Leitner, W. Continuous-Flow Hydrogenation of Carbon Dioxide to Pure Formic Acid using an Integrated scCO<sub>2</sub> Process with Immobilized Catalyst and Base. *Angew. Chem. Int. Ed.* **2012**, *51*, 8585–8588. [\[CrossRef\]](#)
628. Boddien, A.; Federsel, C.; Sponholz, P.; Mellmann, D.; Jackstell, R.; Junge, H.; Laurenczy, G.; Beller, M. Towards the development of a hydrogen battery. *Energy Environ. Sci.* **2012**, *5*, 8907. [\[CrossRef\]](#)
629. Elek, J.; Nádasdi, L.; Papp, G.; Laurenczy, G.; Joó, F. Homogeneous hydrogenation of carbon dioxide and bicarbonate in aqueous solution catalyzed by water-soluble ruthenium(II) phosphine complexes. *Appl. Catal. A Gen.* **2003**, *255*, 59–67. [\[CrossRef\]](#)
630. Jantke, D.; Pardatscher, L.; Drees, M.; Cokoja, M.; Herrmann, W.A.; Kühn, F.E. Hydrogen Production and Storage on a Formic Acid/Bicarbonate Platform using Water-Soluble N -Heterocyclic Carbene Complexes of Late Transition Metals. *ChemSusChem* **2016**, *9*, 2849–2854. [\[CrossRef\]](#)
631. Chatterjee, D.; Sarkar, P. Ru III (edta) catalyzed hydrogenation of bicarbonate to formate. *J. Coord. Chem.* **2016**, *69*, 650–655. [\[CrossRef\]](#)
632. Boddien, A.; Gärtner, F.; Federsel, C.; Sponholz, P.; Mellmann, D.; Jackstell, R.; Junge, H.; Beller, M. CO<sub>2</sub>-“Neutral” Hydrogen Storage Based on Bicarbonates and Formates. *Angew. Chem. Int. Ed.* **2011**, *50*, 6411–6414. [\[CrossRef\]](#) [\[PubMed\]](#)
633. Federsel, C.; Jackstell, R.; Boddien, A.; Laurenczy, G.; Beller, M. Ruthenium-Catalyzed Hydrogenation of Bicarbonate in Water. *ChemSusChem* **2010**, *3*, 1048–1050. [\[CrossRef\]](#) [\[PubMed\]](#)
634. Ziebart, C.; Federsel, C.; Anbarasan, P.; Jackstell, R.; Baumann, W.; Spannenberg, A.; Beller, M. Well-defined iron catalyst for improved hydrogenation of carbon dioxide and bicarbonate. *J. Am. Chem. Soc.* **2012**, *134*, 20701–20704. [\[CrossRef\]](#)
635. Federsel, C.; Ziebart, C.; Jackstell, R.; Baumann, W.; Beller, M. Catalytic hydrogenation of carbon dioxide and bicarbonates with a well-defined cobalt dihydrogen complex. *Chem. A Eur. J.* **2012**, *18*, 72–75. [\[CrossRef\]](#)



636. Liu, Q.; Wu, L.; Gülak, S.; Rockstroh, N.; Jackstell, R.; Beller, M. Towards a sustainable synthesis of formate salts: Combined catalytic methanol dehydrogenation and bicarbonate hydrogenation. *Angew. Chem. Int. Ed.* **2014**, *53*, 7085–7088. [[CrossRef](#)] [[PubMed](#)]
637. Huff, C.A.; Sanford, M.S. Catalytic CO<sub>2</sub> hydrogenation to formate by a ruthenium pincer complex. *ACS Catal.* **2013**. [[CrossRef](#)]
638. Filonenko, G.A.; van Putten, R.; Schulpen, E.N.; Hensen, E.J.M.; Pidko, E.A. Highly Efficient Reversible Hydrogenation of Carbon Dioxide to Formates Using a Ruthenium PNP-Pincer Catalyst. *ChemCatChem* **2014**, *6*, 1526–1530. [[CrossRef](#)]
639. Zhang, Y.; MacIntosh, A.D.; Wong, J.L.; Bielinski, E.A.; Williard, P.G.; Mercado, B.Q.; Hazari, N.; Bernskoetter, W.H. Iron catalyzed CO<sub>2</sub> hydrogenation to formate enhanced by Lewis acid co-catalysts. *Chem. Sci.* **2015**, *6*, 4291–4299. [[CrossRef](#)]
640. Bernskoetter, W.H.; Hazari, N. Reversible Hydrogenation of Carbon Dioxide to Formic Acid and Methanol: Lewis Acid Enhancement of Base Metal Catalysts. *Acc. Chem. Res.* **2017**, *50*, 1049–1058. [[CrossRef](#)] [[PubMed](#)]
641. Spentzos, A.Z.; Barnes, C.L.; Bernskoetter, W.H. Effective Pincer Cobalt Precatalysts for Lewis Acid Assisted CO<sub>2</sub> Hydrogenation. *Inorg. Chem.* **2016**, *55*, 8225–8233. [[CrossRef](#)]
642. Mills, M.R.; Barnes, C.L.; Bernskoetter, W.H. Influences of Bifunctional PNP-Pincer Ligands on Low Valent Cobalt Complexes Relevant to CO<sub>2</sub> Hydrogenation. *Inorg. Chem.* **2018**, *57*, 1590–1597. [[CrossRef](#)]
643. Rivada-Wheelaghan, O.; Dauth, A.; Leitus, G.; Diskin-Posner, Y.; Milstein, D. Synthesis and reactivity of iron complexes with a new pyrazine-based pincer ligand, and application in catalytic low-pressure hydrogenation of carbon dioxide. *Inorg. Chem.* **2015**, *54*, 4526–4538. [[CrossRef](#)]
644. Bertini, F.; Gorgas, N.; Stöger, B.; Peruzzini, M.; Veiros, L.F.; Kirchner, K.; Gonsalvi, L. Efficient and Mild Carbon Dioxide Hydrogenation to Formate Catalyzed by Fe(II) Hydrido Carbonyl Complexes Bearing 2,6-(Diaminopyridyl)diphosphine Pincer Ligands. *ACS Catal.* **2016**, *6*, 2889–2893. [[CrossRef](#)]
645. Kothandaraman, J.; Goeppert, A.; Czaun, M.; Olah, G.A.; Surya Prakash, G.K. CO<sub>2</sub> capture by amines in aqueous media and its subsequent conversion to formate with reusable ruthenium and iron catalysts. *Green Chem.* **2016**, *18*, 5831–5838. [[CrossRef](#)]
646. Kar, S.; Goeppert, A.; Galvan, V.; Chowdhury, R.; Olah, J.; Prakash, G.K.S. A Carbon-Neutral CO<sub>2</sub> Capture, Conversion, and Utilization Cycle with Low-Temperature Regeneration of Sodium Hydroxide. *J. Am. Chem. Soc.* **2018**, *140*, 16873–16876. [[CrossRef](#)] [[PubMed](#)]
647. Treigerman, Z.; Sasson, Y. Generation and Quantification of Formate Ion Produced from Aqueous Sodium Bicarbonate in the Presence of Homogeneous Ruthenium Catalyst. *ACS Omega* **2018**, *3*, 12797–12801. [[CrossRef](#)]
648. Dai, Z.; Luo, Q.; Cong, H.; Zhang, J.; Peng, T. New Ru(II) N'NN'-type pincer complexes: Synthesis, characterization and the catalytic hydrogenation of CO<sub>2</sub> or bicarbonates to formate salts. *New J. Chem.* **2017**, *41*, 3055–3060. [[CrossRef](#)]
649. Bertini, F.; Glatz, M.; Gorgas, N.; Stöger, B.; Peruzzini, M.; Veiros, L.F.; Kirchner, K.; Gonsalvi, L. Carbon dioxide hydrogenation catalysed by well-defined Mn(I) PNP pincer hydride complexes. *Chem. Sci.* **2017**, *8*, 5024–5029. [[CrossRef](#)]
650. Ramaraj, A.; Nethaji, M.; Jagirdar, B.R. Hydrogenation of CO<sub>2</sub>, carbonyl and imine substrates catalyzed by [IrH<sub>3</sub>(<sup>Ph</sup>PN<sup>H</sup>P)] complex. *J. Organomet. Chem.* **2019**, *883*, 25–34. [[CrossRef](#)]
651. Lo, H.K.; Copéret, C. CO<sub>2</sub> Hydrogenation to Formate with Immobilized Ru-Catalysts Based on Hybrid Organo-Silica Mesostructured Materials. *ChemCatChem* **2019**, *11*, 430–434. [[CrossRef](#)]
652. Foster, S.L.; Bakovic, S.I.P.; Duda, R.D.; Maheshwari, S.; Milton, R.D.; Minter, S.D.; Janik, M.J.; Renner, J.N.; Greenlee, L.F. Catalysts for nitrogen reduction to ammonia. *Nat. Catal.* **2018**, *1*, 490–500. [[CrossRef](#)]
653. Hölscher, M.; Precht, M.H.G.; Leitner, W. Can [M(H)<sub>2</sub>(H<sub>2</sub>)(PXP)] pincer complexes (M = Fe, Ru, Os; X = N, O, S) serve as catalyst lead structures for NH<sub>3</sub> synthesis from N<sub>2</sub> and H<sub>2</sub>? *Chem. A Eur. J.* **2007**, *13*, 6636–6643. [[CrossRef](#)]
654. Stucke, N.; Flöser, B.M.; Weyrich, T.; Tuczek, F. Nitrogen Fixation Catalyzed by Transition Metal Complexes: Recent Developments. *Eur. J. Inorg. Chem.* **2018**, *2018*, 1337–1355. [[CrossRef](#)]
655. Nishibayashi, Y. Development of catalytic nitrogen fixation using transition metal-dinitrogen complexes under mild reaction conditions. *Dalt. Trans.* **2018**, *47*, 11290–11297. [[CrossRef](#)]
656. Nishibayashi, Y. Recent Progress in Transition-Metal-Catalyzed Reduction of Molecular Dinitrogen under Ambient Reaction Conditions. *Inorg. Chem.* **2015**, *54*, 9234–9247. [[CrossRef](#)]

657. Tanabe, Y.; Nishibayashi, Y. Catalytic Dinitrogen Fixation to Form Ammonia at Ambient Reaction Conditions Using Transition Metal-Dinitrogen Complexes. *Chem. Rev.* **2016**, *16*, 1549–1577. [\[CrossRef\]](#)
658. Nishibayashi, Y. Molybdenum-catalyzed reduction of molecular dinitrogen into ammonia under ambient reaction conditions. *Comptes Rendus Chim.* **2015**, *18*, 776–784. [\[CrossRef\]](#)
659. Burford, R.J.; Fryzuk, M.D. Examining the relationship between coordination mode and reactivity of dinitrogen. *Nat. Rev. Chem.* **2017**, *1*, 0026. [\[CrossRef\]](#)
660. Shipman, M.A.; Symes, M.D. Recent progress towards the electrosynthesis of ammonia from sustainable resources. *Catal. Today* **2017**, *286*, 57–68. [\[CrossRef\]](#)
661. Cherkasov, N.; Ibhadon, A.O.; Fitzpatrick, P. A review of the existing and alternative methods for greener nitrogen fixation. *Chem. Eng. Process Process Intensif.* **2015**, *90*, 24–33. [\[CrossRef\]](#)
662. Giddey, S.; Badwal, S.P.S.; Kulkarni, A. Review of electrochemical ammonia production technologies and materials. *Int. J. Hydrog. Energy* **2013**, *38*, 14576–14594. [\[CrossRef\]](#)
663. Cui, X.; Tang, C.; Zhang, Q. A Review of Electrocatalytic Reduction of Dinitrogen to Ammonia under Ambient Conditions. *Adv. Energy Mater.* **2018**, *8*, 1800369. [\[CrossRef\]](#)
664. Roux, Y.; Duboc, C.; Gennari, M. Molecular Catalysts for N<sub>2</sub> Reduction: State of the Art, Mechanism, and Challenges. *ChemPhysChem* **2017**, *18*, 2606–2617. [\[CrossRef\]](#) [\[PubMed\]](#)
665. Tanaka, H.; Nishibayashi, Y.; Yoshizawa, K. Interplay between Theory and Experiment for Ammonia Synthesis Catalyzed by Transition Metal Complexes. *Acc. Chem. Res.* **2016**, *49*, 987–995. [\[CrossRef\]](#) [\[PubMed\]](#)
666. van der Ham, C.J.M.; Koper, M.T.M.; Hetterscheid, D.G.H. Challenges in reduction of dinitrogen by proton and electron transfer. *Chem. Soc. Rev.* **2014**, *43*, 5183–5191. [\[CrossRef\]](#) [\[PubMed\]](#)
667. Renner, J.N.; Greenlee, L.F.; Ayres, K.E.; Herring, A.M. Electrochemical Synthesis of Ammonia: A Low Pressure, Low Temperature Approach. *Interface Mag.* **2015**, *24*, 51–57. [\[CrossRef\]](#)
668. Allen, A.D.; Senoff, C.V. Nitrogenopentammineruthenium(II) complexes. *Chem. Commun.* **1965**, *24*, 621–622. [\[CrossRef\]](#)
669. Benedek, Z.; Papp, M.; Oláh, J.; Szilvási, T. Identifying the Rate-Limiting Elementary Steps of Nitrogen Fixation with Single-Site Fe Model Complexes. *Inorg. Chem.* **2018**, *57*, 8499–8508. [\[CrossRef\]](#) [\[PubMed\]](#)
670. Tanabe, Y.; Nishibayashi, Y. Recent advances in nitrogen fixation upon vanadium complexes. *Coord. Chem. Rev.* **2019**, *381*, 135–150. [\[CrossRef\]](#)
671. Clentsmith, G.K.B.; Bates, V.M.E.; Hitchcock, P.B.; Cloke, F.G.N. Reductive Cleavage of Dinitrogen by a Vanadium Diamidoamine Complex: The Molecular Structures of [V(Me<sub>3</sub>SiN(CH<sub>2</sub>CH<sub>2</sub>NSiMe<sub>3</sub>)<sub>2</sub>)(μ-N)]<sub>2</sub> and K[V(Me<sub>3</sub>SiN(CH<sub>2</sub>CH<sub>2</sub>NSiMe<sub>3</sub>)<sub>2</sub>)(μ-N)]<sub>2</sub>. *J. Am. Chem. Soc.* **1999**, *121*, 10444–10445. [\[CrossRef\]](#)
672. Gradert, C.; Stucke, N.; Krahmer, J.; Näther, C.; Tuzek, F. Molybdenum complexes supported by mixed NHC/phosphine ligands: Activation of N<sub>2</sub> and reaction with P(OMe)<sub>3</sub> to the first meta-phosphite complex. *Chem. A Eur. J.* **2015**, *21*, 1130–1137. [\[CrossRef\]](#)
673. Husch, T.; Reiher, M. Mechanistic Consequences of Chelate Ligand Stabilization on Nitrogen Fixation by Yandulov-Schrock-Type Complexes. *ACS Sustain. Chem. Eng.* **2017**, *5*, 10527–10537. [\[CrossRef\]](#)
674. Hidai, M.; Tominari, K.; Uchida, Y. Preparation and properties of dinitrogen-molybdenum complexes. *J. Am. Chem. Soc.* **1972**, *94*, 110–114. [\[CrossRef\]](#)
675. Hidai, M.; Mizobe, Y. Research inspired by the chemistry of nitrogenase Novel metal complexes and their reactivity toward dinitrogen, nitriles, and alkynes. *Can. J. Chem.* **2005**, *83*, 358–374. [\[CrossRef\]](#)
676. Studt, F.; Lehnert, N.; Wiesler, B.E.; Scherer, A.; Beckhaus, R.; Tuzek, F. Spectroscopic Comparison of Dinuclear Ti<sup>+</sup> and Ti<sup>2+</sup> μ-η<sup>1</sup>:η<sup>1</sup> Dinitrogen Complexes with Cp\*/Pentafulvene and Amine/Amide Ligation: Moderate versus Strong Activation of N<sub>2</sub>. *Eur. J. Inorg. Chem.* **2006**, *2006*, 291–297. [\[CrossRef\]](#)
677. Fryzuk, M.D. Transformation of Coordinated Dinitrogen by Reaction with Dihydrogen and Primary Silanes. *Science* **1997**, *275*, 1445–1447. [\[CrossRef\]](#)
678. Bobadova-Parvanova, P.; Wang, Q.; Quinonero-Santiago, D.; Morokuma, K.; Musaev, D.G. Does Dinitrogen Hydrogenation Follow Different Mechanisms for [(η<sup>5</sup>-C<sub>5</sub>Me<sub>4</sub>H)<sub>2</sub>Zr](μ<sub>2</sub>,η<sup>2</sup>,η<sup>2</sup>-N<sub>2</sub>) and {P[Ph](CH<sub>2</sub>SiMe<sub>2</sub>NSiMe<sub>2</sub>CH<sub>2</sub>)PPh}[Zr]<sub>2</sub>(μ<sub>2</sub>,η<sup>2</sup>,η<sup>2</sup>-N<sub>2</sub>) Complexes? A Computational Study. *J. Am. Chem. Soc.* **2006**, *128*, 11391–11403. [\[CrossRef\]](#)
679. Hoffman, B.M.; Lukoyanov, D.; Yang, Z.-Y.; Dean, D.R.; Seefeldt, L.C. Mechanism of Nitrogen Fixation by Nitrogenase: The Next Stage. *Chem. Rev.* **2014**, *114*, 4041–4062. [\[CrossRef\]](#)
680. Hu, Y.; Ribbe, M.W. Nitrogenases-A Tale of Carbon Atom(s). *Angew. Chem. Int. Ed.* **2016**, *55*, 8216–8226. [\[CrossRef\]](#) [\[PubMed\]](#)

681. Solari, E.; Da Silva, C.; Iacono, B.; Hesschenbrouck, J.; Rizzoli, C.; Scopelliti, R.; Floriani, C. Photochemical activation of the N≡N bond in a dimolybdenum-dinitrogen complex: Formation of a molybdenum nitride. *Angew. Chem. Int. Ed.* **2001**, *40*, 3907–3909. [\[CrossRef\]](#)
682. Reiher, M.; Kirchner, B.; Hutter, J.; Sellmann, D.; Hess, B.A. A Photochemical Activation Scheme of Inert Dinitrogen by Dinuclear RuII and FeII Complexes. *Chem. A Eur. J.* **2004**, *10*, 4443–4453. [\[CrossRef\]](#) [\[PubMed\]](#)
683. Kunkely, H.; Vogler, A. Photolysis of Aqueous [(NH<sub>3</sub>)<sub>5</sub>Os(μ-N<sub>2</sub>)Os(NH<sub>3</sub>)<sub>5</sub>]<sup>5+</sup>: Cleavage of Dinitrogen by an Intramolecular Photoredox Reaction. *Angew. Chem. Int. Ed.* **2010**, *49*, 1591–1593. [\[CrossRef\]](#) [\[PubMed\]](#)
684. Huss, A.S.; Curley, J.J.; Cummins, C.C.; Blank, D.A. Relaxation and Dissociation Following Photoexcitation of the (μ-N<sub>2</sub>)[Mo(N[t-Bu]Ar)<sub>3</sub>]<sub>2</sub> Dinitrogen Cleavage Intermediate. *J. Phys. Chem. B* **2013**, *117*, 1429–1436. [\[CrossRef\]](#) [\[PubMed\]](#)
685. Fieser, M.E.; Bates, J.E.; Ziller, J.W.; Furche, F.; Evans, W.J. Dinitrogen Reduction via Photochemical Activation of Heteroleptic Tris(cyclopentadienyl) Rare-Earth Complexes. *J. Am. Chem. Soc.* **2013**, *135*, 3804–3807. [\[CrossRef\]](#) [\[PubMed\]](#)
686. Fieser, M.E.; Johnson, C.W.; Bates, J.E.; Ziller, J.W.; Furche, F.; Evans, W.J. Dinitrogen Reduction, Sulfur Reduction, and Isoprene Polymerization via Photochemical Activation of Trivalent Bis(cyclopentadienyl) Rare-Earth-Metal Allyl Complexes. *Organometallics* **2015**, *34*, 4387–4393. [\[CrossRef\]](#)
687. Miyazaki, T.; Tanaka, H.; Tanabe, Y.; Yuki, M.; Nakajima, K.; Yoshizawa, K.; Nishibayashi, Y. Cleavage and Formation of Molecular Dinitrogen in a Single System Assisted by Molybdenum Complexes Bearing Ferrocenyldiphosphine. *Angew. Chem. Int. Ed.* **2014**, *53*, 11488–11492. [\[CrossRef\]](#)
688. Rebreyend, C.; de Bruin, B. Photolytic N<sub>2</sub> Splitting: A Road to Sustainable NH<sub>3</sub> Production? *Angew. Chem. Int. Ed.* **2015**, *54*, 42–44. [\[CrossRef\]](#)
689. Schrock, R.R. Catalytic reduction of dinitrogen to ammonia by molybdenum: Theory versus experiment. *Angew. Chem. Int. Ed.* **2008**, *47*, 5512–5522. [\[CrossRef\]](#)
690. Yandulov, D.V.; Schrock, R. Catalytic Reduction of Dinitrogen to Ammonia at a Single Molybdenum Center. *Science* **2003**, *301*, 76–78. [\[CrossRef\]](#) [\[PubMed\]](#)
691. Arashiba, K.; Miyake, Y.; Nishibayashi, Y. A molybdenum complex bearing PNP-type pincer ligands leads to the catalytic reduction of dinitrogen into ammonia. *Nat. Chem.* **2011**, *3*, 120–125. [\[CrossRef\]](#) [\[PubMed\]](#)
692. Tanaka, H.; Arashiba, K.; Kuriyama, S.; Sasada, A.; Nakajima, K.; Yoshizawa, K.; Nishibayashi, Y. Unique behaviour of dinitrogen-bridged dimolybdenum complexes bearing pincer ligand towards catalytic formation of ammonia. *Nat. Commun.* **2014**, *5*, 3737. [\[CrossRef\]](#) [\[PubMed\]](#)
693. Kuriyama, S.; Arashiba, K.; Nakajima, K.; Tanaka, H.; Kamaru, N.; Yoshizawa, K.; Nishibayashi, Y. Catalytic Formation of Ammonia from Molecular Dinitrogen by Use of Dinitrogen-Bridged Dimolybdenum–Dinitrogen Complexes Bearing PNP-Pincer Ligands: Remarkable Effect of Substituent at PNP-Pincer Ligand. *J. Am. Chem. Soc.* **2014**, *136*, 9719–9731. [\[CrossRef\]](#)
694. Kuriyama, S.; Arashiba, K.; Nakajima, K.; Tanaka, H.; Yoshizawa, K.; Nishibayashi, Y. Nitrogen fixation catalyzed by ferrocene-substituted dinitrogen-bridged dimolybdenum-dinitrogen complexes: Unique behavior of ferrocene moiety as redox active site. *Chem. Sci.* **2015**, *6*, 3940–3951. [\[CrossRef\]](#)
695. Kuriyama, S.; Arashiba, K.; Nakajima, K.; Tanaka, H.; Yoshizawa, K.; Nishibayashi, Y. Azaferrocene-Based PNP-Type Pincer Ligand: Synthesis of Molybdenum, Chromium, and Iron Complexes and Reactivity toward Nitrogen Fixation. *Eur. J. Inorg. Chem.* **2016**, *2016*, 4856–4861. [\[CrossRef\]](#)
696. Klopsch, I.; Yuzik-Klimova, E.Y.; Schneider, S. Functionalization of N<sub>2</sub> by Mid to Late Transition Metals via N–N Bond Cleavage. In *Topics in Organometallic Chemistry*; Springer: Basel, Switzerland, 2017; pp. 71–112.
697. Silantyev, G.A.; Förster, M.; Schluschaß, B.; Abbeneth, J.; Würtele, C.; Volkmann, C.; Holthausen, M.C.; Schneider, S. Dinitrogen Splitting Coupled to Protonation. *Angew. Chem. Int. Ed.* **2017**, *56*, 5872–5876. [\[CrossRef\]](#)
698. Klopsch, I.; Finger, M.; Würtele, C.; Milde, B.; Werz, D.B.; Schneider, S. Dinitrogen Splitting and Functionalization in the Coordination Sphere of Rhenium. *J. Am. Chem. Soc.* **2014**, *136*, 6881–6883. [\[CrossRef\]](#)
699. Lindley, B.M.; Van Alten, R.S.; Finger, M.; Schendzielorz, F.; Würtele, C.; Miller, A.J.M.; Siewert, I.; Schneider, S. Mechanism of Chemical and Electrochemical N<sub>2</sub> Splitting by a Rhenium Pincer Complex. *J. Am. Chem. Soc.* **2018**, *140*, 7922–7935. [\[CrossRef\]](#)
700. Klopsch, I.; Kinauer, M.; Finger, M.; Würtele, C.; Schneider, S. Conversion of Dinitrogen into Acetonitrile under Ambient Conditions. *Angew. Chem. Int. Ed.* **2016**, *55*, 4786–4789. [\[CrossRef\]](#)



701. Arashiba, K.; Kinoshita, E.; Kuriyama, S.; Eizawa, A.; Nakajima, K.; Tanaka, H.; Yoshizawa, K.; Nishibayashi, Y. Catalytic Reduction of Dinitrogen to Ammonia by Use of Molybdenum–Nitride Complexes Bearing a Tridentate Triphosphine as Catalysts. *J. Am. Chem. Soc.* **2015**, *137*, 5666–5669. [\[CrossRef\]](#) [\[PubMed\]](#)
702. Eizawa, A.; Arashiba, K.; Tanaka, H.; Kuriyama, S.; Matsuo, Y.; Nakajima, K.; Yoshizawa, K.; Nishibayashi, Y. Remarkable catalytic activity of dinitrogen-bridged dimolybdenum complexes bearing NHC-based PCP-pincer ligands toward nitrogen fixation. *Nat. Commun.* **2017**, *8*, 14874. [\[CrossRef\]](#) [\[PubMed\]](#)
703. Matoba, K.; Eizawa, A.; Nishimura, S.; Arashiba, K.; Nakajima, K.; Nishibayashi, Y. Practical Synthesis of a PCP-Type Pincer Ligand and Its Metal Complexes. *Synthesis* **2018**, *50*, 1015–1019. [\[CrossRef\]](#)
704. Kinoshita, E.; Arashiba, K.; Kuriyama, S.; Eizawa, A.; Nakajima, K.; Nishibayashi, Y. Synthesis and Catalytic Activity of Molybdenum–Nitride Complexes Bearing Pincer Ligands. *Eur. J. Inorg. Chem.* **2015**, *2015*, 1789–1794. [\[CrossRef\]](#)
705. Sheng, X.L.; Batista, E.R.; Duan, Y.X.; Tian, Y.H. Dimension and bridging ligand effects on Mo-mediated catalytic transformation of dinitrogen to ammonia: Chain-like extended models of Nishibayashi’s catalyst. *Comput. Theor. Chem.* **2016**, *1095*, 134–141. [\[CrossRef\]](#)
706. Anderson, J.S.; Rittle, J.; Peters, J.C. Catalytic conversion of nitrogen to ammonia by an iron model complex. *Nature* **2013**, *501*, 84–87. [\[CrossRef\]](#)
707. Chalkley, M.J.; Del Castillo, T.J.; Matson, B.D.; Roddy, J.P.; Peters, J.C. Catalytic N<sub>2</sub>-to-NH<sub>3</sub> Conversion by Fe at Lower Driving Force: A Proposed Role for Metallocene-Mediated PCET. *ACS Cent. Sci.* **2017**, *3*, 217–223. [\[CrossRef\]](#)
708. Chalkley, M.J.; Del Castillo, T.J.; Matson, B.D.; Peters, J.C. Fe-Mediated Nitrogen Fixation with a Metallocene Mediator: Exploring pK<sub>a</sub> Effects and Demonstrating Electrocatalysis. *J. Am. Chem. Soc.* **2018**, *140*, 6122–6129. [\[CrossRef\]](#)
709. Arashiba, K.; Eizawa, A.; Tanaka, H.; Nakajima, K.; Yoshizawa, K.; Nishibayashi, Y. Catalytic nitrogen fixation via direct cleavage of nitrogen-nitrogen triple bond of molecular dinitrogen under ambient reaction conditions. *Bull. Chem. Soc. Jpn.* **2017**, *90*, 1111–1118. [\[CrossRef\]](#)
710. Itabashi, T.; Mori, I.; Arashiba, K.; Eizawa, A.; Nakajima, K.; Nishibayashi, Y. Effect of substituents on molybdenum triiodide complexes bearing PNP-type pincer ligands toward catalytic nitrogen fixation. *Dalt. Trans.* **2019**, *48*, 3182–3186. [\[CrossRef\]](#)
711. Fajardo, J.; Peters, J.C. Catalytic Nitrogen-to-Ammonia Conversion by Osmium and Ruthenium Complexes. *J. Am. Chem. Soc.* **2017**, *139*, 16105–16108. [\[CrossRef\]](#) [\[PubMed\]](#)
712. Del Castillo, T.J.; Thompson, N.B.; Suess, D.L.M.; Ung, G.; Peters, J.C. Evaluating Molecular Cobalt Complexes for the Conversion of N<sub>2</sub> to NH<sub>3</sub>. *Inorg. Chem.* **2015**, *54*, 9256–9262. [\[CrossRef\]](#) [\[PubMed\]](#)
713. Kuriyama, S.; Arashiba, K.; Nakajima, K.; Matsuo, Y.; Tanaka, H.; Ishii, K.; Yoshizawa, K.; Nishibayashi, Y. Catalytic transformation of dinitrogen into ammonia and hydrazine by iron-dinitrogen complexes bearing pincer ligand. *Nat. Commun.* **2016**, *7*, 1–9. [\[CrossRef\]](#) [\[PubMed\]](#)
714. Sekiguchi, Y.; Kuriyama, S.; Eizawa, A.; Arashiba, K.; Nakajima, K.; Nishibayashi, Y. Synthesis and reactivity of iron-dinitrogen complexes bearing anionic methyl- and phenyl-substituted pyrrole-based PNP-type pincer ligands toward catalytic nitrogen fixation. *Chem. Commun.* **2017**, *53*, 12040–12043. [\[CrossRef\]](#) [\[PubMed\]](#)
715. Kuriyama, S.; Arashiba, K.; Tanaka, H.; Matsuo, Y.; Nakajima, K.; Yoshizawa, K.; Nishibayashi, Y. Direct Transformation of Molecular Dinitrogen into Ammonia Catalyzed by Cobalt Dinitrogen Complexes Bearing Anionic PNP Pincer Ligands. *Angew. Chem. Int. Ed.* **2016**, *55*, 14291–14295. [\[CrossRef\]](#)
716. Sekiguchi, Y.; Arashiba, K.; Tanaka, H.; Eizawa, A.; Nakajima, K.; Yoshizawa, K.; Nishibayashi, Y. Catalytic Reduction of Molecular Dinitrogen to Ammonia and Hydrazine Using Vanadium Complexes. *Angew. Chem. Int. Ed.* **2018**, *57*, 9064–9068. [\[CrossRef\]](#)
717. Sekiguchi, Y.; Meng, F.; Tanaka, H.; Eizawa, A.; Arashiba, K.; Nakajima, K.; Yoshizawa, K.; Nishibayashi, Y. Synthesis and reactivity of titanium- and zirconium-dinitrogen complexes bearing anionic pyrrole-based PNP-type pincer ligands. *Dalt. Trans.* **2018**, *47*, 11322–11326. [\[CrossRef\]](#)
718. Doyle, L.R.; Woole, A.J.; Jenkins, L.C.; Tuna, F.; McInnes, E.J.L.; Liddle, S.T. Catalytic Dinitrogen Reduction to Ammonia at a Triamidoamine–Titanium Complex. *Angew. Chem. Int. Ed.* **2018**, *57*, 6314–6318. [\[CrossRef\]](#)
719. Tanabe, Y.; Arashiba, K.; Nakajima, K.; Nishibayashi, Y. Catalytic Conversion of Dinitrogen into Ammonia under Ambient Reaction Conditions by Using Proton Source from Water. *Chem. An Asian J.* **2017**, *12*, 2544–2548. [\[CrossRef\]](#)

720. Higuchi, J.; Kuriyama, S.; Eizawa, A.; Arashiba, K.; Nakajima, K.; Nishibayashi, Y. Preparation and reactivity of iron complexes bearing anionic carbazole-based PNP-type pincer ligands toward catalytic nitrogen fixation. *Dalt. Trans.* **2018**, *47*, 1117–1121. [\[CrossRef\]](#)
721. Wickramasinghe, L.A.; Ogawa, T.; Schrock, R.R.; Müller, P. Reduction of Dinitrogen to Ammonia Catalyzed by Molybdenum Diamido Complexes. *J. Am. Chem. Soc.* **2017**, *139*, 9132–9135. [\[CrossRef\]](#) [\[PubMed\]](#)
722. Kiernicki, J.J.; Zeller, M.; Szymczak, N.K. Hydrazine Capture and N-N Bond Cleavage at Iron Enabled by Flexible Appended Lewis Acids. *J. Am. Chem. Soc.* **2017**, *139*, 18194–18197. [\[CrossRef\]](#) [\[PubMed\]](#)
723. Connor, G.P.; Lease, N.; Casuras, A.; Goldman, A.S.; Holland, P.L.; Mayer, J.M. Protonation and electrochemical reduction of rhodium- and iridium-dinitrogen complexes in organic solution. *Dalt. Trans.* **2017**, *46*, 14325–14330. [\[CrossRef\]](#)
724. Stucke, N.; Krahmer, J.; Näther, C.; Tuczek, F. Molybdenum Complexes Supported by PN3P Pincer Ligands: Synthesis, Characterization, and Application to Synthetic Nitrogen Fixation. *Eur. J. Inorg. Chem.* **2018**, *2018*, 5108–5116. [\[CrossRef\]](#)
725. Shiina, K. Reductive silylation of molecular nitrogen via fixation to tris (trialkylsilyl) amine. *J. Am. Chem. Soc.* **1972**, *94*, 9266–9267. [\[CrossRef\]](#)
726. Komori, K.; Oshita, H.; Mizobe, Y.; Hidai, M. Preparation and properties of molybdenum and tungsten dinitrogen complexes. 25. Catalytic conversion of molecular nitrogen into silylamines using molybdenum and tungsten dinitrogen complexes. *J. Am. Chem. Soc.* **1989**, *111*, 1939–1940. [\[CrossRef\]](#)
727. Tanaka, H.; Sasada, A.; Kouno, T.; Yuki, M.; Miyake, Y.; Nakanishi, H.; Nishibayashi, Y.; Yoshizawa, K. Molybdenum-Catalyzed Transformation of Molecular Dinitrogen into Silylamine: Experimental and DFT Study on the Remarkable Role of Ferrocenyldiphosphine Ligands. *J. Am. Chem. Soc.* **2011**, *133*, 3498–3506. [\[CrossRef\]](#) [\[PubMed\]](#)
728. Yuki, M.; Tanaka, H.; Sasaki, K.; Miyake, Y.; Yoshizawa, K.; Nishibayashi, Y. Iron-catalysed transformation of molecular dinitrogen into silylamine under ambient conditions. *Nat. Commun.* **2012**, *3*, 1254. [\[CrossRef\]](#)
729. Araake, R.; Sakadani, K.; Tada, M.; Sakai, Y.; Ohki, Y. [Fe<sub>4</sub>] and [Fe<sub>6</sub>] Hydride Clusters Supported by Phosphines: Synthesis, Characterization, and Application in N<sub>2</sub> Reduction. *J. Am. Chem. Soc.* **2017**, *139*, 5596–5606. [\[CrossRef\]](#)
730. Imayoshi, R.; Nakajima, K.; Nishibayashi, Y. Vanadium-catalyzed Reduction of Molecular Dinitrogen into Silylamine under Ambient Reaction Conditions. *Chem. Lett.* **2017**, *46*, 466–468. [\[CrossRef\]](#)
731. Kawaguchi, M.; Shin-ichi, H.; Mori, M. Incorporation of molecular nitrogen into organic compounds. Titanium catalyzed nitrogenation. *Tetrahedron Lett.* **1993**, *34*, 6907–6910. [\[CrossRef\]](#)
732. Ghana, P.; van Krüchten, F.D.; Spaniol, T.P.; van Leusen, J.; Kögerler, P.; Okuda, J. Conversion of dinitrogen to tris(trimethylsilyl)amine catalyzed by titanium triamido-amine complexes. *Chem. Commun.* **2019**, *55*, 3231–3234. [\[CrossRef\]](#) [\[PubMed\]](#)
733. Siedschlag, R.B.; Bernales, V.; Vogiatzis, K.D.; Planas, N.; Clouston, L.J.; Bill, E.; Gagliardi, L.; Lu, C.C. Catalytic Silylation of Dinitrogen with a Dicobalt Complex. *J. Am. Chem. Soc.* **2015**, *137*, 4638–4641. [\[CrossRef\]](#) [\[PubMed\]](#)
734. Imayoshi, R.; Tanaka, H.; Matsuo, Y.; Yuki, M.; Nakajima, K.; Yoshizawa, K.; Nishibayashi, Y. Cobalt-Catalyzed Transformation of Molecular Dinitrogen into Silylamine under Ambient Reaction Conditions. *Chem. A Eur. J.* **2015**, *21*, 8905–8909. [\[CrossRef\]](#) [\[PubMed\]](#)
735. Dzik, W. Silylation of Dinitrogen Catalyzed by Hydridodinitrogen tris(Triphenylphosphine)Cobalt(I). *Inorganics* **2016**, *4*, 21. [\[CrossRef\]](#)
736. Gao, Y.; Li, G.; Deng, L. Bis(dinitrogen)cobalt(–1) Complexes with NHC Ligation: Synthesis, Characterization, and Their Dinitrogen Functionalization Reactions Affording Side-on Bound Diazene Complexes. *J. Am. Chem. Soc.* **2018**, *140*, 2239–2250. [\[CrossRef\]](#)
737. Suzuki, T.; Fujimoto, K.; Takemoto, Y.; Wasada-Tsutsui, Y.; Ozawa, T.; Inomata, T.; Fryzuk, M.D.; Masuda, H. Efficient Catalytic Conversion of Dinitrogen to N(SiMe<sub>3</sub>)<sub>3</sub> Using a Homogeneous Mononuclear Cobalt Complex. *ACS Catal.* **2018**, *8*, 3011–3015. [\[CrossRef\]](#)
738. Tanabe, Y.; Nishibayashi, Y. Recent advances in catalytic silylation of dinitrogen using transition metal complexes. *Coord. Chem. Rev.* **2019**, *389*, 73–93. [\[CrossRef\]](#)
739. Liao, Q.; Cavaillé, A.; Saffon-Merceron, N.; Mézailles, N. Direct Synthesis of Silylamine from N<sub>2</sub> and a Silane: Mediated by a Tridentate Phosphine Molybdenum Fragment. *Angew. Chem. Int. Ed.* **2016**, *128*, 11378–11382. [\[CrossRef\]](#)

740. Imayoshi, R.; Nakajima, K.; Takaya, J.; Iwasawa, N.; Nishibayashi, Y. Synthesis and Reactivity of Iron- and Cobalt-Dinitrogen Complexes Bearing PSiP-Type Pincer Ligands toward Nitrogen Fixation. *Eur. J. Inorg. Chem.* **2017**, 2017, 3768. [\[CrossRef\]](#)
741. Huber, G.W.; Iborra, S.; Corma, A. Synthesis of Transportation Fuels from Biomass: Chemistry, Catalysts, and Engineering. *Chem. Rev.* **2006**, 106, 4044–4098. [\[CrossRef\]](#) [\[PubMed\]](#)
742. Chheda, J.N.; Huber, G.W.; Dumesic, J.A. Liquid-Phase Catalytic Processing of Biomass-Derived Oxygenated Hydrocarbons to Fuels and Chemicals. *Angew. Chem. Int. Ed.* **2007**, 46, 7164–7183. [\[CrossRef\]](#) [\[PubMed\]](#)
743. Corma, A.; Iborra, S.; Velty, A. Chemical Routes for the Transformation of Biomass into Chemicals. *Chem. Rev.* **2007**, 107, 2411–2502. [\[CrossRef\]](#) [\[PubMed\]](#)
744. Marshall, A.-L.; Alaimo, P.J. Useful Products from Complex Starting Materials: Common Chemicals from Biomass Feedstocks. *Chem. A Eur. J.* **2010**, 16, 4970–4980. [\[CrossRef\]](#) [\[PubMed\]](#)
745. Werpy, T.A.; Holladay, J.E.; White, J.F. *Top Value Added Chemicals from Biomass: I. Results of Screening for Potential Candidates from Sugars and Synthesis Gas*; Pacific Northwest National Lab.: Richland, WA, USA, 2004.
746. Takagaki, A.; Nishimura, S.; Ebitani, K. Catalytic Transformations of Biomass-Derived Materials into Value-Added Chemicals. *Catal. Surv. Asia* **2012**, 16, 164–182. [\[CrossRef\]](#)
747. Zhou, C.-H.; Xia, X.; Lin, C.-X.; Tong, D.-S.; Beltramini, J. Catalytic conversion of lignocellulosic biomass to fine chemicals and fuels. *Chem. Soc. Rev.* **2011**, 40, 5588. [\[CrossRef\]](#)
748. Zakzeski, J.; Bruijninx, P.C.A.; Jongerius, A.L.; Weckhuysen, B.M. The Catalytic Valorization of Lignin for the Production of Renewable Chemicals. *Chem. Rev.* **2010**, 110, 3552–3599. [\[CrossRef\]](#) [\[PubMed\]](#)
749. Cao, L.; Yu, I.K.M.; Liu, Y.; Ruan, X.; Tsang, D.C.W.; Hunt, A.J.; Ok, Y.S.; Song, H.; Zhang, S. Lignin valorization for the production of renewable chemicals: State-of-the-art review and future prospects. *Bioresour. Technol.* **2018**, 269, 465–475. [\[CrossRef\]](#)
750. Azadi, P.; Inderwildi, O.R.; Farnood, R.; King, D.A. Liquid fuels, hydrogen and chemicals from lignin: A critical review. *Renew. Sustain. Energy Rev.* **2013**, 21, 506–523. [\[CrossRef\]](#)
751. van Putten, R.-J.; van der Waal, J.C.; de Jong, E.; Rasrendra, C.B.; Heeres, H.J.; de Vries, J.G. Hydroxymethylfurfural, A Versatile Platform Chemical Made from Renewable Resources. *Chem. Rev.* **2013**, 113, 1499–1597. [\[CrossRef\]](#)
752. Rosatella, A.A.; Simeonov, S.P.; Frade, R.F.M.; Afonso, C.A.M. 5-Hydroxymethylfurfural (HMF) as a building block platform: Biological properties, synthesis and synthetic applications. *Green Chem.* **2011**, 13, 754. [\[CrossRef\]](#)
753. Wright, W.R.H.; Palkovits, R. Development of Heterogeneous Catalysts for the Conversion of Levulinic Acid to  $\gamma$ -Valerolactone. *ChemSusChem* **2012**, 5, 1657–1667. [\[CrossRef\]](#) [\[PubMed\]](#)
754. Liguori, F.; Moreno-Marrodan, C.; Barbaro, P. Environmentally Friendly Synthesis of  $\gamma$ -Valerolactone by Direct Catalytic Conversion of Renewable Sources. *ACS Catal.* **2015**, 5, 1882–1894. [\[CrossRef\]](#)
755. Démolis, A.; Essayem, N.; Rataboul, F. Synthesis and Applications of Alkyl Levulinates. *ACS Sustain. Chem. Eng.* **2014**, 2, 1338–1352. [\[CrossRef\]](#)
756. Raspolli Galletti, A.M.; Antonetti, C.; Ribechini, E.; Colombini, M.P.; Nasso, N.; Bonari, E. From giant reed to levulinic acid and gamma-valerolactone: A high yield catalytic route to valeric biofuels. *Appl. Energy* **2013**, 102, 157–162. [\[CrossRef\]](#)
757. Bond, J.Q.; Alonso, D.M.; Wang, D.; West, R.M.; Dumesic, J.A. Integrated Catalytic Conversion of  $\gamma$ -Valerolactone to Liquid Alkenes for Transportation Fuels. *Science* **2010**, 327, 1110–1114. [\[CrossRef\]](#)
758. Yan, K.; Yang, Y.; Chai, J.; Lu, Y. Catalytic reactions of gamma-valerolactone: A platform to fuels and value-added chemicals. *Appl. Catal. B Environ.* **2015**, 179, 292–304. [\[CrossRef\]](#)
759. Mika, L.T.; Cséfalvay, E.; Horváth, I.T. The role of water in catalytic biomass-based technologies to produce chemicals and fuels. *Catal. Today* **2015**, 247, 33–46. [\[CrossRef\]](#)
760. Horváth, I.T. Solvents from nature. *Green Chem.* **2008**, 10, 1024. [\[CrossRef\]](#)
761. Portillo Perez, G.; Mukherjee, A.; Dumont, M.J. Insights into HMF catalysis. *J. Ind. Eng. Chem.* **2019**, 70, 1–34. [\[CrossRef\]](#)
762. Omoruyi, U.; Page, S.; Hallett, J.; Miller, P.W. Homogeneous catalyzed reactions of levulinic acid: To  $\gamma$ -valerolactone and beyond. *ChemSusChem* **2016**, 9, 2037–2047. [\[CrossRef\]](#) [\[PubMed\]](#)
763. Deng, L.; Li, J.; Lai, D.-M.; Fu, Y.; Guo, Q.-X. Catalytic Conversion of Biomass-Derived Carbohydrates into  $\gamma$ -Valerolactone without Using an External H<sub>2</sub> Supply. *Angew. Chem. Int. Ed.* **2009**, 48, 6529–6532. [\[CrossRef\]](#) [\[PubMed\]](#)

764. Qi, L.; Horváth, I.T. Catalytic Conversion of Fructose to  $\gamma$ -Valerolactone in  $\gamma$ -Valerolactone. *ACS Catal.* **2012**, *2*, 2247–2249. [[CrossRef](#)]
765. Tukacs, J.M.; Király, D.; Strádi, A.; Novodarszki, G.; Eke, Z.; Dibó, G.; Kégl, T.; Mika, L.T. Efficient catalytic hydrogenation of levulinic acid: A key step in biomass conversion. *Green Chem.* **2012**, *14*, 2057. [[CrossRef](#)]
766. Tukacs, J.M.; Novák, M.; Dibó, G.; Mika, L.T. An improved catalytic system for the reduction of levulinic acid to  $\gamma$ -valerolactone. *Catal. Sci. Technol.* **2014**, *4*, 2908–2912. [[CrossRef](#)]
767. Fábos, V.; Mika, L.T.; Horváth, I.T. Selective Conversion of Levulinic and Formic Acids to  $\gamma$ -Valerolactone with the Shvo Catalyst. *Organometallics* **2014**, *33*, 181–187. [[CrossRef](#)]
768. Geilen, F.M.A.; Engendahl, B.; Harwardt, A.; Marquardt, W.; Klankermayer, J.; Leitner, W. Selective and Flexible Transformation of Biomass-Derived Platform Chemicals by a Multifunctional Catalytic System. *Angew. Chem. Int. Ed.* **2010**, *49*, 5510–5514. [[CrossRef](#)]
769. vom Stein, T.; Meuresch, M.; Limper, D.; Schmitz, M.; Hölscher, M.; Coetzee, J.; Cole-Hamilton, D.J.; Klankermayer, J.; Leitner, W. Highly Versatile Catalytic Hydrogenation of Carboxylic and Carbonic Acid Derivatives using a Ru-Triphos Complex: Molecular Control over Selectivity and Substrate Scope. *J. Am. Chem. Soc.* **2014**, *136*, 13217–13225. [[CrossRef](#)]
770. Meuresch, M.; Westhues, S.; Leitner, W.; Klankermayer, J. Tailor-Made Ruthenium-Triphos Catalysts for the Selective Homogeneous Hydrogenation of Lactams. *Angew. Chem. Int. Ed.* **2016**, *55*, 1392–1395. [[CrossRef](#)]
771. vom Stein, T.; Weigand, T.; Merckens, C.; Klankermayer, J.; Leitner, W. Trimethylenemethane-Ruthenium(II)-Triphos Complexes as Highly Active Catalysts for Catalytic C–O Bond Cleavage Reactions of Lignin Model Compounds. *ChemCatChem* **2013**, *5*, 439–441. [[CrossRef](#)]
772. Cui, X.; Li, Y.; Topf, C.; Junge, K.; Beller, M. Direct Ruthenium-Catalyzed Hydrogenation of Carboxylic Acids to Alcohols. *Angew. Chem. Int. Ed.* **2015**, *54*, 10596–10599. [[CrossRef](#)] [[PubMed](#)]
773. Li, Y.; Topf, C.; Cui, X.; Junge, K.; Beller, M. Lewis Acid Promoted Ruthenium(II)-Catalyzed Etherifications by Selective Hydrogenation of Carboxylic Acids/Esters. *Angew. Chem. Int. Ed.* **2015**, *54*, 5196–5200. [[CrossRef](#)]
774. Dutta Chowdhury, A.; Jackstell, R.; Beller, M. Towards the Efficient Development of Homogeneous Catalytic Transformation to  $\gamma$ -Valerolactone from Biomass-Derived Platform Chemicals. *ChemCatChem* **2014**, *6*, 3360–3365. [[CrossRef](#)]
775. Balaraman, E.; Fogler, E.; Milstein, D. Efficient hydrogenation of biomass-derived cyclic di-esters to 1,2-diols. *Chem. Commun.* **2012**, *48*, 1111–1113. [[CrossRef](#)] [[PubMed](#)]
776. Deng, J.; Wang, Y.; Pan, T.; Xu, Q.; Guo, Q.-X.; Fu, Y. Conversion of Carbohydrate Biomass to  $\gamma$ -Valerolactone by using Water-Soluble and Reusable Iridium Complexes in Acidic Aqueous Media. *ChemSusChem* **2013**, *6*, 1163–1167. [[CrossRef](#)]
777. Wang, S.; Huang, H.; Dorcet, V.; Roisnel, T.; Bruneau, C.; Fischmeister, C. Efficient Iridium Catalysts for Base-Free Hydrogenation of Levulinic Acid. *Organometallics* **2017**, *36*, 3152–3162. [[CrossRef](#)]
778. Ortiz-Cervantes, C.; Flores-Alamo, M.; García, J.J. Hydrogenation of Biomass-Derived Levulinic Acid into  $\gamma$ -Valerolactone Catalyzed by Palladium Complexes. *ACS Catal.* **2015**, *5*, 1424–1431. [[CrossRef](#)]
779. Dwivedi, A.D.; Gupta, K.; Tyagi, D.; Rai, R.K.; Mobin, S.M.; Singh, S.K. Ruthenium and Formic Acid Based Tandem Catalytic Transformation of Bioderived Furans to Levulinic Acid and Diketones in Water. *ChemCatChem* **2015**, *7*, 4050–4058. [[CrossRef](#)]
780. Li, W.; Xie, J.-H.; Lin, H.; Zhou, Q.-L. Highly efficient hydrogenation of biomass-derived levulinic acid to  $\gamma$ -valerolactone catalyzed by iridium pincer complexes. *Green Chem.* **2012**, *14*, 2388. [[CrossRef](#)]
781. Gao, H.; Chen, J. Hydrogenation of biomass-derived levulinic acid to  $\gamma$ -valerolactone catalyzed by PNP-Ir pincer complexes: A computational study. *J. Organomet. Chem.* **2015**, *797*, 165–170. [[CrossRef](#)]
782. Phanopoulos, A.; White, A.J.P.; Long, N.J.; Miller, P.W. Catalytic Transformation of Levulinic Acid to 2-Methyltetrahydrofuran Using Ruthenium-N-Triphos Complexes. *ACS Catal.* **2015**, *5*, 2500–2512. [[CrossRef](#)]
783. Deng, L.; Kang, B.; Englert, U.; Klankermayer, J.; Palkovits, R. Direct hydrogenation of biobased carboxylic acids mediated by a nitrogen-centered tridentate phosphine ligand. *ChemSusChem* **2016**, *9*, 177–180. [[CrossRef](#)] [[PubMed](#)]
784. Sullivan, R.J.; Kim, J.; Hoyt, C.; Silks, L.A.; Schlaf, M. Ruthenium-8-quinolinethiolate-phenylterpyridine versus ruthenium-bipyridine-phenyl-terpyridine complexes as homogeneous water and high temperature stable hydrogenation catalysts for biomass-derived substrates. *Polyhedron* **2016**, *108*, 104–114. [[CrossRef](#)]



785. Wozniak, B.; Spannenberg, A.; Li, Y.; Hinze, S.; de Vries, J.G. Cyclopentanone Derivatives from 5-Hydroxymethylfurfural via 1-Hydroxyhexane-2,5-dione as Intermediate. *ChemSusChem* **2018**, *11*, 356–359. [[CrossRef](#)] [[PubMed](#)]
786. Wozniak, B.; Tin, S.; de Vries, J.G. Bio-based building blocks from 5-hydroxymethylfurfural via 1-hydroxyhexane-2,5-dione as intermediate. *Chem. Sci.* **2019**, *10*, 6024–6034. [[CrossRef](#)] [[PubMed](#)]
787. Stadler, B.M.; Puylaert, P.; Diekamp, J.; van Heck, R.; Fan, Y.; Spannenberg, A.; Hinze, S.; de Vries, J.G. Inexpensive Ruthenium NNS-Complexes as Efficient Ester Hydrogenation Catalysts with High C=O vs. C=C Selectivities. *Adv. Synth. Catal.* **2018**, *360*, 1151–1158. [[CrossRef](#)]
788. Yi, Y.; Liu, H.; Xiao, L.P.; Wang, B.; Song, G. Highly Efficient Hydrogenation of Levulinic Acid into  $\gamma$ -Valerolactone using an Iron Pincer Complex. *ChemSusChem* **2018**, *11*, 1474–1478. [[CrossRef](#)]
789. Padilla, R.; Jørgensen, M.S.B.; Paixão, M.W.; Nielsen, M. Efficient catalytic hydrogenation of alkyl levulinates to  $\gamma$ -valerolactone. *Green Chem.* **2019**, *21*, 5195–5200. [[CrossRef](#)]
790. Irrgang, T.; Kempe, R. 3d-Metal Catalyzed N- and C-Alkylation Reactions via Borrowing Hydrogen or Hydrogen Autotransfer. *Chem. Rev.* **2019**, *119*, 2524–2549. [[CrossRef](#)]
791. Corma, A.; Navas, J.; Sabater, M.J. Advances in One-Pot Synthesis through Borrowing Hydrogen Catalysis. *Chem. Rev.* **2018**, *118*, 1410–1459. [[CrossRef](#)]
792. Matsunami, A.; Kayaki, Y. Upgrading and expanding the scope of homogeneous transfer hydrogenation. *Tetrahedron Lett.* **2018**, *59*, 504–513. [[CrossRef](#)]
793. Morris, R.H. Mechanisms of the H<sub>2</sub>- and transfer hydrogenation of polar bonds catalyzed by iron group hydrides. *Dalt. Trans.* **2018**, *47*, 10809–10826. [[CrossRef](#)] [[PubMed](#)]
794. Hashiguchi, S.; Fujii, A.; Takehara, J.; Ikariya, T.; Noyori, R. Asymmetric Transfer Hydrogenation of Aromatic Ketones Catalyzed by Chiral Ruthenium(II) Complexes. *J. Am. Chem. Soc.* **1995**, *117*, 7562–7563. [[CrossRef](#)]
795. Noyori, R.; Hashiguchi, S. Asymmetric Transfer Hydrogenation Catalyzed by Chiral Ruthenium Complexes. *Acc. Chem. Res.* **1997**, *30*, 97–102. [[CrossRef](#)]
796. Ikariya, T. Bifunctional Transition Metal-Based Molecular Catalysts for Asymmetric Syntheses. In *Topics in Organometallic Chemistry*; Springer: Berlin/Heidelberg, Germany, 2011; pp. 31–53. ISBN 9783642207303.
797. Haack, K.-J.; Hashiguchi, S.; Fujii, A.; Ikariya, T.; Noyori, R. The Catalyst Precursor, Catalyst, and Intermediate in the RuII-Promoted Asymmetric Hydrogen Transfer between Alcohols and Ketones. *Angew. Chem. Int. Ed. Engl.* **1997**, *36*, 285–288. [[CrossRef](#)]
798. Zweifel, T.; Naubron, J.-V.; Büttner, T.; Ott, T.; Grützmacher, H. Ethanol as Hydrogen Donor: Highly Efficient Transfer Hydrogenations with Rhodium(I) Amides. *Angew. Chem. Int. Ed.* **2008**, *47*, 3245–3249. [[CrossRef](#)]
799. Samec, J.S.M.; Bäckvall, J.-E.; Andersson, P.G.; Brandt, P. Mechanistic aspects of transition metal-catalyzed hydrogen transfer reactions. *Chem. Soc. Rev.* **2006**, *35*, 237. [[CrossRef](#)]
800. Foubelo, F.; Nájera, C.; Yus, M. Catalytic asymmetric transfer hydrogenation of ketones: Recent advances. *Tetrahedron Asymmetry* **2015**, *26*, 769–790. [[CrossRef](#)]
801. Mai, V.H.; Lee, S.-H.; Nikonov, G.I. Transfer Hydrogenation of Unsaturated Substrates by Half-sandwich Ruthenium Catalysts using Ammonium Formate as Reducing Reagent. *ChemistrySelect* **2017**, *2*, 7751–7757. [[CrossRef](#)]
802. Kayan, C.; Meriç, N.; Aydemir, M.; Ocak, Y.S.; Baysal, A.; Temel, H. Novel cyclohexyl-based aminophosphine ligands and use of their Ru(II) complexes in transfer hydrogenation of ketones. *Appl. Organomet. Chem.* **2014**, *28*, 127–133. [[CrossRef](#)]
803. Ikariya, T.; Blacker, A.J. Asymmetric Transfer Hydrogenation of Ketones with Bifunctional Transition Metal-Based Molecular Catalysts. *Acc. Chem. Res.* **2007**, *40*, 1300–1308. [[CrossRef](#)] [[PubMed](#)]
804. Lundberg, H.; Adolfsson, H. Ruthenium-catalyzed asymmetric transfer hydrogenation of ketones in ethanol. *Tetrahedron Lett.* **2011**, *52*, 2754–2758. [[CrossRef](#)]
805. Castellanos-Blanco, N.; Arévalo, A.; García, J.J. Nickel-catalyzed transfer hydrogenation of ketones using ethanol as a solvent and a hydrogen donor. *Dalt. Trans.* **2016**, *45*, 13604–13614. [[CrossRef](#)] [[PubMed](#)]
806. Sanz, S.; Benítez, M.; Peris, E. A New Approach to the Reduction of Carbon Dioxide: CO<sub>2</sub> Reduction to Formate by Transfer Hydrogenation in i PrOH. *Organometallics* **2010**, *29*, 275–277. [[CrossRef](#)]
807. Wei, Y.; Wang, C.; Jiang, X.; Xue, D.; Li, J.; Xiao, J. Highly efficient transformation of levulinic acid into pyrrolidinones by iridium catalysed transfer hydrogenation. *Chem. Commun.* **2013**, *49*, 5408. [[CrossRef](#)]
808. Crabtree, R.H. Transfer Hydrogenation with Glycerol as H-Donor: Catalyst Activation, Deactivation and Homogeneity. *ACS Sustain. Chem. Eng.* **2019**, *7*, 15845–15853. [[CrossRef](#)]

809. Chen, T.; He, L.-P.; Gong, D.; Yang, L.; Miao, X.; Eppinger, J.; Huang, K.-W. Ruthenium(II) pincer complexes with oxazoline arms for efficient transfer hydrogenation reactions. *Tetrahedron Lett.* **2012**, *53*, 4409–4412. [\[CrossRef\]](#)
810. He, L.-P.; Chen, T.; Xue, D.-X.; Eddaoudi, M.; Huang, K.-W. Efficient transfer hydrogenation reaction Catalyzed by a dearomatized PN3P ruthenium pincer complex under base-free Conditions. *J. Organomet. Chem.* **2012**, *700*, 202–206. [\[CrossRef\]](#)
811. Gladiali, S.; Alberico, E. Asymmetric transfer hydrogenation: Chiral ligands and applications. *Chem. Soc. Rev.* **2006**, *35*, 226–236. [\[CrossRef\]](#)
812. Baldino, S.; Facchetti, S.; Zanotti-Gerosa, A.; Nedden, H.G.; Baratta, W. Transfer Hydrogenation and Hydrogenation of Commercial-Grade Aldehydes to Primary Alcohols Catalyzed by 2-(Aminomethyl)pyridine and Pincer Benzo[h]quinoline Ruthenium Complexes. *ChemCatChem* **2016**, *8*, 2279–2288. [\[CrossRef\]](#)
813. Liu, W.-P.; Yuan, M.-L.; Yang, X.-H.; Li, K.; Xie, J.-H.; Zhou, Q.-L. Efficient asymmetric transfer hydrogenation of ketones in ethanol with chiral iridium complexes of spiroPAP ligands as catalysts. *Chem. Commun.* **2015**, *51*, 6123–6125. [\[CrossRef\]](#) [\[PubMed\]](#)
814. Dubey, A.; Khaskin, E. Catalytic Ester Metathesis Reaction and Its Application to Transfer Hydrogenation of Esters. *ACS Catal.* **2016**, *6*, 3998–4002. [\[CrossRef\]](#)
815. Weingart, P.; Thiel, W.R. Applying Le Chatelier's Principle for a Highly Efficient Catalytic Transfer Hydrogenation with Ethanol as the Hydrogen Source. *ChemCatChem* **2018**, *10*, 4858–4862. [\[CrossRef\]](#)
816. Wang, Y.; Huang, Z.; Leng, X.; Zhu, H.; Liu, G.; Huang, Z. Transfer Hydrogenation of Alkenes Using Ethanol Catalyzed by a NCP Pincer Iridium Complex: Scope and Mechanism. *J. Am. Chem. Soc.* **2018**, *140*, 4417–4429. [\[CrossRef\]](#) [\[PubMed\]](#)
817. Farrar-Tobar, R.A.; Wozniak, B.; Savini, A.; Hinze, S.; Tin, S.; de Vries, J.G. Base-Free Iron Catalyzed Transfer Hydrogenation of Esters Using EtOH as Hydrogen Source. *Angew. Chem. Int. Ed.* **2019**, *58*, 1129–1133. [\[CrossRef\]](#)
818. Krall, E.M.; Klein, T.W.; Andersen, R.J.; Nett, A.J.; Glasgow, R.W.; Reader, D.S.; Dauphinais, B.C.; Mc Ilrath, S.P.; Fischer, A.A.; Carney, M.J.; et al. Controlled hydrogenative depolymerization of polyesters and polycarbonates catalyzed by ruthenium(ii) PNN pincer complexes. *Chem. Commun.* **2014**, *50*, 4884. [\[CrossRef\]](#)
819. Sun, J.; Wang, Y. Recent advances in catalytic conversion of ethanol to chemicals. *ACS Catal.* **2014**, *4*, 1078–1090. [\[CrossRef\]](#)
820. Ndou, A.S.; Plint, N.; Coville, N.J. Dimerisation of ethanol to butanol over solid-base catalysts. *Appl. Catal. A Gen.* **2003**, *251*, 337–345. [\[CrossRef\]](#)
821. Chakraborty, S.; Pizsel, P.E.; Hayes, C.E.; Baker, R.T.; Jones, W.D. Highly Selective Formation of n-Butanol from Ethanol through the Guerbet Process: A Tandem Catalytic Approach. *J. Am. Chem. Soc.* **2015**, *137*, 14264–14267. [\[CrossRef\]](#)
822. Aitchison, H.; Wingad, R.L.; Wass, D.F. Homogeneous Ethanol to Butanol Catalysis-Guerbet Renewed. *ACS Catal.* **2016**, *6*, 7125–7132. [\[CrossRef\]](#)
823. Sheehan, J.; Aden, A.; Paustian, K.; Killian, K.; Brenner, J.; Walsh, M.; Nelson, R. Energy and Environmental Aspects of Using Corn Stover for Fuel Ethanol. *J. Ind. Ecol.* **2003**, *7*, 117–146. [\[CrossRef\]](#)
824. Kim, S.; Dale, B.E. Life cycle assessment of various cropping systems utilized for producing biofuels: Bioethanol and biodiesel. *Biomass Bioenergy* **2005**, *29*, 426–439. [\[CrossRef\]](#)
825. Wu, M.; Wang, M.; Huo, H. Fuel-Cycle Assessment of Selected Bioethanol Production Pathways in the United States. *Renew. Energy* **2006**, *120*.
826. Atsumi, S.; Cann, A.F.; Connor, M.R.; Shen, C.R.; Smith, K.M.; Brynildsen, M.P.; Chou, K.J.Y.; Hanai, T.; Liao, J.C. Metabolic engineering of *Escherichia coli* for 1-butanol production. *Metab. Eng.* **2008**, *10*, 305–311. [\[CrossRef\]](#) [\[PubMed\]](#)
827. Xue, C.; Zhao, X.-Q.; Liu, C.-G.; Chen, L.-J.; Bai, F.-W. Prospective and development of butanol as an advanced biofuel. *Biotechnol. Adv.* **2013**, *31*, 1575–1584. [\[CrossRef\]](#) [\[PubMed\]](#)
828. Dürre, P. Biobutanol: An attractive biofuel. *Biotechnol. J.* **2007**, *2*, 1525–1534. [\[CrossRef\]](#) [\[PubMed\]](#)
829. Jin, C.; Yao, M.; Liu, H.; Lee, C.F.; Ji, J. Progress in the production and application of n-butanol as a biofuel. *Renew. Sustain. Energy Rev.* **2011**, *15*, 4080–4106. [\[CrossRef\]](#)
830. Veibel, S.; Nielsen, J.I. On the mechanism of the Guerbet reaction. *Tetrahedron* **1967**, *23*, 1723–1733. [\[CrossRef\]](#)



831. Xie, Y.; Ben-David, Y.; Shimon, L.J.W.; Milstein, D. Highly Efficient Process for Production of Biofuel from Ethanol Catalyzed by Ruthenium Pincer Complexes. *J. Am. Chem. Soc.* **2016**, *138*, 9077–9080. [[CrossRef](#)]
832. Tseng, K.N.T.; Lin, S.; Kampf, J.W.; Szymczak, N.K. Upgrading ethanol to 1-butanol with a homogeneous air-stable ruthenium catalyst. *Chem. Commun.* **2016**, *52*, 2901–2904. [[CrossRef](#)]
833. Tseng, K.N.T.; Kampf, J.W.; Szymczak, N.K. Base-free, acceptorless, and chemoselective alcohol dehydrogenation catalyzed by an amide-derived NNN-ruthenium(II) hydride complex. *Organometallics* **2013**, *32*, 2046–2049. [[CrossRef](#)]
834. Tseng, K.N.T.; Kampf, J.W.; Szymczak, N.K. Mechanism of *N,N,N*-Amide Ruthenium(II) Hydride Mediated Acceptorless Alcohol Dehydrogenation: Inner-Sphere  $\beta$ -H Elimination versus Outer-Sphere Bifunctional Metal-Ligand Cooperativity. *ACS Catal.* **2015**, *5*, 5468–5485. [[CrossRef](#)]
835. Wingad, R.L.; Gates, P.J.; Street, S.T.G.; Wass, D.F. Catalytic Conversion of Ethanol to n-Butanol Using Ruthenium P-N Ligand Complexes. *ACS Catal.* **2015**, *5*, 5822–5826. [[CrossRef](#)]
836. Everett, M.; Pellow, K.J.; Wass, D.F. Catalytic conversion of methanol/ethanol to isobutanol—A highly selective route to an advanced biofuel. *Chem. Commun.* **2016**, *52*, 5202–5204.
837. Pellow, K.J.; Wingad, R.L.; Wass, D.F. Towards the upgrading of fermentation broths to advanced biofuels: A water tolerant catalyst for the conversion of ethanol to isobutanol. *Catal. Sci. Technol.* **2017**, *7*, 5128–5134. [[CrossRef](#)]
838. Fu, S.; Shao, Z.; Wang, Y.; Liu, Q. Manganese-Catalyzed Upgrading of Ethanol into 1-Butanol. *J. Am. Chem. Soc.* **2017**, *139*, 11941–11948. [[CrossRef](#)]
839. Kulkarni, N.V.; Brennessel, W.W.; Jones, W.D. Catalytic Upgrading of Ethanol to n-Butanol via Manganese-Mediated Guerbet Reaction. *ACS Catal.* **2018**, *8*, 997–1002. [[CrossRef](#)]



© 2020 by the authors. Licensee MDPI, Basel, Switzerland. This article is an open access article distributed under the terms and conditions of the Creative Commons Attribution (CC BY) license (<http://creativecommons.org/licenses/by/4.0/>).